THE
PHYSICAL REVIEW
A Journal of Experimental and Theoretical Physics Established by E. L. Nichols in 1893
VOL. 52, NO. 6 SEPTEMBER 15, 1937 SECOND SERIES

A Long Period Positron Activity: Na^{22}

L. JACKSON LASLETT
Radiation Laboratory, Department of Physics, University of California, Berkeley, California
(Received June 25, 1937)

The bombardment of magnesium with 5.2 Mev deuterons was found to result in a long period radioactivity ascribable to Na^{22}. The half-life, as determined from measurements extending over a period of a year, is 3.0 ± 0.2 years. Absorption measurements on the positrons emitted agree with similar measurements made with a fluorine sample subjected to alpha-particle bombardment; the positron momentum distribution was investigated with a hydrogen-filled cloud chamber in a magnetic field, an upper limit being found at a value corresponding to 0.58 ± 0.03 Mev.

A RADIOACTIVITY ascribable to Na^{22} has been produced by Frisch,[1] who bombarded fluorine in the form of NaF and LiF with alpha-particles from radon. The equations applying are, then,

$$_9F^{19}+{}_2He^4={}_{11}Na^{22}+{}_0n^1,$$
$$_{11}Na^{22}={}_{10}Ne^{22}+e^+.$$

In this laboratory it has been found that, in addition to this long period activity showing up in various fluorides bombarded with artificial alpha-particles, quite strong samples can be produced by the bombardment of magnesium with high speed deuterons.[2] In the latter case we have the reaction

$$_{12}Mg^{24}+{}_1H^2={}_{11}Na^{22}+{}_2He^4;$$

it is the purpose of this paper to present some measurements made on the positrons from this radioelement which is perhaps particularly interesting because of its relatively long period.* The shorter periods arising in magnesium bombarded with deuterons have already been investigated by Henderson,[3] who found that the two negative electron emitters Mg^{27} (10 min. half-life) and Na^{24} (15 hr.) made their appearance.

That the long-period activity in question arises from an isotope of sodium has been confirmed by Dr. M. Kamen, who very kindly carried out a chemical separation on a portion of a sample which had aged six months. Although Na^{22} has been reported to occur in nature[4] in appreciable quantities, a careful investigation by Sampson

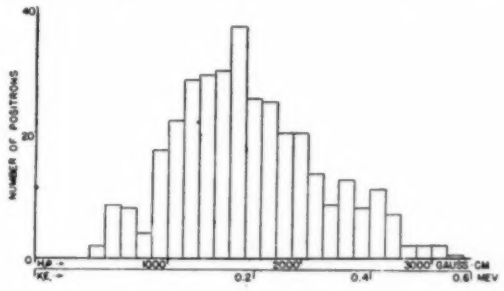

FIG. 1. Momentum distribution of positrons from Na^{22}.

[1] O. R. Frisch, Nature **136**, 220 (1935).
[2] L. J. Laslett, Phys. Rev. **50**, 388(A) (1936).
* *Note added in proof.* The author has been kindly informed by Dr. A. H. Snell that neon, under deuteron bombardment, gives rise to a weak, long period activity. It is likely that this, too, may be ascribed to Na^{22} produced from Ne^{21} with the emission of a neutron.
[3] M. C. Henderson, Phys. Rev. **48**, 855 (1935).
[4] A. K. Brewer, Phys. Rev. **49**, 856(L) (1936).

and Bleakney[5] has convinced these authors this is not the case, an upper limit to the possible abundance being given as one part in fifty thousand of Na^{23}.

In connection with this investigation, two targets of magnesium metal have been bombarded in the Berkeley cyclotron, each with approximately 20 microampere hours of 5.2 Mev deuterons. The older of the two is being kept for

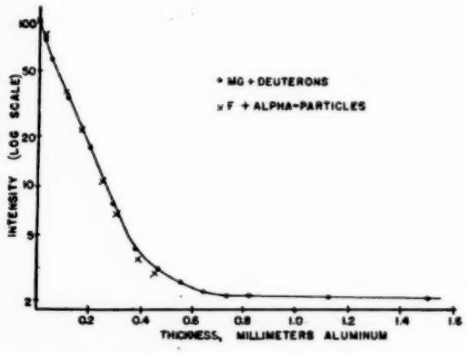

FIG. 2. Absorption curve of radiations emitted by Na^{22}.

further determination of its half-life. The decay of the sample has been followed by comparing the ionization produced by the annihilation radiation with that produced by a radium sample, a pressure ionization chamber coupled to an FP 54 electrometer tube circuit being used for this purpose. In addition, the decay has been followed by measuring the positron intensity and the annihilation radiation with a Lauritsen electroscope. These measurements have been taken over a period of a year and agree in assigning to the half-life the value 3.0 ± 0.2 years.

The momentum distribution of the positrons emitted has been investigated with a hydrogen-filled cloud chamber traversed by a magnetic field of 235 gauss. Some of the photographs were taken with a sample which had aged three months, others with one seven months old; the resulting histogram is shown in Fig. 1 in which the last track and some others in the body of the distribution have been given a weight of one-half, as they were considered poorer than the others. Even with a chamber filled with hydrogen, scattering in the gas distorts such a low energy spectrum, but the upper limit obtained by inspection may be taken as 0.58 ± 0.03 Mev. Absorption measurements made on a magnesium sample are shown in Fig. 2, a logarithmic scale being used. In this figure is also shown the absorption of the positrons from a fluorine sample bombarded in the cyclotron with 10 Mev alpha-particles; the two curves have been fitted at the 0.1 mm point and the similarity of their slopes confirms the belief that the radioactive substances are the same.

Measurements with the electroscope, confirmed by a Geiger counter into which samples could be placed, have indicated that the magnesium targets each emit about six thousand positrons per second. This estimate, together with the known exposure to the deuteron beam, enables one to compute the yield for a thick magnesium target as approximately 2 positron-producing atoms per 10^6 deuterons. This value, applying to 5.2 Mev deuterons, is, of course, much greater than that obtained by Henderson[3] for the similar reaction with Mg^{26} (forming Na^{24}) and 3 Mev deuterons.

The long period positron emission from Na^{22} is of some interest in connection with the theory of Yukawa and Sakata,[6] who suggest K electron capture and neutrino emission as an alternative process. Calculations by Lamb[7] on the basis of this theory and the Konopinski-Uhlenbeck modification of Fermi's β-ray theory show that, with these assumptions, this alternative K electron process is some thirty times more probable than bona fide positron emission—this figure, together with the yield given above, would lead, of course, to a suspiciously large yield of Na^{22} atoms.

The author is greatly indebted to Professor Edwin McMillan and Dr. S. N. Van Voorhis for aid with several of the measurements, as well as to Professor Lawrence for the privilege of using the cyclotron. The work has been aided by grants from the Research Corporation, the Chemical Foundation, and the Josiah Macy, Jr. Foundation.

[5] M. B. Sampson and W. Bleakney, Phys. Rev. **50**, 456 (1936).

[6] H. Yukawa and S. Sakata, Proc. Phys. Math. Soc. Japan **17**, 467 (1935).

[7] W. E. Lamb, Jr., Phys. Rev. **50**, 388 (A) (1936).

The Radioactive Isotopes of Indium

J. L. LAWSON AND J. M. CORK
Department of Physics, University of Michigan, Ann Arbor, Michigan
(Received July 19, 1937)

Although there are but two stable isotopes of indium whose mass numbers are 113 and 115, seven radioactive periods are shown to exist. Six of these whose half-life periods are 13 seconds, 72 seconds, 54 minutes, 2.3 hours, 4.1 hours and 50 days emit negative electrons, and one period of 20 minutes is radiopositive. By bombarding indium with slow neutrons, deuterons and very fast neutrons, and by bombarding cadmium with deuterons it is possible to assign with considerable confidence each period to a certain indium isotope. The conclusions are that the 54 minute and 13 second activities are both due to In^{116}, the 4.1-hour and 50-day periods are both In^{114} and the 20-minute, 72-second and 2.3-hour periods are from isotopes of mass 111, 112, and 117, respectively. Beta-ray energy limits are approximately 2.15 Mev for the 50-day period and 1.75 Mev for the 20-minute positive period.

THERE are at present two known stable isotopes of indium, their relative abundance being 4.5 percent and 95.5 percent for mass numbers 113 and 115, respectively. Fermi[1] and his co-workers have exposed indium to slow neutrons and have observed radioactive half-life periods of 13 seconds and 54 minutes with a very weak activity of a few hours. When slow neutrons produce a radioactive isotope of the bombarded element, the process is considered to be simply the capture of the neutron. Thus one should expect only two radioactive isotopes of indium, 114 and 116, to be formed by this process. The correct assignment of the observed activities to definite isotopes cannot be made from this type of bombardment alone.

The discovery[2, 3] that very energetic neutrons such as those emitted by lithium bombarded by

[1] Amaldi, D'Agostino, Fermi, Pontecorvo, Rasetti and Segrè, Proc. Roy. Soc. **149**, 522 (1935).

[2] Heyn, Physica, **4** 160 (1937).

[3] Pool, Cork and Thornton, Phys. Rev. **51**, 890 (1937).

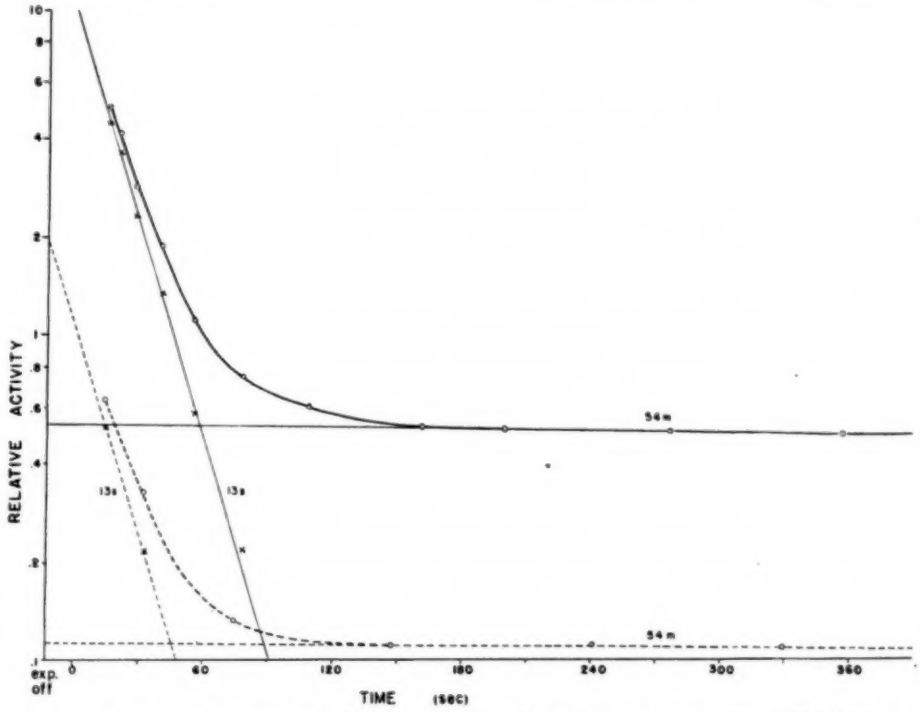

FIG. 1. Decay curves for beta-activity from indium activated by slow neutrons; dotted curves show resolution of gamma-ray activities from a similarly activated indium target.

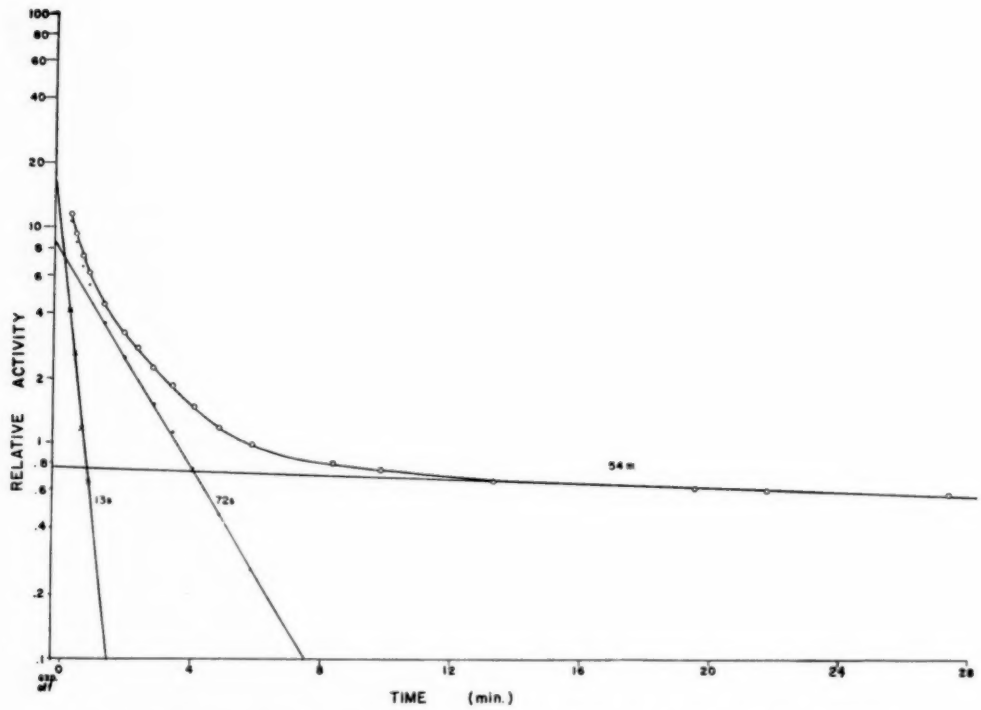

FIG. 2. Decay curves for indium activated by fast neutrons (showing short periods).

deuterons will eject neutrons from the bombarded nucleus allows a more exact assignment of these radioactive periods. Moreover the bombardment of a target directly by very high energy deuterons has been shown to induce the same reactions that are observed when the target is bombarded by slow neutrons except that the intensity of the radioactivities produced may be very greatly increased. To make the assignment of the indium isotopes more complete this investigation includes the results obtained by bombarding the neighboring element, cadmium, with deuterons and subsequently making a chemical separation of the resulting product. Silver has also been radiated with 13 Mev alpha-particles in an attempt to produce one of the active indium isotopes.

RESULTS

Slow neutrons and deuterons

The results obtained with slow neutrons and deuterons are very similar except that the observed activities are much stronger in the latter case. Slow neutron activation was accomplished by imbedding the specimen in a block of paraffin, placed as close as possible to a beryllium target, bombarded by deuterons. Fig. 1 shows a composite decay curve of this activity. This curve resolves satisfactorily into the three periods 13 seconds, 54 minutes and one of a few hours (all negative active). The results with deuterons are not shown but they yield a similar curve except that the increased intensity allows the longer period to be more definitely evaluated as 4.1 hours.

Fast neutrons

Bombardment with the energetic (14→20 Mev) neutrons from lithium exposed to 6.3 Mev deuterons, gave results with indium as shown in Figs. 2 and 3. These results are presented in two figures in order to show more clearly the very different periods. It is quite apparent that certain new periods; namely, 72 seconds and 50 days, both negative, are present in addition to those previously observed. The period of 72 seconds undoubtedly is the same as the period of 1 minute reported by Bothe[4] and Gentner and others[5] induced by means of high energy

[4] Bothe and Gentner, Naturwiss **25**, 284 (1937).
[5] Chang, Goldhaber and Sagane, Nature **139**, 962 (1937).

gamma-rays. A fraction of the high energy neutrons slowed down by scattering always gives a trace of the slow neutron reactions. An estimate of the relative intensities of the various activities at the end of bombardment shows definitely that with fast neutrons or slow neutrons the 13 second and 54 minute periods always have the same ratio with respect to each other. This suggests the assignment of these periods to a single isomeric isotope. The 4.1-hour period appears very strongly with fast neutrons and only very weakly with slow neutrons or deuterons. Since the relative abundance of the isotopes 113 and 115 is about one to twenty such a variation in activity would be expected if it were due to isotope 114. Hence, although the 13-second and 54-minute periods could have been associated with either 114 or 116 they are undoubtedly due to 116. This is substantiated by the fact that they are less strongly excited by fast than by slow neutrons. The 72-second period appears only with fast neutrons and hence must be associated with isotope 112. The 50-day period has so far been observed only when the activation has been with fast neutrons. This therefore might be placed as either an isomer of 112 or 114. It has been tentatively placed as 114. This can be checked by sufficient slow neutron bombardment, but exposures so far have not been sufficient to settle this definitely.

TABLE I. *Stable and radioactive isotopes.*

AT. WT.	106	107	108	109	110	111	112	113	114	115	116	117	118
47 Ag		52.2	2m	47.5	20s	75d							
48 Cd	1.5		1.0		15.2	15.2	21.8	14.9	23.7	4.3h	15.9	58h	
49 In						20m	72s	4.5	4.1h 50d	95.5	13s 54m	2.3h	
50 Sn							1.1		0.8	0.4	15.5	9.1	22.5

Deuterons on cadmium

When 6.3 Mev deuterons are allowed to bombard cadmium certain radioactive isotopes of indium may be formed by the capture of the deuteron with the expulsion of a neutron (i.e., proton capture). One case of this has been reported in the investigation[6] of cadmium. The stable isotopes in this part of the periodic table are shown in Table I. It may be seen from this table that the process of a proton capture might yield many indium isotopes but not 116, and hence not the 13-second and 54-minute periods. The composite decay curve of the indium chemical separation from the bombarded cad-

[6] Cork and Thornton, Phys. Rev. **51**, 608 (1937).

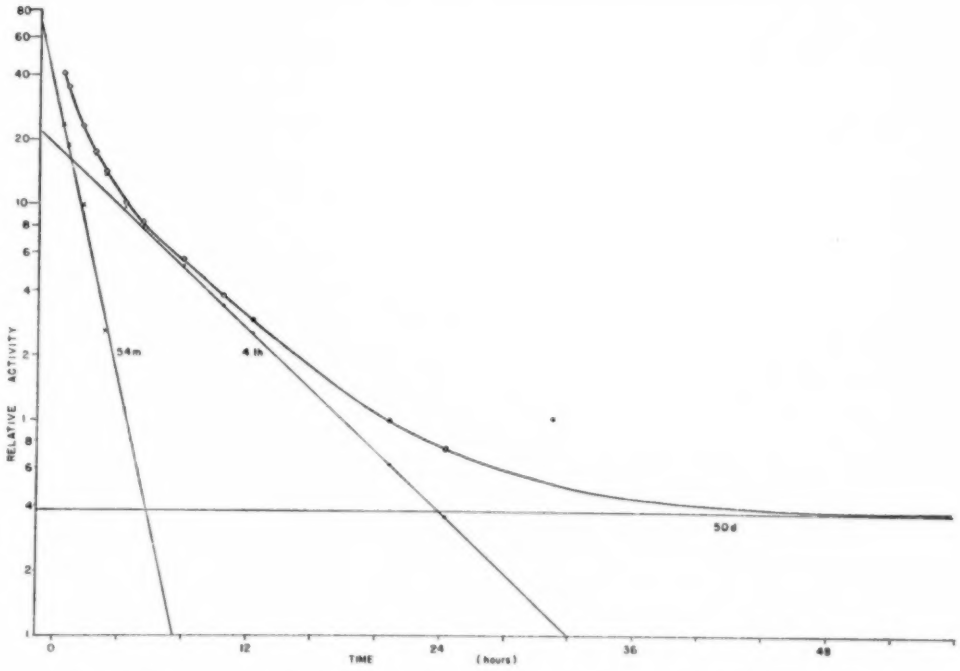

FIG. 3. Decay curves for indium activated by fast neutrons (showing long periods).

mium is shown in Fig. 4. This curve may be resolved into the already well-known periods of 4.1 hours and 2.3 hours, giving in addition a new period of 20 minutes. This 20-minute period was shown to be radiopositive and is accordingly assigned to isotope 111. Other possibilities would be isotopes of mass 107 and 109. These are not probable because of the low relative abundance of the parent cadmium isotopes. Since the minimum time for the chemical separation was about 10 minutes, the period of 72 seconds could not be observed.

Alpha bombardment of silver

By accelerating doubly ionized helium atoms in the cyclotron a beam of alpha-particles of 12 to 13 Mev is obtained. This was allowed to fall on silver, hoping that the reaction corresponding to the absorption of an alpha-particle with the ejection of a neutron might occur. This would lead to the formation of In^{110} and In^{112} from Ag^{107} and Ag^{109}. No evidence of this reaction was observed.

Summary of Probable Reactions

The probable reactions for the various activities are as follows:

(a) Slow neutrons

$${}_{49}In^{N}+{}_{0}n^{1}\rightarrow{}_{49}In^{N+1}$$

$${}_{49}In^{N+1}\rightarrow{}_{50}Sn^{N+1}+{}_{-1}e$$ (13 sec., 54 min., 4.1 hr., 50 da.)

(b) Fast neutrons

$${}_{49}In^{N}+{}_{0}n^{1}\rightarrow{}_{49}In^{N-1}+{}_{0}n^{1}+{}_{0}n^{1}$$

$${}_{49}In^{N-1}\rightarrow{}_{50}Sn^{N-1}+{}_{-1}e$$ (72 sec., 4.1 hr., 50 da.)

(c) Deuterons on cadmium

$${}_{48}Cd^{N}+{}_{1}H^{2}\rightarrow{}_{49}In^{N+1}+n^{1}$$

$${}_{49}In^{N+1}\rightarrow{}_{50}Sn^{N+1}+{}_{-1}e$$, 72 sec., 2.3 hr., 4.1 hr., 50 da.)

$$\rightarrow{}_{48}Cd^{N+1}+{}_{+1}e$$ (20 min.).

Beta- and Gamma-Spectra

There are now shown to be seven radioactive periods in indium. It is evident that a knowledge of the energies of the beta- and gamma-radiations associated with each of these periods should be of value, particularly those relating to the isomeric isotopes. In order to obtain this information it is necessary to isolate each activity for the cloud chamber exposures. This is not easy in every case, and will require much further work. In Fig. 1 is shown in dotted lines the

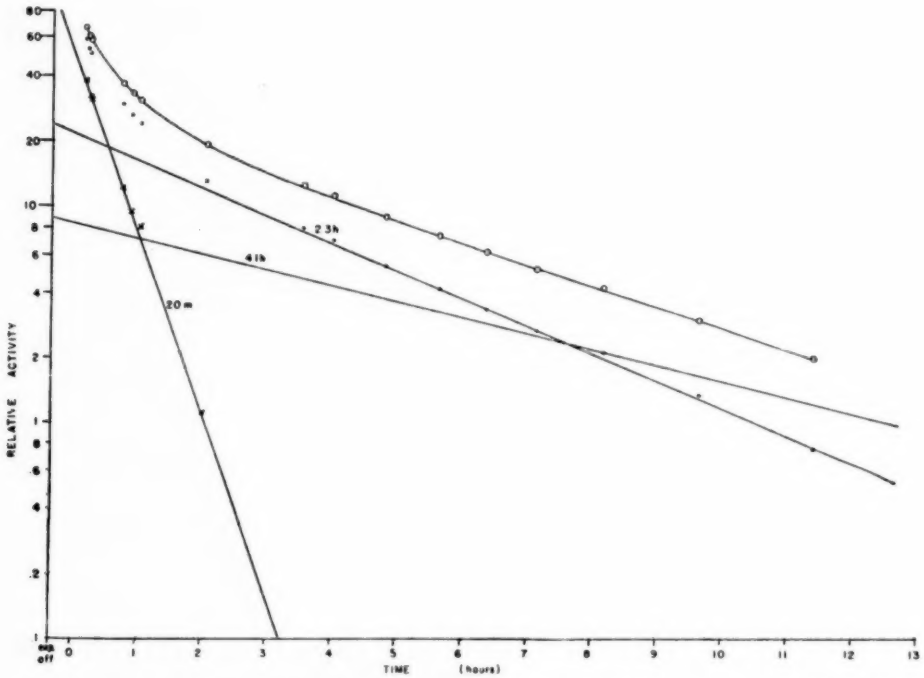

Fig. 4. Decay curves for the indium separation from cadmium bombarded with deuterons.

decay of the gamma-ray activity excited by neutron bombardment. It is apparent that there are gamma-ray periods for the 13-second and 54-minute activities. The energy of each of these has not yet been determined. The energies of the upper limits of the beta-radiations from the 54-minute and 13-second activities have been reported[7] as 1.3 Mev and 3.2 Mev, respectively. In the present investigation about 750 tracks have been measured for the 50-day period and about 100 tracks for the positive 20-minute period. These measurements indicate energies at the upper limit of 2.15 Mev and 1.75 Mev, respectively. Measurements are in progress to determine as far as possible the beta- and gamma-energies for the remaining activities.

We are greatly indebted to Mr. D. W. Stewart for aid in carrying out the necessary chemical separations.

The work has been made possible by a grant from the Horace H. Rackham Trust Fund.

[7] Gaerttner, Turin and Crane, Phys. Rev. **49**, 793 (1937).

SEPTEMBER 15, 1937 PHYSICAL REVIEW VOLUME 52

The Magnetic Moment of the Proton

I. ESTERMANN, O. C. SIMPSON AND O. STERN
Research Laboratory of Molecular Physics, Carnegie Institute of Technology, Pittsburgh, Pennsylvania

(Received July 9, 1937)

The magnetic moment of the proton was measured by the method of the magnetic deflection of molecular beams employing H_2 and HD. The result is $\mu_P = 2.46\mu_0 \pm 3$ percent.

THE magnetic moment of the proton was first measured by Estermann, Frisch and Stern in Hamburg in 1932–33.[1] These measurements gave the surprising result that the proton moment was not one but 2.5 nuclear magnetons with the limit of error of about 10 percent. We have repeated these measurements with the aim of obtaining as great an accuracy as possible. The knowledge of this numerical value is important for several reasons: It allows a check on any theory of the heavy elementary particles, because the theory must give just this numerical value; but it is, of course, also important for the theory of the nuclei and for the theory of the forces between elementary particles.

In addition to the experiments with H_2, we have employed beams of HD[2] and have removed certain sources of error contained in the previous measurements.

I. METHOD

The principle of the method used is the measurement of the deflection of a beam of hydrogen molecules in an inhomogeneous magnetic field. From this measurement the magnetic moment of the proton is obtained in the following way:

Normal hydrogen is composed of 25 percent parahydrogen and 75 percent orthohydrogen. We neglect, at first, the rotation of the molecule. Then in the case of parahydrogen, the two proton spins are antiparallel and the total spin and magnetic moment of the molecule are consequently 0. In the case of orthohydrogen, the two proton spins are parallel, resulting in a total spin of the molecule of 1 and a magnetic moment of twice the proton moment. An infinitely narrow beam of orthohydrogen molecules of a definite velocity should, therefore, be split by the magnetic field into three components corresponding to the deflections 0, $+2s_P$ (H_2) and $-2s_P$ (H_2), where s_P (H_2) would be the deflection under the conditions of our experiment of a H_2 molecule having one proton moment. A beam of parahydrogen would give only the one undeflected component.

In addition to this splitting due to the magnetic moment of the protons, we have to consider the magnetic moment due to the rotation of the molecule as a whole. At very low temperatures all the parahydrogen molecules have the

[1] R. Frisch and O. Stern, Zeits. f. Physik **85**, 4 (1933); U. z. M. 24; I. Estermann and O. Stern, Zeits. f. Physik **85**, 17 (1933); U. z. M. 27. (U. z. M., Untersuchungen zur Molekularstrahlmethode, refers to a series of papers concerning the molecular ray method.)

[2] We wish to express our sincere thanks to Dr. F. G. Brickwedde of the National Bureau of Standards who kindly prepared the HD.

TABLE I. *Distribution of rotational quantum states.*

	l	$T=90°K$	$T=291°K$
ortho-H_2	1	99.98%	88.2%
	3	0.02	11.7
	5		0.1
para-H_2	0	98.3%	51.9%
	2	1.7	46.6
	4		1.5
HD	0	55.5%	20.0%
	1	40.5	39.0
	2	4.0	27.5
	3		10.7
	4		2.4
	5		0.4

rotational state 0, and consequently no rotational magnetic moment; therefore, no magnetic moment at all. This was verified in our Hamburg experiments with pure *para*-H_2 at liquid-air temperature. At room temperature we found a considerable deflection which we ascribed to the rotational moment of the higher quantum states present (see Table I). By further assuming that the rotational magnetic moment is proportional to the rotational quantum number, we found that the rotational magnetic moment per quantum is 0.8 to 0.9 nuclear magnetons.

The orthohydrogen molecules, however, will have the rotational quantum state 1 even at the lowest temperatures. This rotational quantum causes each of the original three components to split again into three, since at the high field strengths used in our experiments the rotational and proton moments can be considered as completely decoupled. The distance between these components is s_R, the deflection of a H_2 molecule having only the magnetic moment associated with the first rotational state, which is about one-third of the proton moment. The total pattern of the orthohydrogen has, thus, nine components, as shown in Fig. 1. Upon adding the 25 percent of the undeflected parahydrogen, we receive the split pattern of ordinary hydrogen at low temperatures. At the temperature of $T=90°K$ where we made measurements, 99.98 percent of the orthohydrogen molecules are in the rotational state $l=1$, and 98.3 percent of the parahydrogen molecules in the rotational state $l=0$ (see Table I). We may therefore neglect the higher rotational states at the temperature of $T=90°K$.

In the case of the HD molecule containing two different atoms, there are no *ortho* and *para* states. At sufficiently low temperatures all the molecules are transformed into the rotational state 0. The experiments, as in the case of H_2, were carried out at $T=90°K$. The distribution of the different rotational states is shown in Table I. Let us consider at first the rotational state 0. In the field strength used we may regard the nuclear magnetic moments of the H and D atoms as completely uncoupled. If the spin and the magnetic moment of the D atom were 0, the deflection pattern of an infinitely narrow monochromatic beam would have just two components $+\frac{1}{2}$ and $-\frac{1}{2}$, because the proton spin is $\frac{1}{2}$. These components correspond to the deflections $\pm s_P$ (HD) of an HD molecule with the magnetic moment of one proton moment. On account of the spin 1 of the D atom, however, each of these components is split into a triplet. The distance between the triplet components is s_D (HD); namely, the deflection of an HD molecule with the magnetic moment of the deuteron. Since the latter moment is only about one-third of the proton moment, s_D (HD) is approximately one-third s_P (HD). For $T=90°K$, 55 percent of the HD molecules are in the state $l=0$, 40 percent in $l=1$ and the rest in $l=2$.

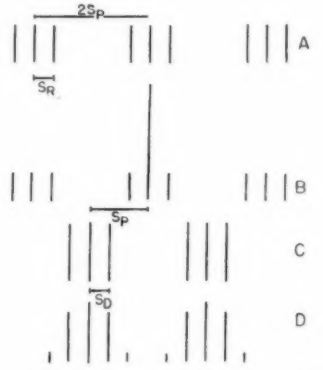

FIG. 1. Magnetic split patterns of H_2 and HD. A, *ortho*-H_2; $T=90°K$. B, normal H_2; $T=90°K$. C, HD without rotation ($l=0$). D, HD; $T=90°K$.

Neglecting state 2, one obtains the split pattern shown in Fig. 1, under the assumption that $s_D=s_R=\frac{1}{3}s_P$. The exact values of s_D and s_R do not matter, because due to the symmetrical arrangement of the s_D and s_R lines around the s_P lines their influence on the intensity distribution

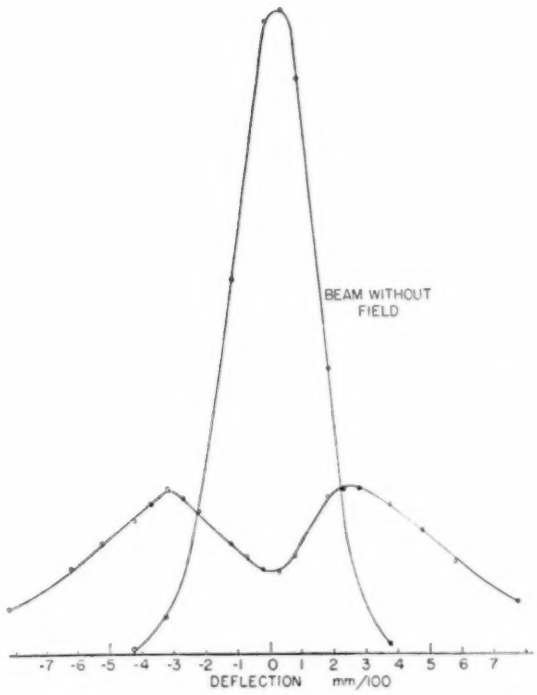

FIG. 2. Magnetic deflection of a beam of HD ($T=90°$K). Intensity in arbitrary units.

of an ordinary nonmonochromatic beam compensates to a large degree.

Actually the experiments were carried out with nonmonochromatic molecular rays of different finite widths in which the molecules have a modified Maxwell distribution of velocities. Each line in Fig. 1 has therefore to be replaced by a Maxwell curve integrated over the finite width of the beam. The actual intensity distribution in the deflected beam is arrived at by superposition of these Maxwell curves.

The characteristic difference in the deflection patterns of H_2 and HD is the absence of a zero beam in the case of HD. With a narrow beam of HD, we receive therefore a deflection curve with a conspicuous minimum in the center (see Fig. 2), in contrast to the H_2 curve (Fig. 3) with a strong maximum in the center.

It should be possible in principle to calculate the unknowns s_P, s_R and s_D from the intensity distribution measured in the experiment. Since the deflection curves, however, are rather insensitive to the value of s_D and s_R, this would be impractical. Being chiefly interested in the moment of the proton, and knowing s_R and s_D from separate experiments with pure parahydrogen and deuterium, respectively, we can calculate s_P from the measured intensity at any point of the deflection curve on the basis of the Maxwell distribution of velocities. $s_P{}^\alpha$ refers then to the deflection of a molecule of the most probable velocity α corresponding to the beam temperature, and the magnetic moment of one proton.[3] For reasons to be explained later (see Section IV), we have used the intensity of the deflected beam at the center of the undeflected beam. We call the ratio of this intensity I to the intensity I_0 of the undeflected beam the "weakening," I/I_0. Assuming a rectangular form for the intensity distribution of the undeflected beam of the half-width $2a$ (see Fig. 4), and a splitting into two beams, as in the case of the alkalies, $I/I_0=F(s^\alpha/a)$, where $F(x)=(1+x)e^{-x}$.[4] For the split pattern of normal H_2 at 90°K (Fig. 1B),

$$\frac{I}{I_0}=\frac{1}{3}+\frac{1}{6}\left[F\left(\frac{s_R{}^\alpha}{a}\right)+F\left(\frac{2s_P{}^\alpha}{a}\right)+F\left(\frac{2s_P{}^\alpha+s_R{}^\alpha}{a}\right)+F\left(\frac{2s_P{}^\alpha-s_R{}^\alpha}{a}\right)\right].$$

For the actual calculations we have used $s_R=\frac{1}{3}s_P$, so that

$$\frac{I}{I_0}=\frac{1}{3}+\frac{1}{6}\left[F\left(\frac{(1/3)s_P{}^\alpha}{a}\right)+F\left(\frac{2s_P{}^\alpha}{a}\right)+F\left(\frac{(7/3)s_P{}^\alpha}{a}\right)+F\left(\frac{(5/3)s_P{}^\alpha}{a}\right)\right].$$

For the pattern of HD at 90°K (Fig. 1D), we have, taking

$$s_D{}^\alpha=s_R{}^\alpha=\tfrac{1}{3}s_P{}^\alpha,$$

$$\frac{I}{I_0}=\frac{1}{3}\left\{F\left(\frac{s_P{}^\alpha}{a}\right)+0.85\left[F\left(\frac{(2/3)s_P{}^\alpha}{a}\right)+F\left(\frac{(4/3)s_P{}^\alpha}{a}\right)\right]+0.15\left[F\left(\frac{(1/3)s_P{}^\alpha}{a}\right)+F\left(\frac{(5/3)s_P{}^\alpha}{a}\right)\right]\right\}.$$

[3] For any given magnetic moment μ, $s^\alpha=(\mu/4kT)\times(dH/ds)\times l^2$ is independent of the mass of the molecule and is therefore the same for H_2 and HD.

[4] O. Stern, Zeits. f. Physik **41**, 563 (1927); U. z. M. 5.

In order to illustrate the small influence of the rotational moment in the case of H_2, and of the rotational and deuteron moment in the case of HD, we refer to Figs. 5 and 6. Fig. 5 shows I/I_0 for H_2 calculated as a function of the half-width $2a$, with and without consideration of the rotational moment; Fig. 6 shows I/I_0 for HD, first setting s_D and $s_R=\frac{1}{3}s_P$ and secondly, $s_D=s_R=0$. The values, $s_D=s_R=\frac{1}{3}s_P$, are in close agreement with the direct measurements of the deuteron moment and the rotational moment of H_2.[5] Under these assumptions, each value of I/I_0 gives a value of $s_P{}^a$. We want to emphasize again that even a comparatively large error in the values of s_R and s_D would influence the value of s_P only to a negligible extent. From $s_P{}^a$ and the constants of the experiment, we calculate the magnetic moment of the proton.

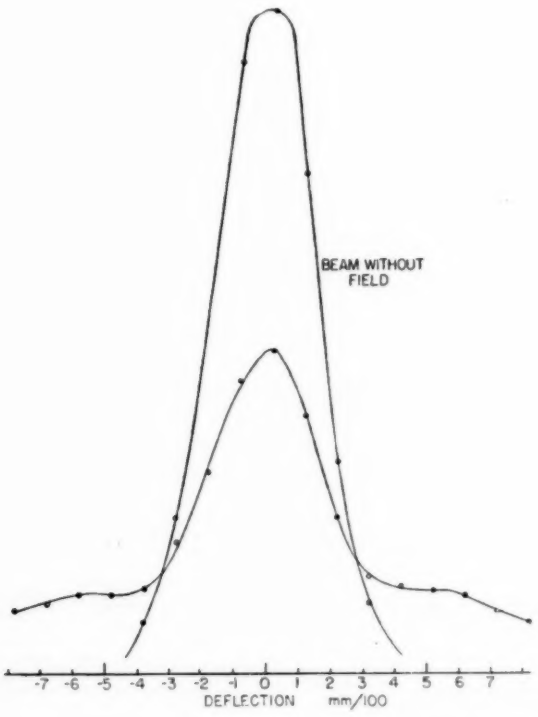

FIG. 3. Magnetic deflection of a beam of H_2 ($T=90°K$). Intensity in arbitrary units.

[5] For the value of the deuteron moment see: I. Estermann and O. Stern; Phys. Rev. **45**, 761 (1934); I. I. Rabi, J. M. B. Kellogg and J. R. Zacharias; Phys. Rev. **45**, 769 (1934); **50**, 472 (1936). There are no direct measurements of the rotational moment of HD. It is to be expected that it is not larger than the rotational moment of H_2. In order to influence our results appreciably, it would have to be of the order of magnitude of the proton moment.

Another series of measurements was made at the beam temperature of 291°K. In this case, the higher rotational states have to be considered (see Table I) and the deflection patterns are more complicated. For H_2 this does not

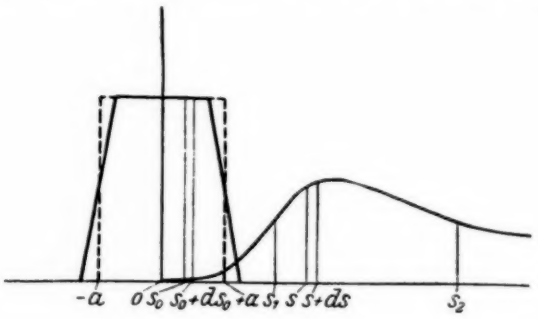

FIG. 4.

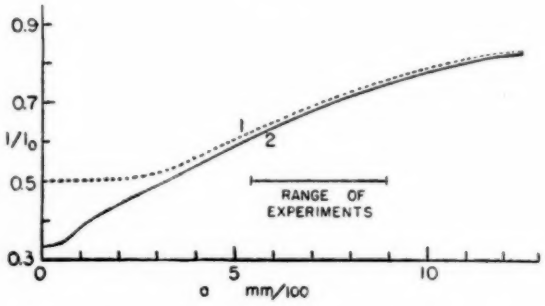

FIG. 5. "Weakening" of a beam of H_2, $T=90°K$; as function of the half-width $2a$. Curve 1, $s_R=0$. Curve 2, $s_R=\frac{1}{3}s_P$.

spoil the correctness of the evaluation of $s_P{}^a$. There are 11 percent of the *ortho*-H_2 molecules in the rotational state $l=3$ and 46 percent of the *para*-H_2 molecules in $l=2$. For the *ortho*-H_2, the influence of the higher temperature is very small, because only one-tenth of the molecules are in a higher rotational state than at liquid-air temperature. For the *para*-H_2, we have directly determined s_R, or rather the "weakening," at room temperature. We were able, therefore, to consider the influence of s_R quite accurately.

For HD, the conditions are less favorable. First, higher rotational quantum states are more populated because of the larger moment of inertia of the HD molecule (see Table I). Secondly, the rotational moment is not so well known (see reference 5). Thirdly, for beams of a width large enough to be employed in our apparatus, the deflection and the weakening are very small, because the effective moment of the

deflected molecules is only about one-half as large as in the case of H_2. For these reasons, we have made only one set of measurements with HD at room temperature.

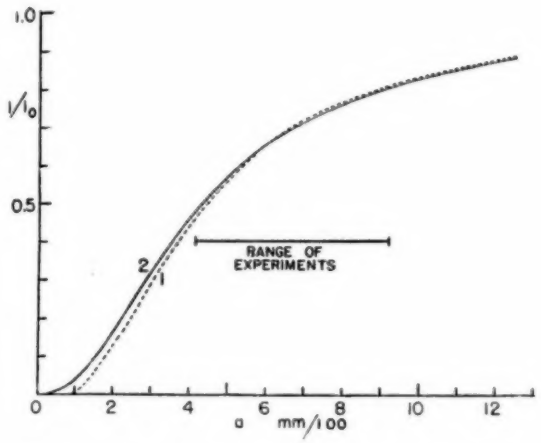

FIG. 6. "Weakening" of a beam of HD, $T=90°K$; as function of the half-width $2a$. Curve 1, $s_R=s_D=0$. Curve 2, $s_R=s_D=\frac{1}{3}s_P$.

II. Experimental Arrangement

The apparatus was essentially the same as the one used in the previous measurements in Hamburg. The principle of the arrangement is shown in Fig. 7. A beam of hydrogen molecules formed by the source slit S_1 and the collimating slit S_2 is deflected in an inhomogeneous magnetic field F. The beam intensity is measured by a receiver R which can be moved across the beam. The receiver is a vessel in which the incoming molecules produce a pressure proportional to the intensity of the beam. This pressure is measured by a sensitive hot-wire manometer.

The actual arrangement is shown in Figs. 8 and 9. They are in general self-explanatory, and only remarks about a few details are necessary. The source slit was $\frac{1}{2}$ mm high and 0.02 mm wide, and was fitted with arrangements for alignment and cooling and with a thermocouple. The foreslit was also 0.02 mm wide, and was somewhat higher than the source slit. The collimating slit was formed by two parallel rods mounted on a piece which could be turned from the outside. Thus the width of the beam could be changed during the experiment. A magnetically operated shutter was arranged between the foreslit and collimating slit. The inhomogeneous magnetic field was produced by a pair of pole-pieces of the slot-wedge type, 9.95 cm long; other dimensions as shown in Fig. 10. The height of the beam was limited to about 0.6 mm by a diaphragm at each end of the field.

The receiving manometer is shown in detail in Fig. 11. The receiving slit was a canal 0.5 mm high, 0.02 mm wide, and 3 mm deep. Since the flow resistance of such a canal is very high, the volume of the whole vessel had to be very small to have a reasonable filling time. In our case the volume was 0.6 cm³, the filling time about $\frac{3}{4}$ minutes. The filament was 9 cm long and was made of 0.001 inch nickel wire from the Driver-Harris Company, and was rolled out in the laboratory shop to a ribbon of 0.085 mm width. With a Wheatstone bridge and a Leeds and Northrup type HS galvanometer, we had a deflection of 155 cm per 10^{-6} mm Hg change in hydrogen pressure. The intensities of the beams used were between 10 and 45 cm deflection. In some experiments, a Kipp and Zonen type Zb galvanometer was used. This instrument was about twice as sensitive, but not very stable.

Further details about the experimental arrangement may be found in the Hamburg papers.

In the measurements with HD, we observed a slight transformation ($2HD=H_2+D_2$) during the experiments. The rate of this decomposition as measured by the weakening of a very narrow beam of HD as a function of time, was found to be about $\frac{1}{2}$ percent per hour. To avoid errors caused by this reaction, we used a fresh supply of HD for each measured weakening.

In agreement with Brickwedde, we found that HD does not decompose if kept in glass vessels for many months. The decomposition observed during our experiments is probably due to the circulation of the gas through metal diffusion pumps.

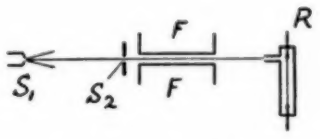

FIG. 7. Schematic diagram of the apparatus. S_1, source slit. S_2, collimating slit. F, magnetic field. R, receiver.

III. Inhomogeneity of the Magnetic Field

Since the uncertainty in the inhomogeneity of the magnetic field was one of the major reasons for the larger limit of error in the Hamburg measurements, we have taken great care in the determination of this quantity. The following different methods were used:

(1) The field strength was measured from point to point by means of the change of the electrical resistance of bismuth wires of 1 cm length and 0.1 and 0.15 mm diameter. The wires were moved repeatedly from point to point, using a micrometer slide from the Gaertner Scientific Company, which was accurate to 0.0005 mm. The differences in field strength divided by the displacements gave the inhomogeneity. The measurements were made in the symmetry plane of the field and 0.2 mm above and below; the results are given in Fig. 12.

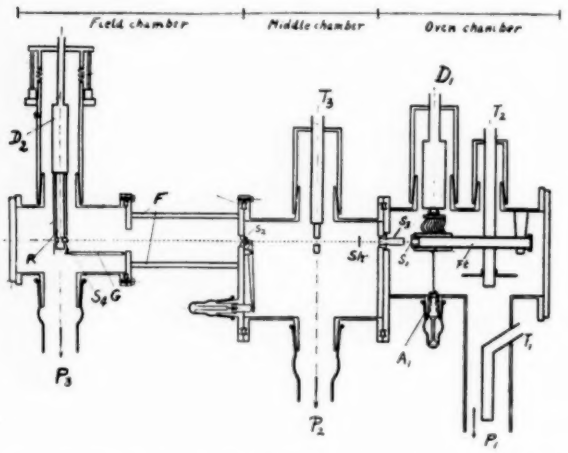

FIG. 8. Vertical cut through the apparatus. P_1, P_2, P_3, pump connections; T_1, T_2, T_3, mercury traps; S_1, source slit; S_2, collimating slit; S_3, foreslit; S_4, receiver slit; D_1, Dewar for cooling of source slit; D_2, Dewar for cooling of manometers R; F, pole-pieces; Sh, shutter; Ft, gas feeding tube; A_1, adjustment screw for vertical displacement of the source slit; G, glass spacer controlling the distance between receiver and pole-pieces.

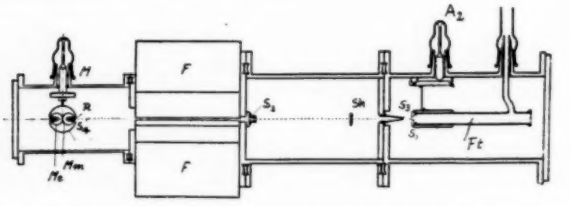

FIG. 9. Horizontal cut through the apparatus. S_1, source slit; S_2, collimating slit; S_3, foreslit; S_4, receiver slit; R, receiver; Ft, gas feeding tube; Sh, shutter; F, pole-pieces; A_2, adjustment screw for the horizontal displacement of the source slit; M, micrometer screw for receiver displacement; Mm, measuring manometer; Mc, compensating manometer.

The bismuth wires were calibrated at six different field strengths of 9380; 13,888; 17,832; 20,330; 21,816 and 22,574 gauss, and at several temperatures by means of an electromagnet with parallel pole-pieces. The values of these standard field strengths were determined with three different flip coils and a ballistic galvanometer which was calibrated by the discharge of a standard capacitance and also with a standard mutual inductance. As a separate check, the field strengths were measured with a magnetic balance. The results obtained by the different flip coil methods agreed within one-half of one percent, and in the average with those measured with the magnetic balance within 2 percent.

(2) A rectangular double flip coil was used for the direct measurement of the inhomogeneity. The coils were made of one turn of copper wire of 0.111 mm diameter and were embedded in paraffin between microscope cover glasses. In this way, the distance between the two flip coils was accurately known (0.138 mm glass plus one wire diameter equals 0.249 mm). Each coil was 37 mm long and 0.207 mm wide (inside between wires). The area of each individual coil was calibrated with the standard field strengths mentioned above. For the measurement of the inhomogeneity, the two coils were connected in series but in opposite directions. If the area of the two coils were exactly the same, their removal from a homogeneous field would produce no deflection of the ballistic galvanometer. In an inhomogeneous field, however, a deflection proportional to the difference of the field strengths at the place of the two coils is obtained. This difference can, therefore, be measured quite accurately; and since the distance between the two coils is known, the inhomogeneity can also be obtained with the same accuracy. In fact, the two flip coils did not have exactly the same area (they were different by 13 percent), but this could be eliminated by taking two series of measurements in which the flip coils were turned by 180°. The flip coil point (see Fig. 12) lies between the two curves but nearer to the curve for the symmetry plane. This is to be expected from the dimensions.

(3) As a final check, we measured the inhomo-

geneity by the ponderomotive force on a bismuth wire which was attached to a quartz fiber, the method used in the previous work.[6] This force is proportional to $H(dH/ds)$, and allows, in connection with the measurement of the field

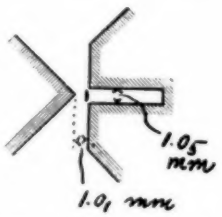

FIG. 10. Cross section of pole-pieces.

strength, the determination of the inhomogeneity. The absolute values of these measurements are not so exact, since the magnetic susceptibility of our bismuth wire was not

FIG. 11. Manometer. S, receiver slit.

known with great accuracy. This method, however, is very well adapted for relative measurements of the inhomogeneity at different parts of the field. In this respect it agreed very well with the other measurements.

The position of the beam in the field was determined in the following way: A quartz fiber was attached to the front end of the pole-piece with the groove. This quartz fiber causes a shadow in a wide molecular beam. The position of this shadow relative to the center of the beam allows the determination of the distance of the center of the beam from the front end of the pole-piece. In a second experiment the quartz fiber was attached to the rear end of the pole-piece. A similar measurement of the shadow gave the position of the center of the beam when leaving the field. The distances so measured were 0.06 and 0.16 mm. The height of the beam was fixed by a diaphragm on each end of the pole-pieces.

Taking into account the size and position of the beam, and the dimensions of the bismuth wire, we obtain the effective inhomogeneity of 154,000 gauss/cm. We consider this value correct to within less than two percent.

[6] See A. Leu, Zeits. f. Physik **41**, 551 (1927); U. z. M. 4.

IV. Sources of Error and Corrections

The uncertainty of about 10 percent in the previous measurements was due mainly to the fact that the inhomogeneity of the magnetic field (see Section III) and the velocity distribution in the beam were not known accurately enough. It is also necessary to apply a few minor corrections which could be neglected in the previous measurements on account of the larger limit of error.

(a) Velocity distribution

In order to calculate the magnetic moment from the observed intensity in the deflected beam, it is necessary to know the molecular velocities and their distribution. In the previous papers and in Section I, these velocities were calculated on the basis of Maxwell's law from the temperature of the beam. This is not quite correct. The molecular beam does not pass through an absolute vacuum, but through an apparatus which contains a small pressure of hydrogen. This leads to a distortion of the Maxwell distribution. It is to be expected theoretically, and is also supported by experiments, that the slow molecules are scattered more than the fast ones. A molecular beam passing through residual gas shows, therefore, a deficiency of slow molecules compared to Maxwell's law. If we measure the intensity I of the deflected beam as a fraction of the intensity I_0 of the undeflected

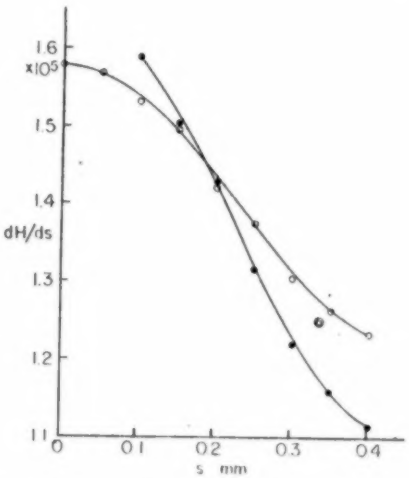

FIG. 12. Inhomogeneity of the field. s, distance from pole-piece fitted with groove. Open circle, points measured in the plane of symmetry. Closed circle, points 0.2 mm above and below the plane of symmetry. Circle within a circle, point measured with double flip coil.

beam, we shall find in the case of small deflections (fast molecules) too large a value; in the case of large deflections (slow molecules) too small a value. It is possible to eliminate this source of

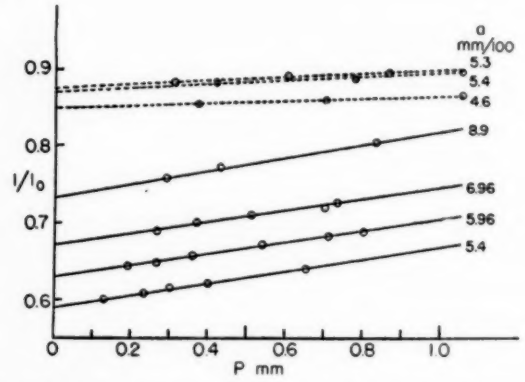

FIG. 13. "Weakening" as function of the scattering pressure for H_2. Full lines, experiments at $T=90°K$. Dotted lines, experiments at $T=291°K$. P, pressure behind the source slit in mm Hg. a, $\frac{1}{2}$ half-width of beam.

error without recourse to special measurements of the scattering by measuring the intensity ratio I/I_0 as a function of the scattering pressure and extrapolating to the pressure 0. Under the obvious assumption that the amount scattered is proportional to the pressure, I/I_0 is, for small pressures, a linear function of the scattering pressure (see appendix). These measurements could be made at any point of the deflected beam, but they are practical only at points where the intensity is large enough. Chiefly for this reason, but also for others mentioned at the end of this section, the measurements used for the final evaluation of the proton moment were those taken at the center of the undeflected beam. We found, in fact, that I/I_0 decreases as a linear function of the scattering pressure, which enabled us to extrapolate safely to the pressure 0 (see Figs. 13 and 14).

The beam passed through three chambers with different scattering pressures (the oven chamber, the middle chamber, and the field chamber, see Fig. 8). We assume that the scattering pressure in all these three rooms is caused by the hydrogen emerging from the source slit, and that the pumping speed at the small pressures in question is constant. Then all the scattering pressures are proportional to each other and proportional to the oven pressure (pressure behind the source slit in the gas reservoir). This was confirmed by direct measurement of the pressures although the very low pressures in the middle and field chamber could not be measured very exactly. Since the oven pressure is the largest of all the pressures involved, it can be measured most accurately. We have plotted I/I_0 as a function of this oven pressure and extrapolated to zero pressure.

It is conceivable that another scattering gas, for instance, mercury vapor, could be present in the apparatus in addition to the scattering hydrogen. If the pressure of this gas were constant, I/I_0 would still be a linear function of pressure, but the curves would be shifted upwards parallel to themselves. The presence of Hg or any other vapor in the apparatus is very unlikely because of the large liquid air cooled surfaces in every part of the apparatus. Furthermore, the presence of such a gas would have a much larger influence on a beam of slow molecules (beam temperature 90°K) than on a beam of fast molecules ($T=291°K$). So if a vapor of constant pressure were present, we would expect to find different values of $s_P{}^a$ from the extrapolated values for different temperatures. A scattering gas of constant pressure should also have a different influence on beams of different widths. No such effects were observed (see Table II).

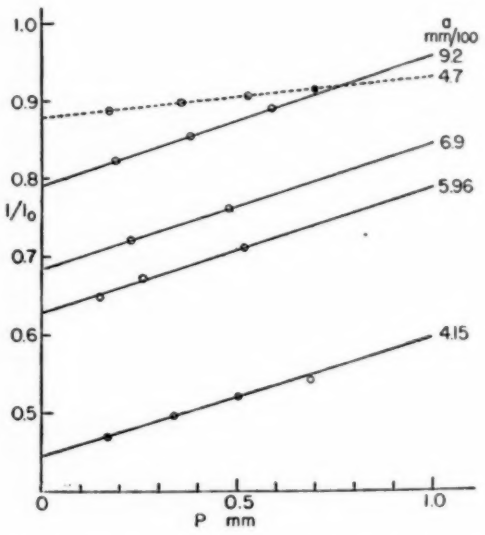

FIG. 14. "Weakening" as function of the scattering pressure for HD. Full lines, experiments at $T=90°K$. Dotted lines, experiments at $T=291°K$. P, pressure behind the source slit in mm Hg. a, $\frac{1}{2}$ half-width of beam.

(b) Other corrections

We have also applied a series of smaller corrections which were omitted in the earlier papers since they were small compared with the uncertainty of 10 percent. With the present accuracy, however, they have to be taken into account.

1. *Form of the undeflected beam.* As stated before, a rectangular intensity distribution of the undeflected beam was assumed as a basis for the calculations. A trapezoid, however, would come much closer to the actual intensity distribution (see Fig. 15). The difference between the calculated results for these two cases is generally less than one percent.

2. *Finite width of the receiver slit.* The measured intensity of the deflected beam in the center of the undeflected beam with a receiver of finite width is the average intensity over the width of the receiver slit (0.02 mm). The difference between this average and the actual intensity at the position $s=0$ is a few tenths of one percent.

3. *Receiver canal.* The receiver is actually not a slit but a canal of 0.02 mm width, 0.5 mm height and 3 mm depth. The alignment of this canal is such that the molecules of the undeflected beam run parallel to its walls (maximum of intensity). The molecules of the deflected beam, however, run obliquely to the walls of the canal; the greater the deflection, the more oblique the path of the molecules. This fact was considered in the previous paper for the intensity measurements of the deflected molecules. It also has, however, an influence on the values of the weakening, but a much smaller one. Since the width of the beam is much larger than the width of the receiver, there are molecules in the deflected beam which hit the receiver at the position $s=0$, but come from the edges of the undeflected beam. For these molecules, the receiver canal is not adjusted correctly and the intensity measured is consequently a little too small (in every case by less than one percent).[7]

4. *Remanent field.* In order to measure the intensity of the undeflected beam a compensation current was sent through the magnet to destroy the remanent field. It was impossible, however, to destroy this field completely, probably because

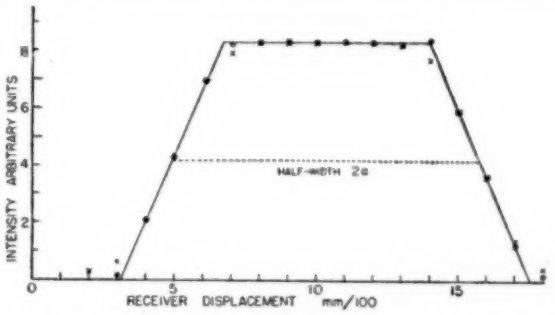

FIG. 15. Form of the undeflected beam. *o*, measured points corrected for finite width of receiver slit. *x*, measured points uncorrected.

the iron of the pole-pieces had a different remanence at different points. The remaining remanence which could not be destroyed by the compensation current was determined in the following way: The intensity of a helium beam was measured as a function of the width. For wide beams the intensity remained constant. When the beams were made very narrow, the intensity decreased. This was expected for geometrical reasons and for imperfections of slits and alignment. The repetition of these measurements with hydrogen showed a greater decrease of the intensity at narrow beams. The difference in the hydrogen and helium results is apparently due to the deflection of the hydrogen molecules in the remaining remanent field.[8] These measurements were used for computing the inhomogeneity of the remanent field. This correction is only a few tenths of one percent.

(c) Deflected molecules

All these corrections have to be applied also in the case of the "deflected molecules" (points of the deflection curve away from the center). Some of them, however, become rather large and uncertain. At larger deflections, the intensities are so small that the extrapolation of I/I_0 to zero pressure is hardly practical. Correction (3) becomes quite large and consequently the uncertainty about the specular reflection plays a role (see reference 7). Furthermore, the inhomo-

[7] This correction as calculated may be a little too large, because it is derived under the assumption of Knudsen's cosine law; whereas at the small angles involved, a certain amount of specular reflection may occur at the walls of the canal. Since this whole correction is less than one percent, an uncertainty of 10 or even 20 percent is of no importance.

[8] This effect may also be partially due to the diffraction of molecules, since the de Broglie wave-length of H_2 is larger than that of He. The applied correction may, therefore, be a little too large.

geneity changes appreciably along the path of the deflected molecules, and its component in the vertical direction influences the intensity also. In fact, we usually observed an asymmetry in the deflection pattern, which is partly due to these causes, but has probably other experimental reasons as well, since our apparatus was not adapted for a thorough investigation of the deflected molecules. At small deflections, I/I_0 depends very much on the actual form of the undeflected beam, which is not so well defined due to small imperfections of slits and alignment. For all these reasons, the measurements of the deflected molecules could be used only as a rough check, but not for the calculation of an accurate value of the proton moment.

V. Results

The results of the experiments are shown in Table II. $2a$ is the half-width of the beam used. I/I_0 (measured) is the value of the weakening obtained by extrapolation to $p=0$ of the straight lines in Figs. 13 and 14 containing the actually measured points at different pressures. I/I_0 (corrected) is corrected as explained in Section IV. $s_P{}^\alpha$ (90°) is the deflection that a molecule with a magnetic moment of one proton moment and the most probable velocity α corresponding to the temperature of $T=90°$ would have under the conditions of our experiments. The numerical values of $s_P{}^\alpha$ (90°) given in the table are those which lead to the value of the weakening listed under I/I_0 (corrected). The values corresponding to $T=291°$K have been reduced to 90°K by multiplication with the factor 291/90. The two starred runs were made with a different slit alignment at a higher inhomogeneity. The values of $s_P{}^\alpha$ belonging to these runs have been reduced to the standard inhomogeneity.

Table II. *Results of experiments.*

	T	a $\frac{\text{mm}}{100}$	$\frac{I}{I_0}$ (measured)	$\frac{I}{I_0}$ (corrected)	$s_P{}^\alpha$ (90°) $\frac{\text{mm}}{100}$	
H_2	90°	8.90	0.732	0.738	7.65	7.61
H_2	90°	7.00	0.672	0.674	7.59	
H_2	90°	5.96	0.628	0.627	7.72	
H_2	90°	5.40*	0.590	0.587	7.49	
HD	90°	9.20	0.790	0.805	7.37	7.56
HD	90°	6.90	0.684	0.700	7.59	
HD	90°	5.96	0.628	0.645	7.54	
HD	90°	4.15	0.445	0.464	7.76	
H_2	291°	5.40*	0.870	0.879	7.56	7.53
H_2	291°	5.29	0.875	0.885	7.52	
H_2	291°	4.62	0.849	0.861	7.50	
HD	291°	4.70	0.880	0.895	7.82	
				Average	7.59 ± 0.08	

Table III. *Values of the proton moment by different observers.*

Year	Observers	Value Given for the Proton Moment: Mean	Lowest	Highest	Method
1933	F. and S.[1]	2-3	2.	3.	Magnetic deflection of H_2
1933	E. and S.[2]	2.5 ±10%	2.25	2.75	Magnetic deflection of H_2
1934	R., K. and Z.[3]	3.25±10%	2.9	3.6	Magnetic deflection of H
1936	K., R. and Z.[4]	2.85±0.15	2.7	3.0	Magnetic deflection of H
1936	L. and S.[5]	2.3 ±10%	2.07	2.53	Susceptibility of solid hydrogen
		2.7 ±10%	2.43	2.97	
1937	E., S. and S.	2.46±3%	2.38	2.54	Magnetic deflection of H_2 and HD

[1] R. Frisch and O. Stern, Zeits. f. Physik **85**, 4 (1933) (U. z. M. 24).
[2] I. Estermann and O. Stern, Zeits. f. Physik **85**, 17 (1933) (U. z. M. 27).
[3] I. I. Rabi, J. M. B. Kellogg and J. R. Zacharias, Phys. Rev. **46**, 157 (1934).
[4] J. M. B. Kellogg, I. I. Rabi and J. R. Zacharias, Phys. Rev. **50**, 472 (1936).
[5] B. G. Lasarew and L. W. Schubnikow, Physik. Zeits. Sowjetunion **10**, 117 1936), **11**, 445 (1937).

The averages for $s_P{}^\alpha$ (90°) for the experiments with H_2 at 291°K and 90°K and for HD at 90°K agree within about one percent. The largest deviation from the average is less than three percent. The probable error in the final average of $s_P{}^\alpha$ (90°) $=7.59\times10^{-2}$ mm is 0.08 or 1 percent.

Systematical errors appear to be excluded to a large extent by the close agreement of the measurements under such different conditions (H_2 and HD at 90° and 291°K). Of course, it would be very desirable to check the value of $s_P{}^\alpha$ by measurements of the intensity at larger distances from the center of the beam. Because of the previously mentioned difficulties, we think such experiments could be carried out in the best way with a monochromatic beam.

$s_P{}^\alpha$ (90°) allows a calculation of the magnetic moment of the proton μ_P from the equation

$$s_P{}^\alpha=\frac{\mu_P}{4RT}\frac{dH}{ds}l_1{}^2\left(1+2\frac{l_2}{l_1}\right),$$

where $l_1=9.95$ cm is the length of the beam in the field, $l_2=5.03$ cm the distance of the receiver from the end of the field. The temperature T was measured with a thermocouple to better than 1°. $(dH/ds)=154{,}000$ gauss/cm is the effective inhomogeneity. With these values, and a value for

the nuclear magneton of 3.023 c.g.s. units per mole, we obtain for the magnetic moment of the proton

$$\mu_P = 2.46 \text{ nuclear magnetons.}$$

The largest uncertainty (less than 2 percent) is due to the inhomogeneity. $s_P{}^a$ and T are accurate to about one percent, while the errors in l_1 and l_2 are negligible. Provided there are no systematical errors, the value of the proton moment should be accurate to within three percent.

A summary of all the published measurements of the magnetic moment of the proton is given in Table III.

The mean value of the proton moment from our new measurements coincides practically with our old Hamburg value. This close agreement is, of course, accidental, considering the limits of error. The values obtained by the method of beams of *atomic* hydrogen are decidedly higher. Although the last measurements with atomic hydrogen come closer to our value, the discrepancy is still outside the limits of error. If this discrepancy were real, it would probably give new information about the interaction between the proton and the electron.[9] It is, however, still possible that the discrepancy is due to imperfections in the experiments. The measurements of the susceptibility of solid hydrogen, which could give an independent check, are at present not quite accurate enough.

We wish to express our gratitude to the Buhl Foundation for financial aid in carrying out the experiments.

[9] L. A. Young, Phys. Rev. **52**, 138 (1937).

Appendix

Proof that for small pressures the weakening is a linear function of the scattering pressure

1. *Weakening without scattering.* We consider a rectangular intensity distribution in the undeflected beam (see Fig. 4). The number of molecules contained in a strip of the width ds is $I_0 ds$. Assuming a magnetic split-up into two components, these molecules produce in the deflected beam at the position $s=0$ an intensity of

$$dI = \frac{I_0}{2} \cdot e^{-c^2/\alpha^2} \frac{c^2}{\alpha^2} d\frac{c^2}{\alpha^2} = \frac{I_0}{2} e^{-y} dy,$$

where $y = s_\alpha/s = c^2/\alpha^2$. The total intensity for $s=0$ is

$$I = 2\frac{I_0}{2}\int_{s_\alpha/a}^{\infty} e^{-c^2/\alpha^2} \frac{c^2}{\alpha^2} d\frac{c^2}{\alpha^2} = I_0 \int_{s_\alpha/a}^{\infty} e^{-y} y dy = I_0\left(1+\frac{s_\alpha}{a}\right) e^{-s_\alpha/a}.$$

2. *Weakening with scattering.* If the beam passes the distance l through scattering gas, the measured intensity I_0' will be smaller than I_0; the intensity of the molecules with the velocity c being weakened by the factor e^{-l/λ_c}. The mean free path λ_c is here an unknown function of the velocity c and the scattering pressure p. We make now the assumption, which should be valid always, that λ_c is proportional to $1/p$ and write $\lambda_c = \lambda_c{}^0/p$. Concerning $\lambda_c{}^0$ we assume only that it increases with c. Then we have

$$I' = 2\frac{I_0}{2}\int_{s_\alpha/a}^{\infty} e^{-(l/\lambda_c{}^0)p} e^{-c^2/\alpha^2} \frac{c^2}{\alpha^2} d\frac{c^2}{\alpha^2}.$$

Being interested only in the limit of I' for small values of p we may replace $e^{-(l/\lambda_c{}^0)p}$ by $1-(l/\lambda_c{}^0)p$. In practice this means that the weakening by the scattering should not be too large. Very slow molecules for which $\lambda_c{}^0$ is so small that $(l/\lambda_c{}^0)p$ is not small any more compared to one are so few that the error due to the replacement of $e^{-(l/\lambda_c{}^0)p}$ by $1-(l/\lambda_c{}^0)p$ is negligible. We have, therefore, for the intensity with field

$$I' = I_0\left[\int_{s_\alpha/a}^{\infty} e^{-c^2/\alpha^2} \frac{c^2}{\alpha^2} d\frac{c^2}{\alpha^2} - p\int_{s_\alpha/a}^{\infty} \frac{l}{\lambda_c{}^0} e^{-c^2/\alpha^2} \frac{c^2}{\alpha^2} d\frac{c^2}{\alpha^2}\right]$$

and without field

$$I_0' = I_0\left[\int_0^{\infty} e^{-c^2/\alpha^2} \frac{c^2}{\alpha^2} d\frac{c^2}{\alpha^2} - p\int_0^{\infty} \frac{l}{\lambda_c{}^0} e^{-c^2/\alpha^2} \frac{c^2}{\alpha^2} d\frac{c^2}{\alpha^2}\right].$$

Hence

$$\frac{I'}{I_0'} = \frac{I - p\int_{s_\alpha/a}^{\infty} (l/\lambda_c{}^0) e^{-c^2/\alpha^2} (c^2/\alpha^2) d(c^2/\alpha^2)}{I_0 - p_0\int_0^{\infty} (l/\lambda_c{}^0) e^{-c^2/\alpha^2} (c^2/\alpha^2) d(c^2/\alpha^2)}$$

and for small values of p

$$\frac{I'}{I_0'} = \frac{I}{I_0}\left\{1 + p\left[\frac{1}{I_0}\int_0^{\infty} e^{-c^2/\alpha^2} \frac{c^2}{\alpha^2} d\frac{c^2}{\alpha^2} - \frac{1}{I}\int_{s_\alpha/a}^{\infty} \frac{l}{\lambda_c{}^0} e^{-c^2/\alpha^2} \frac{c^2}{\alpha^2} d\frac{c^2}{\alpha^2}\right]\right\}$$
$$= \frac{I}{I_0}(1 + Cp).$$

A similar proof can be given for every point of the deflection curve.

Relativistic Effects for the Deuteron

S. SHARE AND G. BREIT
University of Wisconsin, Madison, Wisconsin
(Received July 27, 1937)

It is seen from Tables I, II, and III than an appreciable spin-spin dependence of the neutron-proton interaction can be expected to arise as a result of using Eqs. (1) and (9). This spin dependence is of the wrong sign to account for the empirically known difference in energies of the singlet and triplet states of the deuteron. Its presence suggests that the spatial dependence of spin dependent forces is not wholly the same as that of the other forces. The possibility of finding a simple equation in which the empirical spin dependence will be a natural consequence is still open. It is shown that the relativistic correction to the kinetic energy is only a small part of the corrections called for by invariance. The relativistic refinements made so far in the combined theory of H^2 and H^3 are shown to be questionable from this point of view, as well as on account of the possible presence of terms in relative momenta which are not determined by requirements of invariance alone.

1. INTRODUCTION AND SUMMARY

THE effect of relativity on the energy of the deuteron has been considered by Blochinzew,[1] by Margenau,[1] and by Feenberg.[2] The discussions of Blochinzew and Margenau presuppose that the actual two-body problem can be replaced by a suitable one-body problem and that the latter can be treated by the Klein-Gordon equation. These assumptions are incorrect. Feenberg's calculation takes into account only corrections for the kinetic energy of the two particles. In addition to these, however, it is necessary[3] to consider also the terms in the Hamiltonian which correspond to the interaction of the orbits of the two particles and which are formally of the same order of magnitude as the pure kinetic energy effects. In the present note the results of calculations which take these terms into account, together with all terms of the order v^2/c^2, where v is the velocity of the particles and c is the velocity of light, are presented. Since the Hamiltonian to the order v^2/c^2 can be put into the form of a sum of two relativistic Dirac Hamiltonians and an interaction energy also expressible by means of Dirac's operators[3] the corrections to order v^2/c^2 corresponding to these forms are also given here.

When the motion of two particles is described by means of Diracian equations there appears among other terms an interaction between the spins of the two particles which brings about an energy difference between their triplet and singlet conditions. Calculations given below show that this energy difference is of the same order of magnitude although somewhat smaller than that due to the usual spin dependent Heisenberg force. In the equations used the order of the triplet and singlet terms is opposite to the empirical. Therefore, the spin dependence following from the equations used here cannot be claimed to be the explanation of the Heisenberg force. Nevertheless, the results suggest that a suitable equation could be found in which the Heisenberg force could be replaced by a relativistic correction term to the Majorana force. Whether this is so or not, the fact that a spin dependence of the interaction energy of a magnitude comparable with the empirical arises out of relativistic Diracian equations indicates that the spatial dependence of the spin dependent force is probably different from that of the main Majorana force and that further one should consider in addition to energies of type $(\boldsymbol{\sigma}_1\boldsymbol{\sigma}_2)$ also energies of type $(\mathbf{r}\boldsymbol{\sigma}_1)(\mathbf{r}\boldsymbol{\sigma}_2)$, where $\boldsymbol{\sigma}$ are the Pauli spin operators for particles 1, 2 and $\mathbf{r}$ is the vector from particle 2 to particle 1, $=\mathbf{r}_1-\mathbf{r}_2$. Thus for Eq. (17.6) of reference 3 two spin operators are involved only in the following terms

$$E=2Mc^2-J-\frac{\hbar^2 f}{2M^2c^2}(\boldsymbol{\sigma}_1\boldsymbol{\sigma}_2)-\frac{\hbar^2}{4M^2c^2}\frac{df}{rdr}[r^2(\boldsymbol{\sigma}_1\boldsymbol{\sigma}_2)-(\mathbf{r}\boldsymbol{\sigma}_1)(\mathbf{r}\boldsymbol{\sigma}_2)]+\cdots, \quad f=\frac{dJ}{rdr}.$$

[1] D. Blochinzew, Physik. Zeits. Sowjetunion **8**, 270 (1935); H. Margenau, Phys. Rev. **50**, 342 (1936).
[2] E. Feenberg, Phys. Rev. **50**, 674 (1936).
[3] G. Breit, Phys. Rev. **51**, 248 (1937). Eqs. (16.1), (18.1), (17.6), (18.2) are respectively Eqs. (1), (2), (1'), (2') of present paper.

For S terms this is equivalent to having a spin dependent potential of magnitude[3]

$$-(\hbar^2/6M^2c^2)\Delta J(\boldsymbol{\sigma}_1\boldsymbol{\sigma}_2),$$

which depends on r differently from the dependence of J on r, while for P, D, $\cdots$ terms still different dependences result. The terms in $(\boldsymbol{\sigma}_1\boldsymbol{\sigma}_2)$, $(\mathbf{r}\boldsymbol{\sigma}_1)(\mathbf{r}\boldsymbol{\sigma}_2)$ that are discussed here are not required directly by invariance of order v^2/c^2. It is nevertheless interesting that they disappear only accidentally when relativistic Diracian forms are used. One may expect that neutrino-electron field theories will lead to Diracian forms that are invariant to order v^2/c^2 and it is therefore probable, although not certain, that the $(\boldsymbol{\sigma}_1\boldsymbol{\sigma}_2)$, $(\mathbf{r}\boldsymbol{\sigma}_1)(\mathbf{r}\boldsymbol{\sigma}_2)$ terms have reality. Wheeler's[4] and Wigner's[5] enumerations of possible rotationally invariant interactions include such terms. The fact that they arise as relativistic corrections and are only somewhat smaller than the spin dependent Heisenberg part of the force indicates that not only are they mathematical possibilities but that they most probably correspond to reality.

2. Ordinary Interactions

In reference 3 there were considered two forms of the Hamiltonian for two particles:

$$H=-c(\boldsymbol{\alpha}_1\mathbf{p}_1)-c(\boldsymbol{\alpha}_2\mathbf{p}_2)-(\beta_1+\beta_2)Mc^2-J+\tfrac{1}{2}(\boldsymbol{\alpha}_1\boldsymbol{\alpha}_2)J-\tfrac{1}{2}(\boldsymbol{\alpha}_1\mathbf{r})(\boldsymbol{\alpha}_2\mathbf{r})(dJ/rdr), \tag{1}$$

$$H=-c(\boldsymbol{\alpha}_1\mathbf{p}_1)-c(\boldsymbol{\alpha}_2\mathbf{p}_2)-(\beta_1+\beta_2)Mc^2-\beta_1\beta_2J-\tfrac{1}{2}(\boldsymbol{\alpha}_1\boldsymbol{\alpha}_2)J-\tfrac{1}{2}(\boldsymbol{\alpha}_1\mathbf{r})(\boldsymbol{\alpha}_2\mathbf{r})(dJ/rdr), \tag{2}$$

which when reduced to equivalent Pauli forms give, respectively,[3]

$$H=2Mc^2-J+\frac{p_1^2+p_2^2}{2M}-\frac{p_1^4+p_2^4}{8M^3c^2}+\frac{\hbar f}{4M^2c^2}([\mathbf{r}\times(2\mathbf{p}_2-\mathbf{p}_1)]\boldsymbol{\sigma}_1-[\mathbf{r}\times(2\mathbf{p}_1-\mathbf{p}_2)]\boldsymbol{\sigma}_2)+\frac{J}{2M^2c^2}\mathbf{p}_1\mathbf{p}_2$$
$$-\frac{f}{2M^2c^2}x^ax^bp_1{}^ap_2{}^b-\frac{3\hbar f}{4iM^2c^2}\mathbf{r}(\mathbf{p}_2-\mathbf{p}_1)-\frac{\hbar}{4iM^2c^2}\frac{rdf}{dr}\mathbf{r}(\mathbf{p}_2-\mathbf{p}_1)-\frac{\hbar^2f}{8M^2c^2}(15+4\boldsymbol{\sigma}_1\boldsymbol{\sigma}_2)$$
$$-\frac{\hbar^2}{4M^2c^2}\frac{df}{rdr}[5r^2+r^2\boldsymbol{\sigma}_1\boldsymbol{\sigma}_2-(\mathbf{r}\boldsymbol{\sigma}_1)(\mathbf{r}\boldsymbol{\sigma}_2)]-\frac{\hbar^2r^3}{8M^2c^2}\frac{d}{dr}\left(\frac{df}{rdr}\right). \tag{1'}$$

and

$$H=2Mc^2-J+\sum_{i=1}^{2}\left[\frac{p_i{}^2}{2M}+\frac{p_i{}^2J+2\mathbf{p}_iJ\mathbf{p}_i+Jp_i{}^2}{8M^2c^2}-\frac{p_i{}^4}{8M^3c^2}+\frac{\hbar}{4M^2c^2}[\boldsymbol{\nabla}_iJ\times\mathbf{p}_i]\boldsymbol{\sigma}_i\right]-\frac{J}{2M^2c^2}\mathbf{p}_1\mathbf{p}_2$$
$$-\frac{f}{2M^2c^2}x^ax^bp_1{}^ap_2{}^b-\frac{\hbar}{4iM^2c^2}\left(5f+\frac{rdf}{dr}\right)\mathbf{r}(\mathbf{p}_2-\mathbf{p}_1)-\frac{\hbar^2}{8M^2c^2}\left[15f+10\frac{rdf}{dr}+\frac{r^2d}{dr}\left(\frac{df}{rdr}\right)\right]. \tag{2'}$$

In Eqs. (1), (2) the quantities $\boldsymbol{\alpha}$, β are the usual Dirac matrices, the momenta are denoted by p, and the indices 1, 2 refer to the two particles. In Eqs. (1′), (2′) the notation is similar. The quantities $\boldsymbol{\sigma}$ are Pauli's two row square matrices. Summations are understood for $x^ap_1{}^a$. Also

$$f=dJ/rdr. \tag{2''}$$

The nonrelativistic approximation to the deuteron equation is

$$\Delta\psi+(M/\hbar^2)(E+J)\psi=0. \tag{3}$$

By using this equation, terms in Eqs. (1′), (2′) which occur in addition to $2Mc^2-J+(p_1{}^2+p_2{}^2)/2M$

[4] J. A. Wheeler, Phys. Rev. **50**, 643 (1936).
[5] E. Wigner, Phys. Rev. **51**, 106 (1937).

may be said to be of relativistic origin. Inspection of Eqs. (1′), (2′) shows that there are among them terms explicitly involving momenta. In classical analogy these terms depend on the velocity. In addition there are also present terms which do not depend explicitly on the velocity. Their effects are not easily distinguishable from J because from an empirical point of view they can be considered as part of J. The expectation values of the terms are

$$-\frac{1}{8M^3c^2}\int\psi(p_1^4+p_2^4)\psi d\tau=-\frac{1}{4Mc^2}\int(E+J)^2\psi^2 d\tau=-\frac{\alpha a(D+E)(E+D-E/\alpha a)}{4Mc^2(1+\alpha a)}\sim-0.15mc^2,$$

$$\frac{1}{8M^2c^2}\int\psi[(p_1^2+p_2^2)J+J(p_1^2+p_2^2)]\psi d\tau=-\frac{\hbar^2}{2M^2c^2}\int\psi J\Delta\psi d\tau=\frac{(D+E)(D\alpha a-E)}{2Mc^2(1+\alpha a)}\sim0.31mc^2,$$

$$\frac{1}{2M^2c^2}\int\psi\mathbf{p}_1J\mathbf{p}_1\psi d\tau=\frac{\hbar^2}{2M^2c^2}\int J(\nabla\psi)^2 d\tau=\frac{D(E+D)\alpha a}{2Mc^2(1+\alpha a)}\left[1+\frac{2E}{D\alpha^2a^2}+\frac{E}{D\alpha a}\right]\sim0.09mc^2,$$

$$-\frac{1}{2M^2c^2}\int\psi J\mathbf{p}_1\mathbf{p}_2\psi d\tau=-\frac{\hbar^2}{2M^2c^2}\int\psi J\Delta\psi d\tau=\frac{(D+E)(D\alpha a-E)}{2Mc^2(1+\alpha a)}\sim0.31mc^2,$$

$$-\frac{1}{2M^2c^2}\int\psi f x^a x^b p_1{}^a p_2{}^b\psi d\tau=-\frac{\hbar^2}{2M^2c^2}\int\psi f r^2\frac{d^2\psi}{dr^2}d\tau=-\frac{2E(D+E)}{Mc^2\alpha a}-\frac{\alpha a(D+E)(E+D/2)}{Mc^2(1+\alpha a)}\sim0.22mc^2,$$

$$\int\psi\left[-\frac{p_1^4+p_2^4}{8M^3c^2}-\frac{\hbar^2\Delta J}{4M^2c^2}\right]\psi d\tau=-\frac{D+E}{4Mc^2(1+\alpha a)}\left[\alpha a(D+E)+3E+\frac{4E}{\alpha a}\right]\sim0.08mc^2,$$

$$-\frac{\hbar}{4iM^2c^2}\int\psi r\frac{df}{dr}\mathbf{r}(\mathbf{p}_2-\mathbf{p}_1)\psi d\tau=\frac{2\pi\hbar^2}{M^2c^2}\int f\frac{d}{dr}\left(r^4\psi\frac{d\psi}{dr}\right)dr$$

$$=-\frac{E(1-\alpha a)(D+E)}{Mc^2\alpha a}+\frac{\alpha a(D+E)(E+D/2)}{Mc^2(1+\alpha a)}\sim0.34mc^2,$$

$$-\frac{5\hbar}{4iM^2c^2}\int\psi f\mathbf{r}(\mathbf{p}_2-\mathbf{p}_1)\psi d\tau=-\frac{5\hbar^2}{2M^2c^2}\int\psi f\frac{d\psi}{dr}d\tau=\frac{5E(D+E)}{Mc^2\alpha a}\sim-1.14mc^2.$$

The numerical values are for $a=2.3\times10^{-13}$ cm, $E=-4.3mc^2$. In these formulas the second expression in each case refers to Eq. (3) while the last refers to the case of a constant $J=D$ through $0<r<a$ and $J=0$ for $r>a$ (square well). The quantity α is the reciprocal length

$$\alpha=(-ME/\hbar^2)^{\frac{1}{2}}. \tag{4′}$$

Either by means of Eqs. (4) and Eqs. (17.3), (17.4) of reference 3 or by direct calculation using the spherical symmetry of S states one obtains the expectation values

$$\begin{aligned}(\boldsymbol{\alpha}_1\boldsymbol{\alpha}_2)J&=\frac{\hbar^2}{2M^2c^2}\int\{\psi J\Delta\psi-J(\nabla\psi)^2-(2/3)(\boldsymbol{\sigma}_1\boldsymbol{\sigma}_2)[\psi J\Delta\psi+J(\nabla\psi)^2]\}d\tau,\\(\boldsymbol{\alpha}_1\mathbf{r})(\boldsymbol{\alpha}_2\mathbf{r})f&=\frac{\hbar^2}{2M^2c^2}\int\frac{dJ}{dr}\left\{r\psi\Delta\psi-2\psi\frac{d\psi}{dr}-r(\nabla\psi)^2-(2/3)(\boldsymbol{\sigma}_1\boldsymbol{\sigma}_2)\psi\frac{d\psi}{dr}\right\}d\tau.\end{aligned} \tag{5}$$

Here $(\boldsymbol{\sigma}_1\boldsymbol{\sigma}_2)$ stands for the expectation value of the corresponding operator. For a square well

$$(\boldsymbol{\alpha}_1\boldsymbol{\alpha}_2)J=-\frac{(E+D)(D\alpha a+E/\alpha a)}{Mc^2(1+\alpha a)}-\frac{2}{3}\frac{E(E+D)}{Mc^2\alpha a}(\boldsymbol{\sigma}_1\boldsymbol{\sigma}_2),$$

$$(\boldsymbol{\alpha}_1\mathbf{r})(\boldsymbol{\alpha}_2\mathbf{r})f=\frac{E(D+E)}{Mc^2(1+\alpha a)\alpha a}[1+(\alpha a)^2D/2E+\tfrac{2}{3}(1+\alpha a)(\boldsymbol{\sigma}_1\boldsymbol{\sigma}_2)]. \tag{5'}$$

According to Eq. (17′) of reference 3, the sum of corrections of order v^2/c^2 that correspond to Eq. (1) is

$$(\Delta E)_1=-\frac{p_1^4+p_2^4}{8M^3c^2}-\frac{\hbar^2\Delta J}{4M^2c^2}+\tfrac{1}{2}(\boldsymbol{\alpha}_1\boldsymbol{\alpha}_2)J-\tfrac{1}{2}(\boldsymbol{\alpha}_1\mathbf{r})(\boldsymbol{\alpha}_2\mathbf{r})f, \tag{6.1}$$

and according to Eq. (18) of reference 3, the sum of similar corrections that correspond to Eq. (2) is

$$(\Delta E)_2=\sum_{i=1,\,2}\left[-\frac{p_i^4}{8M^3c^2}+\frac{p_i^2J+2\mathbf{p}_iJ\mathbf{p}_i+Jp_i^2}{8M^2c^2}\right]-\tfrac{1}{2}(\boldsymbol{\alpha}_1\boldsymbol{\alpha}_2)J-\tfrac{1}{2}(\boldsymbol{\alpha}_1\mathbf{r})(\boldsymbol{\alpha}_2\mathbf{r})f. \tag{6.2}$$

From these formulas and the Eqs. (5) the corrections can be computed. One finds

$$(\Delta E)_1=\frac{\hbar^2}{4M^2c^2}\int\left\{E\psi\Delta\psi-3J(\nabla\psi)^2-\psi^2\Delta J-\frac{rdJ}{dr}[\psi\Delta\psi-(\nabla\psi)^2]-(2/3)(\boldsymbol{\sigma}_1\boldsymbol{\sigma}_2)\psi^2\Delta J\right\}d\tau, \tag{7.1}$$

$$(\Delta E)_2=\frac{\hbar^2}{4M^2c^2}\int\left\{(E-2J)\psi\Delta\psi+3J(\nabla\psi)^2-\psi^2\Delta J-\frac{rdJ}{dr}[\psi\Delta\psi-(\nabla\psi)^2]\right\}d\tau. \tag{7.2}$$

For square wells these become

$$(\Delta E)_1=-\frac{(D+E)[4D\alpha^2a^2+E(\alpha^2a^2+3\alpha a+8)]}{4Mc^2(1+\alpha a)\alpha a}-\frac{2E(E+D)}{3Mc^2\alpha a}(\boldsymbol{\sigma}_1\boldsymbol{\sigma}_2), \tag{8.1}$$

$$(\Delta E)_2=\frac{D+E}{Mc^2(1+\alpha a)}\left[D\alpha a+E\left(\frac{1}{4}-\frac{\alpha a}{4}+\frac{1}{\alpha a}\right)\right]. \tag{8.2}$$

By using these formulas the numerical values in Table I were obtained. The values for ^3S have a minimum in the range shown and go through zero at $\alpha a\sim0.29$. The deuteron energy was taken to be $-4.35mc^2$ in this and in Table II.

TABLE I. *Relativistic corrections for square wells. Energies in units of* mc^2.

$amc^2/e^2=$		0.50	0.75	1.00	1.25	1.50	2.00
$(\Delta E)_1$	^3S	−0.023	−0.034	−0.026	−0.020	−0.016	−0.012
	^1S	−2.45	−0.82	−0.39	−0.22	−0.14	−0.067
$E_1(^3S)-E_1(^1S)$		2.43	0.79	0.36	0.20	0.12	0.06
$(\Delta E)_2$		1.47	0.50	0.24	0.14	0.09	0.05

TABLE II. *Relativistic corrections for* $J=Ae^{-\alpha r^2}$ *computed by using numerically integrated wave functions, for* $\alpha^{-1}\sim2.3\times10^{-13}$ *cm and* $A=72.3\ mc^2$.

$(\Delta E)_1\ ^3S$	$(\Delta E)_1\ ^1S$	$E_1(^3S)-E_1(^1S)$	$(\Delta E)_2$
−0.025	−0.34	0.32	0.26

Collecting terms of order v^2/c^2 that contain the $\mathbf{p}_i$ explicitly in Eqs. (1), (2) one obtains for a square well

$$(\Delta E)_1'=\frac{D+E}{Mc^2(1+\alpha a)}\left[E\left(\frac{7}{4}+\frac{3\alpha a}{4}\right)-\frac{3}{4}D\alpha a\right]=\frac{(D+E)E}{Mc^2(1+\alpha a)}\left[\frac{3\pi^2}{16\alpha a}+\frac{13}{4}+\left(\frac{3}{2}-\frac{3}{\pi^2}\right)\alpha a+\cdots\right], \tag{8.3}$$

$$(\Delta E)_2'=\frac{D+E}{Mc^2(1+\alpha a)}\left[E\left(\frac{11}{4}+\frac{3}{\alpha a}+\frac{3\alpha a}{4}\right)+\frac{5}{4}D\alpha a\right]$$

$$=\frac{(D+E)E}{Mc^2(1+\alpha a)}\left[\left(3-\frac{5\pi^2}{16}\right)\frac{1}{\alpha a}+\frac{1}{4}+\left(\frac{5}{\pi^2}-\frac{1}{2}\right)\alpha a+\cdots\right], \tag{8.4}$$

where the first three terms of the series

$$\frac{D}{E}=-\frac{\pi^2}{4\alpha^2a^2}-\frac{2}{\alpha a}-\left(1-\frac{4}{\pi^2}\right)-\left(\frac{32}{\pi^4}-\frac{8}{3\pi^2}\right)\alpha a\cdots \tag{8.5}$$

have been used. It is curious that the coefficients in the square bracket of Eq. (8.4) are small and that the first three terms of the series in the square bracket partly cancel each other for $a=2.3\times10^{-13}$ cm. For this range of force $(\Delta E)_2'$ is practically negligible. For the same range $(\Delta E)_1'=-0.58mc^2$.

It should be noted that the relativistic correction to the energy of the deuteron or any other nucleus with atomic weight >1 is not unique. Thus $(\Delta E)_1'$, $(\Delta E)_2'$ are as justifiable corrections as $(\Delta E)_1$, $(\Delta E)_2$ so far as invariance of the equations is concerned. However the $(\Delta E)'$ do not have a simple obvious counterpart in a Diracian form and may from this point of view be regarded as less probable. It should also be noted that terms in relative velocities such as $-(3\hbar f/4iM^2c^2)(\mathbf{r}(\mathbf{p}_2-\mathbf{p}_1))$ may be added to the Hamiltonian without destroying its invariance. These terms are not negligible. Thus for $a=2.3\times10^{-13}$ cm

$$-\frac{5\hbar}{4iM^2c^2}f(\mathbf{r}(\mathbf{p}_2-\mathbf{p}_1))=-1.14mc^2,\quad -\frac{\hbar}{4iM^2c^2}\frac{rdf}{dr}(\mathbf{r}(\mathbf{p}_2-\mathbf{p}_1))=0.34mc^2.$$

Since these values are of the same order of magnitude as $(\Delta E)_1$ and $(\Delta E)_2$ and are larger than the absolute value of the correction to the kinetic energy $-(p_1^4+p_2^4)/8M^3c^2=-0.15mc^2$ one must regard the relativistic corrections made so far in the combined theory of H^2, H^3 as uncertain[6] not only because they do not take into account terms like $J\mathbf{p}_1\mathbf{p}_2/2M^2c^2$ that are essential for invariance but also because the requirement of invariance does not suffice to fix all the parts of the Hamiltonian that contain the velocity explicitly.

3. Exchange Interaction

It can be shown that

$$H=-c(\boldsymbol{\alpha}_1\mathbf{p}_1)-c(\boldsymbol{\alpha}_2\mathbf{p}_2)-(\beta_1+\beta_2)Mc^2-JP^M+\tfrac{1}{2}(\boldsymbol{\alpha}_1\boldsymbol{\alpha}_2)JP^M-\tfrac{1}{2}(\boldsymbol{\alpha}_1\mathbf{r})(\boldsymbol{\alpha}_2\mathbf{r})fP^M$$
$$-\frac{i}{4Mc}\{([(\mathbf{p}_2-\mathbf{p}_1)\times\boldsymbol{\sigma}_1]\cdot\mathbf{r})(\boldsymbol{\alpha}_2\mathbf{r})f+f(\boldsymbol{\alpha}_1\mathbf{r})(\mathbf{r}\cdot[(\mathbf{p}_1-\mathbf{p}_2)\times\boldsymbol{\sigma}_2]+([(\mathbf{p}_2-\mathbf{p}_1)\times\boldsymbol{\sigma}_1]\cdot\boldsymbol{\alpha}_2)J$$
$$+J(\boldsymbol{\alpha}_1\cdot[(\mathbf{p}_1-\mathbf{p}_2)\times\boldsymbol{\sigma}_2])\}P^M \tag{9}$$

is invariant to order v^2/c^2. Here P^M is the Majorana exchange operator which exchanges in this equation only the space coordinates. There are other equations but the above was used because it is analogous to Eq. (1). The proof of the invariance of this equation will be given in another paper. One finds for the expectation values

$$(\boldsymbol{\alpha}_1\boldsymbol{\alpha}_2)JP^M=\frac{\hbar^2}{2M^2c^2}\int\{\psi J\Delta\psi+J(\nabla\psi)^2-(2/3)(\boldsymbol{\sigma}_1\boldsymbol{\sigma}_2)[\psi J\Delta\psi-J(\nabla\psi)^2]\}d\tau$$
$$=\frac{(D+E)E}{Mc^2\alpha a}+\frac{2}{3}(\boldsymbol{\sigma}_1\boldsymbol{\sigma}_2)\frac{(D+E)(D\alpha a+E/\alpha a)}{Mc^2(1+\alpha a)}, \tag{9.1}$$

$$(\boldsymbol{\alpha}_1\mathbf{r})(\boldsymbol{\alpha}_2\mathbf{r})fP^M=\frac{\hbar^2}{2M^2c^2}\int\frac{dJ}{dr}\left\{-2\psi\frac{d\psi}{dr}+r\psi\Delta\psi+r(\nabla\psi)^2-\frac{2}{3}(\boldsymbol{\sigma}_1\boldsymbol{\sigma}_2)\psi\frac{d\psi}{dr}\right\}d\tau$$
$$=\frac{(D+E)E}{Mc^2\alpha a(1+\alpha a)}\left\{\frac{D}{2E}\alpha^2a^2+3+4\alpha a+2\alpha^2a^2+\frac{2}{3}(\boldsymbol{\sigma}_1\boldsymbol{\sigma}_2)(1+\alpha a)\right\}, \tag{9.2}$$

[6] W. Rarita and R. D. Present, Phys. Rev. **51**, 788 (1937).

$$-\frac{i}{4Mc}\{([(\mathbf{p}_2-\mathbf{p}_1)\times\boldsymbol{\sigma}_1]\cdot\mathbf{r})(\boldsymbol{\alpha}_2\mathbf{r})f+f(\boldsymbol{\alpha}_1\mathbf{r})(\mathbf{r}\cdot[(\mathbf{p}_1-\mathbf{p}_2)\times\boldsymbol{\sigma}_2]+([(\mathbf{p}_2-\mathbf{p}_1)\times\boldsymbol{\sigma}_1]\cdot\boldsymbol{\alpha}_2)J$$
$$+J(\boldsymbol{\alpha}_1\cdot[(\mathbf{p}_1-\mathbf{p}_2)\times\boldsymbol{\sigma}_2])\}P^M=\frac{\hbar^2}{3M^2c^2}(\boldsymbol{\sigma}_1\boldsymbol{\sigma}_2)\int\left\{[-\psi\Delta\psi+(\nabla\psi)^2]J-\frac{dJ}{dr}\frac{d\psi}{dr}\psi\right\}d\tau$$
$$=\frac{2}{3}(\boldsymbol{\sigma}_1\boldsymbol{\sigma}_2)\frac{D+E}{Mc^2}\left\{\frac{D\alpha a+E/\alpha a}{1+\alpha a}+\frac{E}{\alpha a}\right\}, \quad (9.3)$$

and the whole correction is obtained by a formula similar to Eq. (6.1). For a square well this is

$$(\Delta E)_{\text{exc}}=-\frac{(D+E)[2D\alpha a+E(8/\alpha a+9+5\alpha a)]}{4Mc^2(1+\alpha a)}+(\boldsymbol{\sigma}_1\boldsymbol{\sigma}_2)\frac{D+E}{Mc^2}\left[\frac{D\alpha a+E/\alpha a}{1+\alpha a}+\frac{E}{3\alpha a}\right]. \quad (10)$$

For $E=-4.3mc^2$, $a=2.3\times10^{-13}$ cm, $\alpha a=0.533$, $D=56.1mc^2$ one obtains from Eq. (10) $(\Delta E)_{\text{exc}}=0.58mc^2$ for the ^3S state and $-0.73mc^2$ for the ^1S state. Other values are given in Table III.

The spin dependence of the interaction following from Eq. (9) is greater than that corresponding to Eq. (1). By using a range of force only somewhat smaller than the accepted range it is possible to have the spin dependence equal in magnitude but opposite in sign to the empirical value $\sim 5mc^2$. Eq. (9) is only one of many possible forms of invariant equations. It is therefore possible, although not certain, that the empirical spin dependence can be explained as a consequence of a simple interaction between particles obeying Dirac's equation. Such an explanation would not be an ultimate one but would be useful in indicating the sort of field theory that should be used for explaining the interaction between heavy particles.

TABLE III. *Relativistic exchange corrections for Eq. (9).*

amc^2/e^2		0.50	0.82	1.00
$(E)_{\text{exc}}$	^3S	2.08	0.58	0.36
	^1S	−2.76	−0.73	−0.45
$E_{\text{exc}}(^3S)-E_{\text{exc}}(^1S)$		4.84	1.31	0.81

The relatively large magnitude of the spin-spin interactions obtained here indicates that: (a) The spatial dependence of spin dependent forces is likely to be different from the forces averaged over all spin directions. (b) The determination of the magnitude of the Heisenberg force from the empirically known spin dependence of the deuteron energy is questionable.

The authors are indebted to the Alumni Research Foundation of the University of Wisconsin for a grant.

Cosmic-Ray Measurements with a Small Ionization Chamber

I. Variation with Altitude and Latitude of the Total Ionization for Various Shields[1]

R. T. YOUNG, JR.
Worcester Polytechnic Institute, Worcester, Massachusetts

and

J. C. STREET
Harvard University, Cambridge, Massachusetts

(Received June 24, 1937)

Ionization data have been obtained with a small ionization chamber (230 cc volume) at three corresponding altitudes (76, 51, and 45 cm Hg) in northern and equatorial latitudes, for shielding thicknesses up to 19.4 cm Pb. It is found that within limits of error the latitude ionization ratios, northern: equatorial, are independent of shield at each elevation studied. The values of the latitude ratios are: 1.16 at 76 cm Hg, 1.27 at 51 cm Hg, and 1.30 at 45 cm Hg. An analysis of the lead absorption curves has been made in terms of a penetrating ionizing radiation and a softer secondary radiation. By comparing the ionization data with counter data on the absorption of vertical rays and on showers, available at two altitudes (76 and 51 cm Hg), an estimate has been made of the individual contributions of the penetrating and secondary rays to the measured ionizations. The analysis shows that the ionization due to secondaries associated with the soft component is to be identified with the shower radiation. The contribution of secondaries is important, even under thick shields. For 19.4 cm Pb it amounts to 50 percent of the total ionization at 51 cm Hg and to 20 percent at 76 cm Hg. The curves of intensity of secondary rays *vs.* thickness of lead indicate a second maximum for thick shields.

1. INTRODUCTION

THE existence of a latitude effect in the cosmic radiation has been well established, though the magnitudes of the effect found by different investigators are somewhat conflicting. At sea level Clay[2] finds with an unshielded vessel a maximum increase of 17 percent between 0° and 45° north magnetic latitude. Millikan and Neher[3] find increases from 8 to 12 percent depending on longitude, for 11 cm lead shield and for no shield, and Compton[4] gives the value 14 percent for 6 cm lead shield. The latitude effect increases rapidly with altitude. Compton[4] finds a 33 percent effect at 4300 m between 0° and 50° north magnetic latitude with both a shielded (6 cm Pb) and an unshielded chamber. Bowen, Millikan, Korff and Neher[5] find a 36 percent effect at 8800 m. Clay[2] reports a 30 percent effect at 5000 m between 18° south and 53° north, and at 15,000 m a latitude ratio of 8 to 1 for the ionization in Holland relative to that in Java. The magnitude of this last ratio is doubtful in view of Millikan's later findings which give a ratio of 2 to 1 between San Antonio, Texas, and Madras, India at about this same elevation.

It is of importance to know whether the radiation changes in quality, as well as intensity, with altitude and latitude. Schindler[6] has obtained a set of transition curves between various media at sea level. Clay and Alphen[7] state that altitude curves based on data from shielded and unshielded chambers are the same in form in equatorial latitudes, but differ in northern latitudes. They note, however, that the shielded curves are the same for both latitudes. Clay's measurements under water and lead[8] indicate the radiation in equatorial regions to be the more penetrating. We have obtained absorption curves in lead at three comparable altitudes up to 4300 m in northern and equatorial latitudes. Our data show that the variation with altitude at both latitudes is a function of the shielding, but that at a given altitude the curves at the two latitudes are similar.

[1] J. C. Street and R. T. Young, Jr., Phys. Rev. **46**, 823 (1934).
[2] J. Clay, Physica **1**, 363 (1934).
[3] R. A. Millikan and H. V. Neher, Phys. Rev. **50**, 15 (1936).
[4] A. H. Compton, Phys. Rev. **43**, 87 (1933).
[5] I. S. Bowen, R. A. Millikan, S. A. Korff and H. V. Neher, Phys. Rev. **50**, 579 (1936).
[6] H. Schindler, Zeits. f. Physik **72**, 625 (1931).
[7] J. Clay and P. M. V. Alphen, Physica **2**, 183 (1935).
[8] J. Clay, Physica **2**, 299 (1935).

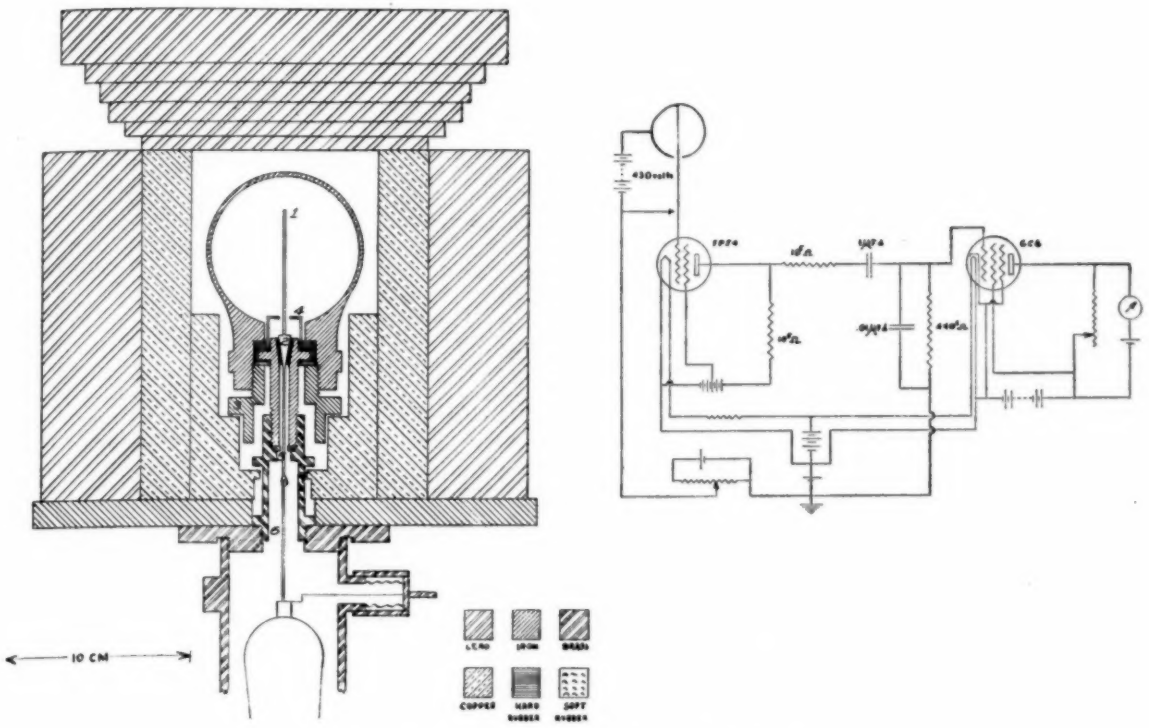

FIG. 1. Ionization chamber and recording circuit.

2. THE EQUIPMENT AND ITS OPERATION

Due to the fact that we wished to measure small bursts along with the total ionization (see II[9]) the volume of the chamber used was small, 230 cc. The design of the chamber and arrangement of shields is shown in Fig. 1. The collecting electrode, 1, passes through a conical plug, 2, to the grid of an FP 54 electrometer tube. The plug is insulated from the outer sphere by a hard rubber sleeve. This sleeve also holds the pressure (200 lb.) and behaved very satisfactorily, particularly when sealed with glyptol. The sphere is insulated from its support by flat hard rubber washers, which, together with a lead washer, likewise hold the pressure. Some trouble was experienced with the rubber flowing away from its supporting surfaces. However, if the large nut, 3, were tightened up at intervals throughout a period of a few days, the flow stopped and the chamber held its pressure. The guard ring, 4, in the shape of a brass hat, shields the collecting electrode from the insulating surfaces. If this electrode is not properly shielded, there is produced a spurious voltage on the inner electrode when the electric field is reversed, due to polarization effects in the dielectric, and a considerable length of time is required before equilibrium is established.

The amplifying system of Fig. 1 was designed to record both small bursts and ionization with the same apparatus. By means of the capacity coupling only sharp changes in potential of the collecting electrode are recorded. The electrometer tube is enclosed in a vacuum, the chamber support at 5 being sealed by a soft rubber washer and stopcock grease, and the threads at 6 by Apiezon putty. The output of the FP 54 is coupled by a 0.1 meg. resistor and a 1 μf condenser to the grid of a 6-C-6 pentode amplifier. The grid of the 6-C-6 is connected to ground by a 4 megohm resistance. The 0.1 meg. resistor and 0.01 μf condenser around this high resistance serve to filter out any high frequency pick-up. Variations of the plate current of the 6-C-6 were recorded by a galvanometer, with the steady plate current balanced out by a suitable battery in the galvanometer line. This circuit provided a convenient means of shifting the zero position of

[9] R. T. Young, Jr., Phys. Rev. **52**, 559 (1937).

the galvanometer. By adjusting the plate, screen, and grid voltages, advantage was taken of the characteristics of the 6-C-6 to obtain a fairly drift-free circuit. The galvanometer deflections were recorded photographically on sensitive paper mounted on a revolving drum.

The grid of the FP 54 was periodically grounded by a clock-driven key mechanism and the net ionization charge accumulated on the collecting electrode during the given interval was recorded as a sharp jump on the photographic trace (see Fig. 1, II). To eliminate the effect of the grid current, runs were made with the sweeping field first in one direction and then in the other. Since the ionization current reverses in direction, while the grid current maintains the same direction, the latter can be averaged out.

The chamber was filled with commercially pure argon at 200 lb. pressure and operated at 430 volts. The side and bottom shields which were used to cut down local radioactivity are equivalent to 6 cm lead. This is sufficient to place the effects of the cosmic radiation incident from the side beyond the transition region. The top shields consist of flat lead plates of areas such that the same solid angle, i.e., that of a 41° cone, is subtended at the center of the sphere for all thicknesses. At each station values of the total ionization were obtained with upper shields up to 20 cm. Corrections for local radioactivity were made by methods similar to those described by Compton,[4] using values of the ionization obtained with and without side shielding. The voltage sensitivity of the FP 54 and amplifier were checked by means of the potentiometer arrangement shown in Fig. 1. For the most sensitive adjustment this amounted to 2 mm deflection on the trace per millivolt. The chamber sensitivity, i.e. the voltage change induced on the collecting electrode by a known amount of radiation, was determined at intervals by using a standard radium source.

TABLE I. *Elevations, barometric pressures and latitudes of stations.*

STATION	ELEVATION	BAROMETRIC PRESSURE	GEOMAGNETIC LATITUDE
Cambridge, Mass.	Sea level	76 cm Hg	53° N
Echo Lake, Colo.	3250 m	51.1	49
Mt. Evans, Colo.	4350 m	44.7	49
Lima, Peru	Sea level	76	1° S
Huancayo, Peru	3340 m	51.3	1
Cerro de Pasco, Peru	4360 m	45.4	1

The value of 2.48 ions per cc per sec. in air at S.T.P.[10] was taken as standard at Cambridge. With the use of this figure to set the value of a measured deflection for no upper shield (corrected for radioactivity), a reduction factor was obtained which enabled us to express all readings in ions per cc per sec. This procedure is justified only if the residual ionization due to radioactive contamination of the chamber is low. We were unable to check this by obtaining readings completely shielded from the cosmic radiation, but since the increase of measured ionization with altitude agrees with that of other observers, we conclude that the chamber contamination was not sufficient to distort our results.

3. IONIZATION DATA

The various stations at which lead absorption data were obtained are listed in Table I.

Because of the fact that a mercury barometer was not carried with the expeditions and since our Aeronoid barometers did not behave satisfactorily in recording barometric differences between different elevations, the barometric pressures for some of the stations are uncertain by 0.1 or 0.2 cm Hg. Curves of barometric pressure against elevation for equatorial and northern latitudes were drawn from values given in Glazebrook's *Dictionary of Applied Physics* (Vol. III, p. 181, Table IX). Barometer readings were available at the Department of Terrestial Magnetism's observatory at Huancayo, and the value for Cerro de Pasco was fixed by subtracting from the Huancayo value the difference given by the curve. The barometric pressure given by Compton[4] was taken as standard for Mt. Evans, and the Echo Lake pressure obtained as above. Corrections were made for fluctuations of barometric pressure at a given station.

The total measured ionizations (corrected for local radioactivity) are given in Table II.

The trace deflections from which the ionization data were obtained were estimated to tenths of a millimeter, which corresponds to about $\frac{3}{4}$ of a percent for the smallest ionization rates. A study of the deviations of individual deflections shows

[10] R. A. Millikan, Phys. Rev. **39**, 397 (1932).

TABLE II. *Total measured ionizations in ions per cc per sec. in air at S.T.P.*

Northern Latitudes

THICKNESS OF LEAD ABOVE CHAMBER IN CM	CAMBRIDGE	ECHO LAKE	MT. EVANS
0.00 no side shields	4.67	10.72	18.25
0.00 with side shields	2.48	7.30	11.31
0.64	2.48	7.92	12.21
1.27	2.43	7.34	11.61
3.18	2.05		8.45
6.66	1.84	4.32	6.06
9.2	1.79		
11.7	1.75		5.20
14.3	1.74		
19.4	1.70	3.74	4.90

Equatorial Latitudes

THICKNESS OF LEAD ABOVE CHAMBERS IN CM	LIMA	HUANCAYO	CERRO DE PASCO
0.00 no side shields	4.41	7.22	11.83
0.00 with side shields	2.14	5.64	8.73
0.64		5.96	9.08
1.27		5.71	8.61
3.18		4.53	6.44
6.66	1.59	3.45	4.55
9.2		3.09	4.07
14.3		2.97	3.80
19.4		2.94	3.74

that the probable error of a single interval is about what one would expect from a consideration of the number of rays passing through the chamber. Taking the data as a whole, one can state the probable error of a measured ionization value at a given station to be within 2 percent. There may be, however, unsuspected systematic errors between values for different stations. The corrections for local radioactivity are only approximate, but since they amount to only 3 percent of the difference between the no-shield and side-shield readings, errors in estimation of the correction cannot affect the ionization values by more than 1 percent. Since the radioactive corrections refer only to ground radiations, contamination of the air above the chamber may lead to slightly greater inaccuracies in the values for no upper shields.

All measurements were made under light roofs. At the North American stations the apparatus was under canvas. At Lima the covering was one-half inch wood, Huancayo one inch wood, and at Cerro de Pasco one inch wood and one-half inch plaster. The stations were chosen to give as level a horizon as possible.

On the basis of Johnson's angular distribution data[11] an estimate was made of the fractional part, F, of the ionization due to radiation which does not pass through the cone subtended by the top shields. If $j(\theta)$ is the number of rays per unit solid angle per sq. cm perpendicular to the radiation, then:

$$F = 1 - \frac{\int_0^{\theta_1} j(\theta) \sin\theta d\theta}{\int_0^{\pi/2} j(\theta) \sin\theta d\theta},$$

where the upper limit, θ_1, is the angle subtended by the upper shield. The integrals were evaluated graphically, allowance being made for the shielding of the horizon. Measurements of the distribution of cosmic rays with varying zenith angle show their angular distribution to be, within limits of experimental error, the same at different latitudes.[11, 12] The factor F was evaluated for Lima and Cerro de Pasco, and the value for Huancayo obtained by interpolation. These same factors were applied to the northern data. The total ionization values for 6.66 cm shield (condition for approximate symmetry of shielding) at a given station were multiplied by the corresponding factor, and the result subtracted from all measured ionizations at that station. The quantities subtracted were: Cambridge, 0.77; Echo Lake, 1.71; Mt. Evans, 2.26; Lima, 0.67;

TABLE III. *Ionizations due to radiation passing through top shields.*

ALTITUDE: CM HG. GEOMAG. LAT.	76		51		45	
	53 N	1 S	49 N	1 S	49 N	1 S
THICKNESS LEAD ABOVE CHAMBER CM	IONIZATION IN IONS PER CC PER SEC. IN AIR AT S.T.P.					
0.00	1.71	1.47	5.64	4.40	8.82	7.12
0.64	1.71		6.26	4.72	9.69	7.47
1.27	1.66		5.68	4.46	9.10	6.99
3.18	1.28			3.24	6.04	4.75
6.66	1.07	.92	2.63	2.13	3.70	2.82
9.2	1.02			1.77		2.33
11.7	.98				2.86	
14.3	.97			1.64		2.04
19.4	.93		2.05	1.61	2.58	1.98

[11] T. H. Johnson, Phys. Rev. **45**, 584 (1934).
[12] W. Kolhörster and L. Janossy, Zeits. f. Physik **93**, 111 (1934).

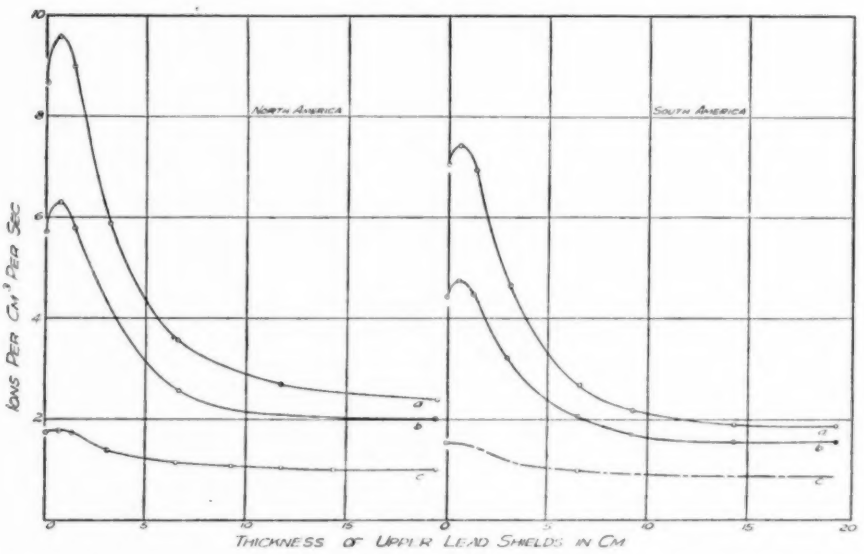

FIG. 2. Absorption curves of cosmic rays in lead. North America: *a*, 45 cm Hg; *b*, 51 cm Hg; *c*, 76 cm Hg. South America: *a*, 45 cm Hg; *b*, 51 cm Hg; *c*, 76 cm Hg.

Huancayo, 1.37; and Cerro de Pasco, 1.80 ions per cc per sec. The resultant ionizations obtained are those arising from the radiation passing through the top shields, and enable one to evaluate the absorption in the upper shields alone. The data thus obtained for corresponding northern and equatorial stations were reduced to the common barometric pressures: 45, 51, and 76 cm Hg, and are listed in Table III.

The curves of Fig. 2 are plotted from the data of Table III. These are essentially air-lead transition curves. Their initial portions may be affected to some extent by radioactive contamination of the air. This would tend to mask the initial rise and may be the explanation for the failure of the Cambridge curve to show any increase for the smaller shielding thicknesses, which Schindler[6] found to amount to 0.5 percent.

TABLE IV. *Latitude ratios.*

Altitude: cm Hg	76	51	45
Thickness Lead Above Chamber cm	Latitude Ratio	Latitude Ratio	Latitude Ratio
0.00	1.16	1.28	1.24
0.64		1.33	1.29
1.28		1.27	1.30
3.18			1.27
6.66	1.16	1.24	1.31
19.4		1.27	1.30
Average all Thicknesses	1.16	1.27	1.30

Also, the material above the chamber at Cerro de Pasco may have influenced the initial portions of that curve.

Two types of comparison may be made: (1) variation with latitude and, (2) variation with altitude.

4. Latitude Effect

In Table IV are recorded latitude effects, as calculated from the values of Table III, in the form of the latitude ratios:

$$I_{\text{northern}}/I_{\text{equatorial}}.$$

Examination of the table leads us to the conclusion that the latitude ratios are independent of the shielding, although the total ionization is reduced by 45 percent, 67 percent and 74 percent at 76, 51, and 45 cm Hg, respectively, when the shield is increased from 0.64 to 19.4 cm Pb. At each of the higher altitudes one or two of the values show a greater deviation from the average than one would expect from statistical considerations. However, the corresponding values at different altitudes for a particular shield do not support an interpretation that these deviations represent any significant trend. The average latitude ratios are in quite good agreement with those found by Compton[4] at the same elevations.

Transition curves represent ionization arising from two factors: (a) ionizing rays incident from

the air which penetrate the shield and (b) secondaries produced in the shielding material. Since the relative contributions of these two factors change markedly with shield (see Section 5) whereas the latitude ratios for the total ionization remain constant, we must conclude that the latitude variation is the same for both. The simplest assumption to make is that they have a common primary origin. The alternative hypothesis that these factors arise from two independent primary components is not ruled out, however, if we assume the same field sensitivety for both.

There is one feature of the above data for which we have no adequate explanation, namely: the latitude ratios decrease from 1.30 to 1.16 as the thickness of the atmosphere increases from 45 to 76 cm Hg, whereas at a given altitude the latitude ratio is independent of thickness of lead up to 20 cm.

5. Variation with Altitude

Several attempts have heretofore been made to analyze transition curves. Johnson[13] has analyzed Schindler's curves in terms of a non-ionizing primary radiation coming into equilibrium with its secondaries in passing from one medium to another, and has evaluated the absorption and production coefficients from Schindler's data. Counter experiments by Rossi[14, 15] and cloud chamber experiments by Street, Woodward and Stevenson,[16] and by Auger and Ehrenfest[17] show however that the assumption of a non-ionizing penetrating radiation does not apply, and one must take account of the ionization produced directly by penetrating particles. Woodward[18] has carried out counter experiments on showers up to 10 cm Pb, and on penetrating rays (using 4 counters in line) up to 91 cm Pb at Cambridge and at Echo Lake. Utilizing his data we can make an analysis of our curves and assign values independently to the contributions of the penetrating and secondary radiations. We assume the measured ionization to be due to:

a. Penetrating ionizing rays, whose absorption in lead and variation with altitude is given by measurements with counters in line.

[13] T. H. Johnson, Phys. Rev. **41**, 545 (1932).

[14] B. Rossi, Zeits. f. Physik **82**, 151 (1933).
[15] B. Rossi, Internat. Conf. Physics, London, Oct. 1934.
[16] J. C. Street, R. H. Woodward and E. C. Stevenson, Phys. Rev. **47**, 891 (1935).
[17] P. Auger and Ehrenfest, Comptes rendus **199**, 1609 (1934).
[18] R. H. Woodward, Phys. Rev. **49**, 711 (1936).

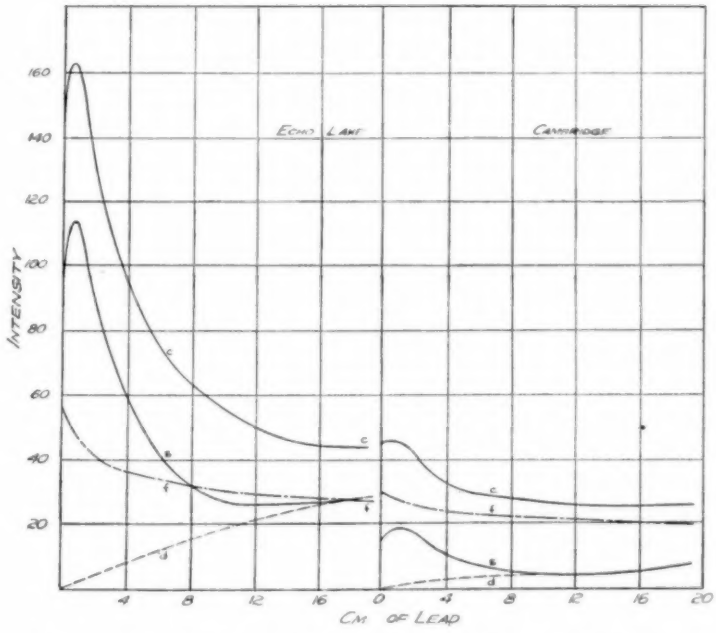

FIG. 3. (left) Curves of absorption of penetrating and secondary rays. *c*, total ionization; *p*, penetrating rays; *s*, secondary rays; *d*, penetrating component in secondary radiation.

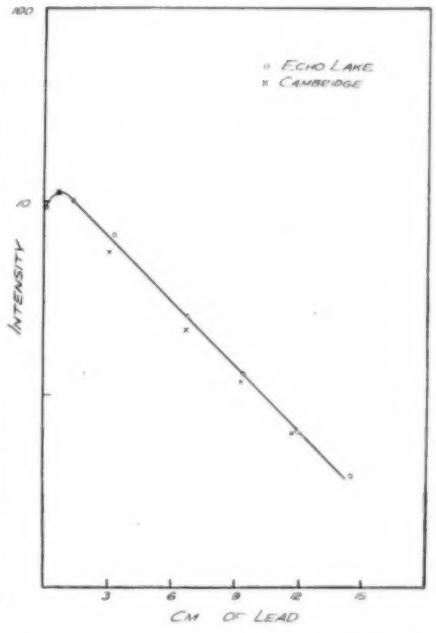

FIG. 4. (right) First peak for secondary rays.

b. Secondary rays, whose production and absorption are given by counter measurements on showers.

Let I_p and I_p' be the intensity of the penetrating rays at sea level and at Echo Lake, respectively, as determined by Woodward's counter arrangement; I_s and I_s' the intensity of secondary rays at sea level and Echo Lake in the same units as I_p and I_p'; J and J' the measured ionizations at sea level and Echo Lake. We can write:

$$J=K(I_p+I_s) \quad \text{and} \quad J'=K(I_p'+I_s').$$

From the counter data on the penetrating rays we obtain $I_p'/I_p=1.39$ at 19.4 cm Pb, and from the data on showers we take $I_s'/I_s=5.0$ for all thicknesses of lead.[19] Using the ratio $J'/J=2.2$ obtained from the ionization chamber measurements for 19.4 cm Pb we can solve the above equations for I_s and I_s' and find $I_s=5.5$ and $I_s'=28$ on the same arbitrary scale as I_p and I_p'. The values of I_p and I_p' for the same lead thickness are 19.2 and 26.7. The contribution of secondary rays is thus a considerable fraction of the total observed ionization under thick shields; roughly, 50 percent at 51 cm Hg and 20 percent at 76 cm Hg. Kulenkampff[20] finds by an entirely independent method that the contribution of secondary rays at sea level and for 30 cm Fe amounts to 17 percent.

In Fig. 3 we have plotted the counter data for the penetrating rays as the dashed curves, *p*, on the above arbitrary scale of intensity. The upper full curves, *c*, are the ionization curves of Fig. 2 reduced by the factor K, and adjusted so that at 19.4 cm Pb they lie 5.5 and 28 units, respectively, above the counter curves at sea level and Echo Lake. Subtracting the curves for the penetrating rays from the ionization curves we obtain the lower full curves, *s*, the values of which are proportional to the ionization produced by the secondary rays.

At zero lead the curves representing the measured ionization lie 95 and 17 units, on the scale chosen, above the counter curves for the penetrating rays at Echo Lake and sea level, respectively. These values are proportional to the ionization due to soft rays from air (and to some extent to those produced in the walls (1 mm steel) of the chamber itself) which will not be recorded by 4 counters in line (112 cm between end counters), due to absorption in the counter walls and to scattering, but will register in an ionization chamber.[21] The curves, *s*, rise from 10 cm on. This means that at greater lead thicknesses the ionization curves are flatter than the counter curves. Curves of a similar form would be obtained if we subtracted the values of the counter curves from those of the ionization curves irrespective of the scales used, but the above method gives the magnitude of the contribution of secondary rays relative to the penetrating rays. Too great significance cannot be attached to the numerical values of the relations between the penetrating and secondary rays, due to lack of exact counter data on showers at sufficiently great thicknesses of lead, but we believe the method of analysis used is of value for the interpretation of ionization chamber data.

The second rise in the curves, *s*, of Fig. 3 indicates the existence of a more penetrating component in the secondary producing radiation. Ackemann,[22] Hummel,[23] and Kulenkampff[20] have noted the appearance of a second peak in counter curves which represent secondary rays. This has been verified by Woodward.[18] We suggest that the rise in our curves is due to the same phenomenon. Making a reasonable estimate of the course of the ionization responsible for this second peak, as shown by the dotted curves, *d*

[19] Woodward states that the altitude ratio for showers between Echo Lake and Cambridge is 5.0 within limits of probable error for all lead thicknesses up to 10 cm (the extent of his measurements). Closer scrutiny of his data indicates that this ratio falls off somewhat with increasing lead; e.g. at 9.85 cm the ratio is 4.5. The behavior of small bursts described in II, Reference 9, indicates a similar decrease of the ratio, but in neither case are the data sufficiently precise to warrant a more refined analysis.

[20] H. Kulenkampff, Physik. Zeits. **35**, 785 (1935).

[21] Street and Woodward (J. C. Street and R. H. Woodward, Phys. Rev. **46**, 1029 (1934)) have discussed this point in connection with their determination of the specific ionization of cosmic rays by comparing the number of rays recorded by a counter set with the volume ionization produced in an ionization chamber. Using the above values for the relation between penetrating and secondary rays at zero lead we find that Street and Woodward's value of 100 ions per cm in air at S.T.P. would be reduced to 71, which is in the range of values found by others (W. F. G. Swann, Phys. Rev. **44**, 961 (1933); R. D. Evans and H. V. Neher, Phys. Rev. **45**, 144 (1934)). Since in the counter arrangement of Street and Woodward the effect of nonrecording of soft secondaries would be less pronounced than in the present case, this figure merely indicates that the relations we find between the penetrating and secondary rays are reasonable.

[22] M. Ackemann, Naturwiss. **22**, 169 (1934).

[23] J. N. Hummel, Naturwiss. **22**, 170 (1934).

of Fig. 3, and subtracting the values of this curve from those for the secondary rays, we obtain curves which should represent the ionization due to the softer secondary component. These curves for Echo Lake and sea level have been reduced to the same scale and plotted logarithmically in Fig. 4. The high altitude and sea level curves are similar in form, and after their initial rise, fall off linearly with a "decrease coefficient" of 0.3 cm^{-1} Pb. Woodward finds the coefficient 0.33 cm^{-1} Pb for the first peak of his shower curves. This indicates that the results of our analysis are in agreement with the assumption that the ionization arising from the transition effect is attributable to the radiation responsible for showers.

The research was supported by grants from the Carnegie Institution of Washington and the Harvard Milton Fund. Acknowledgment is made of the active cooperation given by the late Dr. J. L. Dunham in designing some of the apparatus, and by Professor H. R. Mimno, Dr. J. E. I. Cairns and the staff of the Huancayo Magnetic Observatory in securing the South American data. The authors are also under obligation to Professor J. C. Stearns and the University of Denver for affording laboratory facilities, to the City of Denver which furnished transportation of equipment through the courtesy of Mr. G. E. Cranmer and Mr. R. R. Vail, and to Dr. R. H. Woodward, who took some of the Cambridge data.

SEPTEMBER 15, 1937 PHYSICAL REVIEW VOLUME 52

Cosmic-Ray Measurements with a Small Ionization Chamber

II. Comparison of Small Bursts at Different Altitudes and Their Variations with Thickness of Shield*

R. T. YOUNG, JR.
Worcester Polytechnic Institute, Worcester, Massachusetts

(Received June 24, 1937)

Measurements of bursts produced in a small ionization chamber (230 cc volume) have been carried out at several stations. A comparison is made between frequencies of occurrence of various sized bursts at Cambridge, Mass. (bar. 76), Echo Lake, Colo. (bar. 51.1), Mt. Evans, Colo. (bar. 44.7), and Cerro de Pasco, Peru (bar. 45.4). The altitude ratios for burst groups comprising 10–19 rays, 20–29, and 30 and greater, are: Echo Lake to Cambridge, 4.9, 8.0 and 8.8; Mt. Evans to Cambridge, 7.3, 14.3 and 20.0. The data for the smallest burst groups are in agreement with counter measurements on showers, while the ratios for the largest bursts agree with the ionization chamber data of others on large bursts. The maxima of the burst production absorption curves shift to greater lead thicknesses with increasing burst size.

1. DISCUSSION OF APPARATUS

WE have described in I[1] equipment which is suitable for the measurement of both total ionization and small bursts. The total ionization is determined from measurements of periodic jumps of a photographic trace when the grounding key is closed. While the key is open (see Fig. 1, I) the trace would be a straight line corresponding to the zero position of the galvanometer if the ionization were perfectly steady. However, if the radiation fluctuates within a period comparable to the time constant of the circuit, the trace will fluctuate. Instantaneous bursts of ionization will be recorded as sharp jumps. Fig. 1 is a reprint of a section of one of our records (6.66 cm Pb, Mt. Evans). The time scale is indicated by the large periodic jumps which correspond to the grounding of the collecting electrode every 70 seconds. Arrow 1 indicates a burst of 10 rays (the lower limit of

* Part of a dissertation presented to the Faculty of Arts and Sciences, Harvard University, in partial fulfillment of the requirements for the degree of Doctor of Philosophy. A preliminary report of this work was made at the New York meetings of the American Physical Society, February 21–22, 1936.

[1] R. T. Young, Jr., and J. C. Street, Phys. Rev. **50**, 552 (1937).

FIG. 1. Sample section of traces (Mt. Evans, 6.66 cm Pb)

our measurements), 2 one of 30, 3 one of 60, and 4 one of 100 rays passing simultaneously through the chamber.

The damped period of the galvanometer was $\frac{1}{2}$ second. The maximum time of collection of ions in a burst was calculated by assuming that the electric field inside the chamber could be approximated by that existing between infinite concentric cylinders. The radial electric field, R, at a distance r from the common axis of the cylinders is:

$$R=(E/r)\ \log\ (b/a) \quad a<r<b,$$

where a and b are the radii of the cylinders and E is the potential difference between them. The velocity, u, of an ion in this field is: $u=Rp/P$ where p is the mobility of the ion and P the pressure in the chamber. The time, T, required for an ion to traverse the space between the conductors is:

$$T=\int_a^b dr/u=\frac{P(b^2-a^2)}{2Ep}\log\ (b/a).$$

For our chamber $a=0.21$ cm, $b=3.85$ cm, $E=430$ volts, and $P=13.6$ atm. For argon $p=1.37$ cm per sec per volt per atm. Substituting these values into the above expression we find that $T=\frac{1}{2}$ sec. This is the time required by an ion formed at the wall of the chamber to reach the collecting electrode.

A point which must be checked is whether the recorded deflections are true representations of changes in the grid potential of the FP 54. Analyzing the circuit of Fig. 2 we have (neglecting the fixed e.m.f.'s of the supply batteries and the plate load drop) for the current, i, in R:

$$di/dt+i/RC=(1/R)d\epsilon/dt,$$

where ϵ is the variable potential difference produced in the plate load of the FP 54 by changes in its grid potential. Assume the ions produced in a burst are collected at a steady rate. ϵ is then a linear function of t and during the time of collection $\epsilon=Vt/t_0$, $0<t<t_0$, where t_0 is the time of collection and V the final change in potential of the plate of the FP 54. The potential of the grid of the 6–C–6 with respect to ground is:

$$iR=RCV(1-e^{-t/RC})/t_0.$$

For an instantaneous pulse giving rise to a potential V the initial current i' is V/R. We compare iR at $t=t_0$ and $i'R$.

$$\frac{(iR)_{t=t_0}}{(i'R)_{t=0}}=RC(1-e^{-t_0/RC})/t_0.$$

For $R=4\times10^6$ ohms, $C=1\mu f$ and $t_0=\frac{1}{2}$ second the ratio is .95. Hence we never record less than 95 percent of the full burst value.

Our burst data are presented in terms of the number of rays of average path length contributing to the burst. 80 ions per cm path in air at S.T.P. was taken as the value of the specific ionization.[2] Reduction to number of rays makes the size of burst recorded independent of the chamber dimensions. (Of course, a large chamber will in general record a larger fraction of the rays in a given burst.)

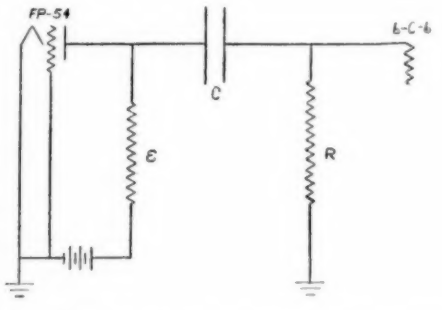

FIG. 2. Diagram for analysis of recording circuit.

[2] Swann (W. F. G. Swann, Phys. Rev. **44**, 961 (1933)) gives the value of 60 ions per cm as determined by direct measurement with a linear amplifier, while Street and Woodward (J. C. Street and R. H. Woodward, Phys. Rev. **46**, 1029 (1934)), by comparing counter data with Millikan's value for the total ionization of 2.48 ions per cc per sec in air at S.T.P., obtain 100 ions per cm path. The value used is the mean of these two.

The essential limitation on the smallness of burst size which can be measured arises from the statistical fluctuations which occur in the chamber. The probability of occurrence of fluctuations which will record as bursts is a rapidly increasing function of the average number of rays passing through the chamber during a period equal to the collecting interval. This number is proportional to r^2 and to the time of collection which, as we have seen above, is an increasing function of the radius, r, of the chamber, proportional to P and inversely proportional to E. Hence we desire P and r to be small and E large. The choice of these values must, however, be consistent with requirements of sensitivity and insulation. The smallest deflection on the traces which could be satisfactorily measured was 1 mm, which corresponded to about 10 rays. The rate of occurrence of kicks due to statistical fluctuations has been evaluated using Poisson's law. It was found that for a collecting time of $\frac{1}{2}$ sec. the contribution of this rate to the measured values for bursts of 10 rays or greater was negligible in all cases. For example, with a 1.27 cm lead shield at Mt. Evans the ionization is due to 3.5 rays per $\frac{1}{2}$ sec. interval. The chance of 13.5 rays passing through the chamber in this interval is 3.2×10^{-5}. The rate per min. due to statistical fluctuations would therefore be 0.0038 which is to be compared with the observed rate of 1.68 for measured kicks. The appearance of the kicks on the traces bears out the conclusion that they are due solely to bursts in that all jumps of 1 mm and greater are uniformly sharp. Some of the kicks below 1 mm are less sharp and are presumably attributable to statistical fluctuations. (See Fig. 1.)

Another source of false kicks is radioactive contamination of the walls of the chamber and consequent emission of alpha-particles. Counts were made of kicks appearing on records taken at reduced pressures; namely, 100 and 17 lb. (gauge). Ionization produced by cosmic rays would be reduced in proportion to the reduction in pressure, while the ionization produced by alpha-particles would increase, due to lessening of the effects of recombination. To evaluate the effective ionization of alpha-particles, a plaque coated with RaF was attached to the interior wall of a chamber similar to the one used in the rest of the work and a curve of average ionization *vs.* pressure obtained. The tests on kicks were made over five hour intervals, and during this time only one kick was observed on the "17 lb." trace which, after applying the alpha-particle ionization factors determined from the curve, would have registered as a 10 ray burst at 200 lb. For this same time interval, our cosmic-ray burst count for the "200 lb." trace was 50. The results obtained from the 100 lb. pressure run were not as conclusive. There were observed about as many kicks which would have recorded as 10–15 ray bursts at 200 lb. as were to be expected from cosmic rays. However, at 100 lb. the cosmic-ray bursts play a larger part, making it difficult to draw definite conclusions concerning the alpha-particle contamination. We consider the evidence from the trace at 17 lb. as quite conclusive that alpha-particle contamination plays little if any part in our results.

2. Results

In Table I are listed the number, N, of observed bursts and their rates of occurrence, R, per min. for each shielding condition.[3] The bursts were arbitrarily classified according to size into the groups listed. On the average a tenth mm deflection on the trace corresponded to the passage of a single ray through the chamber. Uncertainty of measurement amounted to 0.1 or 0.2 mm depending on the sharpness of the trace. (Some of the traces were remeasured after an interval of several months and checks to the above accuracy obtained.) The data were recorded to the nearest ray and then smoothed by dividing the total number of recorded bursts of a given size by three and assigning equal parts to bursts of the given size and to those directly above and below. Since measurements were actually made down to burst sizes of 9 rays the smoothing process could be applied to the 10 ray bursts. There may be some overlapping of the groups, but it is considered that the ranges taken are of sufficient extent that the burst

[3] Though ionization measurements were made at three South American stations (Lima, Huancayo and Cerro de Pasco, Peru), only the Cerro de Pasco burst data are included in the table. While the ionization data for Lima and Huancayo are reliable, the traces at these stations were of such nature that burst measurements were not considered sufficiently accurate to record.

TABLE I. *Frequency of occurrence of bursts.*

Thickness of Lead Above Chamber in cm		0.00	0.64	1.27	3.18	6.66	19.4
Cambridge: Sea Level; Bar. 76; Lat. 53° Mag. N.							
10–14	N	260	158	314	186	343	138
	R	.066	.081	.118	.096	.071	.059
15–19	N	115	97	124	79	237	97
	R	.036	.055	.052	.044	.062	.052
20–29	N	48	28	60	43	101	28
	R	.012	.016	.023	.023	.021	.015
30 and greater	N	22	11	19	13	32	12
	R	.0055	.006	.012	.0085	.0071	.0046
Total 10 and greater	N	485	294	527	321	713	275
	R	.114	.158	.205	.172	.161	.131
Echo Lake: 3250 m; Bar. 51.1; Lat. 49° Mag. N.							
10–14	N	372	277	337		275	149
	R	0.421	0.544	0.588		0.342	0.258
15–19	N	204	153	159		130	75
	R	.217	.249	.277		.162	.130
20–29	N	297	131	87		94	48
	R	.158	.147	.152		.118	.084
30 and greater	N	106	60	49		46	23
	R	.051	.063	.085		.058	.040
Total 10 and greater	N	979	621	632		545	295
	R	.847	1.00	1.10		.680	.512
Mt. Evans: 4350 m; Bar. 44.7; Lat. 49° Mag. N.							
10–14	N	393	601	282	301	312	310
	R	.602	.888	.875	.580	.398	.336
15–19	N	227	277	172	227	232	195
	R	.308	.408	.505	.437	.279	.200
20–29	N	584	284	116	159	192	174
	R	.222	.268	.340	.317	.226	.171
30 and greater	N	341	143	58	97	116	90
	R	.105	.114	.170	.187	.140	.086
Total 10 and greater	N	.1545	1305	640	784	852	769
	R	1.24	1.68	1.93	1.51	1.04	.793
Cerro de Pasco: 4360 m; Bar. 45.4; Lat. 1° Mag. S.							
Thickness of Lead Above Chamber in cm		0.00	.64	1.27	3.18	6.66	9.2	19.4
20–29	N	44	64	74	30	27	17	22
	R	.081	.280	.247	.105	.089	.045	.049
30 and greater	N	22	51	44	57	22	20	23
	R	.040	.218	.147	.153	.060	.034	.041
Total 10 and greater	N	66	115	118	87	49	37	45
	R	.121	.498	.394	.258	.139	.079	.090

groups represent within the probable error, $0.67/(N)^{\frac{1}{2}}$, the correct number within a given range.

To investigate the cause of the high zero rates, measurements were made with no side shields at Echo Lake. The results obtained were the same as with the side shields in place. This indicates there is a considerable contribution from the air above the chamber or from the shell of the sphere (1 mm steel). (See discussion in I[1] of the no shield values of the ionization contributed by secondary rays.)

Only the larger bursts could be measured on the South American traces. Taking the ratio of the average for all thicknesses of lead for bursts of 20 rays and greater, one obtains the latitude ratio: Mt. Evans : Cerro de Pasco, 1.34. This ratio agrees with the latitude ratio for the general ionization (1.30) at this altitude.[1] Since the South American and North American data were obtained from somewhat different types of records the ranges of burst sizes may not correspond, and we do not attach too great significance to this agreement.

In Table II the variations of burst frequency with elevation are tabulated in the form of ratios of rates of occurrence at the higher altitudes to those at Cambridge. It is seen that while the ratios fluctuate somewhat, if one considers the averages over all thicknesses, there is a definitely greater altitude effect for the bursts of larger size. Woodward[4] finds for the relative increase of shower rates between the same stations the ratios:

Echo Lake : Cambridge 5.0
Mt. Evans : Cambridge 8.5

These are in agreement with our ratios for the totals of bursts of all sizes and averaged over all

TABLE II. *Variations of burst frequencies with altitude.*

Thickness of Lead Above Chamber in cm	0.00	0.64	1.27	3.18	6.66	19.4	Average All Thickness
Echo Lake: Cambridge							
Size of burst in rays							
10–19	6.3	5.8	5.1		3.8	3.5	4.9
20–29	13.2	9.2	6.6		5.6	5.6	8.0
30 and greater	9.3	10.5	7.1		8.2	8.7	8.8
Total	7.4	6.3	5.4		4.2	3.9	5.4
Mt. Evans: Cambridge							
10–19	8.9	9.5	8.1	7.3	5.1	4.8	7.3
20–29	18.5	16.7	14.8	13.8	10.8	11.4	14.3
30 and greater	19.1	23.4	14.1	22.0	19.7	18.7	20.0
Total	10.7	10.6	9.4	8.8	8.5	6.1	8.7

[4] R. H. Woodward, Phys. Rev. **49**, 711 (1936).

thicknesses of lead The values for the frequency of occurrence of the net totals are controlled by the observed rates for the groups including only the smaller bursts. Counters record showers of all sizes, but cloud chamber photographs[5] indicate that the average shower tripping a counter set contains 4–6 rays, hence not much below the range of our smallest bursts. D. D. and C. G. Montgomery[6] have found for *large bursts* (40 rays and greater), observed in an ionization chamber shielded by 4 cm Pb, the following relative increases from Swarthmore, Pa. (61 m) to Glen Cove, Colo. (3500 m) and Pikes Peak (4300 m):

Glen Cove : Swarthmore 13.8
Pikes Peak : Swarthmore 26.6

These ratios are in rough agreement with those found by us for the larger bursts. The data in Table II cover the range between showers as observed with counter and large bursts recorded in chambers. One may conclude that counter and ionization chamber results are not contradictory when the size of burst is taken into consideration and that, in dealing with showers or bursts one has to do with a gradual change in the characteristics of the same phenomenon. This increase of altitude ratio with increasing burst (or shower) size is confirmed by the cloud chamber measurements of Anderson and Neddermeyer[7] who find the ratio between Pikes Peak and Pasadena of frequency of occurrence of photographs showing 2–4 tracks to be 8.6; 5–10 tracks, 21; and those showing 11–100 tracks to be 29.

The accuracy of the ratios of Table II is limited by that of the Cambridge data, which are based on a small number of recorded bursts, particularly those of large size. The above ratios can therefore only be considered as indicating general trends in the burst phenomena. There appears to be a definite decrease of the ratios

[5] E. C. Stevenson and J. C. Street, Phys. Rev. **49**, 425 (1936).
[6] D. D. and C. G. Montgomery, Phys. Rev. **47**, 429 (1935).
[7] C. D. Anderson and S. H. Neddermeyer, Phys. Rev. **50**, 263 (1936).

TABLE III. *Contributions of bursts to measured ionizations (in ions per cc per sec).*

Thickness of Lead Above Chamber in cm	0.00	0.64	1.27	3.18	6.66	19.4
Mt. Evans						
Ionization	.67	.87	1.0	.94	.60	.48
Percent contribution	6.0	7.2	9.3	11.2	10.0	10.0
Echo Lake						
Ionization	.44	.54	.57		.38	.26
Percent contribution	6.0	6.8	7.8		8.8	7.0
Mt. Evans						
Ionization	.05	.07	.11	.09	.08	.06
Percent contribution	2.3	3.0	4.3	4.2	4.3	3.5

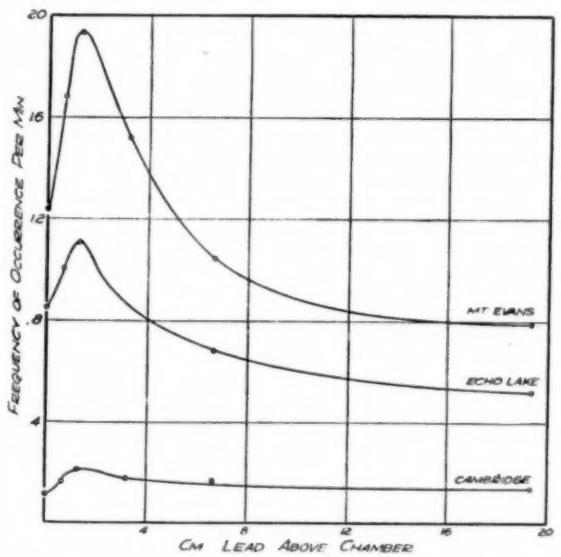

FIG. 3 (left). Curves of total burst frequencies at different altitudes.

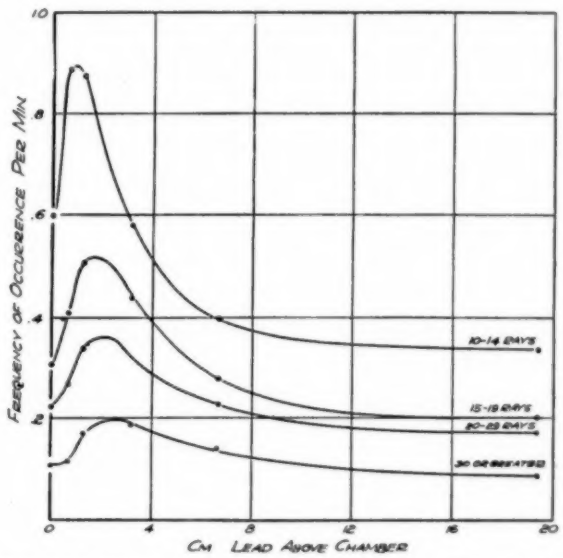

FIG. 4 (right). Curves of burst frequencies for different sized bursts (Mt. Evans).

for smaller bursts with increasing lead, while the ratios for the larger bursts remain sensibly constant.

The variation of total burst frequency with thickness of lead at different altitudes is shown by the curves of Fig. 3. They are of the form of transition curves, and in general shape similar to those for showers as obtained with counters. The set of curves of Fig. 4 are for the different burst groups at Mt. Evans. While the maxima cannot be located exactly, they definitely shift to greater lead thicknesses for the larger sized groups. This is in agreement with the findings of Carmichael,[8] and also with those of Nie[9] who observes the maxima for large bursts to occur at 5 cm lead. Carlson and Oppenheimer[10] show on the theory of multiplicative showers that this shift is to be expected. Bhabha and Heitler[11] also predict a similar shift.

[8] H. Carmichael, Proc. Roy. Soc. **A154**, 223 (1936).
[9] H. Nie, Zeits. f. Physik **99**, 776 (1936).
[10] J. F. Carlson and J. R. Oppenheimer, Phys. Rev. **51**, 220 (1937).
[11] H. J. Bhabha and W. Heitler, Proc. Roy. Soc. **A159**, 432 (1937).

In Table III are given the ionizations contributed by all bursts greater than 10 rays to the total observed ionizations given in I.[1] No extrapolation can be made to smaller showers and hence no estimate can be made of the total contribution of the shower phenomena to the total ionization. Since the values of the tables are lower limits, the actual ionization produced by showers is an appreciable fraction of the total.

The writer wishes to express his appreciation of the advice and encouragement of Professor J. C. Street, who suggested the problem. The writer is also under obligation to Dr. R. H. Woodward who took some of the Cambridge data, to Professor J. C. Stearns and the University of Denver in affording laboratory facilities, and to the City of Denver which furnished transportation of equipment through the courtesy of Mr. G. E. Cranmer and Mr. R. R. Vail. The research was supported in part by grants from the Carnegie Institute of Washington and the Harvard Milton Fund.

SEPTEMBER 15, 1937 PHYSICAL REVIEW VOLUME 52

Shower Production Under Thick Layers of Various Materials*

KARL Z. MORGAN AND W. M. NIELSEN
Lenoire-Rhyne College and Duke University

(Received July 10, 1937)

Observations by G-M counters are reported on showers from lead and iron up to thicknesses of approximately 600 g/cm². As previously noted by others, the transition curves at large thicknesses have approximately the same slope as absorption curves obtained for the general cosmic radiation. Data are presented for the iron-lead and lead-iron transition curves beginning at a material thickness of 274 g/cm² in each case. For the iron-lead transition curve, the number of coincidences increases and attains a maximum in approximately 1 cm of lead, after which the counting rate decreases and finally falls on the air-lead transition curve. For the lead-iron transition curve, the number of coincidences decreases for the first increments of added iron, passes through a minimum and then increases to the air-iron transition curve. It is pointed out that the observations are consistent, in a qualitative way, with the multiplicative theory of the origin of cosmic-ray showers provided one assumes that additional shower producing radiation is generated in the lower layers of material.

THE application of the laws of radiation of high speed electrons and of the production of pairs by quanta has recently led to a fairly complete description of a portion of cosmic-ray shower phenomena. It has been shown[1, 2] that the multiplication theory is capable of accounting in a fairly satisfactory way for showers produced under relatively small thicknesses of material.

* A preliminary report on these experiments was presented at the Chapel Hill-Durham meeting of the American Physical Society, February 1937.

[1] J. F. Carlson and J. R. Oppenheimer, Phys. Rev. **51**, 220 (1937).
[2] H. J. Bhabha and W. Heitler, Proc. Roy. Soc. **159A**, 432 (1937).

The theory is, as yet, unable to account for showers produced under large thicknesses of material and no mechanism is provided for the transmission of the energy represented by such showers through the atmosphere and through large thicknesses of other absorbing material.

Evidence has recently[3, 4] been presented for the existence of a penetrating particle, the properties of which do not seem to be described by the usual properties of electrons in the same energy range. It is the purpose of the present paper to present data, which, while they give no information as to the mechanism by which the cosmic-ray energy is transmitted through large thicknesses of material, do indicate that there are no essential differences between the showers produced under large and small thicknesses of matter.

One of the essential tests of any theory of cosmic-ray showers is that it be capable of accounting for the transition curve. The iron-lead and lead-iron transition curves here presented afford additional evidence for the multiplication theory and indicate furthermore that showers produced under thick layers of producing material are generated in multiplication processes quite similar to those which are associated with the soft component.

The Air-Lead, Air-Iron, and Iron-Lead Transition Curves

Measurements on the frequency of showers were made by recording the number of four-fold coincident discharges in G-M counters arranged as shown in the inset of Fig. 1. With this arrangement the passage of a minimum of two particles through the counters is obviously necessary to cause a coincident discharge in all four counters. The separation of counters and their position with respect to the material is shown on the figure which has been drawn to scale. Sheets of material each 22 cm×30 cm were placed as indicated, the length being parallel to the axis of the counters.

The data shown in Fig. 1 were obtained about a year ago in a light wooden frame structure near the top of Beech Mountain at an altitude of approximately 4500 ft. The air-lead transition curve which is represented by the filled circles shows a maximum at approximately 20 g/cm² of lead. The air-iron transition curve which is represented by the open circles shows a maximum

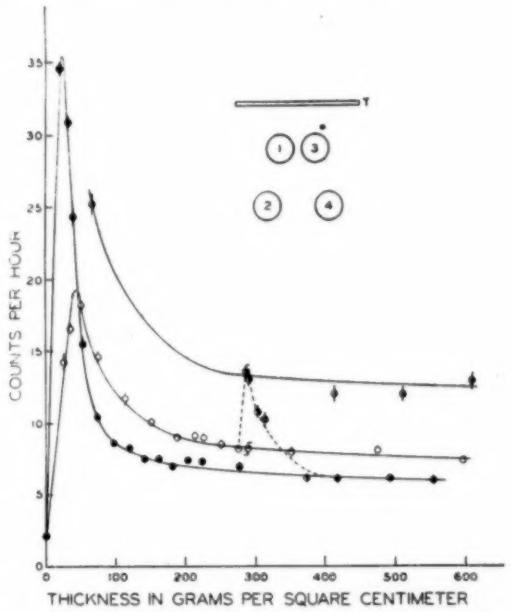

Fig. 1. The frequency of coincidences as a function of material thickness. The data shown by filled circles are for lead, those shown by unfilled circles are for iron. The dashed curve represents the iron-lead transition under 274 g/cm² of iron. The upper curve, shown with half-filled circles, represents the data for various iron thicknesses with a constant lead thickness of 13.12 g/cm² underneath the iron.

at approximately 47 g/cm² of iron. In all cases where the probable errors are larger than the diameters of the circles, they are represented by vertical lines. The relatively small decrease in counting rate in both curves for the larger thicknesses of material has been noted before by a number of investigators[5–8] and is associated with a more penetrating component of cosmic radiation.

While the interpretation of showers on the multiplication theory does not treat the phenomena in such a way that one can assign absorption coefficients to the right-hand side of the transition curve, it is nevertheless of interest to compare the shape of this portion of our curves with the data of Auger and his co-

[3] J. C. Street and E. C. Stevenson, Phys. Rev. **51**, 1005 (1937).
[4] Seth H. Neddermeyer and Carl D. Anderson, Phys. Rev. **51**, 884 (1937).
[5] M. Ackermann, Zeits. f. Physik **94**, 303 (1935).
[6] J. N. Hummel, Naturwiss. **22**, 170 (1934).
[7] H. Kulenkampff, Physik. Zeits. **36**, 785 (1935).
[8] R. H. Woodward, Phys. Rev. **49**, 711 (1936).

workers[9] on the absorption of the general cosmic-radiation as measured by three G-M counters placed in a vertical line. In such a comparison we find it convenient to compute the slopes of the data on semi-logarithmic plots which roughly fall on portions of two straight lines. The calculated slopes are for lead 0.0302 cm²/g and 0.0006 cm²/g. The corresponding values for iron are 0.0072 cm²/g and 0.00044 cm²/g. The coefficients for the data at large thicknesses indicate, as is obvious from inspection of the curves, that the shapes of the transition curves of lead and iron are quite similar for large thicknesses of producing material.[10] It is of some interest to point out that the coefficients for lead, found in this way, are quite closely the same as those observed by Auger and his co-workers. The corresponding coefficients obtained by them in the work referred to above are 0.030 cm²/g and 0.0007 cm²/g. The close correspondence between the shape of the transition curve and the absorption of the general cosmic-radiation has also been noted by Clay.[11]

The dashed curve of Fig. 1 connecting the half-filled circles represents the transition from iron to lead. It is important to observe that this transition begins at an iron thickness equivalent to 274 g/cm² of iron, a thickness of material which is usually regarded as being sufficient to remove a large percentage of the soft component of the shower producing radiation. The full line connecting some of the half-filled circles represents the counting rate for various thicknesses of iron with a constant thickness of 13.12 g/cm² of lead underneath. One would infer from this curve that the iron-lead transition curve at 274 g/cm² would be duplicated in its essential features for other iron thicknesses out to a thickness of 600 g/cm², the maximum iron thickness employed. The data for the point with wings were obtained by placing 13.12 g/cm² of lead above the 274 g/cm² of iron instead of below it.

[9] P. Auger, L. LePrince-Ringuet and P. Ehrenfest, Jr., J. de phys. **7**, 58 (1936).

[10] The coefficients when expressed in terms of the number of electrons per cm³ indicate a variation with the first power of Z. The accuracy of such determinations is not high and it is therefore necessary to regard this as a rough approximation.

[11] J. Clay, A. Van Gemert and J. T. Wiersma, Physica **7**, 627 (1936).

The success of the multiplication theory in accounting for the phenomena at small thicknesses of producing material makes it desirable to examine the observed transition curve in the light of that theory even though it is unable to account for the penetration of the particles considered in that theory through large thicknesses of matter.

According to the multiplication theory of cosmic-ray showers initiated by particles of electronic mass or by quanta, the number of particles in a shower increases by successive radiation of quanta and pair production. This process continues until the probability of energy loss by electrons through ionization becomes comparable to the probability of energy loss by radiation. The maxima in the transition curves are to be associated in a rough way with the energy for which the probabilities of these two methods of energy dissipation are of comparable magnitudes.

According to Bethe and Heitler[12] the ratio of the energy loss by radiation to that by ionization is given approximately by the ratio

$$EZ/1600\ mc^2,$$

where E denotes the energy of the electron or positron, Z represents the atomic number of the element considered, and the other symbols have their usual meaning. This implies that the multiplication of a shower will continue to a lower energy in lead than in iron.

The increase in the counting rate for the first increments of lead in the iron-lead transition curve are, on this theory, to be associated with the fact that the shower particles which come from the iron are more effective in producing new showers in lead than they would be if they were to penetrate additional iron. We would also expect on this theory that the maximum in the iron-lead transition curve would come at a smaller value of lead thickness than in the air-lead transition curve. Our data indicate that the former occurs at a lead thickness of approximately 1 cm and as already noted the latter occurs at a thickness of about 2 cm of lead. These results are then in qualitative agreement with the multiplication theory.

[12] H. Bethe and W. Heitler, Proc. Roy. Soc. **146A**, 83 (1934).

The Lead-Iron Transition Curve

Observations on the lead-iron transition curve were made at Hickory, North Carolina, at an altitude of approximately 1200 feet. The data shown in Fig. 2 were obtained by counting coincidences with the same apparatus, counter, and material arrangements as shown in the inset of Fig. 1. We have also indicated the air-lead and air-iron transition curves observed at this elevation. The dashed curve of Fig. 2 represents the transition from lead to iron beginning with a thickness of approximately 274 g/cm² of lead. The important features of this curve are the initial decrease in the counting rate for the first increments of added iron, followed by the later rise and complete recovery to the air-iron transition curve.[13]

It is of interest to discuss this curve also in the light of the multiplication theory. As in the former case, we must assume that the particles which are responsible for the penetration of cosmic radiation through large thicknesses of matter generate high energy particles of electronic mass or photons[14] and that such secondary particles generate showers by the usual multiplicative processes. The decrease in the observed number of coincidences for small layers of iron (0–15 g/cm² approximately) beneath the lead is interpreted to mean that the showers from the lower layers of lead decrease in size when they pass into iron.[1] One would expect that the energy of such showers would more likely be dissipated by ionization processes in the iron. The increase in the observed number of coincidences for material thicknesses greater than approximately 290 g/cm² must be due to the production of shower producing radiation in the added layers of iron. Two important factors very probably associated with this increase are the rate at which such secondary particles are generated, and the thickness of matter traversed before their energy is dissipated in a shower. It would seem plausible to assume[10] that the

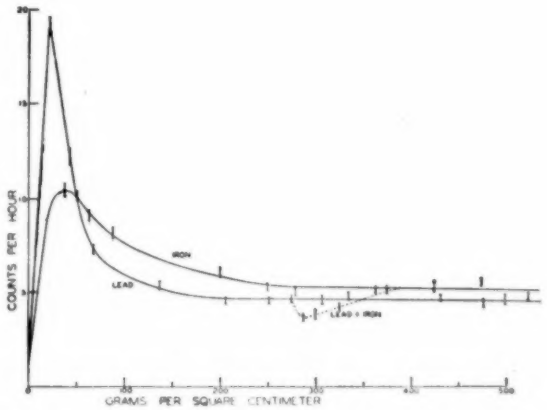

Fig. 2. The frequency of coincidence as a function of material thickness. The dashed curve represents the lead-iron transition under 274 g/cm² of lead.

number of such shower producing particles generated in the same atomic thickness by the penetrating component varies approximately as Z. On the other hand, showers multiply much faster in lead than in iron. It is probable that the longer mean free paths of shower electrons in elements of smaller atomic number more than compensate for the difference in the number of shower producing particles generated in the same atomic thickness. In this way, the intensity of the shower producing radiation increases, and, as the data show, the frequency of coincidences increases with increase in iron thickness to a point characteristic of the air-iron transition curve.

It would appear that all of the results here presented can be interpreted in a qualitative way on the multiplication theory of cosmic-ray showers provided one assumes that particles which are capable of producing showers are generated at large depths of material by the penetrating component of the cosmic radiation.

We are indebted to the Research Council of Duke University for a grant which has made this work possible.

[13] This curve is similar to ionization curves observed by H. Schindler, Zeits. f. Physik **72**, 625 (1931). The fact that such a curve is observed for showers is a point of considerable interest.

[14] The present experiments give no information on certain specific properties of the penetrating component. Thus for example, the data are not inconsistent with the assumption of a decrease in the probability of radiation loss by particles of electronic mass at very high energies although other considerations [L. W. Nordheim, Phys. Rev. **51**, 1110 (1937)] suggest that the radiation theory for electrons and quanta may be valid at high energies.

Note on the Production of Showers in Various Materials

W. M. NIELSEN AND J. E. MORGAN
Duke University, Durham, North Carolina

(Received July 10, 1937)

Data are presented on the increased counting rate due to shower production by layers of equal atomic density for copper, tin and lead. The observed increases of counting rate in the case of these elements are found to vary as a power of the atomic number which is slightly although significantly greater than the second. These results appear qualitatively consistent with our previously reported observations in which the mass per unit area of the producing materials was kept constant for the various elements and for which a dependence on the atomic number of the second power was reported.

DURING the past few years, several papers have been published on the frequency of cosmic-ray shower and Stösse production in various materials.[1–5] Our own measurements[2] indicated the dependence on Z of the observed frequency of shower production to be approximately the second power. In that portion of our work the showers were produced in layers of material having the same mass per square centimeter for each element. The data were then weighted in such a way as to give the relative increases in counting rate per atom, assuming that the increase in each case varied linearly with the number of atoms. In the same paper, however, we also presented evidence showing that the increase in counting rate due to showers, as we observed them, was not a linear function of the thickness of the producing material above the counters for elements of high atomic number such as lead.[6] It is the purpose of the present note to put on record our measurements of shower production in various materials when the number of atoms in the producing layer is maintained equal for each element.

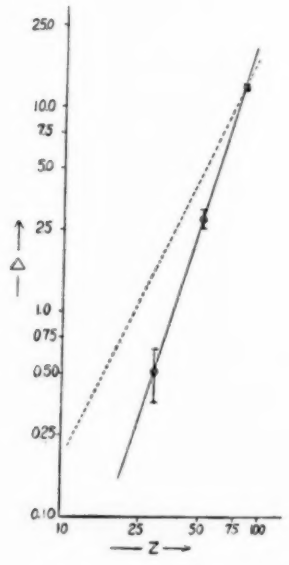

FIG. 1. Increase in counting rate, Δ, as a function of atomic number for layers of copper, tin and lead of equal atomic density.

The same general procedure and counter arrangement (Fig. 1 of reference 2) was followed. As in the previous work, the observations were extended over a considerable period of time in order to reduce the statistical error. The mass of each of the shower producing materials employed in the present experiment was so adjusted as to correspond, in terms of atoms per unit area, to a layer of lead 0.6 cm in thickness. The horizontal area of material above the counters was in all cases 22 cm × 30 cm.

On the curve of Fig. 1 are plotted the respective differences, Δ, between the counting rates due to the background and to each producing material. The dotted line, which has a slope of 2, is included for comparison. These curves indicate that the departure of observed shower production from a simple Z^2 relation is greater than can be accounted for by probable errors. It is of some interest to point out that the observed variation of increased counting

[1] Alocco and Drigo, Ricerca Scient. **5**, 112 (1934).
[2] Morgan and Nielsen, Phys. Rev. **50**, 882 (1936).
[3] C. G. Montgomery and D. D. Montgomery, Phys. Rev. **50**, 490 (1936).
[4] Hu Chien Shan, Proc. Roy. Soc. **158A**, 581 (1937).
[5] J. C. Stearns and D. K. Froman, Contributed Paper No. 13, 215th Meeting American Physical Society.
[6] Since our original publication, Hu Chien Shan (reference 4) has also reported such curves which are concave upwards.

rate with atomic number is appreciably greater in the present data than in that previously reported. This result would appear to be associated with the above noted fact that the increase in counting rate due to showers from the heavier elements, as measured by our arrangement of counters, is not a linear function of the thickness of producing material. This follows because our earlier data were multiplied by the atomic weight to obtain the relative frequency of showers per unit atomic density. Such a procedure would only be accurate if the shower frequency *vs.* thickness curve were linear in each case.

The recent theoretical results of Carlson and Oppenheimer[7] and of Bhabha and Heitler[8] have indicated that the multiplication theory of showers is capable of accounting, in a rough way, for the showers due to the softer component of the general cosmic-radiation. It would appear that such a theory, if correctly applied, can account for a variation of shower production with a second or relatively small power of the atomic number. It is apparently not necessary to assume from such a dependence on atomic number that the showers have their origin in a single act. Any detailed analysis of results such as those herein reported would involve a number of complicating factors. An important one of these factors is the difference in angular spread of the showers from various materials, and its effect on the efficiency of the counting apparatus. Although such a complete analysis is impossible, it appears desirable to record these observations, the results of which are consistent with those of our previous data obtained under identical experimental conditions.

[7] J. F. Carlson and J. R. Oppenheimer, Phys. Rev. **51**, 220 (1937).
[8] H. J. Bhabha and W. Heitler, Proc. Roy. Soc. **159A**, 432 (1937).

SEPTEMBER 15, 1937 PHYSICAL REVIEW VOLUME 52

On Fluctuation Phenomena in the Passage of High Energy Electrons through Lead

W. H. Furry
Research Laboratory of Physics, Harvard University, Cambridge, Massachusetts
(Received June 21, 1937)

It now seems reasonable on both theoretical and experimental grounds to suppose that the formulae of the present radiation theory are valid in the cosmic-ray energy range. The work of Carlson and Oppenheimer and of Bhabha and Heitler has shown that this assumption is capable of accounting for many of the observed features of cosmic-ray absorption and of shower production. These writers concern themselves principally with the mean behavior of a group of electrons and photons moving through matter. Since the fluctuations around this mean behavior are large and for some purposes very important, it is desirable to investigate their nature, even though this involves a loss of accuracy in dealing with other aspects of the situation. In this paper we consider two fluctuation problems: (1) The fluctuations in size of showers produced by single electrons or photons: In dealing with this problem we take the energetic relations into account only very roughly. (2) Fluctuations in energy loss of electrons: The possible production of secondaries is disregarded. The inadequacies in treatment have for both problems the consequence that the results are applicable only to thin layers of heavy substances. The first problem is discussed in Section II. The conclusion is that the distribution in shower sizes should be essentially of the type $P(n;\langle n\rangle) = (\langle n\rangle)^{-1}\{1-(\langle n\rangle)^{-1}\}^{n-1}$, where $\langle n\rangle$ is the mean number; but that under ordinary experimental conditions the number of very small showers should be rather greater than indicated by this law. The results account for two observed phenomena which might at first sight be taken as forming serious objections to the multiplicative hypothesis: First, the occasionally observed production of large showers (~20 or 30 particles) from small thicknesses (~1 cm) of lead; and second, the appearance which many of the larger showers present of having originated at a single point near the bottom of the lead. In Section III we deal with the second problem, with the purpose of providing a way to use energy loss measurements to provide a more detailed check on the theoretical formulae. A method is given for constructing energy loss distribution curves corresponding to any assumed form of the *Bremsstrahlung* spectrum. Also a solution is outlined for the problem of using accurate and detailed information on energy losses to compute an empirical spectrum curve.

I. Introduction

SOME months ago, Anderson and Neddermeyer[1] published the results of a new series of measurements of the energy losses incurred by cosmic-ray electrons in passing through a thin sheet of lead. These results indicate that the formula for the loss of energy by radiative collisions (*Bremsstrahlung*) calculated[2] according to the present radiation theory, is probably obeyed up to primary energies of some hundreds of millions of volts; and on theoretical grounds[3] it is reasonable to suppose that it holds to much greater energies. There is also a strong presumption that the corresponding formula for absorption of photons by pair production[2] is valid in the range of energies of the cosmic rays.

These assumptions make the picture of what happens in the passage of cosmic-ray electrons and photons through matter a quite complicated one. The dominant feature of the process is the rapid decrease in the amount of energy carried by any individual particle, together with a rapid increase in the number of fast electrons and high energy photons present. The events through which these results come about are of an altogether accidental and random character, so that the behavior of such a "multiplicative shower" in any given case may differ widely from the average behavior. The main points to be taken into account in discussing such a situation are accordingly:

(a) Loss of energy by individual particles.
(b) Production of secondary particles.
(c) Fluctuations.

In dealing with so complicated a matter it has been necessary not only to simplify the calculations by using suitable approximations to the theoretical formulae involved, but also to confine attention to certain aspects only. The calculations of Carlson and Oppenheimer[4] and of Bhabha and Heitler,[5] which have shown that this general picture can account for many of the observed facts of cosmic-ray absorption and shower production, were concerned essentially with the treatment of points (a) and (b),[6] the fluctuations being given only slight consideration. The purpose of the present paper is to obtain further evidence about the fluctuations, which is done at the expense of omitting from consideration one or the other of the first two points. Though this may appear a very crude procedure, it is possible to assign physical conditions for which the results should be significant; and the fluctuations are found to be so great that information about them seems comparable in importance with information about the other aspects of the situation.

In Section II the question of fluctuations in the number of particles present in a shower is taken up; that is, the problem is centered about points (b) and (c), point (a) being omitted. Such considerations can be regarded as pertinent only for the case of showers produced in a *small* thickness of a *heavy* material, such as lead: for larger thicknesses the loss of particles by stopping becomes comparable with their production; and in light materials this will be so even at the smallest thicknesses which are capable of occasioning an appreciable production of secondaries. In spite of their limited application, these calculations are of importance because they show to what extent the theory can account for the occasionally observed production of a large shower from a fairly thin layer of lead, which might at first sight seem to be a grave objection against the multiplication hypothesis. The results indicate that the fluctuations are very large indeed, and that the occasional production of showers with several times the expected mean number of particles is quite in accordance with the theory.

In Section III we consider the fluctuations in

[1] C. D. Anderson and S. H. Neddermeyer, Phys. Rev. **50**, 263 (1936).
[2] H. Bethe and W. Heitler, Proc. Roy. Soc. **A146**, 83 (1934); W. Heitler, *The Quantum Theory of Radiation* (Oxford, 1936).
[3] C. F. v. Weizsäcker, Zeits. f. Physik **88**, 612 (1934); E. J. Williams, Phys. Rev. **45**, 729 (1934); D. Kgl. Danske Widensk. Selskab., Math-fys. Meddelelser **13**, 4 (1935).
[4] J. F. Carlson and J. R. Oppenheimer, Phys. Rev. **51**, 220 (1937).
[5] H. J. Bhabha and W. Heitler, Proc. Roy. Soc. **A159**, 432 (1937).
[6] In treating this combination, it is of course necessary to require that the energy lost by the electrons through *Bremsstrahlung* appears as the energy of new light quanta, and that the pairs produced receive the energy of the light-quanta absorbed. The fluctuations in number of particles are neglected in both calculations, the formulae used being concerned only with mean numbers; some account is taken of fluctuations in radiative energy loss, by the use of rough approximations.

radiative energy loss of an electron, leaving out of account the production of secondary electrons. (Points (a) and (c), point (b) omitted.) Here again the results are of interest principally only for a small thickness of a heavy substance: in light substances ionization loss, which cannot be taken into account with any accuracy, is comparable in importance with the radiative loss; and in thicker layers of lead the situation is inevitably obscured by the presence of secondaries. We are thus concerned not with the problem of straggling in range, in which connection such calculations were originally made by Bethe and Heitler, but rather with putting the theory into shape for comparison with energy loss experiments made with thin sheets of lead. The most practical procedure for use with a limited amount of data seems to be to compute the distribution curves for energy losses corresponding to various assumed forms of the *Bremsstrahlung* spectrum; a general method of doing this is developed. At the end of the section a procedure is outlined for solving the converse problem: Given a very large amount of highly accurate energy loss data, to compute the corresponding form of the spectrum.

II. Distribution in Size of Multiplicative Showers

In the calculations of this section we leave out of account the questions of distribution of the particles in energy, and of energy loss; some indication of the probable effects of these considerations on the results will be given at the end of the section. In order for such a treatment to be approximately valid, it is necessary that the primary energy be large compared to the total ionization loss which would be suffered by all the particles of the largest shower to be considered, in traversing a thickness comparable with that in question. This condition is satisfied for primary energies of some hundreds of millions of volts and thicknesses ~ 1 cm Pb, if one wishes to consider showers ranging up to twenty or thirty particles.

Following the notation of Carlson and Oppenheimer,[4] we measure thickness in terms of a variable t, such[7] that $t=1$ corresponds to about 0.5 cm Pb. Then the probability that in traversing thickness dt a high energy electron emits a photon of energy comparable with its own is, very roughly, just dt. The probability that in a thickness dt a high energy photon will produce a positron-electron pair is σdt, with σ equal to about two-thirds.

We solve first a decidedly oversimplified problem, which nevertheless serves to indicate the essential nature of the desired distribution:

Problem A: The probability that in traversing thickness dt one particle is converted into two is just dt. If one particle enters a sheet of thickness t, what is the probability $P(n;t)$ that n particles will emerge?

The probabilities in question satisfy the differential equations

$$\left.\begin{aligned} &(d/dt)P(1;t) = -P(1;t) \\ &(d/dt)P(2;t) = -2P(2;t)+P(1;t) \\ &\quad\cdots\cdots\cdots\cdots \\ &(d/dt)P(n;t) = -nP(n;t) \\ &\qquad\qquad +(n-1)P(n-1;t) \\ &\quad\cdots\cdots\cdots\cdots \end{aligned}\right\} \quad (1)$$

with the boundary conditions

$$P(1;0)=1; \quad P(n;0)=0, \quad n>1. \qquad (2)$$

By successive integration and application of the boundary conditions one obtains

$$P(1;t)=e^{-t}; \quad P(2;t)=e^{-t}(1-e^{-t}); \quad \cdots; \qquad (3)$$

and it is readily established by mathematical induction that

$$P(n;t)=e^{-t}(1-e^{-t})^{n-1}. \qquad (4)$$

The *most probable* number of particles emerging is *one;* the *mean* number is $\langle n\rangle = e^t$. Thus (4) can be written

$$P(n;t)=(\langle n\rangle)^{-1}\{1-(\langle n\rangle)^{-1}\}^{n-1}. \qquad (4')$$

We want the solution to a somewhat different problem:

Problem B: The probability that in dt an electron produces a photon is dt, the electron itself continuing its course; the probability that in dt a photon produces a pair of electrons is σdt, the photon being absorbed. If one electron enters a sheet of thickness t, what is the probability $Q(n;t)$ that n electrons will emerge?

Defining $P(n;m;t)$ as the probability that n

[7] The definition of the variable t is made more precise at the beginning of Section III.

electrons and m photons emerge, one has the differential equations

$$\left.\begin{aligned}
&(d/dt)P(1;0;t) = -P(1;0;t)\\
&(d/dt)P(1;1;t) = -(1+\sigma)P(1;1;t) + P(1;0;t)\\
&(d/dt)P(1;2;t) = -(1+2\sigma)P(1;2;t) + P(1;1;t)\\
&(d/dt)P(3;0;t) = -3P(3;0;t) + \sigma P(1;1;t)\\
&\quad\cdots\cdots\cdots\cdots\cdots\cdots\\
&(d/dt)P(n;m;t) = -(n+m\sigma)P(n;m;t) + nP(n;m-1;t) + (m+1)\sigma P(n-2;m+1;t)\\
&\quad\cdots\cdots\cdots\cdots\cdots\cdots
\end{aligned}\right\} \quad (5)$$

with the boundary conditions

$$P(1;0;0)=1; \quad \text{all other } P(n;m;0)=0. \quad (6)$$

After solving for $P(n;m;t)$, one has

$$Q(n;t)=\sum_{m=0}^{\infty} P(n;m;t). \quad (7)$$

The equations can be solved successively like the first set, without difficulty; but the formulae obtained rapidly become very long, and could scarcely be interpreted except by numerical computation. To carry this through for large values of n would be prohibitively laborious. We shall see that the behavior of $Q(n;t)$ can be obtained more easily.

From (5) and (6) one readily finds for $n=1$:

$$P(1;0;t)=e^{-t}; P(1;1;t)=e^{-t}\sigma^{-1}(1-e^{-\sigma t}); \cdots; P(1;m;t)=(e^{-t}/\sigma^m m!)(1-e^{-\sigma t})^m \quad (8)$$

and on summing,

$$Q(1;t)=e^{-t+[1-\exp(-\sigma t)]/\sigma}. \quad (9)$$

The mean number of photons accompanying the primary if no secondary electrons have been produced is

$$\langle m_1\rangle = \{Q(1;t)\}^{-1}\sum_m mP(1;m;t) = \sigma^{-1}(1-e^{-\sigma t}). \quad (10)$$

Let us also calculate $\langle m_1'\rangle$, the mean number of photons accompanying a primary which has just produced its first pair of secondary electrons. Keeping in mind that the probability of producing this secondary pair is proportional to the number of photons present, we have

$$\langle m_1'\rangle = \{\sum_m mP(1;m;t)\}^{-1}\sum_m m(m-1)P(1;m;t) = \sigma^{-1}(1-e^{-\sigma t}) = \langle m_1\rangle. \quad (11)$$

Thus the mean number of photons belonging to a given electron depends only on the distance the electron has traversed, and not on how many secondaries have been produced by its photons. This makes it possible to formulate the conditions of Problem B in such a way that no explicit reference is made to the photons:

Problem B (restatement): The probability that in dt a given electron will produce a pair is $(1-e^{-\sigma t'})dt$, where t' is the distance the electron has traversed since it was produced or entered the lead. If one electron enters a sheet of thickness t, what is the probability $Q(n;t)$ that n electrons will emerge?

Besides the trivial difference that the secondaries are produced in pairs instead of singly, this formulation differs from Problem A in that an electron's capacity for producing secondaries is not constant, but is zero at the beginning of the electron's path and approaches only asymptotically the constant value assigned to it in Problem A. This dependence on the electron's past history makes the problem much more difficult; it cannot be formulated in terms of ordinary differential equations involving the $Q(n;t)$.[8]

We can use the new formulation to get an expression for $Q(3;t)$. The probability that a secondary pair was produced between t' and $t'+dt'$ and that no other pair was produced is the product of three factors:

(1) The probability that the primary did not produce a pair before reaching t' or after passing $t'+dt'$. Since dt' is infinitesimal, and since the probability of the primary's producing a pair is unaffected by its having already done so, this factor is just $Q(1;t)$.

(2) The probability that the primary did

[8] By introducing the variable $s=\Sigma(1-e^{-\sigma t'})$ and defining $Q(n;s;t)ds$ as the probability that at t there are n electrons and s lies in ds, we can derive the *partial* differential equations

$$\{(\partial/\partial t)+\sigma(n-s)(\partial/\partial s)+(s-\sigma)\}Q(n;s;t)=sQ(n-2;s;t).$$

They seem to be of no particular help in attacking the problem.

produce a pair between t' and $t'+dt'$. This is of course $(1-e^{-\sigma t'})dt'$.

(3) The probability that neither secondary produced a pair in going from t' to t. This is equal to $\{Q(1;t-t')\}^2$. Then, by (9):

$$Q(3;t)=Q(1;t)\int_0^t(1-e^{-\sigma t'})dt'\cdot\{Q(1;t-t')\}^2$$

$$=Q(1;t)e^{2/\sigma}\int_0^t(1-e^{-\sigma t'})dt'e^{-2(t-t')}$$

$$\cdot e^{-(2/\sigma)\exp[-\sigma(t-t')]}.$$

Setting $(2/\sigma)e^{-\sigma(t-t')}=z$, we have

$$Q(3;t)=\tfrac{1}{2}Q(1;t)e^{2/\sigma}\int_{(2/\sigma)e^{-\sigma t}}^{(2/\sigma)}e^{-z}dz$$

$$\cdot(\sigma z/2)^{(2/\sigma)-1}(1-(2/\sigma)e^{-\sigma t}z^{-1}). \quad (12)$$

Thus $Q(3;t)$ is expressed in terms of incomplete gamma-functions. For certain rational values of σ—those which make $(2/\sigma)$ an integer—exponentials suffice. For example, one finds that for $\sigma=1$,

$$Q(3;t)=\tfrac{1}{4}Q(1;t)[e^{2t}\{Q(1;t)\}^2+2e^{-t}-3] \quad (12a)$$

and for $\sigma=\frac{2}{3}$,

$$Q(3;t)=(1/18)Q(1;t)[(2+3e^{-2t/3})e^{2t}$$

$$\cdot\{Q(1;t)\}^2+12\ e^{-2t/3}-17]. \quad (12b)$$

By a similar procedure one can obtain the expressions for $Q(5;t)$, $Q(7;t)$, etc., in terms of multiple integrals; and when $(2/\sigma)$ is an integer, the integrations can be performed in terms of exponentials. This gives a more practicable method for evaluating the $Q(n;t)$ than is provided by Eqs. (5), (6), and (7); but the formulae still increase rapidly in complexity with increasing n, and would require extended numerical computations for their interpretation.

In the case $\sigma=1$ a special method is available for the numerical evaluation of the $Q(n;t)$, and the results suffice to suggest what is almost certainly the form of the answer for other values of σ also. This method depends on the fact that when $\sigma=1$ Problem B differs from Problem A only by our making a distinction between the two kinds of particles (electrons and photons). We then have

TABLE I. *Values of the* q_{nm}.

$n+m$ \ n	1	3	5	7
1	1.00000			
2	1.00000			
3	.50000	.50000		
4	.16667	.83333		
5	.04167	.75000	.20833	
6	.00833	.48333	.50833	
7	.00139	.24861	.66528	.08472
—	—	—	—	—

$$Q(n;t)=\sum_{m=0}^{\infty}q_{nm}P(n+m;t), \quad (13)$$

where the $P(l;t)$ are given by (4), and q_{nm} is the probability that if there are $n+m$ particles, n are electrons. The q_{nm}'s satisfy the relations

$$q_{nm}=nq_{n,\,m-1}/(n+m-1)$$

$$+(m+1)q_{n-2,\,m+1}/(n+m-1) \quad (14)$$

with the boundary condition

$$q_{10}=1, \quad q_{01}=0. \quad (15)$$

Table I shows the values of a few of the q_{nm}. Its manner of construction by the use of (14) is obvious. Each row of entries is computed from the preceding row, and a check is provided by the fact that the sum across each row is unity. Such a table was prepared extending to $n+m=50$, and was used together with (4) and (13) to compute the $Q(n;t)$ for $\sigma=1$.

The results are summarized in Table II. Only

TABLE II. ($\sigma=1$.)

n	$Q(n;1)$	$\rho_n(1)$	$Q(n;1.5)$	$\rho_n(1.5)$	$Q(n;2)$	$\rho_n(2)$	$Q(n;2.5)$	$\rho_n(2.5)$
1	0.69220	—	0.48523	—	0.32132	—	0.20555	—
3	.22083	.3190	.26389	.5439	.23356	.7269	.17649	.8586
5	.06257	.2833	.12911	.4893	.15388	.6588	.13796	.7817
7	.01755	.2805	.06268	.4855	.10071	.6545	.10719	.7770
—	—	—	—	—	—	—	—	—
Limit	—	.2802	—	.4852	—	.6542	—	.7767

a few entries have to be given, for the reason that the quantities

$$\rho_n(t)=Q(n;t)/Q(n-2;t) \quad (16)$$

very rapidly approach a constant limiting value. The distribution for Problem B, $\sigma=1$, is thus of almost exactly the same type as for Problem A.

It is somewhat embarrassing to have such a simple behavior turn up, without being able to give an abstract proof that it should. The writer has devoted considerable time and thought to various attempts to obtain such a proof, but without success. At any rate, for $\sigma=1$ the simple behavior does appear, and the assumption that it holds for other values of σ is very plausible: it is owing to the qualitative difference between Problem B—cf. especially the second formulation—and Problem A, and not to the particular value of σ, that one would have expected any decided departure from the simple type of distribution.

The validity of this assumption for $\sigma=\frac{2}{3}$ was tested by the following procedure: $Q(1;t)$ and $Q(3;t)$ were computed from Eqs. (9) and (12b). The rest of the distribution was approximated by setting

$$Q^*(3+2l;t)=\rho^l Q(3;t) \tag{17}$$

and determining ρ from the requirement that the sum of all the probabilities be unity:

$$\begin{aligned} &Q(1;t)+Q(3;t)/(1-\rho)=1;\\ &\rho=1-Q(3;t)/\{1-Q(1;t)\}. \end{aligned} \tag{18}$$

This approximate distribution was then used to calculate approximate values of $\langle n\rangle$, the mean number of electrons emerging, and $\langle n^2\rangle$, the mean square. One obtains

$$\langle n\rangle \leqq 1+2Q(3;t)/(1-\rho)^2, \tag{19}$$

$$\begin{aligned} \langle n^2\rangle \leqq Q(1;t)+\{Q(3;t)/(1-\rho)\}\\ \times[9+16\rho/(1-\rho)+8\{\rho/(1-\rho)\}^2]. \end{aligned} \tag{20}$$

These values were then checked against the exact values of these quantities, which satisfy the equations:

$$(d/dt)\langle n\rangle=2\sigma\langle m\rangle;\quad (d/dt)\langle m\rangle=\langle n\rangle-\sigma\langle m\rangle, \tag{21}$$

$$\left.\begin{aligned} &(d/dt)\langle n^2\rangle=4\sigma\langle nm\rangle+4\sigma\langle m\rangle\\ &(d/dt)\langle nm\rangle=\langle n^2\rangle-\sigma\langle nm\rangle+2\sigma\langle m^2\rangle-2\sigma\langle m\rangle\\ &(d/dt)\langle m^2\rangle=2\langle nm\rangle-2\sigma\langle m^2\rangle+\langle n\rangle+\sigma\langle m\rangle \end{aligned}\right\} \tag{22}$$

and the boundary conditions

$$\langle n\rangle=\langle n^2\rangle=1,\ \langle m\rangle=\langle nm\rangle=\langle m^2\rangle=0,\ \text{at } t=0. \tag{23}$$

Here as usual m denotes number of photons. From (21), (22), (23) one finds, for $\sigma=\frac{2}{3}$:

$$\langle n\rangle=0.63867e^{0.86852t}+0.36133e^{-1.53518t}; \tag{24}$$

$$\begin{aligned} \langle n^2\rangle=0.79065e^{1.73704t}-0.15073e^{0.86852t}\\ -0.46156e^{-0.66667t}+0.63351e^{-1.53518t}\\ +0.18813e^{-3.07036t}. \end{aligned} \tag{25}$$

The results of the computation are shown in Table III. Values calculated from (19) and (20) are indicated by the sign $\leqq$, the exact values from (24) and (25) by $=$. It is seen that the agreement is good. The increasing discrepancy for larger values of t is presumably due to the increasing importance of slight differences between ρ and the actual limiting ratio; obviously their effect would be most pronounced in the case of $\langle n^2\rangle$. To check this supposition, an alternative calculation was made for $t=2.5$: The approximation (17) was replaced by

$$Q^*(5+2l;t)=\rho^l Q^*(5;t), \tag{17'}$$

and $Q^*(5;t)$ and ρ were determined by the requirements that the sum of all probabilities be unity and that $\langle n\rangle$ receive its correct value as given by (24). The results were:

$$Q^*(5;t)=.15766,\quad \rho=.68426,\quad \langle n^2\rangle\leqq 59.506.$$

The agreement with the exact value of $\langle n^2\rangle$ is now very good, and the difference between the ρ of Table III and the new ρ is seen to be of the same order of magnitude as those between ρ_5 and the limiting ρ in Table II.

Photon-produced showers: Problem B'.—Keeping the essential postulates of Problem B fixed, we may ask: *If one photon enters a sheet of*

TABLE III. ($\sigma=\frac{2}{3}$.)

t	1.0	1.5	2.0	2.5
$Q(1;t)$	0.76328	0.57590	0.40845	0.27712
$Q(3;t)$	.18664	.25882	.26284	.22354
ρ	.21240	.38972	.55568	.69076
$\langle n\rangle\leqq$	1.6005	2.3898	.36628	5.6753
$\langle n\rangle=$	1.6000	2.3861	.36447	5.6087
$\langle n^2\rangle\leqq$	4.0564	10.110	24.971	61.473
$\langle n^2\rangle=$	4.0403	10.045	24.565	59.411

TABLE IV. ($\sigma=1$.)

n	$R(n;1)$	$\rho_n(1)$	$R(n;1.5)$	$\rho_n(1.5)$	$R(n;2)$	$\rho_n(2)$	$R(n;2.5)$	$\rho_n(2.5)$
0	0.36788	—	0.22313	—	0.13534	—	0.08208	—
2	.46728	1.2702	.41604	1.8646	.31377	2.3185	.21631	2.6354
4	.11876	.2542	.18600	.4471	.19079	.6081	.15693	.7255
6	.03316	.2792	.09000	.4839	.12453	.6527	.12164	.7751
8	.00929	.2801	.04366	.4851	.08146	.6541	.09447	.7766
—	—	—	—	—	—	—	—	—
Limit	—	.2802	—	.4852	—	.6542	—	.7767

TABLE V. ($\sigma=\frac{2}{3}$, *photon-produced showers.*)

t	1.0	1.5	2.0	2.5
$\langle n\rangle \leqq$	1.2024	1.9844	3.1166	4.8086
$\langle n\rangle =$	1.2026	1.9856	3.1252	4.8526
$\langle n^2\rangle \leqq$	3.5609	8.624	20.612	48.642
$\langle n^2\rangle =$	3.5628	8.647	20.826	50.077

lead t units thick, what is the probability $R(n;t)$ that n electrons emerge?

Beginning with the case $\sigma=1$, we have

$$R(n;t)=\sum_{m=0}^{\infty} r_{nm}P(n+m;t), \qquad (13')$$

where the r_{nm} obey the same relations (14) as do the q_{nm}, but with the boundary conditions

$$r_{10}(0)=0, \quad r_{01}(0)=1. \qquad (15')$$

Obviously $R(0;t)=e^{-t}$: this follows also because (14) and (15′) give $r_{0m}=0$ for $m>1$. By constructing a table of the r_{nm} similar to that of the q_{nm} (cf. Table I), the results given in Table IV were computed. (Here $\rho_n=R(n;t)/R(n-2,t)$.) It is seen that the sequences, apart from their first terms $R(0;t)$, approach very rapidly to a geometric progression just as do the $Q(n;t)$; and the limiting values of the ratios are the same as for the $Q(n;t)$.

By a procedure analogous to that leading to (12b), one finds that, for $\sigma=\frac{2}{3}$:

$$\left.\begin{aligned} R(2;t)&=(1/9)R(0;t)[(1+3e^{-2t/3})e^{2t}\\ &\qquad\cdot\{Q(1;t)\}^2-4]\\ R(4;t)&=(1/108)R(0;t)[(1+6e^{-2t/3}\\ &\quad+6e^{-4t/3})e^{4t}\{Q(1;t)\}^4-12(1+3e^{-2t/3}\\ &\qquad-4e^{-4t/3})e^{2t}\{Q(1;t)\}^2-13]\end{aligned}\right\} \qquad (26)$$

where $Q(1;t)$ is as defined by (9). If we approximate the rest of the distribution by setting

$$R^*(4+2l;t)=\rho^l R(4;t), \qquad (27)$$

where ρ is determined by requiring that the sum of all probabilities be unity, we can compute approximate values for $\langle n\rangle$ and $\langle n^2\rangle$. Exact values can be computed by integrating (21) and (22) under the boundary conditions

$$\langle n\rangle=\langle n^2\rangle=\langle nm\rangle=0, \ \langle m\rangle=\langle m^2\rangle=1, \text{ at } t=0. \qquad (23')$$

The comparison of the results is given in Table V. It is seen that the agreement is good.

These considerations make it practically certain that the answers to both Problem B and Problem B′ form sequences which rapidly approach the form of a geometrical progression. Lumping together the electron-produced and photon-produced showers, we may say that the law of distribution of shower size should be essentially

$$P(n;\langle n\rangle)=(\langle n\rangle)^{-1}\{1-(\langle n\rangle)^{-1}\}^{n-1}. \qquad (4')$$

This law may be compared with the usual Poisson law for independent events,

$$P_{\text{ind}}(n;\langle n\rangle)=\{(\langle n\rangle)^n/n!\}e^{-\langle n\rangle}. \qquad (28)$$

The Poisson law is applicable to many distribution problems of physical interest, and Bhabha and Heitler[5] assert that it should hold in the present case. Their argument is based on the assumption that the occurrences of particles in various infinitesimal energy ranges may be regarded as independent events; actually these events are not independent, because some of the particles have produced others, and their chance of doing so depends both upon their original energy and upon the energy lost.

The two distributions (4′) and (28) for $\langle n\rangle=5$ are compared in Fig. 1. It is seen that the fluctuations given by (4′) are large and important; the mean value is not marked by any particular feature of the curve, while the curve given by (28) has a well-defined maximum. In

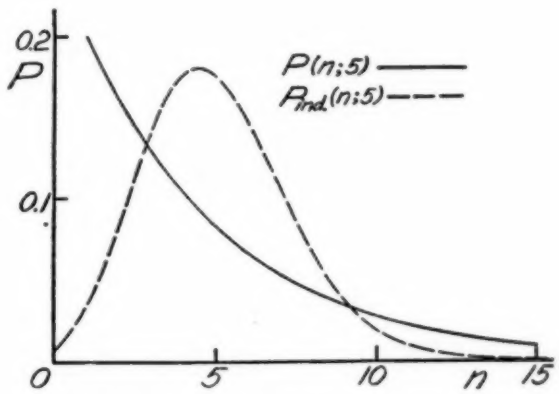

FIG. 1. The distribution law (4′) compared with the Poisson law, for $\langle n\rangle=5$. The functions in question have significance only for integral values of the abscissa, but for convenience continuous curves are plotted.

comparing the probabilities for large showers it is more convenient to consider the quantity

$$S(l;\langle n\rangle)=\sum_{j=l}^{\infty}P(j;\langle n\rangle),$$

which gives the probability for the appearance of l or more electrons. This function, for $\langle n\rangle=5$, together with the corresponding function $S_{\text{ind}}(l;\langle n\rangle)$ given by (28), is plotted in Fig. 2.

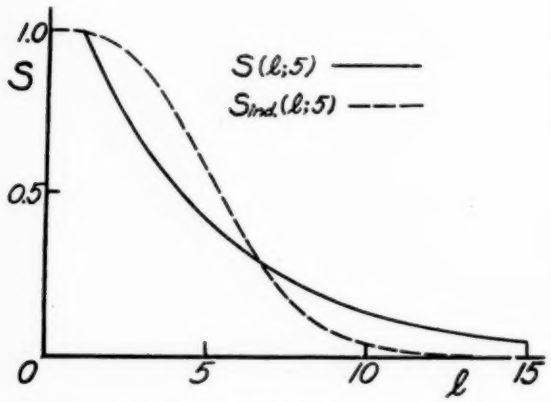

FIG. 2. Total probability for l or more particles according to (4′) and (28), for $\langle n\rangle=5$. As in Fig. 1, smooth curves are plotted although only discrete points are defined.

The quantities $S_{\text{ind}}(l;\langle n\rangle)$ decrease very rapidly with increasing l; one finds

$$S(15;5)=0.044;\quad S_{\text{ind}}(15;5)=0.0002.$$
$$S(20;5)=\ .014;\quad S_{\text{ind}}(20;5)=\ .0000004.$$

The results of some cloud chamber observations on shower sizes were published some time ago by Street and Stevenson.[9] The number of showers observed was rather small, and the results are not corrected for the selective character of the apparatus. Within these limitations, there is qualitative agreement with the type of distribution here suggested. For a thickness of 1.3 cm Pb ($\langle n\rangle\sim5$), 8 out of 107 showers observed contained more than 10 electrons, and 4 had more than 15 electrons.

A more extended investigation is being carried on in this laboratory by Mr. L. M. Fussell. Results so far obtained, corrected in a reasonable way for the selectivity of the apparatus, are in fairly good agreement with a formula of the type (4′). There seems to be an appreciable excess of simple pairs over the number expected from this expression; a plausible reason for this is indicated below.

[9] J. C. Street and E. C. Stevenson, Phys. Rev. **49**, 425 (1936).

Energy considerations

As explained at the beginning of this section, the most important consequence of our having left out of account the energy losses and energy interchanges of the particles is that the pertinence of the results is strictly limited to the case of thin layers of heavy substances. It is possible to estimate qualitatively the nature of some of the effects which consideration of this neglected aspect of the situation would have on our results:

(1) Unless the primary has quite a high energy —some hundreds of millions of volts—there will simply not be enough energy to produce more than a few particles. Thus unless some way of selecting high energy primaries is used, there will be a preponderance of pairs and small showers over and above that indicated by (4′).

(2) Our neglect of the detailed distribution of energy among the particles made it necessary to use a very crude approximation to the law of photon production by *Bremsstrahlung:* we set the probability that in dt an electron produce a photon "of energy comparable with its own" equal to dt. A much better approximation[4] to the *Bremsstrahlung* formula is obtained if we set as the probability that in dt an electron produce a photon of energy between k and $k+\Delta k$,

$$P dt\Delta k=dt\Delta k/k. \tag{28a}$$

This makes the probability that in dt an electron produce a photon whose energy equals or exceeds $(1/q)$ of the original energy of the electron equal to $\ln q\cdot dt$. The full consequences of the more accurate law (28a) could of course be worked out only in a treatment which took account of the detailed energy distribution; two consequences would presumably be roughly as follows:

(a) For a high energy primary, or other particle with many times the energy of an average "low energy" shower particle, $\ln q$ may be several times our estimated value of 1. Such a particle will thus be unusually effective in producing secondaries. It seems likely that the main effect of this will be to increase the *mean*

number of particles produced, without changing the *type* of distribution. From our present point of view the high energy primary is to be regarded as equivalent to a number of primaries; the composition of a number of distributions (4′) does not give one of the exact form (4′), but the general behavior is the same.

(b) The mean population of photons accompanying each electron consists not only of the number $\langle m_1 \rangle$ of high energy photons given by (10), but also of a number of lower energy photons, which are capable of producing pairs. These pairs are not able to play the same role as the particles we have been considering, by producing further secondaries, and are usually stopped a short distance beyond the point where they are produced; but an emergent shower will often contain some of them. Having been produced only a short distance back from the point of emergence, and tending to diverge widely because of their low energies, they help to give many showers an appearance of coming from a single center near the bottom of the lead. This effect, which has been of some importance in discouraging the adoption of the multiplicative hypothesis, is also already partly explained by our unmodified formula (4′): The probability of there being 10 or more electrons at $\frac{3}{4}$ cm Pb ($\langle n \rangle \sim 2.25$) is about 0.005; the probability for 10 or more electrons at 1 cm ($\langle n \rangle \sim 3.5$) is about 0.05. Thus any large shower is likely to consist largely of particles from the last millimeter or two of the lead.

Considerations of the fluctuations in number of particles produced have accordingly led us to a formula indicating the general type of distribution of shower sizes to be expected, and have shown how the multiplicative hypothesis can account for two effects—the appearance of large showers from fairly thin pieces of lead, and the apparent divergence of showers from a point—which at first sight might be regarded as strong evidence against it.

III. Distribution in Fractional Energy Loss

The probability that in penetrating dx centimeters of lead an electron of energy E will emit a photon of energy between k and $k+dk$ is

$$Pdxdk = Kdx \cdot I(E/mc^2,\ k/E)dk/k. \qquad (29)$$

The total mean loss by radiation is then

$$dx \cdot \int_0^E Pkdk = KEdx \cdot \int_0^1 Id(k/E). \qquad (30)$$

Here KI is the spectral intensity of the *Bremsstrahlung*. According to the calculations of Bethe and Heitler,[3] KI is practically independent of E/mc^2 for energies above 100 mc^2 (5×10^7 volts). If we choose the two factors so that

$$\int_0^1 Id(k/E) = 1, \qquad (31)$$

then K is numerically equal to 2. Thus by using the variable t, which we introduced without much comment at the beginning of Section II, we have $Kdx = dt$. The mean total rate of energy loss of an electron in lead is then

$$-(dE/dt)_{Av} = E+\beta, \qquad (32)$$

where $\beta \leqq 6\times10^6$ volts is the ionization loss per unit thickness. From this equation we see that for a large number of high energy electrons whose energies before and after traversing thickness t are E_0 and E, respectively,

$$[(E+\beta)/(E_0+\beta)]_{Av} = e^{-t}. \qquad (33)$$

The results of Anderson and Neddermeyer[1] on mean energy loss are in reasonably good agreement with this formula.

The question of fluctuations in energy loss can be approached from either of two points of view:

(1) *The "straggling problem":* The form of the spectrum $I(k/E)$ being given, to determine the probability $P(t; E)dE$ that an electron has energy between E and $E+dE$, if before passing through the thickness t it had energy E_0.

(2) *The "spectrum problem":* Given the experimental distribution in energy loss of a large number of electrons, to determine the corresponding form of the spectrum $I(k/E)$.

For the solution of either problem, two approximations seem to be indispensable: First, it is assumed that the form of the spectrum and the total intensity $\int_0^1 Id(k/E)$ are independent of the energy E; second, the ionization loss is neglected. Both of these approximations are justified if the only energies considered are of the order of some tens of millions of volts. They

break down, however, when we have to consider particles which are stopped, or even only slowed down to energies of a few million volts. What we have called the "straggling problem" is hence not adapted to any really accurate treatment of straggling in range, but is rather to be regarded simply as the converse of the "spectrum problem." For convenience in dealing with it we introduce a variable

$$\lambda = \ln\,(E_0/E) \tag{34}$$

and a probability function in the scale of λ:

$$P(t;E)dE = w(t;\lambda)d\lambda = P(t;E)E_0 e^{-\lambda}d\lambda. \tag{35}$$

The "straggling problem" was solved by Bethe and Heitler[10] for the case

$$I(k/E) = -(k/E\,\ln\,2)/\ln\,(1-k/E). \tag{36}$$

This is a rather rough approximation to the theoretical spectrum curve,[11] giving too much intensity for small (k/E) and too little for larger (k/E)—hence underemphasizing the fluctuations. Using (36), one can verify[10] by using the functional equation,

$$w(t_1+t_2;\lambda)d\lambda = d\lambda\int_0^\lambda w(t_1;\lambda_1)w(t_2;\lambda-\lambda_1)d\lambda_1, \tag{37}$$

that

$$w(t;\lambda)d\lambda = e^{-\lambda}\lambda^{-1+t/\ln 2}d\lambda/\Gamma(t/\ln 2). \tag{38}$$

We now proceed to show how $P(t;E)$ can be found for any spectrum which can be expressed as a power series,

$$I(k/E) = \sum_{j=0}^{\infty} a_j(1-k/E)^{\alpha+j}, \quad \alpha > -1, \tag{39}$$

or as a sum of a number of such series with different values of α. We begin by finding $P(t;E)$ for a spectrum of the form

$$I(k/E) = b_q I_q(k/E) = (b_q k/E)(1-k/E)^q, \quad q > -1. \tag{40}$$

For this spectrum, the probability that in dt an electron's energy changes from ϵ to a value in the range E to $E+dE$ is

$$\begin{aligned} P_{\text{Rad.}}(dt,\ \epsilon\to(E,E+dE)) &= \{dtdE/(\epsilon-E)\}\cdot b_q I_q(1-E/\epsilon) \\ &= b_q E^q \epsilon^{-q-1}dtdE. \end{aligned} \tag{41}$$

Then $P(t;E)$ satisfies the equation

$$\frac{\partial P}{\partial t} = b_q\int_E^{E_0} E^q\epsilon^{-q-1}P(t;\epsilon)d\epsilon - b_q P(t;E)\int_0^E \epsilon^q E^{-q-1}d\epsilon, \tag{42}$$

which by differentiation reduces to

$$\frac{\partial^2 P}{\partial E\partial t} - qE^{-1}\frac{\partial P}{\partial t} + \{b_q/(q-1)\}\left\{\frac{\partial P}{\partial E} + E^{-1}P\right\} = 0. \tag{43}$$

Introducing the new variable λ by (34), we have:

$$\frac{\partial^2 P}{\partial\lambda\partial t} + q\frac{\partial P}{\partial t} + \{b_q/(q-1)\}\left\{\frac{\partial P}{\partial\lambda} - P\right\} = 0. \tag{44}$$

On making the Laplace transformation,

$$P = \frac{1}{2\pi i}\int_C e^{\lambda z}F(t;z)dz, \tag{45}$$

we see that (44) is satisfied provided

$$(z+q)(\partial F/\partial t) + \{b_q/(q+1)\}(z-1)F = 0. \tag{46}$$

The solution of (42) is then

$$P(t;E) = (1/2\pi iE_0)\int_C \varphi(z)\cdot\exp\,[\lambda z + b_q t\{(z+q)^{-1} - (1+q)^{-1}\}]dz, \tag{47}$$

$$P(t;E) = (1/2\pi iE_0)\int_C \varphi(z)\cdot\exp\,[\lambda z + b_q t\{(z+q)^{-1} - (1+q)^{-1}\}]dz, \tag{47}$$

where the contour C and the function $\varphi(z)$ may be varied to fit the boundary condition at $t=0$.

Now our general spectrum (39) can be written as a sum of spectra of the form (40):

$$I(k/E) = \sum_{j=0}^{\infty} a_j(1-k/E)^{\alpha+j} = \sum_{j=0}^{\infty} b_{\alpha+j}I_{\alpha+j}(k/E), \tag{48}$$

with

$$b_{\alpha+j} = \sum_{l=0}^{j} a_l. \tag{49}$$

[10] Bethe and Heitler, reference 2, p. 101; Heitler, reference 2, p. 225.

[11] The comparison between the theoretical curves and (36) is given in reference 5, Fig. 1. The normalizing factor of (36) relative to the other curves is smaller than ours by about twelve percent. This figure also gives the straight line (28′), with the same difference in normalization.

The essential thing to be remembered at this point is that our fixed spectra assign definite probabilities to given *fractional losses* of energy, independently of the actual value of the energy. The order in which such fractional losses may occur is entirely immaterial. Thus it makes no difference whether the electron is regarded as having passed through thickness t of a substance whose *Bremsstrahlung* spectrum is

$$I_n=\sum_{j=0}^{n} b_{\alpha+j} I_{\alpha+j},$$

or as having passed successively through thicknesses t of substances having the spectra $b_\alpha I_\alpha$, $b_{\alpha+1}I_{\alpha+1}$, $\cdots$, $b_{\alpha+n}I_{\alpha+n}$. We can, accordingly, evaluate the energy distribution by using (47) to define the distributions P_j corresponding to the spectra $b_{\alpha+j}I_{\alpha+j}$ and applying the boundary conditions

$$P_0(0;E)=\delta(E-E_0);\ P_1(0;E)=P_0(t;E);\ \cdots;\ P_n(0;E)=P_{n-1}(t;E). \quad (50)$$

The form of (48) is such that the boundary conditions (50) are easily satisfied. The first of these conditions is satisfied by $\varphi=1$ if C is taken to be a path extending along the imaginary axis from $-i\infty$ to $i\infty$; we agree to deform the path if necessary to insure its passing to the right of the singularity at $-\alpha$. The rest of the boundary conditions are satisfied if we obtain each P_l from P_{l-1} by inserting an additional term in the exponent in the integrand. In the limit $n\to\infty$, I_n becomes the given spectrum (48), and the desired solution is accordingly

$$P(t;E)=(1/2\pi iE_0)\int_C e^{\lambda z+tf(z)}dz \quad (51)$$

with

$$f(z)=\sum_{j=0}^{\infty} b_{\alpha+j}\{(z+\alpha+j)^{-1}-(1+\alpha+j)^{-1}\}. \quad (52)$$

The series (52) converges for all values of z except $z=-\alpha-j$, provided Σa_j converges, which is true for any function I which remains finite for $(k/E)\to 0$. If our spectrum is given not as a single series of the form (39), but as a sum of such expressions, we have only to replace $f(z)$ in (51) by the sum of the corresponding expressions of the form of (52).

Equation (51) therefore gives us a complete formal solution of the "straggling problem." For computing actual values of $P(t;E)$ from (51), the only feasible procedure seems to be the saddle-point method.[12] This gives the asymptotic series

$$P(t;E)=At^{-\frac{1}{2}}e^{\varphi t}\{1+\delta_1/t+\delta_2/t^2+\cdots\} \quad (53)$$

with

$$A=(2\pi f''(\zeta))^{-\frac{1}{2}},\quad g=(\lambda/t)\zeta+f(\zeta),$$
$$\delta_1=-(5/24)\{f'''(\zeta)\}^2/\{f''(\zeta)\}^3+(\tfrac{1}{8})f^{\mathrm{IV}}(\zeta)/\{f''(\zeta)\}^2, \quad (54)$$

and so on; here ζ is the coordinate of the saddle-point, defined by

$$\lambda/t=-f'(\zeta). \quad (55)$$

The quantities (54) are thus all functions of λ/t only.

The distribution (51), (53) has been obtained for the spectrum[11]

$$I(k/E)=1, \quad (28')$$

which corresponds to the approximation (28) mentioned near the end of Section II. This spectrum gives less than the theoretical intensity for small (k/E) and more for larger (k/E), and hence overemphasizes the fluctuations; accordingly we may regard the distribution obtained from (28′) and that obtained from (36) as placing limits on the expected distribution. (28′) is used for some purposes both by Carlson and Oppenheimer[4] and by Bhabha and Heitler.[5]

Using (28′) one finds that[13]

$$f(z)=-\gamma-(d/dt)\ln\Gamma(z)=-\gamma-\Psi(z);\quad \gamma=.577216. \quad (56)$$

The $\Psi(z)$ function and its derivatives have been tabulated very fully.[14] The values of A, g, and δ_1 are given in Table VI. $|\delta_2|$ nowhere takes values greater than about 0.005, while $|\delta_3|$ sometimes exceeds 0.01. Hence one uses only the correction δ_1/t, and the results are presumably in error by less than $0.005t^{-2}$.

[12] Courant-Hilbert, *Methoden der Math. Physik*, second edition (Springer, 1931), p. 455.

[13] Whittaker and Watson, *Modern Analysis*, fourth edition, p. 241.

[14] H. T. Davis, *Tables of the Higher Mathematical Functions*, Vols. I and II (The Principia Press. Bloomington, Indiana).

In Fig. 2 distribution curves $E_0P(t;E)$ plotted against E/E_0 are shown for the thickness[15] $t=0.693$ and for three different spectra:

Curve 1, given by (38), for the spectrum (36).
Curve 2, given by Table VI, for the spectrum (28′).
Curve 3, for the spectrum

$$I(k/E)=2(k/E). \tag{57}$$

Carlson and Oppenheimer at one point in their calculations are obliged to make an approximation which is equivalent to using this spectrum. It badly overemphasizes the fluctuations. For this spectrum, (51) can be evaluated analytically, the result being

$$P(t;E)=e^{-2t}\{\delta(E-E_0)+E_0^{-1}(2t/\lambda)^{\frac{1}{2}}I_1(2[2t\lambda]^{\frac{1}{2}})\}. \tag{57′}$$

For this particular thickness curve 1, which underemphasizes the fluctuations, is simply a straight line; for smaller thicknesses it would show a singularity for $(E/E_0)=1$ and a zero for $(E/E_0)=0$, and *vice versa* for greater thicknesses. Curve 2, which overemphasizes the fluctuations, has a singularity at each end; for $t>1$ it would show a zero at $(E/E_0)=1$. The behavior of curve 2 near $(E/E_0)=1$ is in fact given by

$$E_0P(t;E)\doteq(2\pi t)^{-\frac{1}{2}}e^{t(1-\gamma)}(\lambda/t)^{t-1}\cdot(1-1/12t+\cdots),\quad \lambda\ll 1, \tag{56′}$$

as one finds on making suitable approximations to $\Psi(\zeta)$ and its derivatives. In curve 3 the fluctuations are enormously greater than the upper limit given by curve 2; one-fourth of the distribution is contained in a δ-function singularity at $(E/E_0)=1$.

The spectrum problem

For the comparison of limited amounts of energy loss data with theoretical predictions, the use of calculated distribution curves—such as those of Fig. 1—for a few simple cases should suffice; in fact, the data so far published[1] provide only material for comparison with Eq. (33), which gives just the mean loss. It is, however, of some interest to investigate the possibility of using a large amount of very accurate data to give a detailed check on the theory. This can most readily be done by considering the problem already mentioned at the beginning of this section: Given (empirically) the distribution $P(t;E)$, to find the spectrum $I(k/E)$.

This problem can be solved by obtaining a relation between the moments of the energy distribution,

$$\{(E/E_0)^n\}_{Av}=\int_0^{E_0}(E/E_0)^nP(t;E)dE=\int_0^{\infty}P(t;E)E_0e^{-(n+1)\lambda}d\lambda, \tag{58}$$

and those of the spectrum:

$$\mu_n=\int_0^1(1-k/E)^nI(k/E)d(k/E). \tag{59}$$

By (51) and (58) we obtain

$$\{(E/E_0)^n\}_{Av}=-(1/2\pi i)\int_C(z-n-1)^{-1}e^{tf(z)}dz. \tag{60}$$

In all cases where I does not vanish for $(k/E)\to 0$, one can show that $f(z)\to-\infty$ as $z\to\infty$, $|\arg z|\leq\pi/2$. Thus the expression (60) equals just the residue at $z=n+1$:

$$\{(E/E_0)^n\}_{Av}=e^{tf(n+1)}. \tag{61}$$

Using (52) and (49), we obtain

$$f(n+1)=\sum_{l=0}^{\infty}a_l\sum_{j=l}^{\infty}\{(n+1+\alpha+j)^{-1}-(1+\alpha+j)^{-1}\}=-\sum_{l=0}^{\infty}a_l\sum_{j=0}^{n-1}(1+\alpha+l+j)^{-1},\quad n\geq 1. \tag{62}$$

On the other hand one has by (39) and (59):

$$\mu_n=\sum_{l=0}^{\infty}a_l/(1+\alpha+l+n). \tag{63}$$

Accordingly,

$$\ln\{(E/E_0)^n\}_{Av}-\ln\{(E/E_0)^{n+1}\}_{Av}=t\mu_n. \tag{64}$$

This solves the problem of obtaining the moments of the spectrum in terms of those of the energy-loss distribution.

[15] This is approximately equal to the thickness (0.35 cm of lead) used by Anderson and Neddermeyer (reference 1); it makes $(E/E_0)_{Av}=\frac{1}{2}$, and not very many of the particles produce secondary pairs. The error δ_2/t^2 in curve 2 is about one percent.

This same result (64) can be obtained by integrating the diffusion equations for $\{(E/E_0)^n\}_{Av}$. These may be shown to be

$$(d/dt)\{(E/E_0)\}_{Av}+\{(E/E_0)\}_{Av}=-(\beta/E_0)$$
$$(d/dt)\{(E/E_0)^2\}_{Av}+(1+\mu_1)\{(E/E_0)^2\}_{Av}$$
$$=-2(\beta/E_0)\{(E/E_0)\}_{Av}$$
$$\cdots\cdots\cdots\cdots\cdots\cdots \quad (65)$$
$$(d/dt)\{(E/E_0)^n\}_{Av}$$
$$+(1+\mu_1+\cdots+\mu_{n-1})\{(E/E_0)^n\}_{Av}$$
$$=-n(\beta/E_0)\{(E/E_0)^{n-1}\}_{Av}.$$

Neglecting the right-hand members, we at once get (64). At first sight one is tempted to suppose that by integrating without this neglect one could give a correct account of the effect of ionization loss. This is not so, for the construction of (65) corresponds to letting particles acquire negative energies after being stopped, instead of discarding them from the distribution (e.g., $(E)_{Av}\rightarrow-\beta$ for $t\rightarrow\infty$). The problem of allowing correctly for ionization seems to be a very difficult one; it would in any case not be consistent to do so while retaining the approximation of a *Bremsstrahlung* spectrum independent of the energy.

There is apparently no way to obtain the spectrum $I(k/E)$ itself from the values of the μ_n except by direct numerical computation. The most elegant available method seems to be the use of an expansion in Legendre polynomials.

TABLE VI.

λ/t	A	g	δ_1
0.2	1.9980	−1.0878	−0.0848
0.4	1.0035	− .2953	−.0881
0.6	.6736	.1983	−.0912
0.8	.5091	.5746	−.0934
1.0	.4108	.8840	−.0945
1.2	.3451	1.1503	−.0950
1.4	.2990	1.3862	−.0950
1.6	.2643	1.5996	−.0942
1.8	.2367	1.7952	−.0932
2.0	.2151	1.9768	−.0920
2.2	.1973	2.1466	−.0908
2.6	.1698	2.4584	−.0884
3.0	.1496	2.7407	−.0860
3.4	.1340	3.0003	−.0836
3.8	.1217	3.2421	−.0812
4.2	.1116	3.4691	−.0788
4.6	.1032	3.6827	−.0764
5.0	.0962	3.8861	−.0740

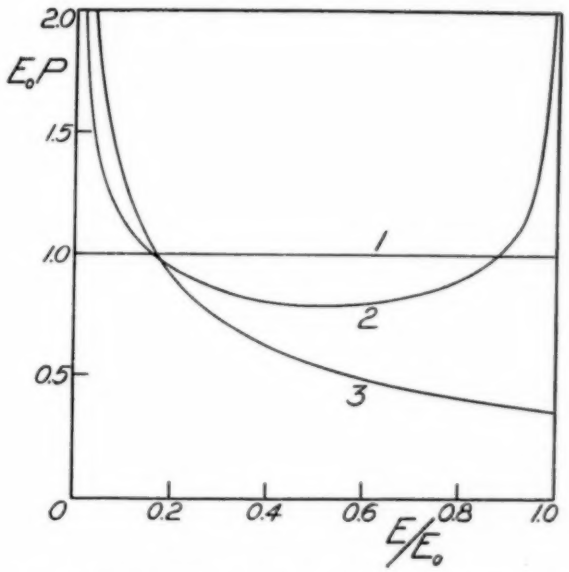

FIG. 3. Distributions in fractional energy loss for $t=0.693$ (~0.35 cm Pb), calculated for certain simple forms of spectrum (see text). Curve 3 is to be thought of as containing the contribution $0.25\,\delta(E-E_0)$, besides the part shown.

Setting

$$I(k/E)=\sum_{n=0}^{\infty}c_nP_n(1-2k/E), \quad (66)$$

we have

$$\begin{aligned}
c_0&=\mu_0\\
c_1&=3(2\mu_1-\mu_0)\\
c_2&=5(6\mu_2-6\mu_1+\mu_0)\\
c_3&=7(20\mu_3-30\mu_2+12\mu_1-\mu_0)\\
c_4&=9(70\mu_4-140\mu_3+90\mu_2-20\mu_1+\mu_0).\\
&\cdots\cdots\cdots\cdots
\end{aligned} \quad (67)$$

From the size of the coefficients in (67) it is evident that extremely accurate knowledge of the μ's is required for a reliable determination of the c's; a reasonable procedure in practice would be to calculate the c_n as far as they decrease steadily with increasing n, and neglect the rest. It is this practical difficulty in the use of (64) which gives importance to our analytic solution of the "straggling problem" and the construction of various comparison curves: from a purely formal point of view, the derivation of (64) directly from (65) could be regarded as a solution of both problems at once.

The writer wishes to thank Mr. L. M. Fussell for assistance with the numerical computations.

Experiments on the Gamma-Radiation from Lithium and Fluorine Bombarded with Protons

E. R. GAERTTNER AND H. R. CRANE
University of Michigan, Ann Arbor, Michigan

(Received July 10, 1937)

The recoil electrons ejected from a 2 mm carbon scatterer by the gamma-radiation from Li+H[1] have been investigated and indicate three lines of energies 17, 14.5, and 11.5 and possibly a fourth line of energy 8.5 Mev. Pairs ejected from the same scatterer were also observed. Most of these may be attributed to the 17 Mev line. Recoil electrons ejected from a 1.5 mm carbon scatterer by the gamma-radiation from F+H[1] have been observed, and indicate two lines of energies 5.7 and 4 Mev. Pairs produced by internal conversion of the gamma-radiation from F+H[1] were also observed, and indicate the same two lines. The cross section for this effect is in good agreement with the theoretical predictions. It is pointed out that a study of the pairs produced by internal conversion affords an excellent method of determining excitation levels in nuclei.

INTRODUCTION

Li+H[1]

THE question whether the gamma-radiation from lithium bombarded with protons is composed of a single line or a number of lines has not been clearly decided by the results of the experiments so far reported. The recoil electrons ejected from the glass wall of a cloud chamber by the radiation were studied by Crane, Delsasso, Fowler and Lauritsen[1] and were interpreted as indicating a complex spectrum extending up to about 16 Mev. During the same measurements a number of pairs was observed, which were grouped principally near the upper energy limit but extended down to 10 Mev. Subsequent measurements of a large number of pairs ejected from a thin sheet of lead were reported by Delsasso, Fowler and Lauritsen.[2] These pairs fell in a band or line at about 17 Mev and it was therefore concluded that there was little if any radiation below about 17 Mev. In a more recent report[3] these authors confirmed this distribution of pairs and suggested the possibility of one or more relatively weak lines of lower energy. The radiation studied in all cases is without doubt due predominantly to the first proton resonance level, the energy of which has been determined by Hafstad, Heydenburg, and Tuve[4] to be 440 kv.

In the experimental arrangement used by Crane, Delsasso, Fowler and Lauritsen for the observation of recoil electrons it was not possible to be sure that all tracks counted had their origin in the glass wall of the cloud chamber, rather than in material outside the wall. The spectrum obtained was therefore open to the objection that a considerable part of it may have been composed of electrons which were due to softened radiation or which originated in material outside the chamber. This objection seemed to be strengthened by the observations of Delsasso, Fowler and Lauritsen that nearly all the pairs fell in a band at about 17 Mev. Because of this disagreement between the results given by the recoil electrons and the pairs, we decided to make more refined measurements on the distribution of recoil electrons. A preliminary report of this work has already been published.[5]

F+H[1]

McMillan,[6] and Crane and Lauritsen[7] first determined the quantum energy of the fluorine radiation by the absorption method. They obtained an absorption coefficient which corresponded to radiation of about 6 Mev. At the same time Crane, Delsasso, Fowler and Lauritsen[7] studied the recoil electrons ejected into a cloud chamber from a thick sheet of lead. The distribution which they obtained extended up to about 6 Mev, and could be attributed to a

[1] Crane, Delsasso, Fowler, and Lauritsen, Phys. Rev. **48**, 125 (1935).
[2] Delsasso, Fowler, and Lauritsen, Phys. Rev. **50**, 389 (1936).
[3] Delsasso, Fowler, and Lauritsen, Phys. Rev. **51**, 391 (1937).
[4] Hafstad, Heydenburg, and Tuve, Phys. Rev. **50**, 504 (1936).
[5] Gaerttner and Crane, Chicago Meeting American Physical Society (1936); Phys. Rev. **51**, 49 (1937).
[6] McMillan, Berkeley Meeting American Physical Society (1934); Phys. Rev. **46**, 325 (1934).
[7] Crane and Lauritsen, Phys. Rev. **46**, 531 (1934).

single line at about this energy. Recently Delsasso, Fowler and Lauritsen[8] extended the cloud chamber method to the investigation of pairs and recoil electrons ejected from thin absorbers placed inside the cloud chamber. The pairs ejected from a thin lead sheet indicated a sharp line at 6 Mev and the recoils ejected from a thin aluminum sheet indicated a line of about the same energy. Using the same experimental arrangement initiated for the study of the lithium gamma-rays we have also investigated the radiation from fluorine. This particular experimental arrangement also made possible a study of the radiation which is internally converted in the target.

Apparatus

The apparatus used in producing the high speed protons necessary in these experiments consists of a one-million-volt transformer and vacuum tube apparatus.[9] A focused ion beam of about 250 microamperes can be obtained at the target. Since no provision is made to analyze the beam, it consists of both atomic and molecular ions. The cloud chamber is 15 cm in diameter and its depth can be varied from 2.5 cm to 3.8 cm. In the present investigation it is found convenient to use the shallower chamber when the chamber is used in the horizontal arrangement shown in Fig. 1, and the deeper chamber when used in the vertical arrangement shown in Fig. 2. The active depth of the chamber is determined by the depth which is illuminated. It is 1 cm in the horizontal arrangement and 2 cm in the vertical one. Nonstereoscopic photographs are taken by means of a Sept 35-mm motion picture camera having an $f:1.9$ lens. The tracks are illuminated by a carbon arc light flashed at 300 amperes. Two water cooled, air core coils, one above and one below the chamber produce the required magnetic field. They are capable of producing a field of 4000 oersteds, when energized only for about 1 second at the time of the chamber expansion. The magnetic field intensity is regulated by varying the field current in a 50 kw generator which supplies the current for the field coils. The rheostat for this and also an accurately calibrated ammeter are located near the cloud chamber, and by means of these the mean deviation of the field current can be kept down to about 1 percent. A motor driven central contact system is used to operate the ion accelerating apparatus and the cloud chamber in synchronism. In this way it is necessary to energize the high voltage transformer and the ion source for only a fraction of a second at the time of the chamber expansion.

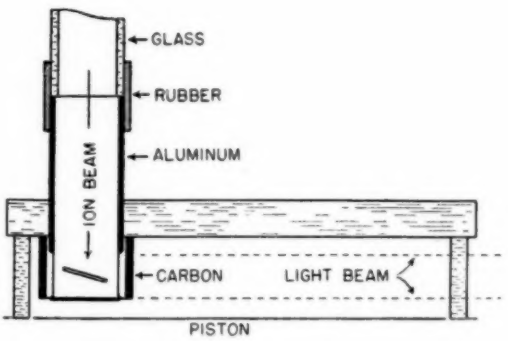

Fig. 1. Horizontal cloud chamber arrangement.

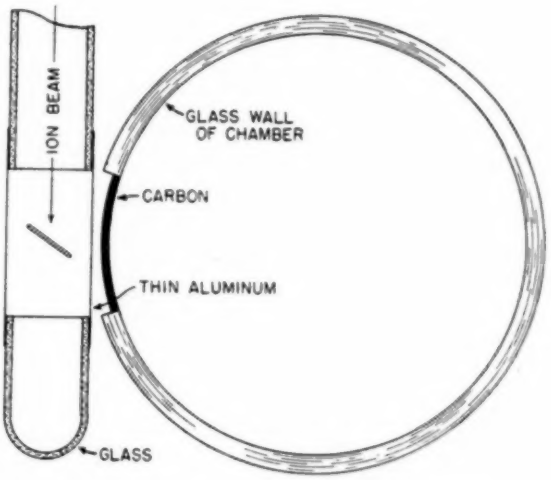

Fig. 2. Vertical cloud chamber arrangement.

The principal object in view in designing the present experimental arrangements was to eliminate doubt as to the origin of the tracks counted, and at the same time to obtain high resolving power by the use of thin scatterers. We accomplished this in our first arrangement, by placing the target in a well in a horizontal cloud chamber, and surrounding the target with a

[8] Delsasso, Fowler, and Lauritsen, Phys. Rev. **51**, 527 (1937).
[9] Crane, Phys. Rev. **52**, 11 (1937).

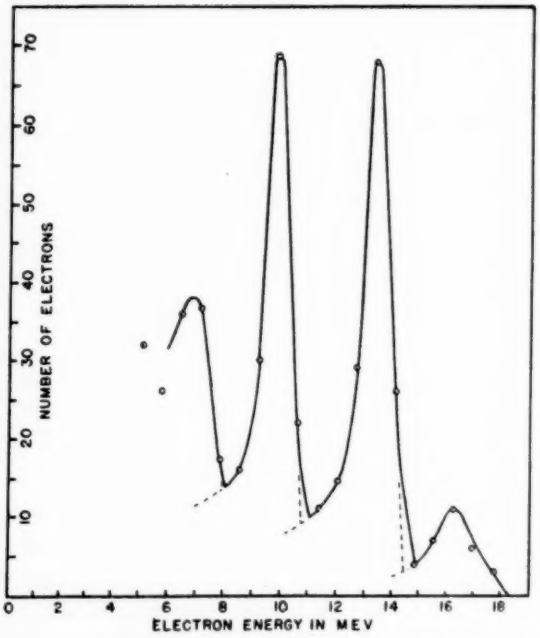

FIG. 3. Negative electrons ejected from 2 mm carbon by the gamma-radiation from $Li+H^1$. Horizontal arrangement. $H=2350$ oersteds.

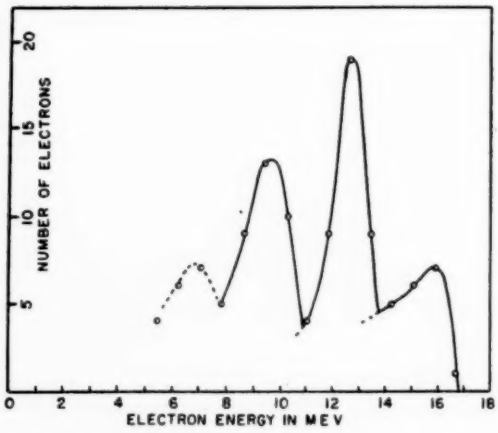

FIG. 4. Negative electrons ejected from 2 mm carbon by the gamma-radiation from $Li+H^1$. Horizontal arrangement. $H=2750$ oersteds.

thin-walled cylinder of scattering material, as sketched in Fig. 1. The large solid angle which the scattering material subtended to the target gave rise to a sufficient number of electrons even though the material had a stopping power of less than 1 Mev for electrons. The fact that the direction of the radiation from the target was everywhere *toward* the outside walls of the chamber, coupled with the fact that at high energies secondaries of all kinds travel predominantly in the direction of the radiation producing them, caused the chamber to be quite free from spurious tracks. We found by actual count that approximately five tracks came directly from the scattering material surrounding the source for every track which appeared elsewhere in the chamber. Thus the chance of a spurious track being situated so that it appears to come from the scatterer, and also to lie in the plane of the chamber is very small. As shown in Fig. 1, the ions were brought vertically downward to the target through a 2 cm brass pipe. The target was lithium metal and was placed at the angle indicated in the sketch, to prevent the gamma-rays from being absorbed in the target. The wall between the target and the scatterer was of thin aluminum (0.1 mm) and could therefore absorb very little of the radiation. The scatterer consisted of a cylinder of pure graphite 2 mm thick.

In an attempt to increase the number of recoil electrons ejected into the chamber from the thin scatterer and also to show that the results obtained were independent of the experimental setup, we made measurements with a second arrangement, using a vertical chamber. In this arrangement a 2 mm carbon scatterer was made part of the cloud chamber wall as shown in Fig. 2. The deeper chamber (3.8 cm), was used and a larger pipe was used to bring the ion beam to the target. Because it was possible to shield the chamber completely from soft x-rays from above, we were able to use considerably higher ion currents and to obtain a correspondingly larger yield of tracks from the lithium radiation. There was also the advantage that the tracks were longer, since the entire diameter of the chamber was available. On the other hand, more tracks due to scattered radiation appeared because the source was outside the chamber. Nevertheless by using a marker indicating the exact position of the scatterer it was possible to select and measure only those tracks which originated in the scatterer.

SELECTION AND MEASUREMENT OF TRACKS

The method generally used for determining the curvature of tracks is to project the full size image upon a white card on which circles of

various radii are drawn, and to determine which circle fits a given track. We have found that the following change in the procedure increases the accuracy of the measurement considerably: The image is projected upon a sheet of blank paper and the image of the track is traced, in full or in part, with a sharp pencil. The curvature of this

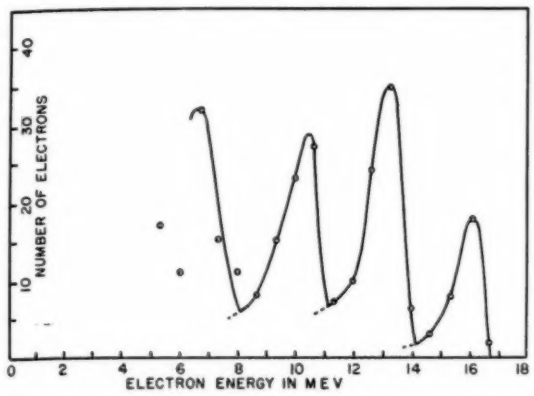

FIG. 5. Negative electrons ejected from 2 mm carbon by the gamma-radiation from Li+H[1]. Vertical arrangement. $H=2200$ oersteds.

arc is then measured by means of a piece of transparent celluloid on which circles are scratched. Parts of tracks which do not stand out with sufficient contrast against the background can easily be traced and measured to a high degree of accuracy.

It was also found that the quality of the tracks could be greatly improved by bombarding the target only for a very short time, 1/10 second, immediately before the photographic exposure. The exposure itself was only 1/10 second long. This rapid procedure accomplished much toward eliminating those changes in curvature of tracks which arise from the drifting and falling of the droplets. It had the further advantage that all tracks photographed were very sharp and narrow.

Before interpreting the present data it was desired to determine the actual amount of spreading of the lines which could be expected to arise from the human error in the measurement of tracks. The following experiment was therefore performed: A list of tracks was traced and measured separately by two observers and the results were later compared, track for track. It was found that the average amount by which the two observers disagreed was 0.3 Mev. This means that for a single observer the average error is somewhat less. The tracks used were of average quality and length and were a representative group having energies greater than 7 Mev.

In order to be selected and measured a track must satisfy the following conditions:

1. It must have its origin in the scatterer. This condition is satisfied if the track is visible to within 1 cm of the surface of the scatterer, and extends at least $\frac{2}{3}$ the distance across the chamber. Any track which starts in the top glass plate or in the floor of the chamber, and appears to come from the scatterer is necessarily short because the active depth of the chamber is only the narrow illuminated portion at the center.

2. A track must not be visibly scattered. The scattering to be expected in air for the high energies encountered here (10 Mev) is extremely small.

RESULTS

Negative electrons from Li+H[1]

In Figs. 3, 4 and 5 are shown the distribution curves of the negative electrons obtained from a

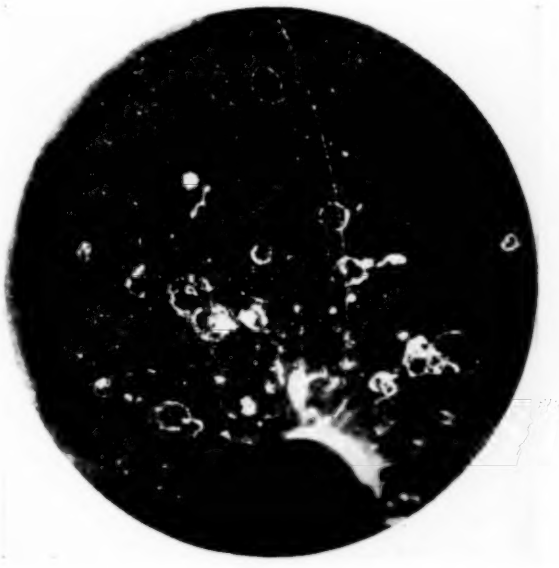

FIG. 6. Example of the pictures obtained with horizontal arrangement. The negative electron (curving to the left) satisfies the requirements for measurement. It is quite certain that the fainter positron track is not associated with this negative electron track.

carbon scatterer 2 mm thick, whose stopping power is about 0.8 Mev for high energy electrons. The electrons plotted in Figs. 3 and 4 were obtained with the horizontal arrangement, and those plotted in Fig. 5 were obtained with the vertical arrangement. Fig. 6 shows an example of the tracks obtained with the horizontal arrangement. Negative electrons which were visibly associated with positrons were not included in these plots. It was not possible, however, to exclude all negative members of pairs, but it is estimated that not more than 10 percent of the negative electrons in the above plots are members of pairs. The data obtained may be interpreted in several ways, as follows:

1. Assuming that the groups of electrons indicated are Compton recoil electrons, we can determine the gamma-ray energies by adding 0.25 Mev to the high energy cut-off of each of the peaks. This procedure gives very closely the same values in each of the sets of data: 17, 14.5, and 11.5 Mev, with the possibility of a fourth line at about 8.5 Mev. However, the data below about 10 Mev are not considered reliable because of the presence of some beta-rays from Li^8, produced by deuteron contamination in the ion beam.

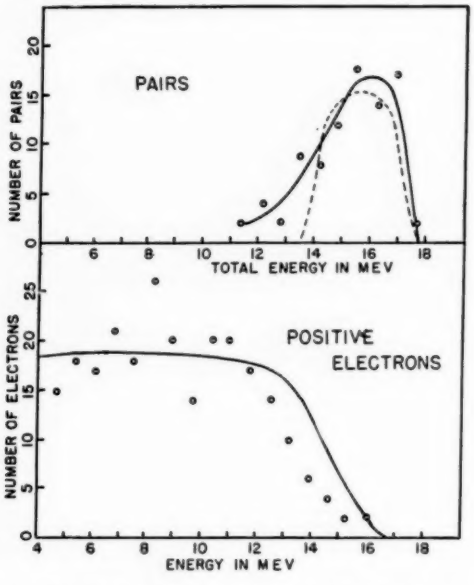

FIG. 7. Upper plot: Pairs ejected from 2 mm carbon by the Li+H^1 radiation, in the horizontal arrangement. $H=2350$ oersteds. The dotted curve is the theoretically expected distribution from a 17 Mev gamma-ray line and 2 mm carbon. Lower plot: Positrons which appear singly or as members of pairs. The curve shows the expected distribution from a 17 Mev gamma-ray line.

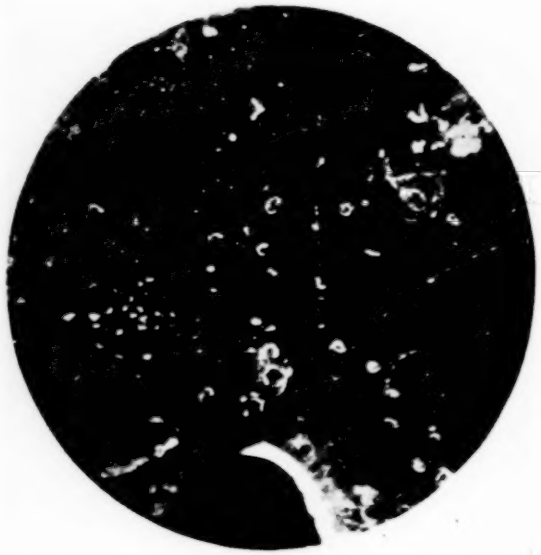

FIG. 8. Pair ejected from the 2 mm carbon scatterer in the horizontal arrangement. By extending the tracks until they intersect it can be shown that the pair originates in the carbon, rather than in the target. This indicates that it is not due to internal conversion.

2. Internal conversion, giving rise to discrete beta-ray groups, can take place with very high efficiency, when only a particular kind of nuclear transition is available ($i=0$ to $i=0$). An example of this exists in the Ra C spectrum. In the present experiment such beta-rays from the target could pass through the carbon scatterer and enter the chamber with only about 0.8 Mev loss in energy. It seems unlikely that several lines could be due to this cause; nevertheless, an investigation of this possibility is being made.

3. It may be suggested that nearly all of the primary radiation has an energy of 17 Mev and that the electrons of lower energy are due to softened radiation, to *Bremsstrahlung*, or are electrons which have suffered large energy losses. It would be difficult to reconcile this hypothesis with (a) the sharpness of the peaks, (b) the fact that the same distribution is obtained with two quite different experimental arrangements, (c) the relatively small number of tracks (20 percent of the total) which do not appear to originate in the carbon scatterer, and (d) the fact that the ratio of positive to negative electrons changes roughly in the expected manner with the atomic

number of the scattering material used. This latter point was checked by replacing the carbon scatterer with a 0.7 mm brass scatterer. If the lower energy tracks were produced in the chamber walls the ratio of positives to negatives would not be sensitive to the material in the scatterer.

Pairs from Li+H[1]

Because of the low atomic number of carbon, which was the scattering material used, the amount of data obtained on pairs was smaller than that obtained on recoil electrons. A plot of 95 pairs obtained with the horizontal arrangement is shown in Fig. 7. Examples of the pairs obtained are shown in Figs. 8 and 9. In addition to pairs produced in carbon, there is the possibility that the plot includes some pairs produced by internal conversion in the target. The spreading in the distribution which results from the thickness of the scatterer and errors in measurement is expected to be roughly twice the spreading in the recoil electron plots, since two electron energies must be added. A dotted curve is shown in Fig. 7 to indicate the distribution of pairs which would be expected from a 17 Mev gamma-ray falling upon a 2 mm carbon scatterer, with an average error in measurement of 0.5 Mev. It is quite definite from this distribution that the majority of the pairs are produced in the carbon scatterer rather than by internal conversion in the lithium target, for if the distribution were due predominantly to internally converted pairs, one would expect the distribution to be an error curve with its center at 15 Mev. The dotted curve apparently accounts for the majority of the pairs observed. At most, about 20 percent of the pairs could be attributed to radiation below 17 Mev. These results are in good agreement with those obtained by Delsasso, Fowler and Lauritsen.[2, 3]

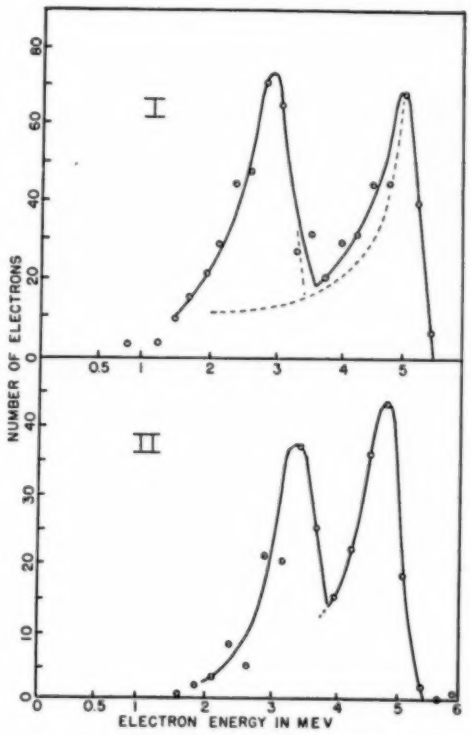

FIG. 10. Negative electrons produced by the gamma-radiation from F+H[1]. I: Horizontal arrangement of Fig. 1, 1.5 mm carbon scatterer. II: Collimated gamma-ray beam falling upon a 1.5 mm carbon sheet placed across the center of the chamber. $H = 1850$ oersteds.

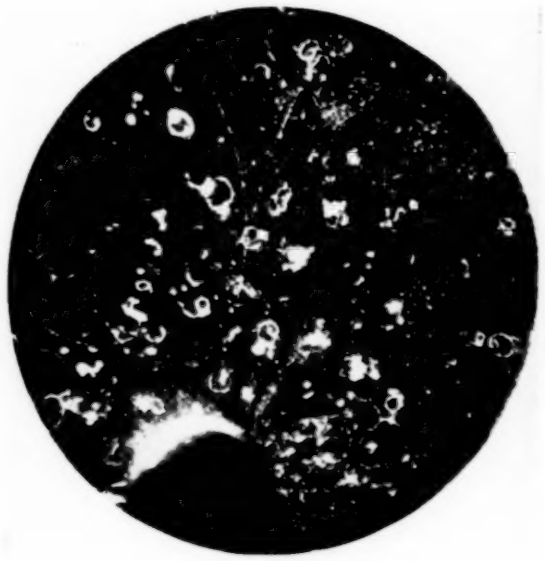

FIG. 9. A pair which originates in the gas in the cloud chamber. Its total energy is 17.1 Mev, with an uncertainty due to measurement and fluctuation in the magnetic field of at least ±0.5 Mev. One pair of this kind gives a good approximation to the quantum energy of one of the gamma-ray lines, because it suffers no absorption.

Positrons from Li+H[1]

In order to show that the distribution of electrons is not fortuitous, and also to get an independent check on the upper limit of the gamma-ray spectrum all the positives obtained in both arrangements were measured and plotted

on a common energy scale in Fig. 7. The criteria for selecting and measuring them were the same as for the electrons except that both associated and unassociated positives were counted. It is evident that the distribution shows no line structure and has a cutoff value of about 16 Mev. According to the theory of pair formation this places an upper limit of 17 Mev on the spectrum, a value in good accord with that obtained with pairs and recoil electrons.

Judging from the distribution of pairs, this distribution of positrons should be consistent with that expected from a 17 Mev line. To test this point we have plotted the theoretical distribution of positrons for 17 Mev gamma-radiation falling on 2 mm of carbon. This curve is also shown in Fig. 7. It appears that the experimental distribution is in fair agreement with this curve if allowance is made for the fact that there is some tendency to discriminate against the higher energy tracks. However, it is impossible to decide definitely from this data whether or not the positron distribution is due entirely to the 17 Mev line.

Negative electrons from F+H[1]

The upper curve in Fig. 10 shows the distribution of negative electrons obtained by bombarding a crystal of calcium fluoride with 400 kv protons, using the horizontal chamber arrangement of Fig. 1. The scatterer in this case was 1.5 mm of carbon. The distribution indicates two gamma-ray lines, at 5.7 and 4.0 Mev. The energy of the higher line is in good agreement with the recent results of Delsasso, Fowler and Lauritsen,[8] who investigated both the pairs and the negative electrons ejected from sheets of material in the center of a cloud chamber. Their results do not, however, show the presence of the lower line. Because of this discrepancy we carried out an experiment using an arrangement similar to theirs; a sheet of carbon 2 mm thick was placed across the center of the cloud chamber, and gamma-radiation, collimated by a lead channel 15 cm long was allowed to fall upon the center of the carbon sheet. The negative electrons originating in the carbon gave the lower curve in Fig. 10. This is in substantial agreement with the curve obtained by the other method, although it falls off more rapidly at the low energies. The latter is undoubtedly due to the difference in the geometry involved in the two methods. The number of pairs obtained was too small, with either arrangement, to give any indication of the distribution of pairs.

Since the excitation curves of Herb, Kerst, and McKibben[10] indicate the possibility of a second resonance level at about 600 kv, we made a separate investigation of the spectrum of recoil electrons at a bombarding voltage of about 750 kv. The resulting distribution curve revealed the same two lines; consequently there appears to be no appreciable dependence of the spectrum upon bombarding voltage between 400 and 750 kv. However, it is possible that the molecular ions of 656 kv may completely mask the effect of a higher resonance level.

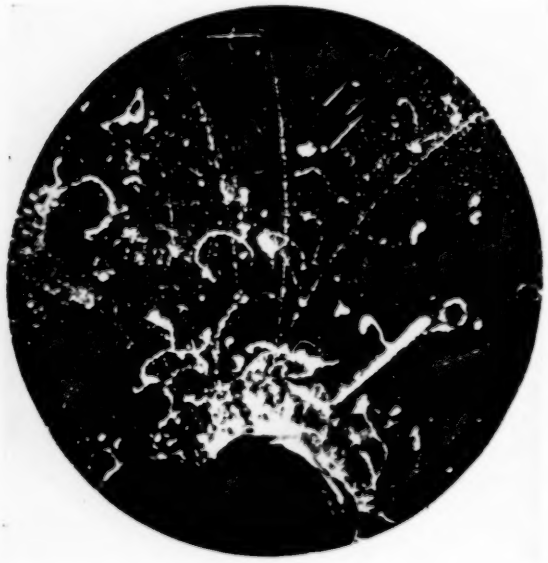

FIG. 11. Example of positive and negative electrons produced by internal conversion of the F+H[1] radiation into pairs. Negative electrons curve to the right. $H=820$ oersteds.

Internal conversion of the F+H[1] radiation

The well in the cloud chamber shown in Fig. 1 was replaced with a very thin aluminum tube (0.1 mm wall thickness). A thin target was made by depositing powdered CaF_2 upon a piece of 0.05 mm aluminum, and was sloped toward the chamber as shown in Fig. 1. An abundant emission of pairs was observed when the target

[10] Herb, Kerst, and McKibben, Phys. Rev. **51**, 691 (1937).

was bombarded with 400 kv protons. The ratio of negatives to positives, which was 15 to 1 in the previous experiment (carbon scatterer) now became 2 to 1. An example of the photographs obtained is shown in Fig. 11, and energy distributions of the pairs, positive electrons and negative electrons are shown in Fig. 12. The extreme sharpness of the peak in the pair distribution at 5.7 Mev should be noted. Because the pair receives the entire energy of excitation of the nucleus, and because there is practically no material in the path to reduce the energy of the pair, this proves an excellent means of measuring the energy levels in the excited nucleus. A second peak in the distribution, which may be somewhat doubtful, appears at 4 Mev. Those pairs which fall outside these two peaks most probably result from associating, in the measuring process, positive and negative electrons which are not members of the same pair. The average angle between the directions of emission of the members of a pair increases rapidly as the energy of the pair decreases. This makes it much more difficult to recognize pairs belonging to the lower line than to the upper line, and therefore the relative intensities in the plot are distorted.

The plot of negative electrons includes negative members of pairs and also recoil electrons from the small amount of aluminum surrounding the target. A part of the area under the curve is shaded to suggest what portion of the tracks might be negative members of pairs. The maximum at about 1.2 Mev is rather higher than expected. Judging from Fig. 10 there is probably no strong gamma-ray of this energy. There is, however, the possibility that this is a discrete beta-ray group from internal conversion. From a consideration of the ratio of the number of recoil electrons to the number of negative (or positive) members of pairs, it is estimated that the efficiency of production of internal conversion pairs is of the order of 1 pair per 10^3 gamma-rays. This is in good agreement with the theoretical predictions.[11]

It is worth pointing out here that the above experiments in which the carbon scatterer was removed furnish good proof that the origin of the tracks counted is not uncertain in the experimental method described.

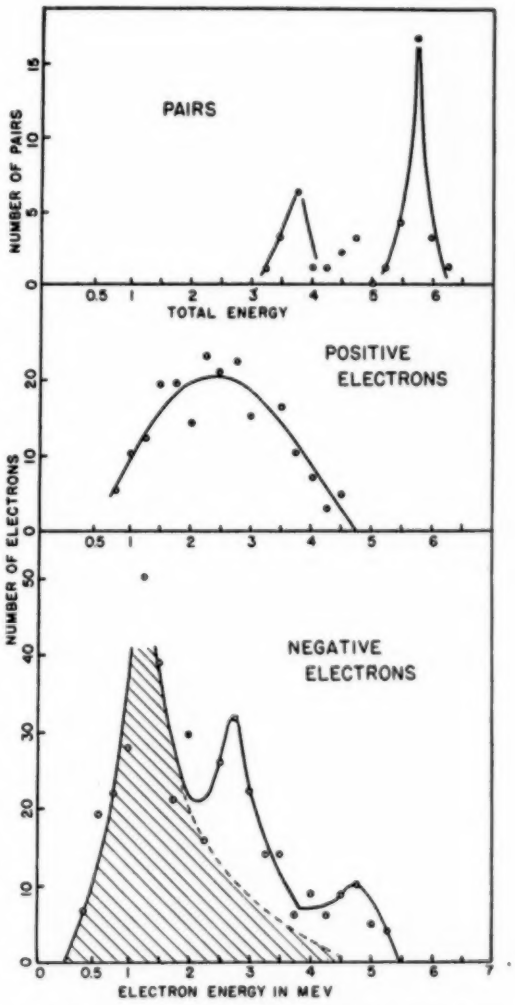

FIG. 12. Pairs, positive electrons and negative electrons obtained with only 0.1 mm aluminum between the target and the cloud chamber. The plots of single electrons include both associated and unassociated members of pairs. $H = 820$ oersteds.

DISCUSSION

Origin of the radiation

Detailed discussions of the possibilities for the origin of the $Li+H^1$ radiation have been given by several authors.[12] It is agreed, from the standpoint of energy available, that one of the two reactions

[11] Oppenheimer and Nedelsky, Phys. Rev. **44**, 948 (1933); Uhlenbeck and Rose, Phys. Rev. **48**, 211 (1935); Jager and Hulme, Proc. Roy. Soc. **148**, 708 (1935).

[12] Crane, Delsasso, Fowler and Lauritsen, Phys. Rev. **48**, 125 (1935); Hafstad, Heydenburg and Tuve, Phys. Rev. **50**, 510 (1936).

$$Li^7+H^1\rightarrow Be^{8*}\rightarrow Be^8+\gamma\rightarrow He^4+He^4+\gamma \quad (1)$$

$$Li^7+H^1\rightarrow He^{4*}+He^4\rightarrow He^4+He^4+\gamma \quad (2)$$

is responsible for the radiation; the only question is whether the radiation comes from Be^{8*} or He^{4*}. It is also clear that the radiation so far studied is associated with the first proton resonance level, 440 kv. The recent discovery by Lewis, Burcham and Chang[13] of a continuous alpha-particle group which is probably due to the reaction

$$Li^8\rightarrow Be^{8*}+e^-\rightarrow He^4+He^4+e^- \quad (3)$$

indicates that those levels in Be^8 which are permitted to disintegrate into two alpha-particles are extremely broad. If reaction 1 is responsible for the gamma-radiation, some lines might arise from transitions to lower states of Be^8 which are permitted to disintegrate into two alpha-particles. Such lines would be very broad. Since the 17, 14.5 and 11.5 Mev peaks in the negative electron distribution which we have obtained are almost exactly of the width expected from the Klein-Nishina scattering formula, it seems unlikely that these particular lines arise from transitions of this kind. Theory predicts[14] the existence of many levels in Be^8, and there is therefore no particular difficulty in accounting for all the observed radiation by means of reaction 1. Reaction 2 would give rise to sharp lines, but brings up at least two difficulties: First, the alpha-particle is not expected, on theoretical grounds, to possess more than one real excited level.[15] Second, unless the $He^{4*}+He^4$ were formed with an extremely small amount of kinetic energy, the peak in the excitation curve (proton energy) would be excessively broadened. This is known experimentally to be very narrow: its half-width is of the order of 10 kv.

Reactions analogous to those for $Li+H^1$ have been put forward to account for the gamma-radiation from $F+H^1$.

$$F^{19}+H^1\rightarrow Ne^{20*}\rightarrow O^{16}+He^4+\gamma, \quad (4)$$

$$F^{19}+H^1\rightarrow O^{16*}+He^4\rightarrow O^{16}+He^4+\gamma. \quad (5)$$

Here the question is whether the radiation comes from Ne^{20*}, O^{16*} or He^{4*}. He^4 may be eliminated tentatively on theoretical grounds because no levels of such low energy are expected. About 9 Mev is released in the over-all reaction, in both 4 and 5. If the energy of the highest line (5.7 Mev) is subtracted, more than 3 Mev is left to appear as kinetic energy of the $O^{16}+He^4$. The consequent short lifetime for separation of the O^{16} and He^4 would broaden the gamma-ray line in 4, and would broaden the peak in the excitation curve (proton energy) in 5, by 0.5 to 1 Mev. Such a breadth certainly does not exist in the excitation curve, and probably does not exist in the gamma-radiation. By subtracting the sum of the gamma-ray energies (5.7+4 Mev) from the total energy available, and allowing for some errors in the data, we find that the $O^{16}+He^4$ would have about zero kinetic energy, and the difficulty of the line breadth would disappear in both 1 and 2. A third possible reaction is that Ne^{20*} radiates to its ground state by several successive transitions. Here about 13 Mev is released, and it is not easy to see how the observed gamma-ray lines fit into such a scheme. One thing may be concluded with some confidence: The emission of a group of alpha-particles of any considerable energy, associated with the observed gamma-radiation is excluded because of the broadening effect it would necessarily have on the gamma-ray lines or on the peaks in the excitation curve.

Errors in the determination of energies

A summary of the errors involved in the present method can be given as follows:

1. The absolute value of the magnetic field intensity was determined both by means of a flip coil and by calculation from the geometry of the coils and the current. The error in this is not greater than 3 percent.

2. The average deviation of the magnetic field strength from the mean value during all the measurements was 1 percent.

3. The average error in the measurement of tracks was found by actual test to be not more than 2 percent.

4. No estimate of the error caused by scattering in the air has been made, but for electrons of such high energy this error is certainly much smaller than the other errors involved.

[13] Lewis, Burcham and Chang, Nature **139**, 24 (1937).
[14] Feenberg and Phillips, Phys. Rev. **51**, 597 (1937).
[15] Feenberg, Phys. Rev. **49**, 328 (1936).

5. Because nonstereoscopic pictures were used, a small error is involved due to the angle a track may make with the plane of the cloud chamber. From the criteria used in selecting tracks for measurement, the angle with the plane of the chamber is estimated to be less than 10°. Therefore, the maximum error introduced is 1.5 percent.

All of the errors mentioned, except the first, are of the kind which tend only to broaden the peaks. The first may introduce an error in the energy scale. For lithium, the most probable energies of the lines are 17, 14.5, 11.5 and possibly 8.5 Mev, with a maximum absolute error in the energy scale of about 1 Mev. For fluorine the most probable energies are 5.7 and 4 Mev, with a maximum absolute error of about 0.3 Mev.

Relative intensities

While the energies of the gamma-ray lines can be determined with some confidence from the recoil electron distributions, estimates of the relative intensities of the lines are less certain. The difficulty arises from a number of causes:

(1) Each line contributes some tracks to neighboring lines which lie at lower energy.

(2) There is some tendency to discriminate against tracks of large radius of curvature because they must be of greater length to afford accurate measurement. This is evidenced by the fact that the 17 Mev peak appears stronger in Fig. 4 than in Fig. 3. The magnetic field strength was greater in Fig. 4 than in Fig. 3.

(3) The angular distribution of recoil electrons emerging from the scattering material depends upon the energy of the gamma-ray line producing them, because of both the Klein-Nishina angular distribution, and scattering of the electrons in the material.

(4) An appreciable number of electrons fail to emerge at all from the scattering material, and this number is dependent upon the energy of the electrons. Whether this effect is due to multiple scattering or to a new process by which electrons are absorbed is not yet known, but it has been noticed by several investigators.[16]

It will be noticed, both in the case of lithium and of fluorine that the various sets of data do not show the same relative intensities. This is undoubtedly because of the difference in geometry in the various cases and, to some extent, because of the different magnetic field strengths used. The simplest method of estimating the relative intensities is to determine the relative numbers of tracks under the peaks (the average of all the data is used) and to apply a correcting factor for the variation in cross section for Klein-Nishina scattering as a function of energy. In this way we obtain the relative intensities 2 : 4 : 3 for the 17, 14.5 and 11.5 Mev lines of lithium, and 5 : 2 for the 5.7 and 4 Mev lines of fluorine.

Because of the fact that the cross section for pair formation increases with energy, while the cross section for Klein-Nishina scattering decreases with energy, the higher energy lines in the spectrum tend to appear relatively stronger in the pair distribution than in the negative electron distribution. The corrections of this kind which we are able to apply to the distributions at present do not seem to be sufficient to bring the pair and negative electron distributions into entire agreement. Although our data on pairs are not so extensive as those of Delsasso, Fowler and Lauritsen, they are in good agreement with theirs. It is our opinion at present that a further investigation of the number of electrons which are lost before emerging from the scattering material may be of help in explaining the apparent contradiction between the pair and the negative electron distributions.

The authors wish to express their gratitude to the Rackham Endowment Fund for the support of this work.

[16] Turin and Crane, Phys. Rev. **52**, 63 (1937).

The Production and Properties of Low Temperature Neutrons

W. F. Libby and Earl A. Long
Department of Chemistry, University of California, Berkeley, California

(Received June 7, 1937)

Evidence has been found that (a) hydrogenous substances so cold that nearly all the molecules are in the ground state can cool only those neutrons whose kinetic energies are great enough to excite the molecules to their first state, e.g., the temperature of neutrons cooled by a crystal of such molecules at the absolute zero will approximate the temperature at which the specific heat begins to rise above the normal curve of the Debye type for crystalline specific heat; (b) the probability of energy loss to a liquid or crystal as a whole seems to be small; (c) for hydrocarbons, the limiting temperature for cooling neutrons appears to decrease with increase in length of the hydrocarbon chain. A neutron thermometer, using the absorption by boron, has been tested and calibrated approximately.

Introduction

THE evidence reported by many investigators,[1–7] that neutrons emerging from thick layers of hydrogenous matter have approximately thermal energies, suggested the importance of measuring neutron temperatures.

It is necessary that the qualified way in which the term "temperature" of neutrons is used in this discussion be made clear. The processes of absorption of the slower neutrons and of production by slowing of the fast neutrons both act to distort the velocity distribution from the Maxwellian. Velocity seleçtor experiments (reference 6) and data for lower temperatures presented below both reveal this. The term "neutron temperature" is used only to specify the approximate average neutron energy. Some of the results below were reported briefly several months ago.[8, 9]

Table I. *Data on temperature variation of gamma-radiation from capture of slow neutrons in paraffin.*

Difference in Count Rate. With and and Without Paraffin Plugs. (Counts/Minute.)	Temperature
9.2±1.5	300°K
8.2±2	90°K
8.0±2	25°K
With and Without CCl_4 Instead of Paraffin	
2.4±1	300°K

Preliminary Experiments

Among the first experiments tried was an attempt to use the gamma-radiation produced by the capture of slow neutrons by protons in paraffin as a means of studying the rate of capture and therefore the average velocity of the neutrons. The assumption that the probability of capture is inversely proportional to the velocity of the neutron (the "$1/v$" law of capture), should then allow a study of the variation of neutron velocity to be made. The arrangement and apparatus are shown in Fig. 1, and the data in Table I.

At a given temperature, counts were taken, first with the Dewars empty, and second with paraffin plugs (3.5 inches in diameter and 16 inches long, coated with sufficient H_3BO_3 to prevent escape of slow neutrons) in place inside each of the Dewars. The control experiment with CCl_4 gives an upper limit to the effect of scattering of gamma-radiation from the source and leads to a prediction of approximately 25 counts per minute as the effect to be expected at 25°K, if the capture production of gamma-radiation were to vary as the reciprocal of the square root of the absolute temperature. The data show quite clearly that the effect is much smaller. This apparent temperature independ-

[1] Dunning, Pegram, Mitchell and Fink, Phys. Rev. **47**, 888 (1935).
[2] Moon and Tillman, Nature **135**, 904 (1935).
[3] Dunning, Pegram, Fink, Mitchell and Segrè, Phys. Rev. **48**, 704 (1935).
[4] Westcott and Niewodniczanski, Proc. Camb. Phil. Soc. **31**, 617 (1935).
[5] Moon and Tillman, Proc. Roy. Soc. **A153**, 476 (1936).
[6] Fink, Phys. Rev. **50**, 738 (1936).
[7] Preiswerk and von Halban, J. de phys. et rad. **7**, 29 (1937).
[8] Libby and Long, Phys. Rev. **50**, 575 (1936).
[9] Libby and Long, Phys. Rev. **50**, 576 (1936).

ence of the capture can be understood as evidence that even at 300°K a large fraction of the thermal neutrons produced are captured in so large a block of paraffin, eliminating the possibility of any large increase on cooling. This agrees with the considerations of Fermi[10] on the diffusion of thermal neutrons in paraffin. Calcu-

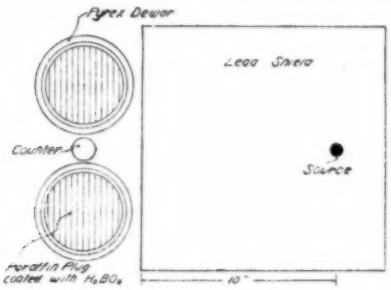

FIG. 1. Paraffin neutron-proton gamma-radiation assembly.

lation for the arrangement used, assuming the "$1/v$" law of capture, gave 46 percent as the expected increase of gamma-radiation intensity on cooling from 300°K to 25°K, in agreement with the measured effects within the rather large limits of error. Consequently, it was concluded that any measurement of temperature effects must be accomplished by observing effects produced in a small region of the larger system used to cool the neutrons, e.g., activation of a target imbedded in the system or preferably exposed to the neutrons emitted from the surface of such a system. Some of the later experiments further illustrate this point.

TEMPERATURE CURVES FOR DIFFERENT HYDROGENOUS MOLECULES

The apparatus finally selected for comparison studies of several different hydrogenous molecules is shown in Fig. 2. A metal Dewar of 5.25 inches inside diameter, with inner wall of brass and outer of monel metal, each about one millimeter thick, was surrounded with a paraffin cylinder of 10 cm wall thickness. The neutron source, either radon-beryllium (60–210 millicuries) or radium-beryllium (200 millicuries) was placed in the paraffin jacket as shown. This jacket, surrounding the whole Dewar, produced slow neutrons which diffused into the Dewar space, activating the silver target. Inside the metal Dewar a soft glass Dewar was mounted to the Dewar cap to serve as protection for the silver target cylinders which were dropped into place inside the surrounding can of cold hydrocarbon. The walls of the soft glass Dewar absorbed about seven percent of room temperature neutrons. The copper can used to hold the cooling hydrocarbon in position had 0.3 mm walls, thick ends (approximately 1 mm), and a set of radial vanes inside to facilitate the establishment of temperature equilibrium. Thirteen hundred cubic centimeters was the total volume. When in position, at least ninety percent of the neutrons activating the target passed through the can. In order to estimate this fraction, the can was filled with 3.7 molal $CdCl_2$ solution, which diminished the activity by eighty percent. Half of the residual twenty percent was not absorbed by cadmium.

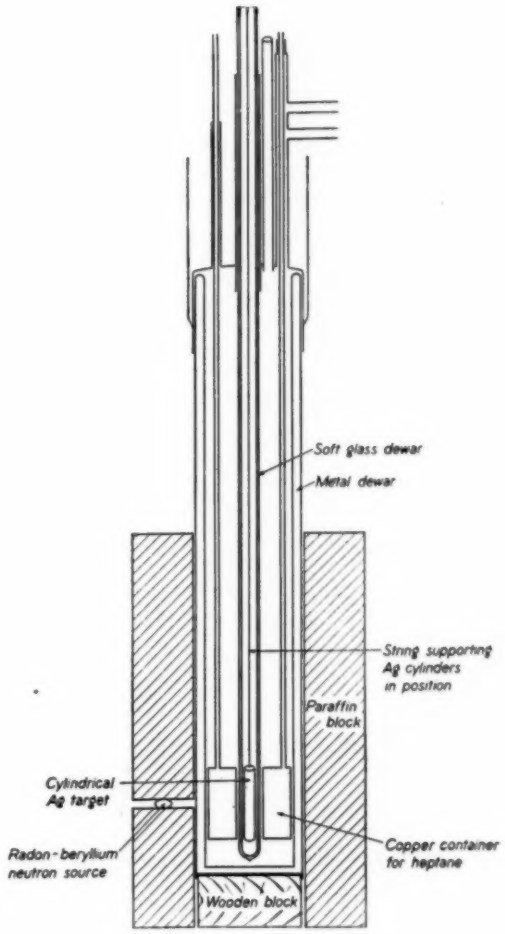

FIG. 2. Large Dewar assembly.

[10] Fermi, Ricerca Scient. 7, 13 (1936).

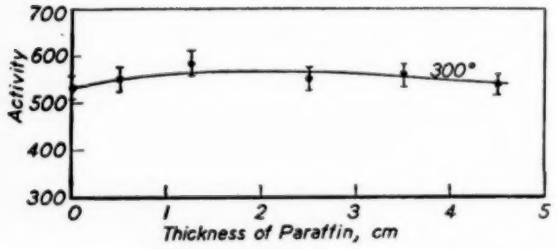

FIG. 3. Effect of introduction of paraffin cylinders of different thicknesses on activity of target.

The procedure used was to activate the silver cylinder (11 cm long, 1 cm in diameter, and approximately 0.1 mm thick) for 7 minutes, with the hydrogenous substance at a temperature constant within one or two degrees during the activation period. The Dewar contents were generally cooled with either liquid air or liquid hydrogen, and allowed to come to thermal equilibrium. The cooling liquid was then removed and silver activations were taken as the contents slowly warmed. Since the temperature drift in the important low temperature range was considerably greater than at higher temperatures, an accurate point at 20°K was obtained by making activation runs while the liquid hydrogen was still surrounding the can (as shown by the thermocouples), and then extrapolating the activity data to the time the last hydrogen left. Several runs from 20° to 300° gave enough data to average over each interval of a few degrees. The target activities were measured with a solid-wall tube counter for the interval of nine minutes between the end of the second and the beginning of the twelfth minute after the end of the activation period. This assured that the effects measured were mainly due to the 2.3 minute silver activity. For purposes of comparison a theoretical curve which was calculated on the assumption that all neutrons captured were absorbed by "$1/v$" law nuclei is shown with each set of data. The expression for the curve is

$$\text{Activity} \sim e^{-\gamma T^{-1}}(1-e^{-0.77 T^{-1}}), \qquad (1)$$

where T is the absolute temperature and 0.77 was determined by the dimensions of the target and the absorption cross section of silver for neutrons exciting the 2.3-minute period. This treatment obviously cannot be expected to be rigorous because it assumes that the neutrons pass through the target only once. However, at the lower temperatures where the absorption cross sections are larger, it might be expected to be more rigorous. The smeared velocity distribution resulting from the capture and creation processes introduces an additional reason for this relation's being only approximate. The constant γ, presumably measuring the thickness of hydrogenous material traversed on the average by the neutrons after they have been cooled, is fitted to the data in each case.

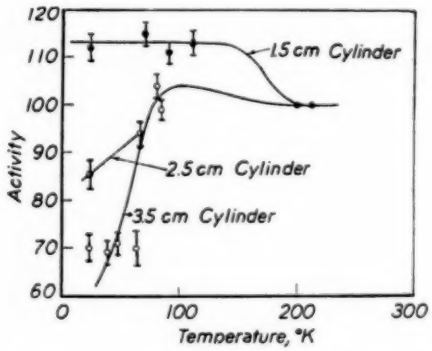

FIG. 4. Temperature effects with different thicknesses of cold paraffin.

DATA FOR PARAFFIN

Paraffin was studied by replacing the copper can shown in Fig. 2 with paraffin cylinders of the same height and various thicknesses. At room temperature, introduction of the paraffin cylinders inside the Dewar altered the activity of the target very little, as shown in Fig. 3. The data for the cold paraffin cylinders are shown in Fig. 4. These effects are similar to those reported by Moon and Tillman, but somewhat smaller, presumably because the neutrons were able to pass through the target several times. As shown later, the effect of such multiple passage would tend to decrease the temperature effects.

The general character of the curves in Fig. 3 suggests that the initial rise on cooling is due to the effect of slowing the neutrons on the capture probabilities for both the silver target (2.3 minute period) and the paraffin protons, the two capture effects being so balanced as to lead to an initial rise in target capture which is more

than compensated at lower temperatures by capture by the protons and soft glass Dewar. The paraffin temperatures were measured by two copper-constantan thermocouples imbedded at the top and bottom of the cylinders. The temperatures differed by less than two degrees during the runs and their mean was used.

Data for *n* Heptane

Normal heptane was selected for careful study because it has a straight chain molecule of considerable length and was rather easily obtained. The sample was 99 percent pure. Fig. 5 shows the data. They obviously closely resemble those for paraffin.

Data for a 1.5 cm layer of heptane in a can similar to the 4.5 cm can described are also shown. Again, they seem to show the same characteristics as those found with paraffin of approximately the same thickness, an initial rise

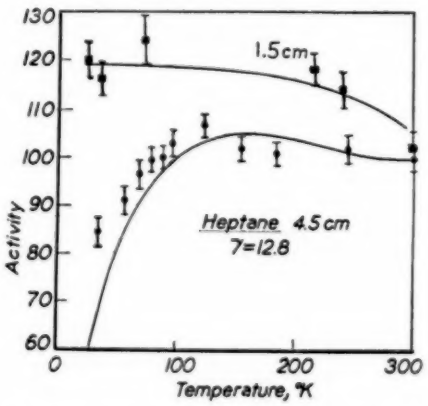

Fig. 5. Heptane data for 4.5 cm and 1.5 cm thicknesses.

and then temperature independence at lower temperatures. This is expected for small γ values from Eq. (1) and checks our supposition that the γ values increase with the average thickness of hydrogenous material through which the cold neutrons diffuse.

Data for Ethane

Ethane was introduced into the apparatus by immersing the 4.5 cm thick copper can in liquid air and condensing gas from a commercial cylinder. Measurements of the boiling point gave an estimate of less than three percent of impurities. Fig. 6 shows the data.

Comparison of these data with those shown in Fig. 5 for heptane reveals a definite difference below 80°K. For ethane, there seems to exist a temperature below which no further cooling changes the activity. Since for all the hydrogenous substances used, except liquid hydrogen, the numbers of protons per cubic centimeter were the same within four percent, it seems evident that at low temperatures the ethane ceases to cool the neutrons as well as does heptane. The curve was drawn for $\gamma=13.5$, approximately the same as for heptane. The data of Witt and Kemp[11] on the heat capacity of ethane show that the heat capacity first rises above the Debye curve for heat capacity due to crystalline vibrations at about 50°K, indicating the appearance of some new type of excitation, probably molecular, at about this temperature. This temperature agrees fairly well with the temperature at which ethane appeared to stop cooling and seems to point to a connection between ability to cool neutrons and this new type of excitation.

Data for Methane

Methane condensed from natural gas, pure to at least 95 percent, was condensed in the can just as in the case of ethane. Since it boils at 112°K no data for higher temperatures were obtained. The data for the lower range are shown in Fig. 6. The point for 300°K was written in on the basis of the observation mentioned above, that the placing of 300° paraffin, heptane, or water around the target cylinder caused no appreciable change in the activity produced.

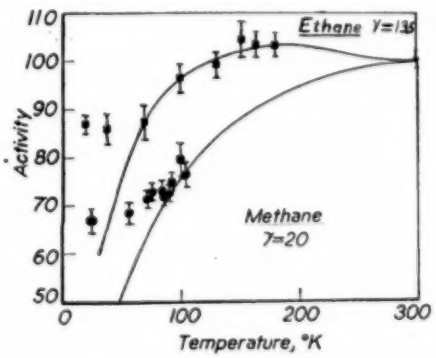

Fig. 6. Ethane and methane data.

[11] Witt and Kemp, J. Am. Chem. Soc. **59**, 273 (1936).

Assuming that 300° methane would not differ appreciably from these substances, the value of the activity at 100°K becomes remarkably low. Apparently the methane is cooling more rapidly than either heptane or paraffin, so that the neutrons have a thicker average layer of hydrocarbon to traverse before reaching the target. It is also clear that at some temperature around 80°K the ability to cool neutrons further is being lost rapidly. However, since the number of carbon nuclei per unit volume is considerably smaller in this case an effect similar to that found with pure liquid hydrogen reported elsewhere in this paper might be expected. The hydrogen experiment seems to show that the absence of any heavy nuclei to scatter the neutrons and keep them in the cooling medium as long as they would have remained otherwise made it difficult for the hydrogen to cool them. Such an effect in the methane would have given too low an activity at 300°K and our assumption that the methane would be quite equivalent to heptane at 300°K would then be wrong. Against this view, experiments reported later, in which liquid hydrogen itself was used in the Dewar instead of the hydrocarbon, and compared directly with an hydrocarbon solution of the same proton density at 300°K, showed that the activity due to the liquid hydrogen (which was unable to cool to temperatures lower than about 120°K, and was therefore not greatly different from 300°K liquid hydrogen) was nearly the same as that for the hydrocarbon solution. The surrounding paraffin jacket seems to help keep the neutrons in the cooling medium in both cases. Consequently, the authors believe the best explanation is that methane has more ways of absorbing neutron energy, possibly because its molecular rotation is so easily excited.

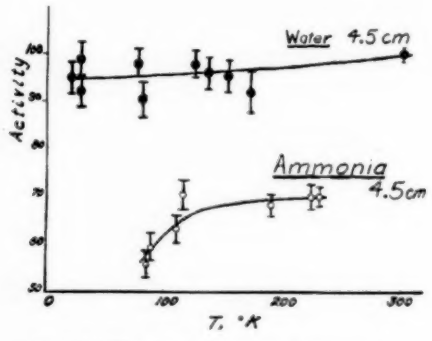

FIG. 7. Data on water and ammonia.

The solid curve on the graph is for γ equal to 20, agreeing with the previous interpretation of γ as a measure of the average thickness of hydrocarbon traversed after the average neutron was cooled.

DATA FOR WATER

The principal difficulty in the work with water was the expansion on freezing, which stretched the can and changed the geometry to a slight extent. However, the distortion, occurring principally in the radial direction perpendicular to the surface of the target, could hardly have caused a serious change in the shape of the temperature curve. The data are shown in Fig. 7.

On the lines of the previous interpretations the temperature independence of the activities with water in the can probably means that it has ceased to cool at some temperature not lower than 100°K where the large temperature effects are expected to appear first (with this apparatus). In addition, it is clear that water does not cool as rapidly as does methane, for there is no appreciable drop between 300°K and 100°K. It appears that the two molecules differ markedly in the rate at which they cool thermal neutrons.

These conclusions are not surprising in view of the well-known character of the ice crystal. Investigations of the temperature variation of the dielectric constant (for infinite frequency) with temperature shows that a constant value is reached on cooling to 110°K. In addition, the heat capacity of water first rises above the Debye curve at about 185°K.[12] One would expect, therefore, that any neutron cooling process depending on excitation of states of individual molecules rather than of the ice crystal as a whole (Debye curve) would cease to function at some neutron temperature between 110°K and 185°K, agreeing with the results obtained.

In more detail, the lethargic slowing by water as compared to ammonia can be understood on the basis of the crystal structure of ice. Bernal and Fowler[13] have shown that a structure in-

[12] Giaque and Stout, J. Am. Chem. Soc. **58**, 1144 (1936).
[13] Bernal and Fowler, J. Chem. Phys. **1**, 515 (1933).

TABLE II. *Data on first liquid H_2 experiment.*

CONDITIONS	ACTIVITY
Empty Dewar (300°K)	400±15
Liquid H_2 (20°K)	500±15
Water (300°K)	540±15

volving random orientation of hydrogen bonds[14] accounts very well for the known properties of water. The verifications[12, 15] of Pauling's[16] prediction on the basis of this model, of a discrepancy between the entropy of ice deduced from specific heat data and the third law of thermodynamics and the entropy from spectroscopic data, has established the model even more firmly. Therefore any mechanism of transfer of energy from a neutron to a water molecule which requires excitation of rotational states would be expected to be quite inhibited in the ice crystal. On the other hand, the methane crystal is known to allow molecular rotation, agreeing with our observation that methane apparently cooled more rapidly than ice. The indication afforded by these facts, that the excitation of rotational states in the cooling molecule is an important mechanism for neutron cooling, is further born out by work described below on the relative effects with *ortho* and *para* liquid hydrogen.

DATA ON AMMONIA

Ammonia from a commercial cylinder (99 percent pure) was condensed in the can immersed in a bath of ether cooled with solid carbon dioxide. The corrosive action of the liquid and solid ammonia on the copper made the manipulation somewhat difficult, so data were not obtained at liquid hydrogen temperatures. The data down to 80°K are shown in Fig. 7.

One might suppose at first sight that the difference between the empty can activity and the asymptotic value of 80 percent for the 300° ammonia is due to rapid cooling of the type shown by methane. However, it has been shown by several observers that nitrogen has a rather large cross section for capture ($\sim 8 \times 10^{-24}$ cm^2). The simplest explanation seems to be that the nitrogen absorption in the ammonia caused this decrease in activity. The character of the data indicates that it is still cooling at liquid-air temperatures, though it will probably soon stop because the specific heat of ammonia drops to the Debye limiting curve at about this temperature.

DATA ON DIATOMIC HYDROGEN

Since the investigation of liquid and solid hydrogen over any appreciable range of temperatures was quite impossible, it was necessary to use special experiments employing some of the results reported above to study this very important molecule. The first experiment tried was performed in the small assembly shown in Fig. 8. The Dewar was filled with liquid hydrogen to a level two or three inches above the top of the silver target. The activities so obtained (2.3-min. activity, after 7 minutes activation) were compared with activities from the same arrangement when the liquid hydrogen was replaced with water at room temperature. Table II contains the data.

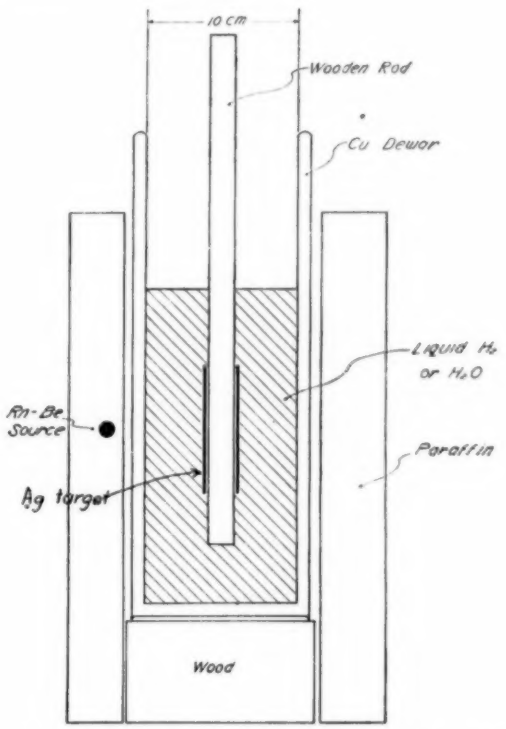

FIG. 8. First experiment on cooling by liquid hydrogen. Small copper Dewar assembly.

[14] Latimer and Rodebush, J. Am. Chem. Soc. **42**, 1529 (1920).
[15] Long and Kemp, J. Am. Chem. Soc. **58**, 829 (1936).
[16] Pauling, J. Am. Chem. Soc. **57**, 2680 (1935).

TABLE III. *Data for liquid H_2 runs in large assembly.*

CONDITIONS	ACTIVITY
Empty Dewar (300°K)	540±15
Liquid H_2(20°K)	730±15
Solid H_2 (13°K)	720±15
"Equivalent" (300°K) Liquid (21.2% CH_3OH in acetic acid)	700±15
Paraffin Cylinder (1.5 cm thick) +Liquid H_2 (20°K)	560±15
Carbon Cylinder (0.5 cm thick)+Liquid H_2 (20°K)	700±15

Since the relative proton densities of liquid hydrogen and water are 1 and 1.4, from these data it seemed probable that the liquid hydrogen and water were having about the same effect, allowing for the higher proton concentration of the water. To further elucidate this point, the large assembly shown in Fig. 2 was used with the copper sample can removed. The level of liquid hydrogen was adjusted by placing two thermocouples approximately two inches apart on the soft glass Dewar, at a level about three inches above the top of the silver target. The experiments described above were then repeated with this assembly. In addition, runs were made with solid hydrogen (obtained by pumping till the vapor pressure fell to 4 cm) and with a solution of methyl alcohol in acetic acid which had the same number of protons per cubic centimeter as the liquid hydrogen. The composition of this solution is 21.2 percent alcohol by volume. The data are shown in Table III.

Table III also includes results from an experiment in which a paraffin cylinder 1.5 cm thick and of the same height as the target, was placed around the soft glass Dewar so as to cover the target as completely as possible, and the rest of the volume filled with liquid hydrogen.

It is apparent from the data that liquid and solid hydrogen both have nearly the same effect as a room temperature hydrocarbon liquid of the same proton density. The interposition of the paraffin cylinder caused a large decrease incommensurate with its dimensions, in view of the experiments with paraffin and pure hydrocarbons described above. One is led to conclude that the process probably consists of a cooling by liquid hydrogen to a certain temperature, e.g. 180°K, well above 20°K and a further cooling by the paraffin. This further cooling would lead to high absorption by the paraffin protons and by the soft glass Dewar, causing the observed drop in activity. An alternative explanation, of course, is that the carbon in the paraffin cylinder is absorbing or scattering to such an extent that the activity is reduced. This point was settled, however, by replacing the paraffin cylinder with a thinner one of carbon containing the same number of carbon atoms. The result, shown in Table III, is conclusively in favor of the explanation given.

The correlations already obtained between the ability to cool neutrons and the specific heats involving excitation of the individual molecules, rather than crystals as a whole, made the inability of the hydrogen molecule to cool to low temperatures quite understandable. It also suggested that in this case a more direct check on the mechanism of the energy transfer might be made by studying the relative effects of *ortho* and *para* liquid hydrogen in the Dewar.

This was done by filling the Dewar with non-equilibrium liquid hydrogen (75 percent *ortho*) and converting it to *para* by dropping active charcoal into the Dewar and allowing it to stand for approximately an hour. Samples of the gas were taken in both cases for subsequent analysis by the standard heat conductivity method. The

TABLE IV. *Data for runs with equilibrium (75% ortho) and para liquid H_2 in large assembly.*

ACTIVITIES	
75% *ortho*	100% *para*
2998	2858
2861	3140
2854	2975
2766	3115
2610	3150
2620	2990
2980	3188
2837	2900
—	3160
2817±35	3018
	3049±27

% Increase on conversion to *para* state = 8.3±1.5

TABLE V. *Data on production of slow neutrons by water and liquid hydrogen.*

LIQUID	ACTIVITY
Water (300°K	14±1
Liquid H_2 (20°K)	1±1

compositions were found to be 75 percent *ortho* in the first case and 99 percent *para* in the second, within one or two percent. The data for the runs on the activities in the two cases are given in Table IV.

Since the first excited state of the *para* molecule loses its population at a much lower temperature than does the *ortho* molecule, these results are in complete agreement with the hypothesis advanced. Fig. 9 shows the populations of the ground and first excited rotational state for the two molecules at various temperatures. The curves were calculated from the data of Giauque.[17]

From these data a lower limit of approximately 100°K for *para* hydrogen and approximately 200°K for the nonequilibrium mixture (75 percent *ortho*) might be expected. The agreement with the results seems to indicate, in this case at least, that the cooling mechanism is mainly the excitation of rotation in the cooling molecule.

Another experiment was done to determine the ability of liquid hydrogen (75 percent *ortho*) to slow the very fast neutrons from the source. The large metal Dewar was used without the surrounding paraffin cylinder, and the source was placed inside a Pyrex Dewar of the same dimensions as the soft glass Dewar described previously. Targets of dysprosium oxide mounted on varnished linen with rubber cement (0.20 g of Dy_2O_3/cm^2) were placed in the cooling liquid. The Dewar was filled to a level about 20 inches from the bottom. A cross section of the assembly is shown in Fig. 10 and the data in Table V.

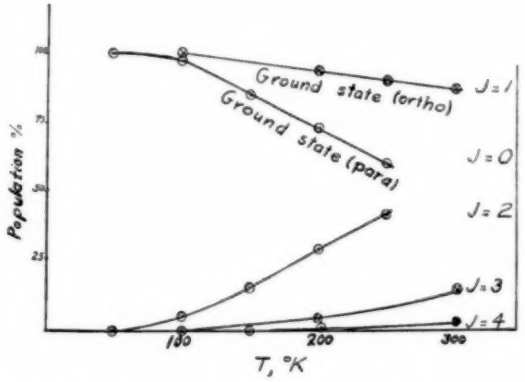

FIG. 9. Level populations for ortho- and parahydrogen.

[17] Giauque, J. Am. Chem. Soc. **52**, 4816 (1930).

These results agree with those of Fomin, Houtermans, Leipunsky, and Schubnikow,[18] who also found that water is much more efficient in

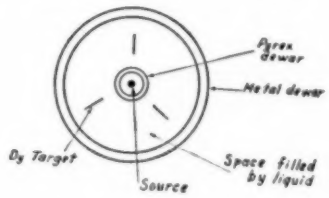

FIG. 10. Arrangement for determining relative effects of water and liquid hydrogen in slowing fast neutrons.

producing slow neutrons. A plausible explanation seems to be that the smaller mass of the H_2 molecule and the absence of the additional scattering due to O prevents the neutrons from staying in the cooling liquid as long as in the case of water, and consequently allows them less chance to attain temperature equilibrium. The experiment is interesting in that it indicates, as did all the previous experiments with heavier hydrogenous molecules, that cooling by recoil of the whole molecule is of small importance in the liquid or solid state. It seems probable that this conclusion should necessarily apply to all heavier molecules in the liquid or solid states.

CONCLUSIONS FROM COOLING EXPERIMENTS WITH DIFFERENT HYDROGENOUS MOLECULES

Figure 11 shows the collected data for the molecules most thoroughly studied, other than H_2. These curves in conjunction with the detailed considerations given above seem to justify the following conclusions:

1. An hydrogenous molecule in its ground state can cool only those neutrons whose kinetic energies are at least equal to the energy necessary to excite the molecule to its first state, e.g., the temperature of neutrons emerging from a crystal of such molecules at 0°K will approximate the temperature at which the specific heat curve begins to rise above the Debye curve for the crystalline specific heat.

2. The probability of energy loss to a crystal or liquid as a whole seems to be small.

3. For hydrocarbons, the limiting temperature for cooling appears to decrease with increase in length of the hydrocarbon chain.

[18] Fomin, Houtermans, Leipunsky, and Schubnikow, Physik Zeits. Sowjetunion **9**, 696 (1936).

4. The speed of cooling by hydrogenous solids, i.e., the probability of energy loss by a high temperature neutron, seems to be highest for those molecules having the largest number of rotational degrees of freedom in the solid state.

Measurement of Neutron Temperature

If the absorption of slow neutrons by boron nuclei really obeys the "$1/v$" law, it should be possible to use this absorption as a rather sensitive neutron "thermometer." A first attempt was made to study the absorption in H_3BO_3 sheets (absorbed on filter paper) of the neutrons passing through the walls of the large metal Dewar shown in Fig. 3, when it was filled with paraffin and all surrounding hydrogenous material removed to a distance of at least two feet. The absorption curve was run at both 300°K and 90°K, using rhodium as a detector. No change in absorption coefficient greater than about five percent was found. Presumably this was due to absorption of the slower neutrons in the Dewar walls at both temperatures, reducing the effect of temperature change. The large component of neutrons not absorbable in cadmium exciting the rhodium also made the measurements more uncertain. For this reason the target was changed in the later work to dysprosium.

About 98 percent of the neutrons exciting dysprosium are absorbed by cadmium. At first it seemed that this choice would lead to difficulties because it had been commonly supposed that the very high absorption cross section for

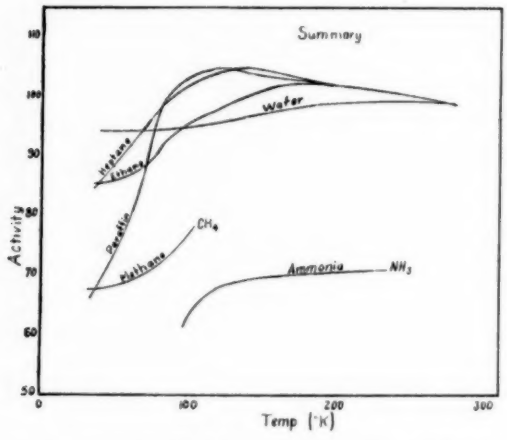

Fig. 11. Summary of data on hydrogenous molecules.

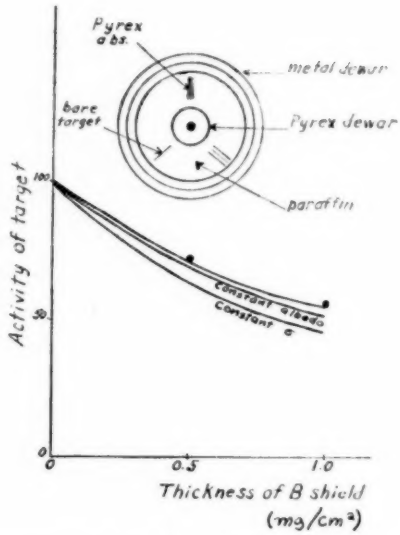

Fig. 12. Arrangement and 90°K curve for multiple passage boron absorption.

this element must be due to the existence, for one of the isotopes, of a resonance level in or near the thermal region, which would necessarily distort the absorption from the "$1/v$" law. However, test runs made in collaboration with Dr. P. W. Schutz, with dysprosium and silver targets placed between paraffin blocks, first at room temperature, and then at liquid-air temperature, gave the same relative change (approximately 10 percent increase) for the activity of the dysprosium as for the 2.3-minute activity of silver. Data described later on a comparison between B and Dy further check the "$1/v$" character of the dysprosium absorption. The activities of the targets were measured with a Lauritsen quartz fiber electroscope.

"Multiple Passage" Boron Absorption

Figure 12 shows a cross section of the apparatus used in the first experiment with the dysprosium targets. The long period (2.3 hours) of the dysprosium activity allowed the target to be placed inside the Dewar and so eliminated Dewar wall absorption. Three targets were used. All were squares with 3 cm sides and having a total of 0.20 g of dysprosium, as Dy_2O_3, mounted on varnished linen with a thin layer of rubber cement. Calibration showed the three targets to be identical within a small error. The targets were placed symmetrically around the source (in the central small Pyrex Dewar) in slits cut in

the paraffin cylinder just wide enough for the targets and absorbers. In this way each run gave two points on the absorption curve at each temperature.

Since the thickness and absorption cross sections for the H_3BO_3 absorbers and Dy_2O_3 absorbers as well as the reflection coefficient (albedo) for the neutrons succeeding in passing through both absorbers and the target were all known for 300°K neutrons it seemed possible to calculate the absorption curve. This proved to be the case. Furthermore, by assuming the "$1/v$" law throughout, also that the albedo varies as indicated by Fermi's considerations, and that the neutrons were at thermal equilibrium inside the block, the curves could be calculated for 90°K and 20°K. If the absorption coefficient of the dysprosium target is expressed as $bT^{-\frac{1}{2}}$ and for the boron absorbers as $taT^{-\frac{1}{2}}$, where b and a are constants and t is the thickness of the boron absorbers, the activity of the target, A, is given at 300°K by

$$A=K(1-[\exp -b(300)^{-\frac{1}{2}}]) \times\frac{[\exp -ta(300)^{-\frac{1}{2}}]}{1-\zeta[\exp -(b+2ta)(300)^{-\frac{1}{2}}]}, \quad (2)$$

in which K is a constant and ζ is the albedo coefficient (0.82 for 300°K neutrons). At any other temperature ζ should be calculated, on the above assumptions, from the expression

$$\frac{2}{1-\zeta}=(N)^{\frac{1}{2}}, \quad (3)$$

where N is the average number of collisions of the neutron with protons necessary for capture by the protons. The assumption of the "$1/v$" law for proton capture requires N to vary as the reciprocal of the square root of the temperature, so that

$$\zeta=1-0.75T^{-\frac{1}{2}}. \quad (4)$$

Substitution of expression 4 in Eq. (2) gives the final equation used for calculating the expected curves. Figs. 12 and 13 show the curves and data for 90°K and 20°K, respectively. Curves are also shown for the effect of assuming the dysprosium cross section, σ, to be independent of temperature in one case, and the albedo to be constant in the other case. The experimental error of the points is about equal to their width so that the agreement seems to be satisfactory in both cases. For purposes of comparison, one point of the 300°K curve is shown on the 20°K plot to indicate how small the temperature effect is in this arrangement where the neutrons are allowed to make as many passages as possible through the target and absorbers. For this reason the arrangement was discarded as a means of measuring neutron temperatures and the following single passage arrangement was substituted.

Single Passage Boron Absorption

The arrangement for this series of experiments is shown in Fig. 14. The three dysprosium targets were placed symmetrically around the source at the surface of the 4.5 cm paraffin cylinder. Each had a sheet of cadmium behind it to prevent multiple passage. The whole assembly was moved as far as possible (approximately two feet) from the nearest hydrogenous material. Thin Pyrex plates, made by etching thicker plates with hydrofluoric acid, were used as absorbers. Use of several thicknesses showed the absorption to be exponential at each temperature. The averages from twenty runs are shown in Fig. 14, with the probable errors indicated by the vertical lines through each point. The two low points refer to measurements described later, made with a BF_3 neutron counter.

Apparently the data do not fit the straight line expected if the "$1/v$" law holds for B and Dy and the neutrons are at the temperature of the block. It seemed probable that the assumption of the "$1/v$" law for dysprosium was the weakest of the three assumptions involved, so

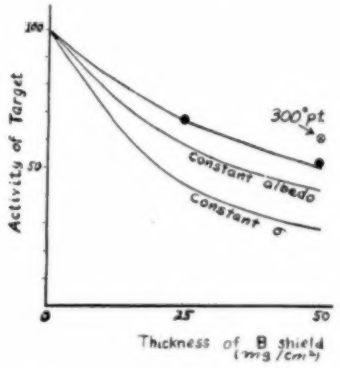

FIG. 13. Multiple passage boron absorption curve for 20°K.

determinations of the absorption coefficients were made with a neutron counter filled with boron trifluoride, instead of the dysprosium.

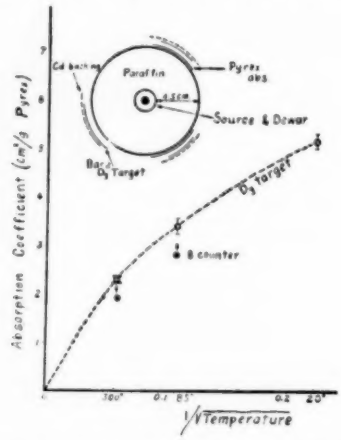

FIG. 14. "Single passage" boron absorption assembly. Data obtained.

The counter is an ordinary tube counter with an iron wire, 0.22 mm in diameter, filled to 12.5 cm pressure with BF_3 gas. It is quite possible by use of a linear amplifier of standard type to adjust the counter to respond to slow neutrons quite efficiently (probably 5 percent of the 300°K neutrons traversing the counter register), without giving counts of more than two or three per minute due to the gamma-radiation from 200 mg of Ra+Be at a distance of six inches or less even when the counter is unshielded with lead. The voltage adjustment for the counter is not very critical, a variation of twenty volts in the counting voltage of 1600 being quite unimportant. It is necessary to remove all hydrogenous material, such as paraffin, from contact with the gas to prevent its decomposition and destruction of the selective characteristics of the instrument.

The arrangement used for the boron counter work consisted of the paraffin plug and Pyrex Dewar for the source as shown in Fig. 14. The paraffin was cooled, for the 90°K run, by immersion in liquid air, and was then removed to a position in mid-air at considerable distance (approximately two feet) from hydrogenous material. The boron counter, 17 cm long and 2.3 cm in diameter, was placed 8 inches distant with its axis parallel to that of the paraffin cylinder. A thick Pyrex plate was interposed at intervals between the paraffin and the counter to absorb the neutrons coming directly from the paraffin, and to allow the slow neutrons being scattered from the floor to be counted. The cold paraffin runs were only two minutes long and a test run with a thermocouple imbedded in the block showed that the temperature rise during this interval was certainly less than 5°.

The absorption curves were obtained for both the paraffin and "floor" neutrons by slipping Pyrex cylinders (etched to appropriate thickness with hydrofluoric acid), around the counter. Fig. 15 is a logarithmic plot of the data obtained. The data obviously check the dysprosium data within the limits of error, for the ratio of the absorption coefficient for 90°K to that for 300°K was 1.5 ± 0.1 in the case of the dysprosium targets and is 1.44 ± 0.05 in this case, indicating again that dysprosium acts like a "$1/v$" absorber. However, this test, using the B and Dy as targets rather than absorbers, is not as reliable as a test using them as absorbers would be. The small amount of dysprosium available (approximately 1 gram) prevented the latter experiment. The two coefficients are plotted in Fig. 14. They are lower in absolute value than those for the Dy work by about the fraction one would expect from the difference in the two cases in the average angles between the paths of the incident neutrons and the normals to the Pyrex absorbers. The average angle in the case of the counter work was smaller.

The most plausible view now remaining seems to be that the neutrons emerging from such a

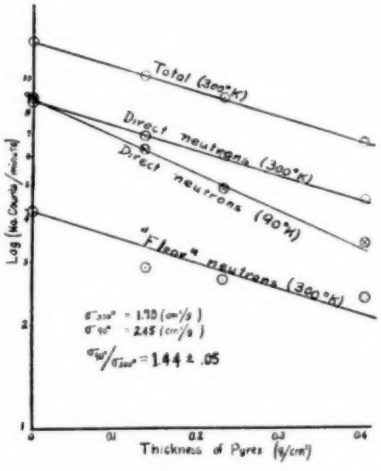

FIG. 15. Data for boron counter determination of boron absorption coefficient.

block have not attained thermal equilibrium. The experiments on "multiple passage" seemed to show that in this case thermal equilibrium was nearly attained, though the low sensitivity of the measured effects to change in temperature may have masked any small failure to cool. It seems reasonable, however, that in the case of multiple passage the repeated reflections may offer more opportunity for the neutrons to cool and even select those that have cooled. Further evidence for this conclusion was obtained by consideration of the results of Amaldi and Segrè,[19] on the apparent equality of the albedo coefficient for 90°K to that for 300°K.

Temperature Variation of Albedo (Reflection) Coefficient

The results of Amaldi and Segrè were checked in the following way. A dysprosium target was activated when exposed on the top of a cube of paraffin (approximately 8 cm on a side) which was so placed beside the radium-beryllium source that a second identical cube placed on top of the target would occupy a position symmetrical to that of the first cube with respect to the source. The arrangements are shown in Fig. 16.

The ratio of the activity with two blocks to that with one block was obtained first with the blocks at 300°K and later with them immersed in liquid air at 90°K. The ratio was 8.1 ± 0.2 in both cases, a somewhat lower value than reported by Amaldi and Fermi,[20] probably because the effect of neutrons of intermediate energy above thermal produced in one block which are cooled on addition of the second block is neglected. This was justified because such an effect should be expected to be nearly independent of temperature and should also be small in absolute magnitude. This ratio, R, is easily shown[10] to satisfy the relation

$$R=2/(1-\zeta), \qquad (5)$$

if the absorption cross section of the target for neutrons present inside a block of paraffin and that for those emitted from the surface can be assumed to be the same. This, however, is the point discussed above. If σ_i represents the cross section inside the block and σ_e that for the neutrons coming from the surface, Eq. (5) becomes

$$R=(\sigma_i/\sigma_e)(2/(1-\zeta)), \qquad (5')$$

where ζ is the albedo coefficient, as usual.

Assuming that σ_i and ζ vary with the temperature in the way expected from the "$1/v$" law, and that the neutrons inside the block are at the temperature of the paraffin block, the ratio of R for 90°K to R for 300°K can be calculated from the experimental value of 1.47 for the ratio of σ_e at 90° to σ_e for 300°. The result is unity within the error of measurement, agreeing with the experimental results.

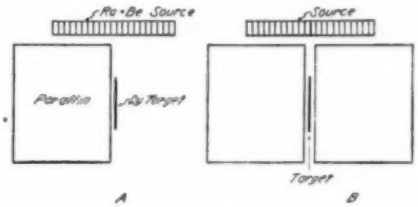

Fig. 16. Arrangements for measuring temperature variation of the "albedo" coefficient.

In addition to such a failure to cool due to proximity to the surface, there probably is an effect in the paraffin analogous to that found in lighter molecules which limits the cooling because of absence of likely mechanisms at the lower energies. The authors are much indebted to Professor J. R. Oppenheimer and Mr. W. E. Lamb of the physics department for helpful discussions and suggestions about this and other phases of the problem.

Temperature of "Ice Neutrons"

Having a temperature scale empirically calibrated, the paraffin cylinder in Fig. 14 was replaced by one of ice of the same dimensions and the absorption curve obtained when the ice was at 20°K. The value for the absorption coefficient was 3.4 ± 0.4 cm²/g of Pyrex, corresponding to a neutron temperature of about 100°K, in agreement with the previous conclusions.

The authors wish to express their gratitude to Professors Gilbert N. Lewis and W. M. Latimer for their continued interest and support. They are also much indebted to Professor W. F. Giauque for assistance with the low temperature work. It is also a pleasure to thank Dr. L. R. Taussig and the University of California Hospital for the donation of the large quantities of radon used in this research.

[19] Amaldi and Segrè, Phys. Rev. **50**, 571 (1936).
[20] Amaldi and Fermi, Phys. Rev. **50**, 899 (1936).

The Beta-Ray Spectra of Li^8 and B^{12}

D. S. Bayley and H. R. Crane
University of Michigan, Ann Arbor, Michigan

(Received July 15, 1937)

Cloud chamber measurements have been made on the beta-ray spectra of Li^8 and B^{12}. The use of strict criteria in the selection of tracks for measurement is thought to have reduced preference for tracks at one or the other end of the spectrum. Separate measurements near the upper limits give for both spectra upper limits by inspection of 12.0 ± 0.6 Mev. Evidence is presented that the protons emitted during the formation of Li^8 have nearly zero energy. It is thus possible to determine the energy available in the radioactive disintegration of Li^8 into an electron, neutrino and two alpha-particles. Comparisons are made between the experimental Li^8 spectrum and those predicted by using the K-U and Fermi theories in conjunction with the recently measured alpha-particle distributions. It is shown that the K-U theory demands a reaction energy 5 Mev greater than that which is available. An indication is given that the protons emitted during the formation of B^{12} have an energy of at least 1 Mev, while a proton energy of nearly zero is required if the K-U upper limit, 14.5 Mev, is correct.

Introduction

THE cloud chamber method of measuring beta-ray spectra is most effective when applied to such high energy spectra as those of Li^8 and B^{12}. Distortion of the spectra due to scattering of the electrons in the gas is entirely negligible over the greater part of the energy range. The short lifetimes of Li^8 and B^{12} give no inconvenience, as they would in a spectrograph, because the target can be bombarded immediately before each expansion.

Accurate measurements of the high energy spectra lead to results of considerable theoretical importance: The mass differences in such isobaric pairs as Li^8-Be^8 and $B^{12}-C^{12}$ give promise of being important in the determination of the energy level schemes of light nuclei. The recent observation by Lewis, Burcham and Chang[1] of a continuous alpha-particle emission associated with the disintegration of Li^8 indicates that the beta-ray spectrum of this isotope is complex. It is therefore of interest to compare this spectrum with that of B^{12}, which is presumably not complicated by subsequent splitting into alpha-particles. A further point of interest is that the energy balances in the Li^8 and B^{12} disintegrations furnish by far the most clear proof that the energy lost by a nucleus during a beta-disintegration is that corresponding to the upper limit of the spectrum. It is also possible, by means of the energy balances, to discover whether or not the K-U upper limit demands more energy than is available in the reaction.

The beta-rays from Li^8 and B^{12} were first observed and measured by Crane, Delsasso, Fowler and Lauritsen,[2] by the cloud chamber method. The present experiment is an attempt to measure with greater accuracy the shapes and upper energy limits of these spectra. The principal improvements in the method used lie in the strict criteria used in selecting the tracks for measurement, and in the fact that overlapping measurements were made at several magnetic field strengths. In this way it is believed that the preference for tracks at one or the other end of the spectrum has been reduced.

Experimental Method

The cloud chamber used in the work described is 15 cm in diameter and 3 cm deep, filled with air and ethyl alcohol vapor at atmospheric pressure. It is equipped with a pair of air core coils which produce a magnetic field for bending the tracks in the plane of the chamber. Calibration of the field strength was made by means of a pick-up coil and standard mutual inductance. The measurement was made automatically at the time of expansion of the cloud chamber, in order to eliminate any question as to the building up of the field, and is considered accurate to within 2 percent. The error introduced by the nonuniformity of the field over the area of the chamber is less than 1 percent. A vernier resistance in the field circuit of the generator supplying the current to the coils made it

[1] Lewis, Burcham and Chang, Nature **139**, 24 (1937).

[2] Crane, Delsasso, Fowler and Lauritsen, Phys. Rev. **47**, 971 and 887 (1935).

FIG. 1. Li^8 beta-rays from a thin walled thimble inside the cloud chamber. Three of these tracks satisfy the requirements for measurement.

possible to keep the field strength constant to within 1 percent at all times.

Li^8 and B^{12} were produced by bombarding targets of lithium metal and amorphous boron with deuterons of about 500 kv energy, accelerated by a high potential transformer-vacuum tube apparatus.[3] For measurements of the shapes of the beta-ray spectra the target was placed in a thin walled (0.2 mm) aluminum thimble, which projected into the cloud chamber through the glass top plate. The targets were sloped toward the center of the chamber, so that the only material which the beta-rays passed through was the 0.2 mm aluminum wall. The tracks were illuminated by means of a carbon arc, flashed at 300 amperes, and were photographed with a Sept camera mounted directly above the chamber. An example of the photographs obtained is shown in Fig. 1 and indicates the position of the target in the cloud chamber. A motor driven contact system was used to operate the tube and cloud chamber in the proper sequence. For lithium (0.9 second half-life) the expansion occurred about two seconds after bombardment, and for boron (0.02 second half-life) the expansion was delayed only 1/25 second. The length of time of bombardment was 1 second for lithium and 0.1 second for boron.

[3] Crane, Phys. Rev. **52**, 11 (1937).

In order to obtain additional data at the upper limits of the spectra, an arrangement was used in which the target was placed outside the cloud chamber and coils, and the particles were allowed to pass into the chamber through a thin window. The path of the particles in the magnetic field outside the chamber was such that only those of radius of curvature greater than 6 cm were able to reach the window. All other particles were stopped by suitably placed absorbing blocks or were bent away by the magnetic field. A graphical estimate showed that for particles with radius of curvature greater than 8 cm (7 Mev) the variation with curvature of the solid angle subtended at the target by the chamber window was not appreciable. It was not possible for particles scattered from the faces of the field coils to enter the chamber and still remain closely enough in the horizontal plane to satisfy the criteria for measurement. The picture shown in Fig. 2 was obtained with this arrangement.

The curvatures of the tracks were measured by matching their full size projected images with circles drawn on a card. The size of the projected image was adjusted by means of a photograph of a meter stick placed in the chamber at the position in which the tracks were formed. This method of adjustment is accurate to about 1 percent. To eliminate a curvature

FIG. 2. Li^8 beta-rays entering the cloud chamber through a thin window. This is the arrangement used for measuring the upper limits of the Li^8 and B^{12} spectra.

dependent preference in the selection of tracks for measurement the following criteria were set up:

(1) In order to make sure that all selected tracks could travel 10 cm without striking the chamber wall, it was required that they emerge from the source within the region marked by the white line in Fig. 1.
(2) The measurable portion of each track selected was required to be at least 10 cm long.

It is seen that three of the tracks in Fig. 1 satisfy these requirements. The criteria used insure that the effective solid angle subtended at the source by the active part of the cloud chamber is independent of the curvature of the tracks. This is a frequent source of distortion in cloud chamber measurements where the only requirement for the selection of tracks is measurability.

Results

In measuring the shapes of the spectra, three different values of the magnetic field were used for lithium, and two for boron. The data obtained with the various fields were adjusted to the same scale by making the areas under the overlapping portions equal. The curves are shown in Figs. 3 and 4. The fact that the overlapping portions of the curves have about the same shape is some indication that there is no great preference for the selection of tracks of either high or low curvature. The results of the measurements on the upper limits of the spectra, made with the target outside the chamber, are shown in Fig. 5. The values obtained for the upper limits by inspection are 12 Mev for both lithium and boron, and are considered accurate to within 5 percent, as far as the errors in the actual measurements are concerned. K-U and Fermi plots are given for boron (Fig. 6) but are not given for lithium because it is not a simple spectrum.

With the use of the boron target, a number of photographs were taken of expansions made during bombardment, and with a low magnetic field strength. One of these is reproduced in Fig. 7. The total thickness of the aluminum windows between the target and cloud chamber was such that only the 90 cm group of protons

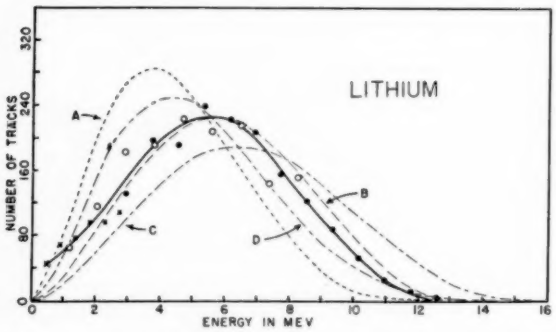

FIG. 3. Heavy curve: experimental spectrum of Li^8. Crosses are for 780 gauss field, circles are for 1490 gauss, dots are for 2670 gauss. The same ordinate scale applies to all points. Curve *A*: K-U theory with F-L alpha-particle distribution. Curve *B*: Fermi theory with F-L alpha-particle distribution. Curve *C*: Fermi theory with R-R-H alpha-particle distribution. Curve *D*: K-U theory with R-R-H alpha-particle distribution.

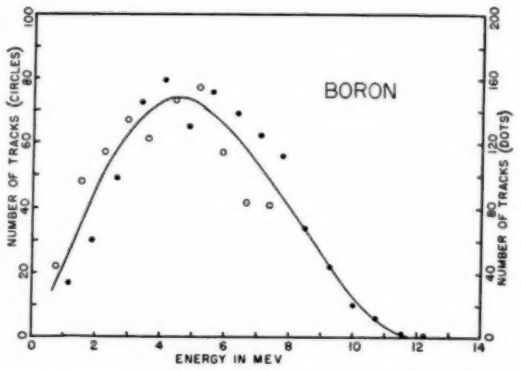

FIG. 4. Experimental spectrum of beta-rays from B^{12}. Circles are for 1220 gauss field (right-hand ordinate scale). Dots are for 2440 gauss field (left-hand ordinate scale).

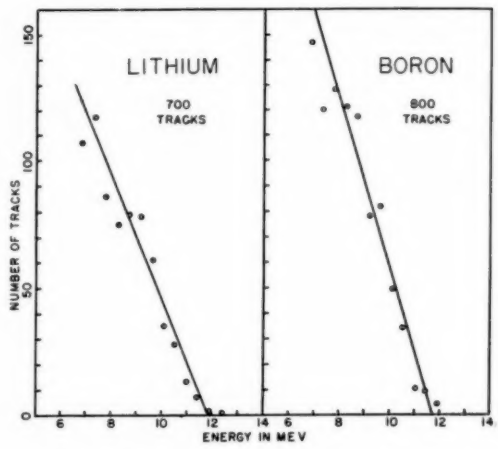

FIG. 5. Plots of separate data obtained near the upper limits of the Li^8 and B^{12} spectra.

from $B^{10}+H^2$ were able to enter the chamber. It was found that the electrons greatly outnumbered the protons of this range group. Our observations gave no reason for modifying the ratio of 20 to 1 given by Crane, Delsasso, Fowler and Lauritsen.[2]

Discussion

Lithium

The reaction describing the formation of Li^8 by deuteron bombardment is probably

$$Li^7+H^2\rightarrow Li^8+H^1+Q_1. \quad (1)$$

Q_1 has never been measured directly, but evidence that it is nearly zero can be obtained by comparing the excitation curve for reaction (1) with that of the alternative reaction

$$Li^7+H^2\rightarrow 2He^4+n^1+Q_2, \quad (2)$$

which is responsible for most of the neutrons from Li^7+H^2. The reaction probability for (1) is, to a first approximation, proportional to P_DP_P/E, where P_D and P_P are the potential barrier penetrabilities of the incident deuteron and the escaping proton, and E is the bombarding voltage. Since the neutron is uncharged, the corresponding reaction probability for (2) is proportional to P_D/E. For the bombarding voltages E_1 and E_2 at which the two reactions just become observable, the reaction probabilities should be about equal. On the assumption that the internal reaction probabilities are of the same order of magnitude, we can write

$$\frac{P_D(E_1)P_P(E_p)}{E_1}\leqq\frac{P_D(E_2)}{E_2}, \quad (3)$$

where E_p is the energy of the escaping proton in reaction (1). According to the excitation curves obtained by Rumbaugh and Hafstad,[4] $E_1\sim 400$ kv and $E_2\sim 200$ kv. Eq. (3) can now be solved for E_p by using the expressions for the barrier penetrabilities given by Bethe.[5] The result is $E_p\sim 200$ kv. Hence $Q_1\sim 0$.

Another indication that Q_1 is of this order of magnitude has been given by Rumbaugh, Roberts and Hafstad,[6] as a result of experiments on the separated isotope Li^7. They found no protons emitted with range greater than 1.7 cm when Li^7 was bombarded with deuterons at 860 kv. This sets an upper limit for Q_1 of 260 kv. A lower limit, $Q_1=-300$ kv, is set by the fact that reaction (1) occurs at all at 400 kv bombarding voltage.

The radioactive decay of Li^8 is probably described by

$$Li^8\rightarrow 2He^4+e^-+\nu+2Q_a+W_0. \quad (4)$$

The total energy released in (4) is 15.8 ± 0.5 Mev. This is determined by using 0 ± 0.3 Mev for Q_1, and the mass scale of Livingston and Bethe.[7] It has been found by Rumbaugh, Roberts and Hafstad,[6] and also by ourselves that no gamma-rays are emitted in reaction (4). We can therefore write

$$W_0+2Q_a=15.8\pm 0.5 \text{ Mev}, \quad (5)$$

on the assumption that the energy lost by the nucleus in the beta-process is equal to the upper limit of the beta-ray spectrum, W_0.

In order to determine the expected shape of the beta-ray spectrum on the basis of the K-U or the Fermi theory, we must treat the spectrum as a superposition of an infinite number of simple spectra, and may represent it by

$$\int_0^{15.8} A(W_0)F(W, W_0)dW_0, \quad (6)$$

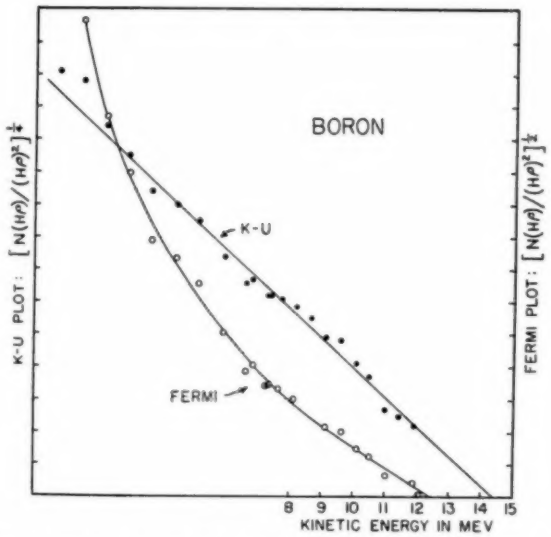

FIG. 6. K-U and Fermi plots for B^{12}. These include the separate upper limit data shown in Fig. 5.

[4] Rumbaugh and Hafstad, Phys. Rev. **50**, 681 (1936).
[5] Bethe, Rev. Mod. Phys. **9**, 69 (1937).
[6] Rumbaugh, Roberts and Hafstad, Phys. Rev. **51**, 1106 (1937).
[7] Livingston and Bethe, Rev. Mod. Phys. **9**, 245 (1937).

in which $F(W, W_0)$ is a simple spectrum with upper limit W_0 and in which $A(W_0)$ is its weight factor given by

$$A(W_0)\int_0^{W_0} F(W, W_0)dW = N_\alpha, \qquad (7)$$

where N_α is the number of alpha-particles of energy $\frac{1}{2}(15.8 - W_0)$.

In Fig. 3 we compare our experimental lithium spectrum (heavy curve) with that predicted by Eq. (6). Curves A and B are obtained by using for $F(W, W_0)$ the K-U and the Fermi distributions, respectively, together with the continuous alpha-particle distribution given by Fowler and Lauritsen.[8] The calculated curves are adjusted to the same area as the experimental curve. The calculation of curve A from the K-U theory involves only the conservation Eq. (5), and is not fitted except for the adjustment of the ordinate scale. The usual method of fitting K-U curves to experimental spectra is to make the maxima and center portions of the curves coincide. This method leads to the prediction of a theoretical upper limit. In order to make the maximum in curve A coincide with that of the experimental curve we would have to use a reaction energy more than 5 Mev greater than that which is known to be available.

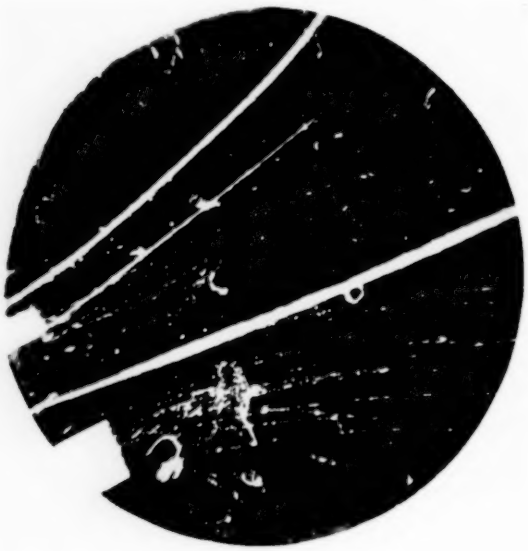

FIG. 7. Protons of the 90 cm range group and electrons from a target of $B^{10}+B^{11}$ bombarded with deuterons.

The true upper limit of the Li^8 spectrum must be the difference between the total energy, 15.8 Mev, and twice the minimum alpha-particle energy. Although the alpha-particle intensity may become exceedingly small near zero energy, it is reasonable, from a theoretical standpoint, to expect it to reach to zero energy; therefore the true upper limit is probably 15.8 Mev. Fowler and Lauritsen's curve tends to indicate that there are relatively few alpha-particles below 0.8 Mev, and our beta-ray spectrum supports this by giving a fairly definite cut-off at about 12 Mev. However, if enough data were obtained (7000 photographs were used in the present lithium spectrum) the experimental spectrum should eventually extend to 15.8 Mev.

Rumbaugh, Roberts and Hafstad[6] have found an alpha-particle distribution which seems to show no tendency to decrease at an energy as low as 0.9 Mev, whereas the Fowler and Lauritsen distribution decreases below 1.3 Mev. Taking an extreme case, namely assuming that the alpha-particle distribution has a maximum at zero energy, we have derived the curves C and D, Fig. 3, from the Fermi and K-U formulae, respectively.

The maximum in the neighborhood of 1 Mev which probably exists in the alpha-particle distribution can be made understandable by postulating a virtual level for the system of two alpha-particles (Be^8) at an energy of 2 or 3 Mev. This would be a very short lived state and would therefore have a great breadth in energy. One cannot be sure, however, that the maximum owes its position to a level of that energy in Be^8. Let us assume (1) that the intensity of alpha-particles decreases at low (alpha) energy because of the potential barrier for the separation of the pair of alpha-particles, and (2) that the intensity of beta-rays falls off at low (beta) energy according to the Sargent relation. The product of the Sargent and Gamow probabilities would predict an alpha-particle distribution of about the shape observed by Fowler and Lauritsen, but with a maximum at an energy corresponding to half the height of the mutual barrier for two alpha-particles. Using Bethe's value for the alpha-particle radius, the maximum is found to

[8] Fowler and Lauritsen, Phys. Rev. **51**, 1102 (1937).

be at 0.9 Mev. This is somewhat below that found by Fowler and Lauritsen, but is consistent with the distribution of Rumbaugh, Roberts and Hafstad.

Boron

The reactions involved in the case of boron are probably

$$B^{11}+H^2\rightarrow B^{12}+H^1+Q_3; \quad (8)$$

$$B^{12}\rightarrow C^{12}+e^-+\nu+Q_4. \quad (9)$$

We have been able to observe no gamma-ray emission during the radioactive decay. Q_4 should therefore be the energy of the upper limit of the beta-ray spectrum, given by

$$Q_4=14.5\pm0.2 \text{ Mev}-Q_3.$$

The protons emitted from boron bombarded with deuterons have only been investigated when both isotopes are present, and the emission of several range groups of protons from B^{10} have made it difficult to identify the slow proton group which should accompany the formation of B^{12}. Q_3 is therefore not known from direct experiment.

By counting the number of beta-ray tracks in the cloud chamber as a function of the bombarding voltage, we have obtained the excitation curves for the reactions producing Li^8 and B^{12}. These are shown in Fig. 8. The voltage scale was calibrated by means of the resonance[9] for the $F+H^1$ gamma-rays at 328 kv. It appears that the boron reaction begins at a voltage as low as 250 kv, while the lithium reaction, as already found by other observers,[4] sets in at about 400 kv. This may be interpreted as indicating that the emitted proton in the boron reaction has sufficient energy to escape easily through the potential barrier, which is effectively

[9]Hafstad, Heydenburg and Tuve, Phys. Rev. **50**, 504 (1936).

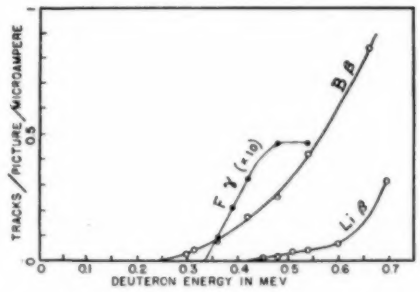

FIG. 8. Excitation curves for the reactions producing the Li and B beta-rays (unresolved ion beam). The voltage scale is calibrated by the excitation curve for the $F+H^1$ gamma-rays. For the beta-rays the solid angle subtended by the chamber window at the source was about $\pi/4000$.

about 1.4 Mev high. That is, the proton probably has an energy of at least 1 Mev. The upper limit of the beta-ray spectrum given by the K-U plot (Fig. 6) is 14.5 Mev, which leaves about zero energy for the escaping proton at 250 kv bombarding voltage. Although the errors in such a calculation may easily be 0.5 Mev, this is slight evidence that the upper limit given by the K-U plot is too high. On the other hand, the fact that the boron reaction sets in at about 150 kv lower voltage than does the lithium reaction could be accounted for by assigning to the boron reaction an internal probability fifty times greater than that of the lithium reaction. Positive evidence as to whether or not the K-U upper limit is too high in this case will be obtained when the protons belonging to the reaction are identified.

It is clear from the excitation curves that the bombardment of boron with deuterons forms an excellent low voltage source of high energy electrons for experiments upon the electrons themselves. By bombarding with an unresolved ion beam of 100 microamperes at 300 kv, about 10^5 beta-rays per second can be obtained.

The authors wish to express their appreciation to the Rackham Endowment Fund for the support of this work.

The Absorption of High Energy Electrons, Part II

J. J. Turin and H. R. Crane
University of Michigan, Ann Arbor, Michigan
(Received July 15, 1937)

Cloud chamber measurements of the energy loss of electrons in passing through lead and carbon absorbers have been extended up to 11 Mev by using the beta-rays from Li^8. The values for the average energy loss for lead are more than 50 percent greater than those predicted by the Bethe-Heitler theory. Part of this difference, at least, is accounted for by the fact that the actual length of path of an electron in lead is somewhat greater than the thickness of the lead. If a reasonable value (1.25 to 1.75) is used for the path length-thickness ratio, the experimental values can be said to be in agreement with theory to within 30 percent. The results for carbon are in good agreement with theory, using a path length-thickness ratio of unity, which is reasonable, because of the smaller amount of scattering in carbon than in lead.

Introduction

WE have previously reported[1] an experiment on the energy loss of the recoil electrons from the $F+H^1$ gamma-radiation in passing through carbon and lead absorbers. The energies of the incident particles extended up to 6 Mev. We wish now to report similar experiments on the high energy beta-rays from Li^8, by which we have extended the energy range up to 11 Mev. Inasmuch as the energy ranges covered in the two experiments overlap somewhat, we have also found it of interest to try to notice whether or not electrons of nuclear origin and recoil electrons are absorbed alike.

Experimental Method

The apparatus used was essentially the same as that described in our previous paper (Part I) except for the arrangement of the path of the beta-rays between the lithium target and the cloud chamber. In the present experiment, stereoscopic photographs were taken. A sketch of the cloud chamber and camera arrangement is shown in Fig. 1. By simply moving the lead slits A and B, and changing the position of the source with respect to the chamber, any desired band of electron velocities could be selected out. Throughout the experiment these slits and the strength of the magnetic field were adjusted so that the range of radii of curvature of the tracks was 10 to 15 cm. The mirror system shown in the sketch produces a complete picture of the chamber from directly above, and shows the halves of the chamber on the two sides of the absorber separately. The advantage of this system is that all the images lie in the focal plane; this was found to be important when using a camera lens of small depth of focus (f : 1.9). An example of the stereoscopic views is shown in Fig. 2, which at the same time shows a typical example of a beta-ray which loses energy. The camera and mirror system was left intact during the reprojection and measuring process, so that the plane in which the images of the track coalesced represented the plane in which the track was photographed.

Results

The method of treatment of the data in the present study is the same as that described in Part I of this report. The data were divided into groups according to energy of the electrons striking the absorber. Plots of the loss of energy against the number of electrons for 5 mm carbon, primary energy 4 to 6 Mev, and for 0.5 mm lead, primary energies 4 to 6, 6 to 8 and 8 to 11 Mev are shown in Figs. 3, 4, 5 and 6.

Table I. *Average and most probable energy losses of electrons in various absorbers.*

Absorber	Incident Energy (Mev)	Average Loss (Mev)	Most Probable Loss (Mev)
0.5 mm lead	4 to 6	1.68	1.2
0.5 mm lead	6 to 8	2.18	1.3
0.5 mm lead	8 to 11	2.26	1.4
5 mm carbon	4 to 6	1.70	1.6

[1] J. J. Turin and H. R. Crane, Phys. Rev. **52**, 63 (1937).

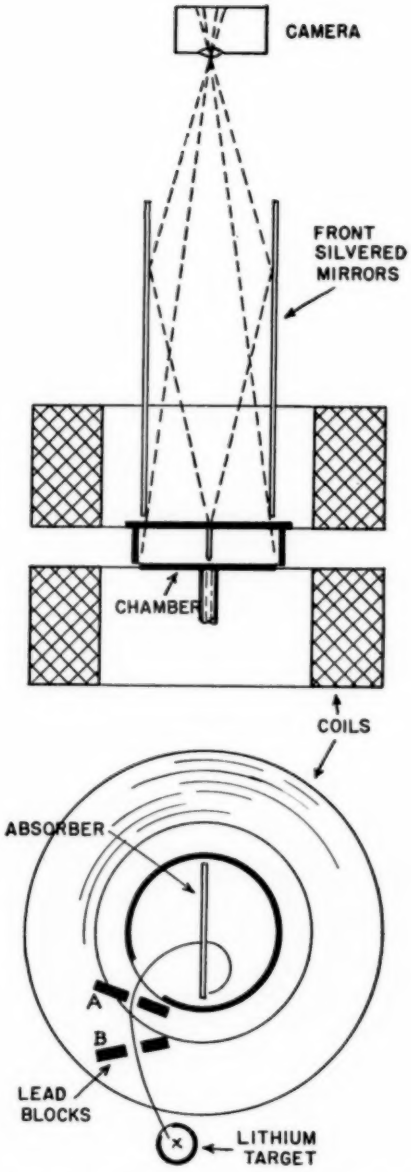

FIG. 1. Sketch showing stereoscopic camera arrangement, and showing the slit system by which the beta-rays were roughly selected as to energy before entering the cloud chamber.

In Table I are given the average energy losses and the most probable energy losses.

DISCUSSION

The diagram in Fig. 7 shows a comparison of the collected results for lead with the values of the average energy loss calculated from the Bethe-Heitler theory. The abscissa scale represents the average energy in the absorber for the electrons of each group, rather than the incident energies. This is the average incident energy minus one-half the average energy loss, for each group. The diagram therefore gives approximately the differential energy loss as a function of energy. The experimental values are all more than 50 percent greater than the theoretical. At least part of this difference can be well accounted for by the fact that the actual length of path of an electron in a lead absorber is somewhat greater than the thickness of the absorber. However, because of the rapid decrease of the amount of scattering with increasing energy, one should expect the path length-thickness ratio to be much less at 8 to 11 Mev than at 2 to 4 Mev. The many other factors involved make it difficult to say whether the theory gives values which are too low over the whole energy range. With reasonable limits (1.25 to 1.75) for the path length-thickness ratio it can be stated that the difference between the present results and theory is not more than 30 percent.

An important question in this experiment, as in the previous one, concerns the treatment of

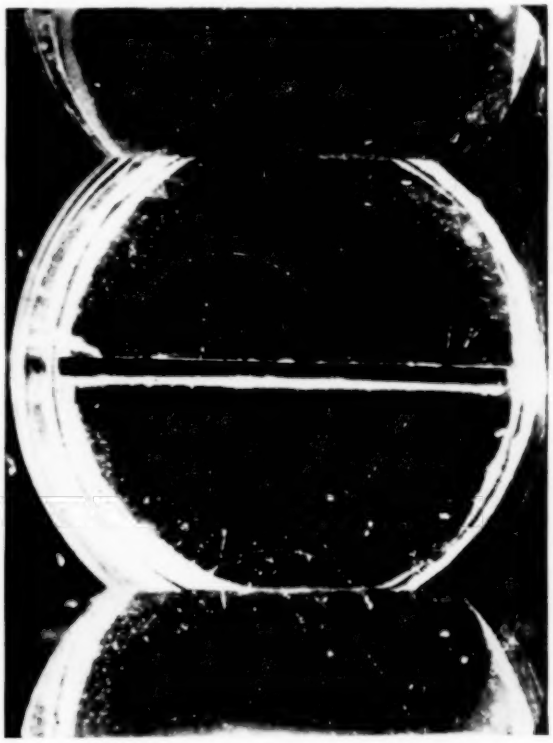

FIG. 2. Example of cloud chamber picture, which shows the kind of stereoscopic views obtained and which also shows a typical energy loss by a 6 Mev beta-ray.

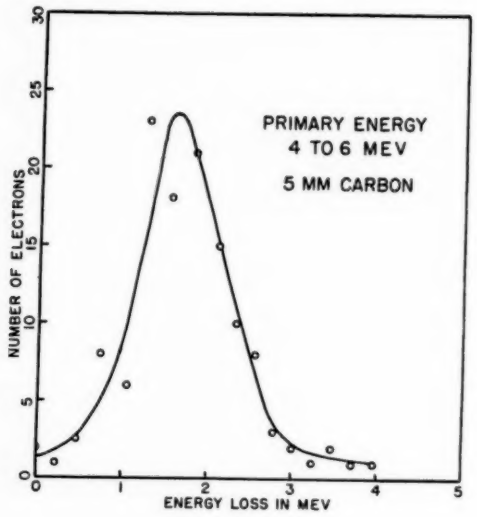

FIG. 3.

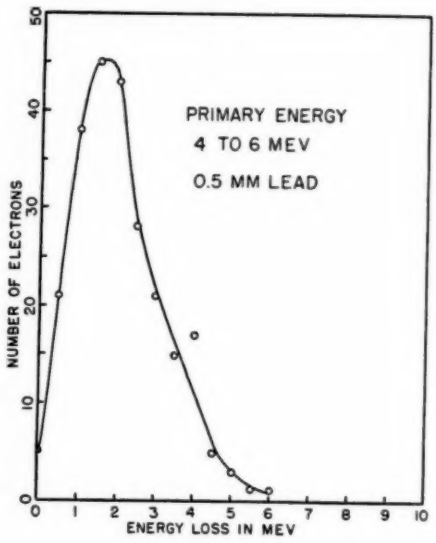

FIG. 4.

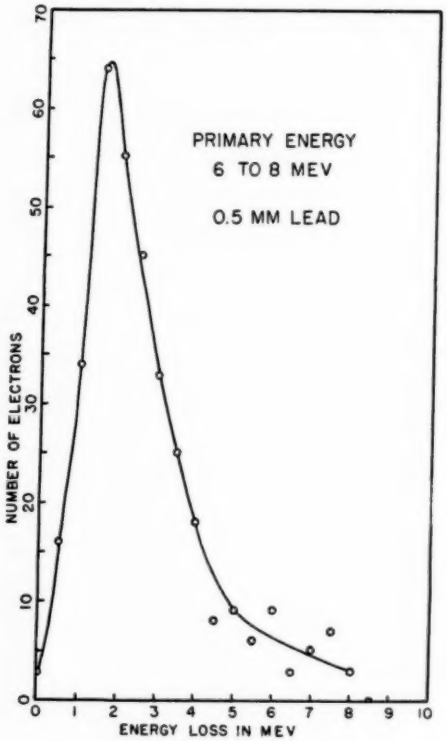

FIG. 5.

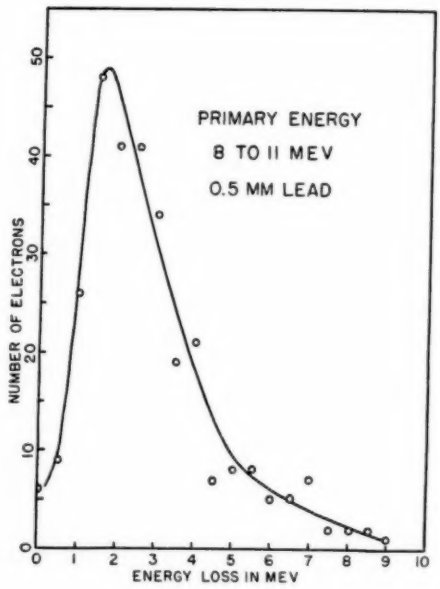

FIG. 6.

those electrons which are apparently completely stopped by the absorber. These have not been included in the curves on the assumptions (1) that they represent primarily electrons which are scattered out of the visible solid angle in the cloud chamber, and (2) that the electrons which emerge from the absorber within the visible part of the chamber give a fair representation of the energy loss of all the electrons, because multiple scattering is large enough to obliterate the dependence of angle upon energy loss. The complete validity of such a treatment is open to question. If there does remain some dependence of angle upon energy loss of the emergent elec-

TABLE II. *Percent of tracks transmitted through lead and carbon as a function of incident energy.*

	2 to 4 Mev	4 to 6 Mev	6 to 8 Mev	8 to 11 Mev
Lead	20	40	58	75
Carbon	36	64		

trons, the effect is in the direction of causing discrimination against those electrons which have suffered large energy losses. This would mean that the true values for the losses are even greater than those obtained.

Comparisons of the numbers of tracks incident upon the absorber with the numbers which pass through and are measurable on the opposite side have been made, by using about 1000 tracks, and the percent transmitted as a function of energy is given in Table II. This tends to indicate that scattering is large (unless some new mechanism is postulated to account for the stopping), and shows that the results would be radically changed if those electrons which appear to be stopped completely were included in the data.

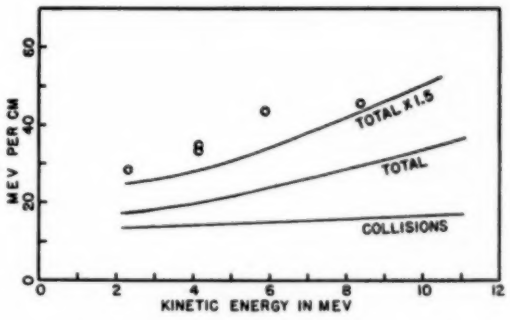

FIG. 7. Comparison of experimental points with theoretical curves, in terms of differential energy loss, Mev per cm of lead. The highest curve is that obtained by using 1.5 for the path length-thickness ratio.

The authors wish to express their gratitude to the Rackham Endowment Fund for the support of this work.

SEPTEMBER 15, 1937 PHYSICAL REVIEW VOLUME 52

Energy of Lattice Distortion in Cold Worked Permalloy

F. E. HAWORTH
Bell Telephone Laboratories, New York, New York

(Received June 4, 1937)

The lattice distortion produced by severe cold working of permalloy of 70 percent Ni content has been studied by measuring the broadening of the reflection of the Fe $K\alpha$ doublet by the (311) planes, with a focusing camera. The broadening decreases upon annealing and recovery is complete at 650°C, when the breadth of the x-ray intensity curve at half-maximum is as small as that obtained by use of the two-crystal spectrometer. The mean square distortion in the lattice spacing due to cold work is derived from the x-ray measurements after photometering the x-ray film, converting the curve into an x-ray intensity curve, fitting the latter with an empirical equation and using an analysis worked out by S. O. Rice. The energy of the distortion is then calculated by using an equation derived by G. R. Stibitz. The root-mean-square distortion was found to be 0.31 percent of the lattice spacing after the material had been reduced 96 percent in cross-sectional area by cold working. The energy of distortion in the hard worked condition is thus found to be 23×10^6 ergs/cm^3 or 0.065 calorie/gram.

ONE of the interesting problems in the physics of metals is to explain the increase in internal energy which takes place when a metal is severely cold worked. This increase has been measured by Taylor and Quinney[1] in copper and steel, and Cagliotti and Sachs[2] have shown on the basis of x-ray measurements on copper that the lattice strain as measured by the broadening of the x-ray lines does not nearly account for the energy increase.

The purpose of this work is to study the internal strain in more detail, using a material on which parallel measurements[3] of electrical

[1] G. I. Taylor and H. Quinney, Proc. Roy. Soc. London **A143**, 307 (1934).
[2] V. Cagliotti and G. Sachs, Zeits. f. Physik **74**, 647 (1932).
[3] J. F. Dillinger, Phys. Rev. **49**, 863 (1936).

resistivity, mechanical hardness, and various magnetic properties have been made for various reductions in area by hard rolling or drawing and for various times and temperatures of annealing after such reduction. The state of strain is derived in a new way from the broadening of x-ray diffraction maxima.

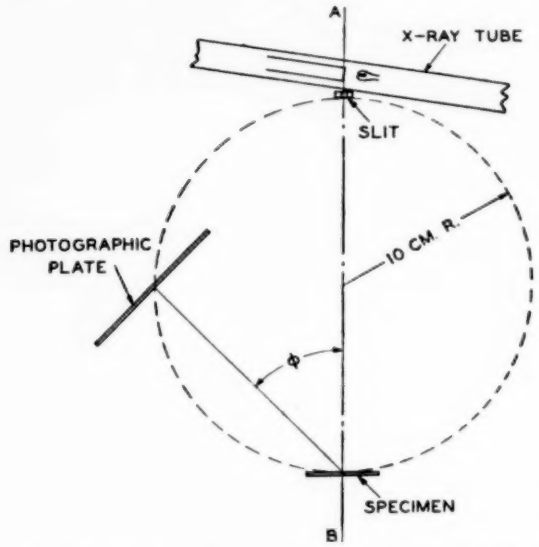

FIG. 1. Arrangement of apparatus for focusing and photographing the x-ray reflections.

The derivation of the internal energy increase proceeds in four steps, as follows: (1) measurement of the distribution of reflection angles by photographic densitometry; (2) separation of overlapping α_1 and α_2 components of the K radiation by an empirical method; (3) derivation of the strain distribution from the distribution of α_1 radiation so obtained; (4) computation of the increase in potential energy density from the derived strain distribution.

The material chosen was an alloy containing 70 percent nickel and 30 percent iron. Bozorth and Dillinger[4] obtained a maximum permeability of over 500,000 for this alloy by heat treatment in a magnetic field, and measurements had been made of the properties listed above. Two series of specimens were prepared from this material, which was received from the manufacturer (Driver-Harris) in quarter-inch rods. For a study of the recovery of the material from cold rolling, rods were rolled to tape 0.006 inch (0.015 cm) thick—this involving a reduction in cross-sectional area of 96 percent—and then annealed in hydrogen for two hours at selected temperatures up to 1090°C. In the other series, to test for a possible grain size effect, specimens were annealed at a temperature of 1000°C at various stages in the rolling schedule, but all were finally cold rolled to tape of the standard thickness, thus giving various degrees of reduction since the last anneal, in otherwise similar pieces.

[4] Richard M. Bozorth and Joy F. Dillinger, Physics **6**, 279–291 (1935).

APPARATUS

The apparatus used for photographing the x-ray reflections is shown schematically in Fig. 1. The x-ray source is a Philips Metalix tube with an iron target, and the slit, specimen, and plate are arranged on the circumference of a circle to focus the (311) reflections of the $K\alpha$ doublet sharply on the plate. The slit was 0.1 mm wide and 5 mm high, made in a quarter-inch brass plate. The specimens were mounted with a flat surface perpendicular to the axis AB and were rotated about this axis in order to produce smooth lines. The angular divergence of the beam was such that at the specimen it was a millimeter wide. The reflection angle θ, was about 64.5°, making $\varphi = 51°$. The photographic plate was placed at right angles to the reflection to eliminate any broadening due to emulsion thickness. To obtain the density distribution of the reflections a Moll microphotometer was used with its optical system so arranged that the area scanned on the plate was 0.014 mm by 1.0 mm. It was difficult to obtain good microphotometer curves with x-ray plates on account of their large grain size and Eastman 33 plates were used instead.

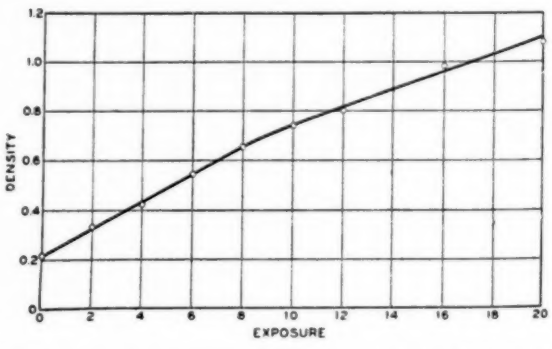

FIG. 2. Curve of exposure *vs.* density for the photographic plates used (Eastman 33).

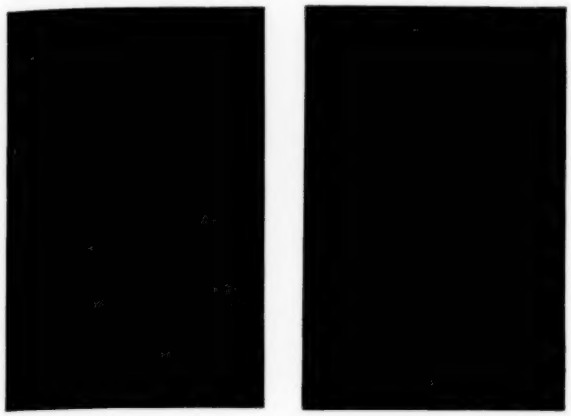

(a) (b)

FIG. 3. Reflection of the Fe $K\alpha_1$, α_2 lines by the (311) planes: (a) in the hard rolled tape; and (b) in the tape annealed at 650°C. The exposure time for (a) was twenty times that for (b).

For accurate measurements of the lattice spacing a symmetrical focusing camera of the Seeman-Bohlin type was used. The distances between lines on the film were measured with a comparator to about 0.01 mm, the calculated spacings plotted against $\varphi \tan \varphi/2$, and the resultant curve extrapolated to $\varphi=0$. Repeated measurements indicate that spacings determined in this manner are accurate to within 0.01 percent.

MEASUREMENT OF THE LINE BROADENING

Photographs of the (311) reflections from the proposed specimens were made using the arrangement as described above. Exposure times varied from one to twenty hours and care was taken that the maximum density on the plate did not exceed that at the knee of the exposure-density curve. This curve had been determined previously and is shown in Fig. 2. Figs. 3a and b are reproductions of the $K\alpha$ doublet from the specimens hard rolled from a $\frac{1}{4}$ inch rod to 0.006 inch tape and from the same tape annealed at 650°C, respectively. The microphotometer records for these photographs are shown in Figs. 4a and b. From the relation between plate density and transmission of light it is easily shown that if δ_B is the microphotometer deflection for the background, δ_M that for maximum density, and $\delta_{\frac{1}{2}}$ that for half-maximum then

$$\delta_{\frac{1}{2}}=(\delta_B\delta_M)^{\frac{1}{2}},$$

and if all three points lie on the linear part of the exposure-density curve, this will also be the deflection for the half-maximum x-ray intensity.

The curve of the specimen annealed at 650°C, Fig. 4b, shows the $K\alpha$ doublet well resolved. Comparing this with published curves obtained by the two crystal spectrometer it not only shows as good resolution, but has the same asymmetry and breadth at half-maximum intensity. Correcting for the effect of the finite slit width the breadth of the $K\alpha_1$ line is here 1.06 X.U., to be compared with Allison's value of 1.00 X.U. and Parratt's of 1.02 X.U.[5] From this it appears that after annealing at 650°C the mean lattice distortion has fallen to zero, as nearly as can be detected. A mean distortion of 0.01 percent of the lattice spacing would increase the breadth of the $K\alpha_1$ line to about 1.25 X.U. and hence could readily be observed. Fig. 5 shows the breadths at half-maximum of the whole series as a function of annealing temperature.

Since these data were obtained from reflections by (311) planes only in the surface of the specimen, there was some question as to whether they were representative of the whole specimen. Measurements were therefore made of the broadening of the (222) reflections, and of the broadening for (311) planes after etching the specimen

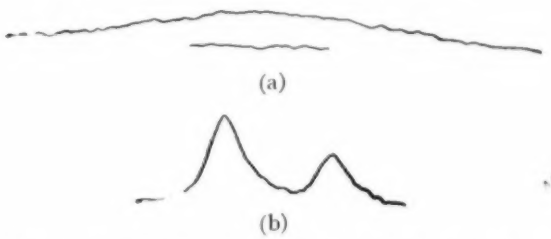

(a)

(b)

FIG. 4. Microphotometer curves of the reflections shown in Fig. 3: (a) for the hard rolled tape; and (b) for the tape annealed at 650°C.

to about one-third of its thickness. In both cases the broadening, corrected for resolving power, was the same as previously measured.

To see how much of the observed broadening is due to strain it is necessary to estimate the broadening due to grain size. Wood[6] concludes

[5] Compton and Allison, *X-Rays In Theory and Experiment*, p. 745 (D. Van Nostrand Co., 1935).

[6] W. A. Wood, Phil. Mag. **20**, 964 (1935) and Phil. Mag. **15**, 555 (1933).

from comparisons of hard drawn and electrodeposited metals that line broadening in the former is to be attributed to lattice distortion. If the broadening is measured for various reductions by cold working he found that it quickly reached a maximum and then changed very little. This finding agrees with the present measurements on the series with varying amounts of reduction after annealing as shown in Fig. 6. The greatest breadth is very much less than that for particles which are known to be less than 10^{-5} cm in diameter such as occur in colloids and electrodeposits, and hence the indication is that hard working has not reduced the crystal size sufficiently to account for the broadening observed. An actual estimate of the size of the crystals can be made from the photomicrographs of rolled permalloy published by F. F. Lucas.[7] In these the slip planes are shown to be from 3 to 5×10^{-5} cm apart, and it is reasonable to suppose that the crystal fragments extend from one slip plane to the next. Substituting in Scherrer's formula for line broadening shows that (311) planes in crystals of this size would have a line broadening at half-maximum of about 5×10^{-4} radian, approximately one-tenth the total broadening observed. Thus all available evidence indicates that lattice distortion, and not crystal size, is the primary cause of line broadening produced by cold working, though not necessarily responsible for all of it.

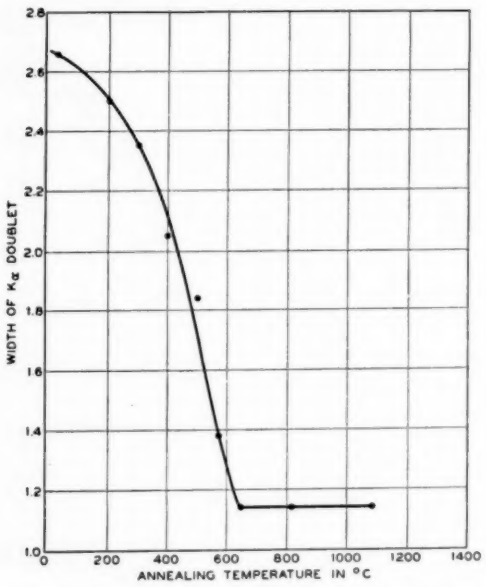

FIG. 5. Breadth at half-maximum x-ray intensity of the reflected $K\alpha$ doublet after annealing for two hours at the indicated temperatures.

[7] F. F. Lucas, J. Frank. Inst. **201**, 177 (1926).

SEPARATION OF THE α-COMPONENTS

Assuming that the substance is elastically isotropic and that the stresses are independent and oriented at random with zero mean values, G. R. Stibitz has derived the following expression for the potential energy density V of the distortion,

$$V=3E[(\Delta d^2)_{Av}/d^2]/[2(1+2v^2)]. \quad (1)$$

E is Young's modulus, v Poisson's ratio, and $(\Delta d^2)_{Av}$ the mean square increment of the plane spacing d. The derivation of this equation is given in Appendix A. An evaluation of the last term requires a knowledge of the distribution curve of Δd. To obtain this the first step was to fit an empirical equation to the observed intensity curves. The microphotometer curves were first reduced to curves of x-ray intensity *vs.* angle of reflection, and then various distribution curves fitted to them. As has been shown by others the normal Gauss distribution falls off too rapidly at the base, and Hoyt's[8] curve, of the form $y=a/(1+bx^2)$, does not fit at the base of the curve, and in addition yields an infinite value for $(x^2)_{Av}$. As has been pointed out by R. C. Spencer[9] if a fourth power term is added to Hoyt's equation a much better fit is obtainable and the following expression was found to fit the curves for both the hard worked and annealed specimens:

$$I=\frac{A}{1+0.828(x/B)^2+0.172(x/B)^4}+\frac{A/2}{1+0.828[(x-x_0)^2/B]+0.172[(x-x_0)^4/B]}, \quad (2)$$

where the origin is chosen as shown in Fig. 7, and x_0 is the separation of the α_1 and α_2 components, one unit in x corresponding to $\Delta\theta=10^{-3}$ radian. This equation has only two adjustable constants, A being the maximum ordinate of the α_1 component and B being the half-breadth of

[8] A. Hoyt, Phys. Rev. **40**, 477 (1932).
[9] R. C. Spencer, Phys. Rev. **46**, 1108 (1934).

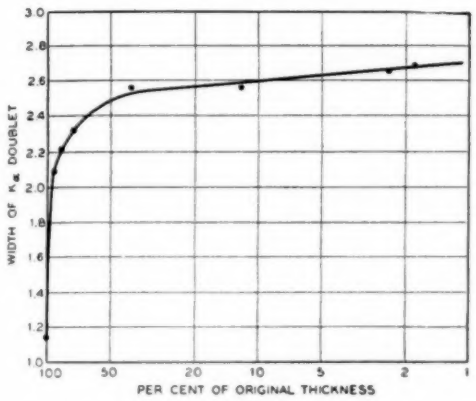

FIG. 6. Breadth at half-maximum x-ray intensity of the reflected $K\alpha$ doublet for various amounts of reduction.

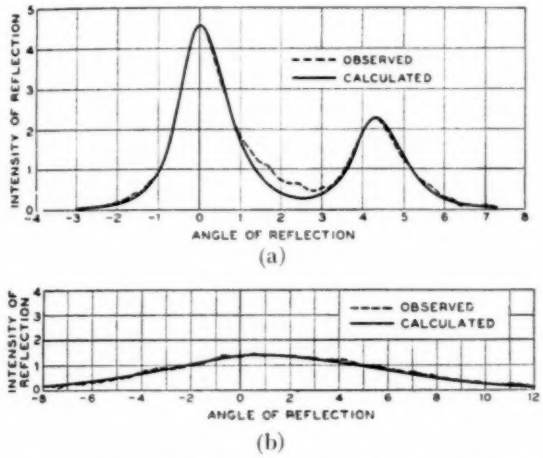

FIG. 7. Comparison of calculated and observed x-ray intensities for the $K\alpha$ doublet reflected (a) from the annealed specimen, and (b) from the hard rolled specimen. The calculated curves are defined by Eq. (2).

either single component at half-maximum intensity. On account of the asymmetry of the reflection from the annealed specimen, two values of B had to be used, and Fig. 7a shows the accurate fit obtained. For the right side of the components B is 0.8, and for the left it is 0.6. Fig. 7b shows the equation fitted to the curve for the unannealed specimen with $B=4.3$. No asymmetry was here assumed.

DETERMINATION OF THE STRAIN DISTRIBUTION AND CALCULATION OF THE ENERGY

Since the intensity curve for the annealed specimen shows no evidence of lattice distortion the assumptions are made that the equation fitted to it represents the distribution of $\Delta\theta$ caused by the variation $\Delta\lambda$ in the wave-lengths of the α components and that the equation fitted to any intensity curve in which distortion is present represents a distribution of $\Delta\theta$ caused by $\Delta\lambda$ and Δd. The next problem is to evaluate the distribution for Δd from the distribution for the combination of $\Delta\lambda$ and Δd. This involves the solution of an integral equation, solved by S. O. Rice, as given in Appendix B, where functions and symbols used in the process are defined. The function $f_d(u)$, which gives the distribution of Δd, has been evaluated by graphical integration for the values of M and m equal to 6.0 and 1.0, respectively, the former being about the value obtained from the unannealed specimen, and the latter being that from the annealed specimen. The resulting distribution curve of Δd is shown in Fig. 8.

The mean square values of the functions $F(\theta)$, $f_\lambda(\theta)$, and $f_d(u)$ are M^2, m^2, and M^2-m^2, respectively, and from Eqs. (2) and (2a) of Appendix B, and Eq. (2) given above, it follows that $M=1.55B$, giving $M^2-m^2=(2.4B^2-1)$ for B in thousandths of a radian. From the camera dimensions 10^{-3} radian corresponds to a change in d of 0.048 percent. Therefore

$$(\Delta d^2)_{AV}/d^2=0.23(2.4B^2-1)10^{-6}.$$

The values of $(\Delta d^2)_{AV}/d^2$ have been calculated for the specimens from which Fig. 5 was plotted. For the hard worked specimen, the root mean square strain is 0.3 percent. It is interesting that this is about the value obtained for the maximum strain in iron or nickel if the breaking stress of the hard worked metal is divided by Young's modulus.

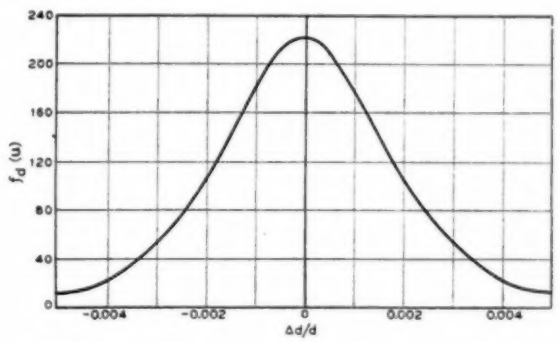

FIG. 8. Derived distribution of the distortion in the hard rolled specimen. Here Δd is the change in the lattice spacing d.

The stored specific energy[9a] of the distortion, obtained by substituting $(\Delta d^2)_{Av}/d^2$ in Stibitz's equation, is shown in Fig. 9.

Discussion of the Results

It is of interest to compare these energy densities with others reported in the literature. Taylor and Quinney[1] measured calorimetrically energies stores in the hard working of wires by twisting, and obtained maximum values of 1.15 cal./g for copper and 1.27 cal./g for steel. W. A. Wood,[10] measuring a shift in lattice parameter of copper on cold working calculated energies of the same order of magnitude but C. G. Maier[11] has stated that the assumptions on which those calculations were based are doubtful. Wood obtained a shift of the (420) reflection in cold worked copper corresponding to $\Delta d/d = 2.8 \times 10^{-4}$ at the peak of the line, 16.7×10^{-4} at the base. For cold rolled α-brass he calculated from the line broadening for (331), $\Delta d/d = 3 \times 10^{-3}$, and from that for (420), $\Delta d/d = 6 \times 10^{-3}$. These values are all of the same order of magnitude as the distortions derived from the present measurements or are less, and according to the analysis here offered indicate energy changes not greater than those reported here.

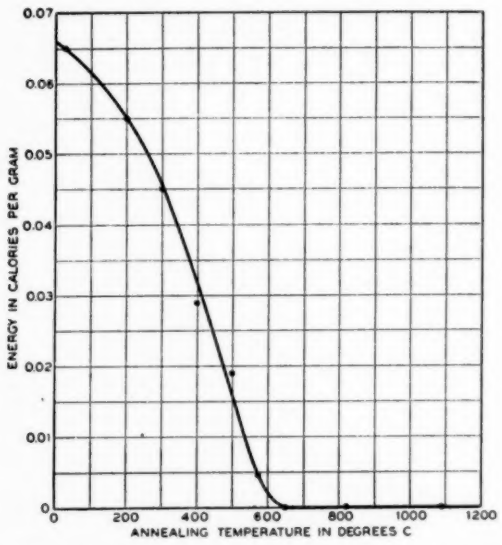

Fig. 9. The latent energy of distortion which produced the x-ray line broadening for the tape which had been hard rolled and then annealed at the temperatures indicated.

In studies of the nature of cold working of copper and iron, Maier[11] made some calculations of the potential energy due to observed changes of density. These energies are of the same order of magnitude as the ones obtained here, but since a density change would affect x-ray reflections by shifting the reflected line instead of merely broadening it, the effect he measures is of a different nature, and the agreement has no significance. To see if density changes occurred in the regions where $\Delta d/d$ was here estimated, the lattice constants of the annealed and cold worked specimens were measured by use of the symmetrical focusing camera and no difference was found, though a change as little as 0.02 percent should have been detectable. Maier's theory, however, would permit density changes by the formation at crystal boundaries of regions of higher than average density, the material in such regions having no definite crystal structure, and hence not affecting a measurement of average lattice spacing.

Brindley and Spiers[12] in measurements of the atomic scattering of copper and nickel powders found it to be lowered by lattice distortions resulting from filing. Assuming an exponential factor similar to that used in calculating atomic displacements due to heat motions they calculated $(\Delta d^2)_{Av}^{\frac{1}{2}} = 0.106 \times 10^{-8}$ cm for filed copper, 0.083×10^{-8} cm for nickel. From these values they calculated the thermal energy necessary to give a corresponding change in lattice dimensions and obtained 7.4 cal./g for copper and 6.4 cal./g for Ni. Boas, in a recent paper,[13] considers these too high by a factor of about thirty, and sets the upper limit for the latent energy for copper at about 0.23 cal./g, as measured by Rosenhain and Stott.[14] From this he concludes that the cause of the intensity changes must be

[9a] A sample of the material was cold rolled to 0.035 inch (0.089 cm) and sent to Professor P. W. Bridgman, who kindly reduced and sheared it to approximately 0.006 inch (0.015 cm) under tremendous pressure. Measurement of the line breadth at half-maximum x-ray intensity of the reflection from the (311) planes of this specimen gave a value of 3.5 units on the same scale as in Fig. 5. Provided there is no grain-size effect, this broadening corresponds to a root-mean-square distortion of 0.48 percent and an energy of 0.17 cal./g.

[10] W. A. Wood, Phil. Mag. **18**, 495 (1934).

[11] C. G. Maier, A. I. M. M. Technical Publication No. 701 (1936).

[12] G. W. Brindley and F. W. Spiers, Phil. Mag. **20**, 882 (1935).

[13] W. Boas, Zeits. f. Krist. **96**, 214 (1937).

[14] Rosenhain and Stott, Proc. Roy. Soc. London **140**, 9 (1933).

looked for elsewhere, ignoring the value of 1.15 cal./g for copper obtained by Taylor and Quinney as mentioned above. If the atomic displacements calculated by Brindley and Spiers are substituted in Stibitz's equation the latent energy is 3.0 cal./g for copper and 3.7 cal./g for nickel, values which differ from Taylor and Quinney's results by a factor of only three. From this it is evident that a great amount of the energy of cold rolling may be absorbed by lattice distortions extending over volumes too small to cause broadening of the reflected x-ray lines. To measure this in cold rolled materials it would be necessary to compare the integrated intensities of the reflections from the unannealed and annealed specimens, but unfortunately in removing the distortions by annealing the specimen recrystallizes with a change of special orientation, so that the usual intensity comparisons become meaningless. Nevertheless, experiments are being continued in hope of finding a suitable heat treatment which relieves strains without affecting crystal orientation or grain size.

Appendix

A. Energy of lattice distortion[15]

Assuming that the substance is elastically isotropic, and that the magnitudes of the principal stresses at a point are independent of each other and of the crystallographic indices of the principal directions, we choose the coordinate axes in the directions of the principal stresses, which then are F_x, F_y and F_z. It is necessary to find the elongation of the material in the direction of the normal to the reflecting planes.

The elongation in the x-direction in the neighborhood of the given point when $F_y=F_z=0$ is F_x/E, where E is Young's modulus. This is accompanied by negative elongations in the y and z directions of amount $-\nu F_x/E$, where ν is Poisson's ratio. Similar effects follow when $F_x=F_z=0$ and $F_y\neq 0$, and likewise when $F_z\neq 0$. Summing them we have the total elongations

$$A_x=(F_x-\nu F_y-\nu F_z)/E,$$
$$A_y=(F_y-\nu F_z-\nu F_x)/E,$$
$$A_z=(F_z-\nu F_x-\nu F_y)/E.$$

Next consider the change in the distance between parallel planes, the normal N of which makes an angle ψ with the z-axis in a plane zN at an angle θ with the x-z plane. The elongation in the direction of N is the sum of the projections on N of the elongations in the x, y, z-directions. It is easily seen that the angles $[xN]$, $[yN]$, $[zN]$ are given by

$$\cos[zN]=\cos\psi,$$
$$\cos[xN]=\sin\psi\cos\theta,$$
$$\cos[yN]=\sin\psi\sin\theta.$$

The required elongation is

$$\begin{aligned}\Delta d/d&=A_x\cos[xN]+A_y\cos[yN]+A_z\cos[zN]\\&=(1/E)[(F_x-\nu F_y-\nu F_z)\sin\psi\cos\theta\\&\quad+(F_y-\nu F_z-\nu F_x)\sin\psi\sin\theta\\&\quad+(F_z-\nu F_x-\nu F_y)\cos\psi].\end{aligned}$$

Now let a beam of x-rays fall normally on the surface of the material, the reflected rays being received at a specified angular distance from the normal. In general, all such reflected rays arise from crystal planes of which the normals make a specified angle ω with the surface normal. The small deviations of the reflected rays from various points on the material will be proportional to the values of $\Delta d/d$ for those points, and will thus depend on ψ, θ, F_x, F_y, F_z. The intensity of the reflected ray corresponding to a certain value D of $\Delta d/d$ is proportional to the number of elementary areas for which ψ, θ, F_x, F_y, F_z are such that $\Delta d/d=D$. In particular if we wish the root mean square value of $\Delta d/d$, we multiply $(\Delta d/d)^2$ for each value of ψ, θ, F_x, F_y, F_z by the distributions of ψ, θ, F_x, F_y, F_z and average the product. Averaging with respect to θ, which is unrestricted, we have

$$\begin{aligned}\text{av}\,(\Delta d/d)^2=(1/E^2)\,\text{av}[&\tfrac{1}{2}(F_x-\nu F_y-\nu F_z)^2\sin^2\psi\\&+\tfrac{1}{2}(F_y-\nu F_z-\nu F_x)^2\sin^2\psi\\&+(F_z-\nu F_x-\nu F_y)^2\cos^2\psi].\end{aligned}$$

The assumptions regarding F_x, F_y and F_z imply that, for average values $F_x^2=F_y^2=F_z^2=F^2$, $F_xF_y=F_yF_z=F_zF_x=0$, in which case the average is independent of ψ, and

$$[(\Delta d)_{\text{av}}/d]^2=[(F^2)_{\text{av}}/E^2](1+2\nu^2).$$

It may be emphasized at this point that the median value of $\Delta d/d$ could not be obtained without an additional assumption giving the form of the distribution functions for the F's, whereas the present computation required only qualitative hypotheses about that function.

The potential energy V, stored in the metal by the residual stresses is easily obtained as

$$V=(1/2E)(F_x^2+F_y^2+F_z^2)-(\nu/E)(F_xF_y+F_yF_z+F_zF_x).$$

Averaging for the type of distribution assumed for F_x, F_y and F_z, we have

$$V=3(F^2)_{\text{av}}/2E.$$

From this and the equation for strain it follows that

$$V=\frac{3E}{2(1+2\nu^2)}(\Delta d/d)^2_{\text{av}}.$$

B. Analysis of line broadening due to strain[16]

By solving the equation

$$F(\theta)=\int_{-\infty}^{+\infty}f_\lambda(\theta-u)f_d(u)\,du \qquad (1)$$

[15] This analysis was supplied by G. R. Stibitz. It is abstracted in Phys. Rev. **49**, 862 (1936).

[16] This analysis was supplied by S. O. Rice. It is abstracted in Phys. Rev. **49**, 862 (1936).

for the Δd distribution $f_d(u)$, when the $\Delta\lambda$ distribution $f_\lambda(\theta)$, and the combined distribution $F(\theta)$ for a single α component are given by the expressions

$$f_\lambda(\theta)=q/(1+r\theta^2+s\theta^4) \quad \text{and} \quad F(\theta)=Q/(1+R\theta^2+S\theta^4) \tag{2}$$

Rice[16] derives a series giving $f_d(u)$. This series proved to be difficult to handle with the values of the constants derived from the experimental curves, and consequently one of the preceding integral equations was evaluated graphically. The following derivation has been provided by Rice.

Equation (1) may be solved by using the multiplication theorem for Fourier integrals.[17] The result is

$$f_d(u)=\frac{1}{2\pi}\int_{-\infty}^{+\infty} e^{iug}\frac{S_1(g)}{S_2(g)}dg, \tag{3}$$

where

$$S_1(g)=\frac{1}{2\pi}\int_{-\infty}^{+\infty} e^{-i\theta g}F(\theta)d\theta, \tag{4}$$

$$S_2(g)=\frac{1}{2\pi}\int_{-\infty}^{+\infty} e^{-i\theta g}f_\lambda(\theta)d\theta. \tag{5}$$

Since Eqs. (2) are distribution functions, Q, R, and S are not independent, and neither are q, r, and s. By using the necessary relations between these coefficients (2) may be written

$$F(\theta)=\frac{2M(M^2-N^2)/\pi}{\theta^4+2(M^2+N^2)\theta^2+(M^2-N^2)^2} \tag{2a}$$

and

$$f_\lambda(\theta)=\frac{2m(m^2-n^2)/\pi}{\theta^4+2(m^2+n^2)\theta^2+(m^2-n^2)^2}. \tag{2b}$$

It is now convenient to express $F(\theta)$ in the form

$$F(\theta)=\frac{M^2-N^2}{2\pi N}\left[\frac{1}{\theta^2+(M-n)^2}-\frac{1}{\theta^2+(M+N)^2}\right],$$

which may be readily verified. Then upon using the result

$$\int_{-\infty}^{+\infty}\frac{e^{-i\theta g}}{\theta^2+\alpha^2}d\theta=\pi/\alpha\, e^{-|g|\alpha} \qquad \alpha>0$$

we have from (4)

$$S_1(g)=\frac{M^2-N^2}{4\pi N}\left[\frac{e^{-|g|(M-N)}}{M-N}-\frac{e^{-|g|(M+N)}}{M+N}\right]$$
$$=\frac{M+N}{4\pi N}e^{-|g|(M-N)}[1-Ze^{-2|g|N}],$$

where $Z=(M-N)/(M+N)$.

In a similar manner, writing $z=(m-n)/(m+n)$, we find from (5)

$$S_2(g)=\frac{m+n}{4\pi n}e^{-|g|(m-n)}[1-ze^{-2|g|n}].$$

When these values of $S_1(g)$ and $S_2(g)$ are inserted in Eq. (3) we have

$$f_d(u)=\frac{1}{2\pi}\frac{M+N}{m+n}\frac{n}{N}\int_{-\infty}^{+\infty}dge^{iug}\left[\frac{1-Ze^{-2|g|N}}{1-ze^{-2|g|n}}\right]e^{-|g|p}$$

or
$$f_d(u)=\frac{1}{\pi}\frac{M+N}{m+n}\frac{n}{N}\int_0^\infty dg\cos ug\frac{1-Ze^{-2gN}}{1-ze^{-2gn}}(e^{-gp}), \tag{6}$$

where $p=M-N-m+n$, which is assumed positive so that the integral converges.

This may be further simplified if we let N and n equal zero, which will be true if $R^2=4S$ and $r^2=4s$. This adjustment of the constants was made in the equations for the experimental curve given above. Therefore evaluating (6) for the limit as N and n approach zero we have:

$$f_d(u)=\frac{1}{\pi}\int_0^\infty dg\cos uge^{-g(M-m)}\frac{1+Mg}{1+mg}$$
$$=-\frac{M-m}{\pi m}\int_0^\infty\frac{e^{-g(M-m)}\cos ugdg}{1+mg}$$
$$+\frac{M}{\pi m}\int_0^\infty e^{-g(M-m)}\cos ugdg \tag{7}$$
$$=-\frac{M-m}{\pi m}\int_0^\infty\frac{e^{-g(M-m)}\cos ugdg}{1+mg}+\frac{M}{\pi m}\frac{M-m}{(M-m)^2+u^2}.$$

Finally,

$$f_d(u)=\frac{M-m}{\pi m}\left[\frac{M}{(M-m)^2+u^2}-\int_0^\infty\frac{e^{-g(M-m)}\cos ugdg}{1+mg}\right]. \tag{8}$$

The mean square values of the functions $F(\theta)$, $f_\lambda(\theta)$, and $f_d(u)$ when N and n are zero, are M^2, m^2 and M^2-m^2, respectively.

[17] Campbell and Foster, *Fourier Integrals for Practical Application*, Bell System Monograph B-584 (1931). Pair 202.

The Extreme Ultraviolet Spectra of Scandium VI, Scandium VII and Other Elements Isoelectronic with Phosphorus I and Sulphur I*

P. GERALD KRUGER AND H. S. PATTIN
Department of Physics, University of Illinois, Urbana, Illinois
(Received July 6, 1937)

The spectra of Sc, Ti, V and Cr have been photographed in the region 80A to 700A with a large grazing incidence vacuum spectrograph. The irregular doublet law and constant second difference law have been used to aid in the identification of multiplets in ions of these elements. In the S I isoelectronic sequence, Sc VI multiplets involving the $3s^23p^4\ ^3P$, ^1D, $^1S-3s3p^5\ ^3P^0$; $3s^23p^34s\ ^3S^0$, $^{1,3}D^0$, $^{1,3}P^0$ terms and the Ti VII multiplet involving the $3s^23p^4\ ^3P-3s3p^5\ ^3P^0$ terms have been observed. A number of intercombination lines have been identified, making possible an accurate calculation of the term values relative to the ground state. In the P I isoelectronic sequence, Sc VII multiplets involving the $3s^23p^3\ ^4S^0$, $^2D^0$, $^2P^0-3s^23p^24s\ ^4P$, ^2D, ^2P and $3s3p^4\ ^4P$ terms; Ti VIII multiplets involving the $3s^23p^3\ ^4S^0$, $^2D^0$, $^2P^0-3s^23p^24s\ ^4P$, ^2P, ^2D terms; and V IX multiplets involving the $3s^23p^3\ ^4S^0$, $^2D^0-3s^23p^24s\ ^4P$, ^2D terms have been observed. Since no intercombination lines have been observed it is impossible to assign relative term values to the doublet and quartet systems.

THE spectra of all ions of the first eight elements of the periodic table are well known. A great deal of work has been done also on the isoelectronic ions of elements following oxygen. However, previous to the beginning of the present investigation, the spectra of scandium were known only for Sc I, Sc II, Sc III, and Sc XI. This was undoubtedly due to the fact that the highly ionized spectra of scandium was very hard to excite. There was also a lack of information about the spectra of various ions of the neighboring elements Ti, V, and Cr, though these elements are not particularly hard to excite.

Other members of this laboratory have reported the work done on Sc IV,[1] Sc V,[2] Sc VIII, IX[3] and other neighboring ions in isoelectronic sequences related to these scandium ions. It is the purpose of this paper to present the results of the investigation of the spectra of Sc VI, Sc VII and related ions in the S I and P I isoelectronic sequences.

The spectra of the elements Sc, Ti, V, and Cr were photographed throughout the region 80 to 700A by means of a large grazing incidence vacuum spectrograph.[4] Titanium, vanadium, and chromium electrodes, made in the conventional way by inserting a piece of the metal into the hollow end of a $\frac{1}{4}$-inch diameter rod (Al or Cu) and wedging it fast, were used as the anode of a vacuum spark.

Satisfactory scandium electrodes were made by packing a mixture of four parts of scandium oxide and one part of boron oxide in a copper (Al) shell electrode and hardening the mixture by heating the electrode to a red heat in a small electric furnace.

The energy for excitation was supplied by a four kenotron bridge rectifier which charged a bank of condensers of 0.2 mf (0.45 mf) capacity, to 100 kv (40 kv).

Usually, copper lines from the copper shell of the electrodes were used as wave-length stand-

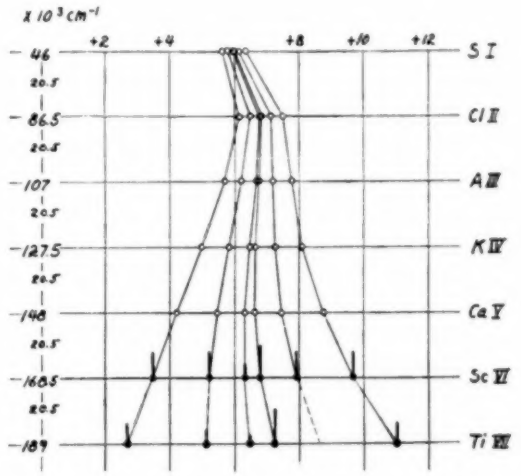

FIG. 1. Displaced frequency diagram. The $3s^23p^4\ ^3P-3s3p^5\ ^3P^0$ multiplets of the sulphur I sequence.

* A preliminary report of these data was given at the Washington meeting of the American Physical Society, April 1937: Phys. Rev. **51**, 1019A (1937).

[1] Kruger, Weissberg and Phillips, Phys. Rev. **51**, 1090 (1937).

[2] Kruger and Phillips, Phys. Rev. **51**, 1087 (1937).

[3] Kruger and Phillips, Phys. Rev. **52**, 97 (1937).

[4] Kruger, Rev. Sci. Inst. **4**, 128 (1933).

TABLE I. *Multiplets in Scandium VI.*

$3s^23p^4$		$^3P_2$	$^3P_1$	$^3P_0$	$^1D_2$	$^1S_0$
	TERM VALUES	0	3350	4476	21,397	49,238
$3s3p^5$						
$^3P_2^0$		(5) 570.295	(4) 581.399			
	175,348	175,348	171,999			
$^3P_1^0$		(4) 561.183	(4) 571.916	(2) 575.573		
	178,195	178,195	174,851	173,740		
$^3P_0^0$			(4) 566.794			
	179,775		176,431			
$3s^23p^34s$						
(^4S) $^5S_1^0$		(30) 221.203	(6) 222.855	(2) 223.419		
	452,073	452,073	448,722	447,590		
(^2D) $^3D_1^0$		(0) 211.696	(4) 213.194	(5) 213.701		
	472,406	472,375	469,056	467,930		
$^3D_2^0$		(5) 211.615	(8) 213.124			
	472,556	472,556	469,210			
$^3D_3^0$		(15) 211.423				
	472,985	472,985				
(^2D) $^1D_2^0$		(1) 209.050	(1) 210.530		(15) 218.840	
	478,354	478,354	474,991		456,955	
(^2P) $^3P_0^0$			(4) 204.725			
	491,810		488,460			
$^3P_1^0$		(2) 203.214	(2) 204.604	(4) 205.067		
	492,092	492,092	488,750	487,646		
$^3P_2^0$		(6) 202.922	(5) 204.310		(1) 212.132	
	492,800	492,800	489,452		471,405	
(^2P) $^1P_1^0$		(1) 200.810		(0) 202.638	(8) 209.826	(3) 222.844
	497,984	497,983	(494,634)*	493,491	476,585	448,744

* Masked by oxygen line.

ards,[5] but in the case of scandium, oxygen[6] lines excited from the oxide were used also. The exposures using aluminum shell electrodes were made in order to find any lines which might be masked by lines of the copper spectrum.

In the analysis of these spectra the regular doublet law, the irregular doublet law and corresponding displaced frequency diagrams, and the constant second difference law have been used. That the latter is applicable to cases where the total quantum number n changes by some integer a, can be seen from the following. If the term value is expressed by $T=R(Z-s)^2/n^2$ the radiated frequency is given by

$$\nu=T_1-T_2=\frac{R(Z-s_1)^2}{n_1^2}-\frac{R(Z-s_2)^2}{(n+a)^2},$$

which reduces to $\nu=c_1Z^2+c_2Z+c_3$ where c_1, c_2 and c_3 are constants involving R, n, a and $s_{1,2}$. This expression is quadratic in Z, and explains the constant second differences between radiated frequencies when n changes by a, and provided there is no change in the screening constant in successive ions. Experimentally, the second differences vary by small amounts so that the screening constants must vary in a similar way.

SPECTRA OF IONS IN THE S I SEQUENCE

A major portion of an analysis of the spectra of the ions Sc VI, Ti VII, V VIII and Cr IX, in the S I isoelectronic sequence, had been completed when the commendable work of Edlen[7] appeared, giving an analysis of most of these spectra. Since Edlen's work agrees with our analysis, only that part of our analysis not duplicated by him is included here. This includes the spectra of Sc VI and one multiplet of Ti VII.

The normal electron configuration of scandium VI is $3s^23p^4$, which gives rise to the normal

[5] Kruger and Cooper, Phys. Rev. **44**, 826 (1933).
[6] Edlen, Nova Acta Reg. Soc. Sci. Upsaliensis, Ser. IV, Vol. 9, No. 6 (1934).
[7] Bengt Edlen, Zeits. f. Physik **104**, 188 (1937).

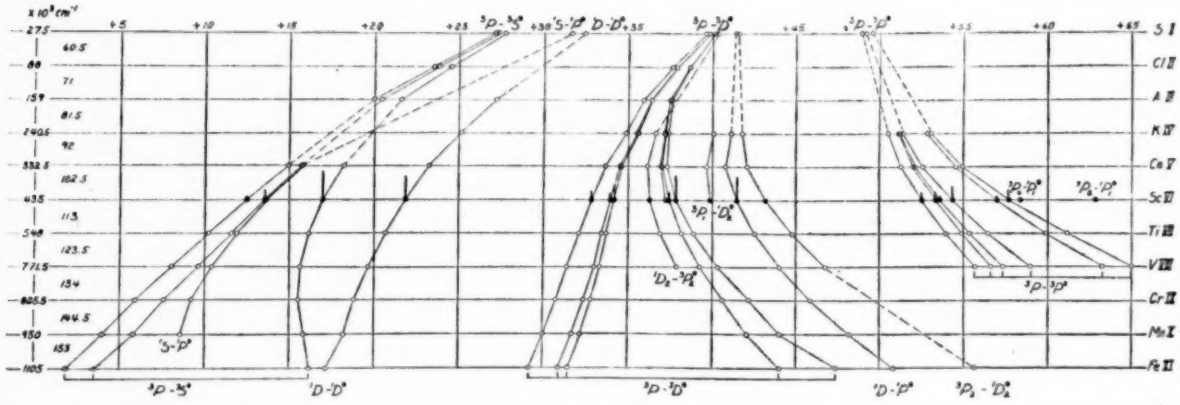

FIG. 2. Displaced frequency diagram. Multiplets of the $3s^23p^4-3s^23p^34s$ transition in the sulphur sequence.

TABLE II. *Radiated frequencies with first and second differences for some of the strongest lines arising from transitions between the $3s^23p^4-3s^23p^34s$ configurations of the sulphur isoelectronic sequence.*

	$^3P_2-{}^3S_1^0$			$^3P_2-{}^3D_3^0$			$^1D_2-{}^1D_2^0$		
	ν	First Difference	Second Difference	ν	First Difference	Second Difference	ν	First Difference	Second Difference
S I	55331			67843			60000		
		57274			58939			(58000)	
Cl II	112605		10799	126782		10961	(118000)		(10308)
		68073			69900			(68308)	
A III	180678		(11549)	196682		11404	186308		(11373)
		(79622)			81304			79681	
K IV	(260300)		(10992)	277986		10669	265989		10212
		(90614)			91973			89893	
Ca V	350914		(10545)	369959		11053	355882		11180
		101159			103026			101073	
Sc VI	452073		11008	472985		10989	456955		10782
		112167			114015			111855	
Ti VII	564240		10843	587000		10975	568810		10645
		123010			124990			122500	
V VIII	687250		10890	711990		10890	691310		10640
		133900			135880			133140	
Cr IX	821150		10940	847870		10430	824450		10750
		144840			146310			143890	
Mn X	965990		10440	994180		11960	968340		10050
		155280			158270			153940	
Fe XI	1121270			1152450			1122280		

states ^3P, ^1D and ^1S. The ^3P term is the ground state and above this are the ^1D and ^1S in the order named. The ^3P term is inverted. Above the normal states are the excited states $^3P^0$ and $^1P^0$ arising from the $3s3p^5$ electron configuration. The $3s3p^5\,{}^3P^0$ term is also inverted. The next excited states above these should be $^{3,5}S^0$, $^{1,3}D^0$ and $^{1,3}P^0$ arising from the $3s^23p^34s$ electron configuration. All terms arising from this configuration are normal.

In the analysis of the spectrum, radiations involving transitions from all excited states, except the $3s3p^5\,{}^1P^0$ and the $3s^23p^34s\,{}^5S^0$, to the normal states have been found. Table I gives the intensity, wave-length, frequency and classification of all the spectral lines identified, together with the term values of the energy levels. All intermultiplet separations have been checked experimentally wherever possible. All other multiplet separations which are involved in only one transition, have been checked for agreement with the regular doublet law. A number of intercombination lines have been identified; thus it is possible to give accurately the relative term values of all the levels, with respect to the $3s^23p^4\,{}^3P_2$ level as zero.

The relation of the multiplets of Sc VI to similar multiplets of the sulphur isoelectronic sequence is shown in the displaced frequency graphs, Figs. 1 and 2. Fig. 1 is a constant first difference graph for the $3s^23p^4\,{}^3P-3s3p^5\,{}^3P^0$ multiplet and follows the irregular doublet law. Fig. 2 is a constant second difference graph and illustrates the constant second difference law. The regularity of the second differences is apparent in Fig. 2, and is further illustrated in Table II where the frequencies, and first and second differences for some of the strong lines arising from transitions between the $3s^23p^4-3s^23p^34s$ configurations are tabulated.

The data for S I, Cl II, A III, K IV and Ca V are available in the literature.[8–11] The data for

TABLE III. *The $3s^23p^4\,{}^3P-3s3p^5\,{}^3P^0$ multiplet of titanium VII.*

$3s^23p^4$		$^3P_2$	$^3P_1$	$^3P_0$
	Term Values	0	4535	5893
$3s3p^5$		(12)	(5)	
		509.518	521.561	
$^3P_2^0$	196,264	196,264	191,732	
		(6)	(2)	(3)
		499.850	511.444	515.021
$^3P_1^0$	200,060	200,060	195,525	194,167
$^3P_0^0$	(202,198)		(197,663)*	

* Obscured by second-order titanium line.

[8] J. E. Ruedy (S I), Phys. Rev. **44**, 757 (1933).
[9] K. Murakawa (Cl II), Zeits. f. Physik **96**, 117 (1935).
[10] J. C. Boyce (A III, IV), Phys. Rev. **48**, 396 (1935).
[11] I. S. Bowen (K V, VI; Ca VI, VII), Phys. Rev. **46**, 791 (1934).

Ti VII, V VIII, Cr IX, Mn X and Fe XI are to be found in Edlen's publication,[7] except for the $3s^23p^4\ ^3P-3s3p^5\ ^3P^0$ multiplet of Ti VII. The intensities, wave-lengths and frequencies of the lines in thus multiplet are given in Table III. The $^3P_1-^3P_0{}^0$ line of this multiplet was obscured by the second order of an intense titanium line of frequency 395,318 cm^{-1}. The value given for this line in Table III was that predicted by the regular doublet law, as applied to the $3s3p^5\ ^3P_0{}^0-{}^3P_1{}^0$ separation in successive ions of the sequence.

TABLE IV. *Multiplets in scandium VII.*

$3s^23p^3$		$^4S^0_{3/2}$	$^2D^0_{3/2}$	$^2D^0_{5/2}$	$^2P^0_{1/2}$	$^2P^0_{3/2}$
	Separations		678		910	
$3s3p^4$		(4)				
$^4P_{5/2}$		571.256				
		175,053				
	2710	(3)				
$^4P_{3/2}$		562.547				
		177,763				
	1441					
$^4P_{1/2}$		(2)				
		558.023				
		179,204				
$3s^23p^24s$						
		(7)				
$(^3P)\ ^4P_{1/2}$		184.607				
		541,691				
	(1960)					
$^4P_{3/2}$						
		(543,650)*				
	(2818)	(12)				
$^4P_{5/2}$		182.993				
		546.469				
			(8)		(2)	(1)
$(^3P)\ ^2P_{1/2}$			191.602		199.163	199.524
			521,916		502,101	501.193
	3276				(1)	(5)
$^2P_{3/2}$				(8)	197.871	198.229
			(525,192)	524,511	505,380	504,467
			(1)	(10)		(15)
$(^1D)\ ^2D_{5/2}$			185.675	185.808		193.000
			538,866	538,190		518,135
	142		(7)		(8)	
$^2D_{3/2}$			185.526		192.607	
			539,008	(538,330)	519,192	(518,282)*

* Masked by oxygen line.

TABLE V. *Multiplets in titanium VIII.*

$3s^23p^3$		$^4S^0_{3/2}$	$^2D^0_{3/2}$	$^2D^0_{5/2}$	$^2P^0_{1/2}$	$^2P^0_{3/2}$
	Separations		1077		1456	
$3s^23p^24s$						
		(10)				
$(^3P)\ ^4P_{1/2}$		151.485				
		660 130				
	2719	(20)				
$^4P_{3/2}$		150.864				
		662,849				
	3653	(20)				
$^4P_{5/2}$		150.037				
		666,502				
			(3)		(1)	(0)
$(^3P)\ ^2P_{1/2}$			156.442		162.019	162.401
			639,215		617,212	615,760
	4234			(10)	(0)	(4)
$^2P_{3/2}$				155.673	160.914	161.293
			(643,449)	642,372	621,450	619,990
			(1)	(20)		(3)
$(^1D)\ ^2D_{5/2}$			151.915	152.164		151.527
			658,263	657,186		634,812
	227		(8)		(3)	(2)
$^2D_{3/2}$			151.863		157.107	157.470
			658,488	(657,411)	636,509	635,042

TABLE VI. *Multiplets in vanadium IX.*

$3s^23p^3$		$^4S^0_{3/2}$	$^2D^0_{3/2}$	$^2D^0_{5/2}$
	Separations		1523	
$3s^23p^24s$				
		(5)		
$(^3P)\ ^4P_{1/2}$		126.732		
		789,066		
	3630	(8)		
$^4P_{3/2}$		126.152		
		792,696		
	4625	(12)		
$^4P_{5/2}$		125.420		
		797,321		
			(0)	(10)
$(^1D)\ ^2D_{5/2}$			126.810	127.068
			788,501	786,978
	358		(5)	
$^2D_{3/2}$			126.765	
			788,859	(787,336)

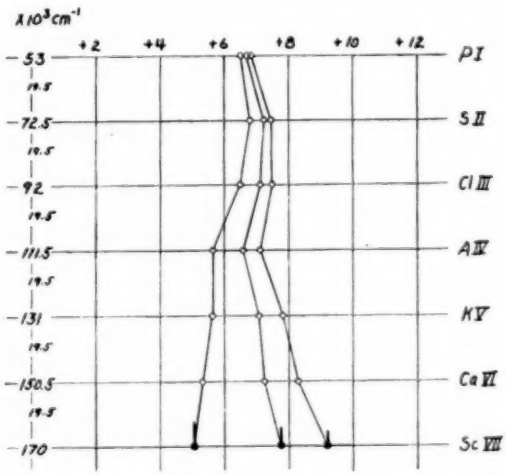

FIG. 3. Displaced frequency diagram. The $3s^23p^3\ ^4S^0-3s3p^4\ ^4P$ multiplet of the phosphorus sequence.

THE SPECTRA OF IONS OF THE P I SEQUENCE

The ions Sc VII, Ti VIII and V IX are isoelectronic with phosphorus. The normal electron configuration of these ions is $3s^23p^3$, which gives rise to the normal states $^4S^0$, $^2D^0$ and $^2P^0$. The $^4S^0$ is the ground state, above which are the $^2D^0$ and $^2P^0$ states respectively. The first excited states are $^{2,4}P$, ^2D and ^2S arising from the $3s3p^4$ configuration. The ^4P term is inverted,

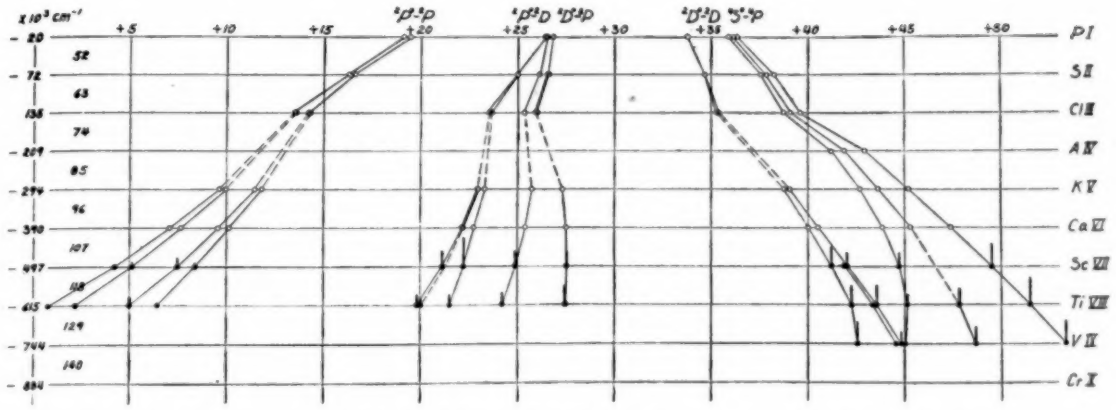

FIG. 4. Displaced frequency diagram. Multiplets of the $3s^23p^3-3s^23p^24s$ transition in the phosphorus sequence.

as it should be. The next excited states above these are $^{2,4}P$, ^2D and ^2S arising from the $3s^23p^24s$ configuration. The ^4P and the ^2P terms are normal but the ^2D term is inverted in all the ions of the sequence.

In the analysis of the spectra of the ions Sc VII, Ti VIII and V IX, the $3s^23p^3\ ^4S^0-3s3p^4\ ^4P$ multiplet has been identified in Sc VII only. No multiplets involving the $3s3p^4\ ^2D$, ^2P and ^2S terms appear on our spectrograms. Multiplets involving the transitions $3s^23p^3\ ^4S^0-3s^23p^24s\ ^4P$ and $3s^23p^3\ ^2D^0$, $^2P^0-3s^23p^24s\ ^2P$, ^2D have been found in Sc VII and Ti VIII. The term value of the $3s^23p^24s\ ^2S$ term is not known for any ion of the phosphorus sequence.

An attempt was made to extend the identification of the radiations of the P I-like ions into V IX, but only the lines belonging to the $3s^23p^3\ ^4S^0-3s^23p^24s\ ^4P$ and to the $3s^23p^3\ ^2D^0-3s^23p^24s\ ^2D$ multiplets were identified. The other multiplets did not appear on our spectrograms.

The intensity, wave-length, frequency and classification of all the lines identified in Sc VII, Ti VIII and V IX are given in Tables IV, V and VI, respectively. Some of the weaker lines of the multiplets are missing or obscured by oxygen lines, but fortunately the doublet separations could still be checked experimentally, making positive identification possible. The separations of the ^4P terms have been checked for agreement with the regular doublet law.[12] Unfortunately no intercombination lines have been identified, hence it is not possible to assign term values to any of the doublet terms relative to the $^4S^0$ ground state.

The relation of the multiplets of Sc VII, Ti VIII and V IX to similar multiplets of ions isoelectronic with phosphorus is shown in the displaced frequency graphs, Figs. 3 and 4. Fig. 3 is a constant first difference graph for the $3s^23p^3\ ^4S^0-3s3p^4\ ^4P$ multiplet, while Fig. 4 is a constant second difference graph for multiplets arising from transitions between terms of the $3s^23p^3$ and the $3s^23p^24s$ configurations. The data for the ions P I, S II, Cl III, A IV, K V and Ca VI are available in the literature.[10, 11, 13–15]

[12] Gibbs and White, Phys. Rev. **29**, 655 (1927).
[13] H. A. Robinson (P I), Phys. Rev. **49**, 297 (1936).
[14] S. B. Ingram (S II), Phys. Rev. **32**, 172 (1928).
[15] I. S. Bowen (Cl III), Phys. Rev. **31**, 34 (1928).

The Ultraviolet Bands of Magnesium Hydride

LOUIS A. TURNER AND WILBUR T. HARRIS
Palmer Physical Laboratory, Princeton University, Princeton, N. J.

(Received July 26, 1937)

Extension of the $^2\Pi^*-{}^2\Sigma$ system of MgH leads to the following values of the constants of the $^2\Pi^*$ state.

$B_0'=6.090$, $B_1'=5.951$,
$B_e'=6.159$, $\alpha'=0.139$,
$D_0'=-3.1\times10^{-4}$, $D_1'=-2.9\times10^{-4}$,
$\omega_e'=1709$, $\omega_e'\chi_e'=43.3$.

Previous erroneous assignments of K values in the bands of both MgH and MgD are corrected. Difficulties in the interpretation of the λ2348 band of MgH and λ2360 band of MgD are discussed.

THE spectrum of MgH includes several band systems. In the ultraviolet lies the $^2\Pi^*-{}^2\Sigma$ system which was discovered and studied by Pearse,[1] and further extended by Guntsch.[2] The 0−0 band of this system shows an abrupt disappearance of the P and R branches for $K'>10$, without any such discontinuity in the Q branch. This was explained by Kronig[3] as a predissociation, in accord with the selection rules for that process. In an attempt to study effects of pressure on this band the whole system was brought out more completely than in previous experiments. This paper presents the new experimental results and the more complete analysis of the spectrum to which they lead.

Experimental Methods

The spectra were obtained from arcs in hydrogen at a pressure of ¼ to 1 atmosphere. The cathode was made of copper and water-cooled. The lower electrode was the anode and consisted of a cup made of nickel into which scraps of magnesium were placed. A current of 2–3 amperes was run for several hours. This was supplied by a 700-volt generator with suitable ballast resistance in series. For some exposures the supply of Mg had to be renewed several times. Hydrogen was admitted to a side tube to which a quartz window was attached, and was pumped out on the other side. This arrangement helped to keep the window from becoming coated with magnesium. A Hilger E-1 quartz spectrograph and Ilford Q plates were used. The iron lines from an iron arc were put on some of the plates for standards of measurement.

[1] R. W. Pearse, Proc. Roy. Soc. **A125**, 157 (1929); **122**, 442 (1929).
[2] A. Guntsch, Zeits. f. Physik **87**, 312 (1934); **93**, 534 (1935).
[3] R. deL. Kronig, Zeits. f. Physik **62**, 300 (1930).

Experimental Results

In addition to extensions to the already known branches of these bands the following results

TABLE I. *Wave numbers of the lines of the 0−0 band.*

K	$P(K)$	$Q(K)$	$R(K)$
1		41226.49(?) 41235.45	41262.00*b*
2	41215.43 41212.66	41238.05	41275.63*b*
3	41204.18	41240.44	41289.87
4	41195.20	41243.44	41305.03
5	41186.84	41247.14	41320.94
6	41179.61	41251.47	41337.54
7	41172.50	41256.41	41354.84
8	41166.64	41262.00*b*	41372.77
9	41161.43	41269.04	41390.25*b*
10	41157.04	41275.63*b*	
11	41152.85	41283.88	
12		41292.62	
13		41302.00	
14		41312.30	
15		41323.33	
16		41335.04	
17		41347.66	
18		41360.92	
19		41375.11	
20		41390.25*b*	
21		41405.67	
22		41422.08	
23		41439.55	
24		41457.14	
25		41476.31	
26		41496.08	
27		41516.52	
28		41539.33*b*	
29		41560.34	
30		41582.94	
31		41605.72	
32		41631.45?	

TABLE II. *Wave numbers of the lines of the 0−1 band.*

K	P(K)	Q(K)	R(K)
1		39803.44	39829.45
2	39782.70	39806.71	39843.39*b*
3	39774.42	39810.80	39859.86
4	39766.61	39814.85	39875.94*b*
5	39759.97	39820.27	39894.10
6	39754.70	39826.52	39913.15
7	39750.31	39834.35	39932.74
8	39747.50	39843.39*b*	39952.87?*b*
9		39852.76	39971.15?*b*
10	39745.60	39863.68	
11		39875.94*b*	
12		39888.86	
13		39902.98	
14		39918.39	
15		39934.54	
16		39952.87*b*	
17		39971.15*b*	
18		39990.77	
19		40012.19	
20		40034.21	
21		40057.76?*b*	
22		40083.10?*b*	
23		40111.78?*b*	

were obtained. Twelve lines of the Q branch of the $1-0$ band were measured. (Because of the predissociation only a Q branch appears.) Pearse had observed only the head of this band and Guntsch's plates did not show it at all. The predictable P and R branches of the $0-1$ band were observed. Neither Pearse nor Guntsch were able to observe these lines. These branches break off because of the predissociation in the $^2\Pi^*$, $v'=0$ term. Because of the crowding of the lines near the P head and the overlapping of R and Q lines it is impossible to say definitely that the bands stop at $K'=10$. Undoubtedly, however, such is the case. A few unresolved lines of what is apparently the $2-2$ band were observed. They give the same appearance as the lines of the $1-1$ band do with light exposure.

The dispersion in the region of these bands was 40 cm^{-1} per mm of plate. Measurements of the strong lines could be repeated to 0.001 mm, but successive measurements of fainter lines would differ by several times that amount. The relative wave numbers in any band should be correct to about 0.1 cm^{-1}. The absolute values are not so accurate. The wave numbers of several atomic lines were measured and found to be in error systematically by as much as 1.3 cm^{-1}. Apparently the superposed iron spectrum was slightly shifted, as often happens with prism spectrographs. We were not able to get a good picture with both the Fe lines and Mg bands from the same discharge. All wave numbers were shifted to give the correct ones for the atomic lines. The dispersion and relative wave numbers depend on the Fe lines but the absolute values depend upon a rather small number of atomic lines of Mg. The wave numbers differ from those of Guntsch in each sequence of bands by about 0.3 cm^{-1} but not in the same direction. He does not give any details as to how his measurements were obtained but his grating spectrograph was more favorable for getting accurate superposition of spectra from different sources. Probably his absolute values are more accurate. Because of the greater intensity of our source our relative values are probably more accurate for the weaker lines.

Tables I–III give the wave numbers of the lines. Lines which are blended with others are indicated by a *b*. The faintest ones are marked with a question mark.

Comparison with the tables of Guntsch will show that the K values of the lines in the $1-1$ and $1-2$ bands are here increased by one unit. The necessity for such a change was shown first by a combination relation. One should have

$$\nu_{1,\,0}(K)-\nu_{0,\,0}(K)=\nu_{1,\,1}(K)-\nu_{0,\,1}(K).$$

The differences so calculated showed a divergence increasing with increasing K, until the K values

TABLE III. *Wave numbers of the lines of the 1−0, 1−1, 1−2 and 2−2 bands.*

K	1−0 Q(K)	1−1 Q(K)	1−2 Q(K)	2−2
1	42861.54 (head)	41426.62	40057.76*b*	41596.03 (head)
2		41429.68	40061.59	
3		41432.16	40065.98	
4		41436.01	40070.92	
5	42865.64	41439.55*b*	40076.63	
6	42868.59	41444.37	40083.10*b*	
7	42871.80	41450.11	40091.92	
8	42875.19	41457.14*b*	40101.58	
9	42879.30	41463.88	40111.78*b*	
10	42883.56	41472.14	40123.90	
11	42889.09	41481.20	40136.99	
12	42894.24	41491.10	40152.27*b*	
13	42900.38	41502.04	40167.38?	
14	42906.28*b*	41513.80	40184.60?	
15	42912.76	41526.21	40202.82?	
16	42921.78	41539.33*b*	40222.68?	
17		41554.75		
18		41570.33		
19		41586.73		
20		41603.96		
21		41622.89		
22		41641.40		

for the 1,1 band were raised by one unit. That this change is correct and also necessary for $1-2$ is shown by the method discussed in the next paper. The above combination relation is satisfied by all unblended lines to less than one wave number unit. There is a systematic discrepancy of about 0.7 cm^{-1} with lesser fluctuation about it.

Constants of the Molecule

By the method given in the following paper the constants for the Q branches of the different bands were found. They are given in Table IV. For three of the bands the points scattered so that no accurate value of $D_0'-D_0''$ could be determined. The values of B_v' and D_v' were found by using the accurate determinations of the B_v'''s and D_v'''s by Guntsch[4] given in a recent paper. These were obtained from the analysis of the $^2\Pi-^2\Sigma$ bands which lie in the visible region. From the B_v''s can be calculated B_e' and α'. All of the rotational constants are grouped in Table V. From his analysis of the $0-0$ band of the $^2\Pi^*-^2\Pi$ system Guntsch[2] obtained $B_0'=6.088$ and $D_0'=-3.20\times10^{-4}$.

For all K values above 2 these bands show no splitting of the lines so that the energy expressions for case b are applicable. In general, the expression for case b is

$$\nu_Q(K)=\nu_{e,v}+B_{v'}'\{K(K+1)-\Lambda'^2\}-B_{v''}''\{K(K+1)-\Lambda''^2\}.$$

In the present case $\Lambda'=1$ and $\Lambda''=0$ so that this becomes

$$\nu_Q(K)=\nu_{e,v}+CK(K+1)-B_v'.$$

Table IV. *Constants of the bands.*

Band	$C=B_v'-B_v''$	$D_v'-D_v''$	B_v'	D_v'
$0-0$	0.357	2.19×10^{-5}	6.090	-3.1×10^{-4}
$0-1$	0.54	—	6.09	—
$1-0$	0.23	—	5.96	—
$1-1$	0.399	5.15×10^{-5}	5.951	-2.9×10^{-4}
$1-2$	0.60	—	5.95	—

Table V. *Rotational constants of* $^2\Pi^*$.

$B_0'=6.090$	$D_0'=-3.1\times10^{-4}$
$B_1'=5.951$	$D_1'=-2.9\times10^{-4}$
$B_e'=6.159$	$\alpha'=0.139$

[4] A. Guntsch, Zeits. f. Physik **104**, 584 (1937).

In particular for $K=5$ one gets

$$\nu_{cv}=\nu_Q(5)-30C+B'.$$

The values for the $\nu_{e,v}$'s so calculated are given in Table VI. The one for the $2-2$ band, however, was obtained by assuming that the head corresponds to $K=1$, and by using an extrapolated value for B_2'. From these values one calculates $\omega_e'=1709$, $\omega_e'\chi_e'=43.3$.

Constants of $^2\Pi^*$ of Magnesium Deuteride

The lines of three of the $^2\Pi^*-^2\Sigma$ bands of MgD were studied by Guntsch.[2] Application of the methods of the following paper shows that his assignments of K values in the $0-0$ band is correct, but that they must be raised by one unit for the $0-1$ band. The values for the $1-1$ band are uncertain because of the irregularity of the points, but presumably correct.

The revised constants are given in Table VII with the values for B' calculated as above. The values of B'' used in computing those of B' are the accurate ones taken from the paper of Fujioka and Tanaka.[5] The calculated B_e' and α' for MgD are 3.283 and 0.136, respectively.

According to theory

$$(B_e'(\mathrm{MgD})/B_e'(\mathrm{MgH}))=\rho^2=(\mu_{\mathrm{MgH}}/\mu_{\mathrm{MgD}}).$$

The ratio of the B_e''s is 0.533, while the ratio of the reduced masses is 0.52061. Starting with B_e' for MgH and the theoretical value of ρ^2 we can compute a value of 3.206 to be expected for B_e' of MgD. It does not seem possible to account for the discrepancy between this and the value of 3.283 from the bands by experimental error or wrong assignment of K's. The $^2\Pi^*$ state may be perturbed by the other $^2\Pi$ state which should exist at nearly the same energy, according to Pearse and Guntsch. As Van Vleck[6] points out the relations between bands of isotopic molecules are upset by perturbations.

The λ2348 Band of MgH and λ2360 Band of MgD

Guntsch[2] discovered a band consisting of a single Q branch at 2348. This band was strong

[5] Y. Fujioka and Y. Tanaka, Sci. Pap. Inst. Phys. Chem. Tokyo **30**, 121 (1936).

[6] J. H. Van Vleck, J. Chem. Phys. **4**, 327 (1936).

TABLE VI. *Deslandres table for the band system.*

v' \ v''	0	1	2
0	41242.5 (1432.3) (1622.2)	39810.2 (1623.3)	
1	42864.7 (1431.2)	41433.5 (1368.7)	40064.8 (1536.1)
2			41600.9

TABLE VII. *Constants of MgD.*

BAND	C	B'
0−0	0.216	3.214
0−1	0.285	3.217
1−1	0.15	3.08

on all of our plates. Table VIII gives our measurements of these lines. They differ from those of Guntsch by about one wave number. Also, it will be noted that the K values have been lowered by one unit for the same reason that they were raised in the other bands. With this change one gets $C=B'-B''=0.618$ and $E=D'-D''=-1.26\times10^{-4}$. If it be assumed that the lower state is the $v''=0$ of the normal $^2\Sigma$ state this gives $B'=6.351$ and $D'=4.6\times10^{-4}$, using Guntsch's new values of B'' and D'', as before.

Guntsch found a similar band for MgD at 2360 and gives the wave numbers of 13 of the lines. Apparently his K values should be lowered by 2 although there are not enough lines of the band measured for this to be as certain as in the other cases. If this change be made one gets $C=0.236$ and $E=-1.58\times10^{-4}$. Again, assuming that the lower state is the $v''=0$ of the normal $^2\Sigma$ one gets $B'=3.234$ and $D'=-2.50\times10^{-4}$.

If these bands in MgH and MgD are analogous bands of another $^2\Pi-{}^2\Sigma$ system, as seems probable, the ratio of B_0'(MgD) to B_0'(MgH) should not be greatly different from the ratio of the $B_e''s$. This ratio is 0.509, less than the theoretical value, 0.52061. This is what one would expect if the $^2\Pi$ of these bands is what is causing the perturbation of the $^2\Pi^*$ state. The changes of energies which would make the ratio too great in the one perturbing state would presumably occur in the other direction in the other state.

The large difference of wave numbers between these two bands of MgH and MgD introduces difficulties in their interpretation. As above one can compute values of $\nu_{e,\,v}$ from the relation

$$\nu_{ev}=\nu_Q(5)-30C+B'.$$

One gets

$$\nu_{ev}(\mathrm{MgH})=42569.4,$$
$$\nu_{ev}(\mathrm{MgD})=42360.3.$$

Neglecting all but the first power terms in the expression for the vibrational energy one has by the usual theory of the isotope effect for analogous bands

$$\nu_{ev}(\mathrm{MgH})-\nu_{ev}(\mathrm{MgD})=(1-\rho)\{\omega'(v'+\tfrac{1}{2})-\omega''(v''+\tfrac{1}{2})\}.$$

Substitutions of the ν's and of $\rho=(0.52061)^{\frac{1}{2}}=0.723$ gives

$$\omega''(v'+\tfrac{1}{2})-\omega''(v''+\tfrac{1}{2})=209/0.277=755.$$

If these bands are 0−0 bands this gives $\omega'-\omega''=2\times755=1510$. If the lower state be the normal state of MgH then ω'' equals approximately 1450 (see Table VI) and ω' would have to be 2960. This seems implausibly large, especially in view of the fact that the B' calculated above in the same hypothesis (6.351) is not much greater than that of the $^2\Pi^*$ state for which the ω' is about 1650. If values of v'' greater than those of v' be taken absurdly high values for ω' result. Assuming $v'=1$, $v''=0$ one gets $\omega'=990$, which is rather low. The assumption $v'=1$, $v''=1$ leads to the more plausible result that $\omega'=1954$. It seems incredible, however, that a 1−1 band could appear with no trace of the 0−0 band of the same system.

Whatever the explanation of these bands may be it is peculiar that the other bands given by transitions to states with higher values of v'' are not found. They do not appear with any

TABLE VIII. *2348 band of MgH.*

K		K	
2	42571.18	13	42641.01
3	42574.13	14	42651.36
4	42577.43	15	42662.38
5	42581.61	16	42674.04
6	42586.51	17	42685.36
7	42591.98	18	42697.99
8	42598.53	19	42710.73
9	42605.81	20	42723.21
10	42613.54	21	42738.78
11	42622.21	22	42757.76
12	42631.27		

TABLE IX. *Unclassified lines.*

41226.49	39764.89
41330.31	39883.71
41528.77	39928.12
41577.24	39986.54
41613.49	39996.89
41637.85	40002.66
41644.82	40192.06
41667.28	40208.24
	40226.57
	40266.32
	40290.08
	40291.26

strength in the places that one would calculate for MgH, assuming the 2348 band to be 0−0. Perhaps the unassigned lines discussed in the next paragraph belong to this system.

UNCLASSIFIED LINES

In addition to the lines included in Tables I–III there appeared regularly on our plates some other lines which seem to belong to MgH. Their wave numbers are given in Table IX. They are all of low intensity but not as faint as some of the classified lines. Those of the group of smaller wave numbers gave the superficial appearance of belonging to P and R branches of the 1−2 band. This was reported in the abstract which appeared in the program of the April, 1937, meeting of the American Physical Society in Washington. Analysis showed this to be a false conclusion and the error was corrected in the proof. These lines do not belong to possible O-type or S-type branches. It is also possible that they may belong to the $^2\Sigma^*-{}^2\Sigma$ band system. One band of this system was observed in absorption by Grundström.[7] We have not been able to classify these lines.

[7] B. Grundström, Nature **137**, 108 (1936).

SEPTEMBER 15, 1937 PHYSICAL REVIEW VOLUME 52

The Determination of Rotational Quantum Numbers in Single Q Branches

LOUIS A. TURNER AND WILBUR T. HARRIS
Palmer Physical Laboratory, Princeton, N. J.

(Received July 26, 1937)

A graphical method is given for determining the rotational quantum numbers and rotational constants of Q branches. It is applicable to a single band. It seems to be more accurate than methods used hitherto.

AS a result of predissociation many of the ultraviolet bands of MgH consist of single Q branches. The levels which would give emission of the P and R branches are unstable. This condition will probably be encountered in other spectra in the ultraviolet. It is necessary to find a way to assign the rotational quantum numbers in such bands. Jenkins and McKellar[1] gave one method applicable in such cases. It involves comparison of lines in two bands having one vibrational state in common. The method was applied by Guntsch[2] to the bands of MgH, but it does not give unambiguous results for those bands. The method described below seems to be more reliable and gives immediately the coefficients of both the quadratic and fourth-power terms for each band separately. It offers a convenient way of beginning the analysis of bands even when P and R branches are also present.

To be definite, consider a molecule of case b for both upper and lower states. The wave number of a Q line will be given by the expression

$$\nu_Q(K)=\nu_{v,v}+B'\{K(K+1)-\Lambda'^2\}-B''\{K(K+1)-\Lambda''^2\}+(D'-D'')K^2(K+1)^2.$$

By subtraction one gets

$$\nu_Q(K+n)-\nu_Q(K-n)=(B'-B'')\{(K+n)(K+1+n)-(K-n)(K+1-n)\}+(D'-D'')\{(K+n)^2(K+1+n)^2-(K-n)^2(K+1-n)^2\}.$$

[1] F. A. Jenkins and A. McKellar, Phys. Rev. **42**, 473 (1932).

[2] A. Guntsch, Zeits. f. Physik **93**, 534 (1935).

By tedious but straightforward algebra this can be put in the form

$$y=\frac{\nu_Q(K+n)-\nu_Q(K-n)}{2K+1}=2n[(B'-B'')-(2n^2-0.5)(D'-D'')]+n(D'-D'')(2K+1)^2.$$

To use this one assigns tentative K values and computes the y's for different pairs of lines, using the same value of n ($n=3$ proves to be a convenient value). If now these y's be plotted against the corresponding values of $(2K+1)^2$ a straight line will result, provided that the K's have been properly chosen. The slope of this line is $n(D'-D'')$ and its intercept is $2n[(B'-B'')-(2n^2-0.5)(D'-D'')]$, from which $B'-B''$ can be calculated. Fig. 1 shows the results of such a plot for the lines of the 1−1 band of the $^2\Pi^*-{}^2\Sigma$ system of MgH (see previous paper). The three sets of points correspond to three different assignments of the K's, differing from each other by a shift of one unit. The K's corresponding to the middle set, through which the line is drawn, are those given in the previous paper and the constants for the band are computed from this line. The K's of the other bands of MgH and MgD were determined in the same way.

The question arises as to what is the best choice of n in order to show most plainly any error in the assignment of the K's. If the K's have been wrongly assigned the curvature becomes greatest for low K values and for a small n; on the other hand, the scattering of the points about the line are relatively great for small n. The average experimental error in the difference between two lines will be the same whether they be adjacent ($n=\frac{1}{2}$), or eight lines apart ($n=4$). The ratio of the departure of the point from the line to the intercept will, however, vary as $1/n$, for the same mean K. Thus, one obtains a closer fit to a straight line for large n values. The analytical solution of the problem is too involved to be worth while. Empirically it was found that $n=3$ seemed to give a good compromise.

Obviously this method is applicable to Q branches whenever the levels are accurately given by expressions involving only terms of the form $J(J+1)$ and $J^2(J+1)^2$. It takes explicit account of the fourth-power term which the method of Jenkins and McKellar does not.

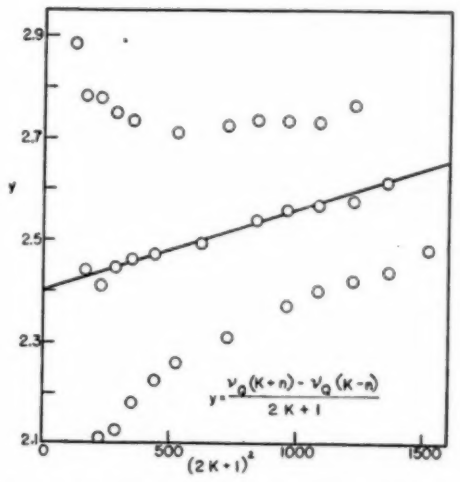

FIG. 1. Illustration of the graphical method for the case of the lines of the 1−1 band of the $^2\Pi^*-{}^2\Sigma$ system of MgH.

This method is not applicable to P and R branches since the expression for such branches includes terms in the first and third-power of $K+\frac{1}{2}$ even when the K's are correctly assigned. If the K's be shifted by one unit and the coefficients changed correctly the new expression will give as good a representation of the lines as the old one. Thus there is no basis for discrimination.

Stepwise Fluorescence in Mercury-Nitrogen Mixtures

The 3650 Line

LOUIS A. TURNER
Princeton University, Princeton, New Jersey

(Received June 24, 1937)

The experiments of Wood and of Gaviola show that when mercury vapor is illuminated by light from a mercury arc, and nitrogen is added in increasing amounts, the concentration of atoms in the $^3P_2$ state passes through a minimum. No simple theory accounts for this result. An explanation involving excitation of atoms in the $^3P_1$ state by vibrating nitrogen molecules is discussed. The results obtained when a filter of bromine vapor is used indicate a transfer of excited mercury atoms from one to another ^3D state upon collision with nitrogen.

SOME years ago R. W. Wood performed experiments on the optical excitation of mercury vapor. They were continued in collaboration with E. Gaviola, who wrote several papers on the theory. In this splendid series of papers[1] by these authors the principal effects were explained. Nevertheless, the theory developed by Gaviola does not adequately account for the observed changes of the intensity of the 3650 line ($2\,^3P_2-3\,^3D_3$). The purpose of the present paper is to consider the behavior of this line, point out the questions which it raises, and suggest interpretations of the results.

THE 3650 LINE IN THE FLUORESCENCE OF PURE MERCURY VAPOR

First, it is desirable to reconsider the behavior of the 3650 line in the fluorescence excited in pure mercury vapor by the full light of the mercury arc. Fig. 1 gives the Grotrian diagram of the levels of the mercury atom with which we are concerned. 1*a* is drawn to scale, 1*b* is schematic. On it are indicated the wave-lengths of the principal lines and their relative intensities in the arc as given by Wood (II, p. 782; III, p. 474). Wood and Gaviola interposed neutral screens between the source of exciting light and the fluorescing vapor (V). For each screen there was a factor, f, by which the intensities of all exciting lines were reduced. They found that the intensity of the 3650 line in the fluorescence was reduced by the factor f^3, and the intensity of the 3654 line by the factor f^2. In earlier experiments (II, p. 784) the intensities of the 5461, 4358, 4046, 3663, 3131, 3125, and 2967 lines had been found to vary in the same way as that of 3654, so these other lines must also vary in intensity as f^2. One concludes from the change of the 3650 line that the concentration of excited atoms in the $^3D_3$ state must vary with f^3, and that the concentration of the atoms in the $^3P_2$ state must vary with f^2. This is apparent from Eq. (1) for the steady state.

$$[^3P_2]a_{3650}\cdot I_{3650}\cdot f=[^3D_3]\cdot A_{3650}=J_{3650}\ (\propto f_3). \quad (1)$$

(Notation: In this equation and in the following ones, the square brackets, [ ], will be used to represent concentrations of excited atoms in the states indicated by the symbols within the brackets.

The a's are effective absorption coefficients,
The I's are intensities in the exciting light before modification by screens,
f is the transmission factor of the screen,
The A's are Einstein emission coefficients,
The J's are intensities of emitted light in fluorescence.)

These conclusions were drawn by Wood and Gaviola, of course, but the argument is repeated here for elucidation of the equations and notations which are used in this paper. In all of these equations the left side will represent the rate of formation of excited atoms (no. per cc per sec.) and the right-hand side will represent the rate of disappearance. The concentration of the variety

[1] Henceforth these papers will be referred to by the Roman numerals given to them here. I. R. W. Wood, Proc. Roy. Soc. London, **A106**, 679 (1924); II. R. W. Wood, Phil. Mag. **50**, 774 (1925); III. Ibid. **4**, 466 (1927); IV. R. W. Wood and E. Gaviola, Phil. Mag. **6**, 271 (1928); V. **6**, 352 (1928); VI. E. Gaviola, Phil. Mag. **6**, 1154 (1928); VII. **6**, 1167 (1928); VIII. E. Gaviola and R. W. Wood, **6**, 1191 (1928).

of excited atoms under consideration appears as a common factor on the right-hand side.

Next consider the equation for the balance of $^3P_2$ atoms.

$$[^3S]A_{5461}=[^3P_2](f\Sigma aI+b). \qquad (2)$$

On the left-hand side of this equation there should also appear other terms corresponding to the emission of the 3663, 3654, and 3650 lines which results in the formation of atoms in the $^3P_2$ state. Since these lines are very much weaker than 5461 these terms may be neglected. The term ΣaI on the right is the sum of four separate terms, each of which represents absorption of one of the four lines just mentioned. 5461 is much the strongest line in the exciting light but its absorption is not detectable experimentally, whereas that of 3650 has been observed (VII, p. 1171). The b term includes all other processes by which $^3P_2$ atoms are removed, such as collisions with other atoms, and with the walls. Since the $^3P_2$ atoms are metastable, their mean life is large enough for such effects to be of importance. The $(^1S-^3P_2)$ forbidden line, 2270, does not appear so that its emission need not be included. The left-hand side of Eq. (2) gives J_{5461}, the intensity of the green line in emission. It is experimentally observed to be proportional to f^2. We have just seen above that $[^3P_2]$ is also proportional to f^2. These two facts are reconcilable only if $\Sigma aI \ll b$, because of the f which multiplies into ΣaI. Thus, we must conclude that the $^3P_2$ metastable atoms are removed principally by collision and not by absorption of radiation. This is exactly opposite to the suggestion of Gaviola (VI, p. 1165). The point was one of minor importance in his considerations, so he did not make as careful an analysis of the factors involved. Since the pressure in the experimental tube could not have been much above the vapor pressure of mercury ($\sim$0.001 mm) the mean free path of these excited atoms is presumably large compared to the size of the tube. The metastable atoms can get to the walls quickly. The probability of losing energy and being reduced to $^3P_1$, $^3P_0$ or $^1S_0$ atoms at the first collision must be large, since the decrease of intensity of the 3650 line in fluorescence across the tube does not indicate an equalized, uniform distribution of $^3P_2$ atoms.

It is obvious that Eq. (2) represents an average behavior, rather than being one which takes proper account of the balance in any particular portion of the tube. Such an equation would have to include terms both for the loss and gain of $^3P_2$ atoms by thermal motion. These would contain geometrical factors and be complicated. Because of the low pressure the ordinary equations for

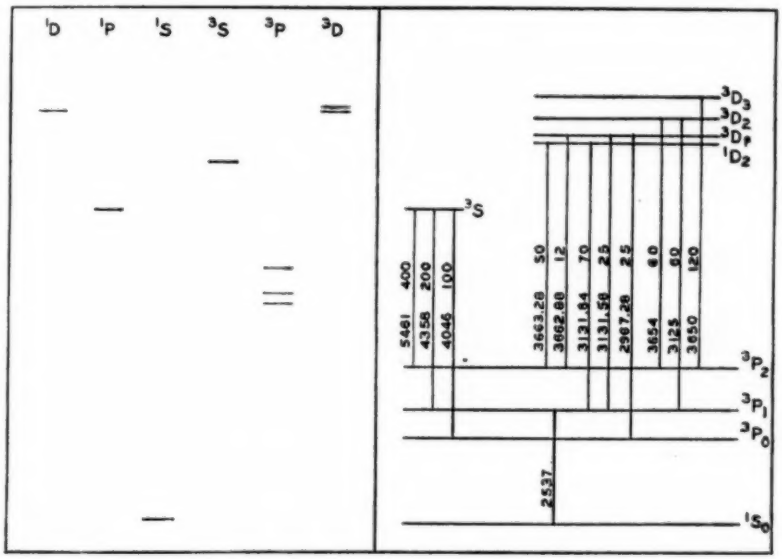

FIG. 1. Grotrian diagram of certain levels of the mercury atom.

diffusion would not be relevant. The b of Eq. (2) puts such terms together as a net loss. The b is different for different places in the tube. Such considerations for the other excited states lead to the same conclusions as those reached by Wood and by Gaviola by substantially equivalent methods.

It should be noted that the above and the following remarks refer only to the conditions in a small region of volume of the experimental tube. It is to be thought of as close to the side where the exciting light enters, since nearly all of the experimental data cited were obtained for such places. The question of the distribution of density of the exciting atoms across the tube is a vastly more complicated one. The equations of Gaviola (VI, p. 1161) can represent only a very rough first approximation, even when diffusion is unimportant, because of his assumption of exponential absorption. The over-all absorption of an emission line can be accurately exponential only when there is the same coefficient of absorption for all parts of the line. In general, in such reversals of emission lines the variation of the absorption coefficient with frequency is more rapid than that of the intensity of the absorbed line.

Effects of Added Nitrogen on the 3650 Line

Wood found that the addition of nitrogen to the tube gave rise to marked changes in the intensities of the different lines in fluorescence. Most of them become stronger. The 3650 line was first markedly diminished in intensity by small amounts of nitrogen and then augmented by larger amounts. As is well known, many of the effects are the result of a great increase of the concentration of atoms in the $^3P_0$ state. The absorption of 4047 by such excited atoms was directly observed and accounts for the great enhancement of 5461, 4358 and 4047.

This great enhancement of 5461 would lead one to expect a corresponding increase of 3650, since $^3P_2$ atoms are being produced by emission of 5461. The contrary result must mean that the $^3P_2$ atoms are destroyed upon collision with N_2 molecules. Gaviola presents a theory based on this hypothesis (VII, p. 1173) which is in good accord with the experiments as far as the principal effect of a diminution of intensity is concerned. Unfortunately it does not lead to the observed result that the intensity again increases at higher pressures. In order to explain this discrepancy one might be tempted to suggest production of $^3D_3$ atoms by some process other than the absorption of the 3650 line by the $^3P_2$ atoms (as in the last section of this paper). This will not suffice, however, since the more direct experiments on the absorption of the 3650 line show slight absorption at zero pressure of nitrogen, no absorption at intermediate pressures, and increased absorption again at higher pressures (VII, p. 1171). The concentration of $^3P_2$ atoms evidently goes through a minimum, and this is reflected in the intensity of the 3650 line in fluorescence.

The difficulty of understanding this behavior can be seen by consideration of the equation for the steady state of the $^3P_2$ atoms. It is

$$[^3S]A_{5461}=[^3P_2]\{\Sigma aI+K_2+k_2p+\Delta/p\}. \quad (3)$$

As above, the production of $^3P_2$ atoms by emission of lines other than 5461 is negligible. Further, the term representing absorption of light, ΣaI, is undoubtedly even less important here than above, where it was negligible. K_2 takes care of any manner of disappearance of $^3P_2$ atoms which is independent of the pressure of the nitrogen. Collisions with nitrogen molecules and with impurities in the nitrogen used are represented by the k_2p term, p being the pressure of the nitrogen. The Δ/p term is of the form which has been found suitable for taking account of the decreased rate of diffusion to the walls at higher pressures.[2]

The experimentally observed fivefold decrease in the intensity of the 3650 line produced by the addition of 0.05 mm of nitrogen can mean only that the k_2p term far outweighs the Δ/p term, which latter tends to give an initial change in the opposite direction. The right-hand side of (3) can thus be represented to a fair approximation by a term of the form K_2+k_2p. This is essentially the same as Gaviola's theory. Noting that the left-hand side of (3) is proportional to

[2] E. W. Samson, Phys. Rev. **40**, 940 (1932); Klumb and P. Pringsheim, Zeits. f. Physik **52**, 610 (1929). Obviously this is incorrect for very low pressures since it goes to infinity for zero pressure. $\Delta/(p+p_0)$ would be a better form. See E. Gaviola, Phys. Rev. **34**, 1373 (1929).

TABLE I. *Ratio of intensities as a function of pressure.*

P (mm)	0	0.05	0.1	0.2	0.43	1.25	2	4	11
J_{5461}/J_{3650}	1	7.5	8	8	6	12	7.5	4.3	12.7

J_{5461}, and taking the intensity of 3650 as proportional to $[^3P_2]$ (3) becomes

$$K_2+k_2p=CJ_{5461}/J_{3650}, \tag{4}$$

C being a constant of proportionality. The values of the ratio J_{5461}/J_{3650} are given in Table I. These ratios in Table I are computed from Wood's provisional values of the relative intensities (III, p. 485). Although they do not lie on a smooth curve the approximate constancy of the ratio at higher pressures is apparent. This requires that k_2 be much less than K_2, which leaves unaccounted for the marked change produced by a change from a pressure of 0 to one of 0.05 mm. Eqs. (3) and (4) are completely inadequate for representing the facts.

One way to approach the problem is to inquire what changes in Eqs. (3) and (4) would be necessary to get a better agreement with experiment. There seems to be no reasonable way to modify the right-hand side of Eq. (3). Collisions with the nitrogen molecules are clearly very effective in removing the $^3P_2$ atoms. It is hard to see how this effect could be other than proportional to the pressure of the nitrogen. The experimental results can be taken to indicate that there is some process of production of $^3P_2$ atoms which increases with pressure, in addition to their production by radiation of the 5461 line. If we add such a term, $C'p$, to the left-hand side of (3) and eliminate the same terms on the right as before we get

$$[^3P_2]=\frac{[^3S]A_{5461}+C'p}{K_2+k_2p}=\frac{J_{5461}+C'p}{K_2+k_2p}. \tag{5}$$

Wood's relative values of J_{5461} can be represented approximately by an empirical formula of the form

$$J_{5461}=1+ap-bp^2,$$

in which a and b are positive. This merely expresses the finding that J_{5461} grows less rapidly at higher pressures. It is perhaps better to use the more general form

$$J_{5461}=1+ap-(bp^2+cp^3+\cdots).$$

Putting this expression in (5) we get

$$[^3P_2]=\frac{1}{K_2}\cdot\frac{1+(a+C')p-(bp^2+cp^3+\cdots)}{1+pk_2/K_2}. \tag{6}$$

Inspection of Eq. (6) shows that if $[^3P_2]$ is to decrease with rising pressure, at low pressures, k_2/K_2 must be greater than $(a+c')$. If this be so there can be no minimum for $^3P_2$. Because of the negative term $-(bp^2+cp^3+\cdots)$ this concentration will decrease even faster at higher pressures. Thus we are led to the conclusion that no process which supplies $^3P_2$ atoms at a rate proportional to the pressure of nitrogen will suffice to give the observed minimum. It is necessary that there be some process of supplying $^3P_2$ atoms which is proportional to p^2, or some higher power of p, large enough to outweigh the term $-(bp^2+cp^3+\cdots)$. This conclusion seems to be a necessary one on the basis of the experimental evidence. It does not depend on the exact values of J_{5461}, which are given by Wood as being merely provisional, but on the general experimental evidence that the concentration of $^3P_2$ atoms passes through a minimum.

A process of the sort required is suggested by consideration of the sensitivity of the $^3P_2$ atoms to collision with nitrogen. These excited atoms must give up some energy to become one of three other kinds of excited atoms, either $^3P_1$, $^3P_0$, or $^1S_0$. The energy difference between $^1S_0$ and $^3P_2$ is 5.43 volts. There is no known or expected electronic difference of this magnitude in the nitrogen molecule and it is unlikely, by the Frank-Condon principle, that such large vibrational transitions should occur. Presumably $^3P_2$ atoms lose their energy to become $^1S_0$ atoms only very infrequently upon collision with nitrogen molecules. The energies involved in the changes $^3P_2\rightarrow{}^3P_1$ and $^3P_2\rightarrow{}^3P_0$ are 0.571 and 0.789 volts, respectively. Compare these with the energies of the nitrogen molecule in its $v''=0$, 1, 2, and 3 vibrational states, which are 0, 0.287, 0.570, and 0.850 volts.[3] The very close agreement between the energy of the $^3P_2\rightarrow{}^3P_1$ change and the $v''=2\rightarrow v''=0$ change leads one to suspect that the process which makes the $^3P_2$ atoms sensitive to nitrogen is the excitation

[3] Computed from the $a\leftrightarrow X$ bands of Birge and Hopfield, Astrophys. J. **68**, 257 (1928).

of normal nitrogen molecules to the $v''=2$ state, the mercury atoms becoming $^3P_1$ atoms. Probably the better way to put it is the following: The complex unstable triatomic molecule formed by the union of a $^3P_2$ atom of mercury and a normal molecule of nitrogen can break up either into these original constituent parts or into a $^3P_1$ atom and a vibrating nitrogen molecule having $v''=2$, the energies being practically the same.

The reverse process should also occur. Some $^3P_1$ atoms should be raised to the $^3P_2$ state upon collision with vibrating nitrogen molecules. The concentration of atoms in the $^3P_1$ state is nearly constant regardless of the pressure of the nitrogen. (Collisions negligible in comparison with radiation for the balance in the $^3P_1$ state.) If there be a sufficient concentration of nitrogen molecules with two quanta of vibrational energy, and if this concentration be proportional to the square of the pressure, this process of excitation can account for the increase in the $^3P_2$ concentration at higher pressures.

Let us assume that the $^3P_2$ atoms are removed by the production of molecules of nitrogen having two quanta of vibrational energy and consider the fate of the latter. They may collide with normal nitrogen atoms, with the walls of the tube, with normal mercury atoms, with $^3P_0$ and $^3P_1$ atoms, and with each other. In which of these collisions can they be expected to lose the vibrational energy?

The collisions with normal molecules of nitrogen will be the most frequent. According to the work of Zener,[4] and of Jackson and Mott[5] it is very improbable that such a vibrating molecule will give its energy of excitation to another nitrogen molecule. Such an exchange would still leave a molecule in the $v''=2$ state and be of no significance for our consideration. It is even less probable that two molecules in the $v''=1$ state should be produced at collision. Further, collisions with normal mercury atoms, and both kinds of metastable mercury atoms should be ineffective since there are no other states into which these atoms will be put by the 0.570 or 0.283 volts which the nitrogen molecule can give without large changes of kinetic energy. One has left only the excitation of the $^3P_1$ atom to the $^3P_2$ state and collisions with the walls. The nearly exact agreement of energy is favorable for the former process. Presumably, because of the excited electron of the mercury atom, the excited atoms and vibrating nitrogen molecule will make a temporary triatomic molecule more closely bound than those resulting from the collision of a vibrating molecule with an atom in the ^1S state, or another molecule in the $^1\Sigma$ state. The effectiveness of collisions with the walls is problematical. No theory of such collisions has been developed, so far as I am aware. One might expect that the wall of the tube, on which water molecules are adsorbed, might show a sort of "stickiness" which would favor interchange of energy with the nitrogen molecules.

If we assume that the two processes mentioned are the ones responsible for the removal of the energy of the vibrating nitrogen molecules the equation for the steady state is

$$k_2'[^3P_2]p=[N_2'(2)]\{\Delta_2/p+k_1'[^3P_1]\}. \quad (7)$$

The term on the left gives the rate of formation of vibrating nitrogen molecules. Their concentration is represented by $[N_2'(2)]$. (In pure nitrogen k_2' will equal k_2 of Eq. (3)). The Δ_2/p gives the rate of loss by collision at the walls as modified by diffusion, and the $k_1'[^3P_1]$ term the rate of loss by formation of $^3P_2$ atoms. Thus we get a term $[N_2'(2)]k_1'[^3P_1]$ to be added to the left-hand side of Eq. (3). From (7)

$$[N_2'(2)]k_1'[^3P_1]=\frac{k_1'[^3P_1]k_2'[^3P_2]p}{\Delta_2/p+k_1'[^3P_1]}. \quad (8)$$

As long as $\Delta_2/p \gg k_1'[^3P_1]$ this new term is proportional to $[^3P_2]p^2$. It will appear in the denominator of the proper modification of Eq. (6) with a negative sign and will lead to a minimum for the expression just as a positive p^2 term in the numerator would do. This is fairly involved, but all that it amounts to is that in effect at the higher pressures of nitrogen the $^3P_2$ atoms lost by collision are not all irrevocably lost.

This explanation of the experimental results is, to be sure, somewhat *ad hoc*. Other explanations which have been suggested do not seem even remotely plausible.

[4] C. Zener, Phys. Rev. **37**, 556 (1931).
[5] J. M. Jackson and N. F. Mott, Proc. Roy. Soc. **A137**, 703 (1932).

Excitation by Light Filtered by Bromine Vapor

In the light of the discussion in the preceding section Wood's results obtained when a bromine filter was used are most astonishing (III, p. 473). The bromine filter removes the 4047 and 4358 lines so that these lines and the 5461 line do not appear in the fluorescence at all. The concentration of atoms in the $^3S_1$ state is zero. As with no filter, the absorption of 2537 gives a considerable concentration of $^3P_1$ atoms. With no added gas the further excitation is presumably the result of the absorption of the 3125 and 3131 lines to form $^3D_1$ and $^3D_2$ atoms. By the emission of the 3663 and 3654 lines $^3P_2$ atoms are formed. The process of removal of these atoms by collision at the walls is the same as before. Because of the weakness of all of these lines compared to the 4047, 4358 and 5461 lines the concentration of $^3P_2$ atoms would be expected to be slight. The 3650 line should be exceedingly weak in fluorescence, as is found to be the case.

On the admission of 0.25 mm of nitrogen the intensity of the 3663 line (unresolved pair) is doubled and that of the 3654 line remains unchanged. Since it is principally the emission of these lines which results in the formation of the $^3P_2$ atoms the rate of formation is evidently no more than doubled. At the same pressure, with no bromine filter, the intensity of the 5461 line and proportional rate of formation is quadrupled. The removal of $^3P_2$ atoms by collision must be just as effective in both cases so that we expect less than half the concentration of $^3P_2$ atoms when the bromine filter is used. In spite of that, the intensity of the 3650 line is *increased* to twice its original value instead of being decreased to half of its original value as it is with no filter. Thus, the 3650 line is more than four times as intense as we should expect it to be from the result obtained with no filter.

There seems to be little possibility of doubt that the concentration of atoms in the $^3P_2$ state is markedly less in the presence of 0.25 mm of nitrogen. The observed increase of the intensity of the 3650 line must mean that atoms are put into the $^3D_3$ state by some process other than the absorption of 3650 light by $^3P_2$ atoms.

One possible process is the transfer of atoms from the lower $^3D_1$ and $^3D_2$ states to the slightly higher $^3D_3$ state upon collision. Undoubtedly such transfers can go in both directions, as they do among the ^3P states, but the very low concentration of atoms in the $^3D_3$ state would lead to a preponderance of upward transfers to it over downward transfers away from it. The number of such upward transfers should be proportional to the product of the concentration of the atoms in the $^3D_2$ state and to the pressure (neglecting the less likely transfers from the lower $^3D_1$ state). A rough test of this theory of the enhancement of the intensity of the 3650 line can be obtained as follows. The intensities of the 3654 and 3125 lines are proportional to the concentration of atoms in the $^3D_2$ state. At pressures of nitrogen of 4 and 0.25 mm their intensities relative to the values for zero pressure are 2 and 1, respectively. The concentration of $^3D_2$ atoms must therefore be in a ratio of 2 to 1 at these two pressures. The concentration times pressure products are 2×4 and 1×0.25, respectively, in a ratio of 32 to 1. The ratio of the corresponding intensities of the 3650 line is 30 to 2. Of the intensity of 2 at the lower pressure 0.5 is to be attributed to 3650 light absorbed by $^3P_2$ atoms. The proper ratio is thus 30 to 1.5 or 20 to 1. The agreement with the prediction of 32 to 1 is unimpressive, but not too bad in view of the difficulties of the photometry of the very weak 3650 line and neglect of transfers in the opposite direction.

As Wood pointed out (III, p. 479) the changes of relative intensity of the yellow lines gives evidence for similar transfer of atoms from the $^3D_2$ state to the very close $^1D_2$ state.

Such transfers must also contribute to the enhancement of the 3650 line at higher nitrogen pressures in the experiments without the bromine filter, discussed in the first part of this paper. They could not account for the observed changes in the concentration of atoms in the $^3P_2$ state.

The lifetime of the ^3D atoms is presumably of the order of 10^{-8} sec. It is apparent that the cross section of collisions for such transfers must be large compared to ordinary kinetic theory cross sections in order that an appreciable effect should appear at pressures as low as 2 to 4 millimeters of nitrogen.

Analysis of a New Band System of the C_2 Molecule

J. G. Fox and G. Herzberg
Department of Physics, University of Saskatchewan, Saskatoon, Saskatchewan, Canada

(Received July 7, 1937)

The 0–3, 0–4, 0–5 and 0–6 bands of a new band system of the C_2 molecule are analyzed. The lower state, $^3\Pi$, is the same as the lower state of the Swan bands (in all probability the ground state). The upper state is a new $^3\Pi_g$ state. The rotational and vibrational constants of the upper and lower state are given in Table VII. While the constants for the upper state are entirely new those for the lower state (ground state) are considerably improved over those at present in the literature. The triplet splitting and staggering in the new bands is much larger than in the Swan system. In the $^3\Pi_0-{}^3\Pi_0$ component a reversal of the staggering is observed. The electron configuration of the new state is briefly discussed. Finally a number of other bands, very probably due to C_2, but not yet analyzed, are given.

A. Introduction

In recent years the spectrum and the structure of the C_2 molecule have received little attention. However, a more complete knowledge of this molecule would be of considerable interest both because of its chemical and its astrophysical importance.

We have therefore thought it worth while to re-investigate the spectrum of the C_2 molecule in order to find, if possible, new information about the structure of this molecule.

B. Experimental

A weakly condensed discharge was passed through an ordinary discharge tube (capillary of 5 mm diameter and 8 cm length) which was filled with helium of 2–5 cm pressure and was in connection with a side tube containing pure C_6H_6. In some experiments the tube was used without He while the C_6H_6 was streaming through rapidly. Solid carbon was of course quickly deposited on the walls of the discharge tube, so that for longer exposures it had to be cleaned several times.

The spectra were taken partly with a Hilger E3 and partly with a smaller spectrograph of higher light power which could be used both with quartz and with glass prism and lenses.

Under the best conditions the spectrum consisted only of the known bands of C_2 and CH and some unidentified bands but showed no trace of common impurities such as CN and CO. The absence of the strong violet CN bands, which, as is well known, occur so easily as impurities, was considered as a satisfactory proof that a pure spectrum, due solely to C_2 and CH, had been obtained and that the unidentified bands were due to C_2 or CH.

Among the new bands were two at 2855A and 2987A which were shaded to the red but did not show pronounced heads. These two bands were found to be identical with two bands previously obtained by one of us (H) with high dispersion (2.7A/mm, second order of a 3 m grating) under conditions which did not allow any definite conclusions about the carrier of these bands. They had been obtained, for instance, in an uncondensed discharge through argon containing a slight amount of CO_2. The new spectrograms seemed to show that they were due to C_2 (the fine structure being much too narrow for CH). This was unambiguously confirmed by the fine structure analysis which was consequently carried out with the older grating plates. In the course of the measurements two further bands having the same fine structure and therefore belonging to the same system were found on the grating plates. They were however badly overlapped by other bands and could only partly be measured.

C. Rotational Analysis of the New Bands

In Fig. 1 a spectrogram of part of the band at 2987A is reproduced. As can be seen by inspection six branches are present. It will be noticed that in every alternate group of six lines the spacing seems to be somewhat different from that in the intermediate groups.

If a quadratic formula, $\nu=a+bm+cm^2$, is roughly fitted to the component of lowest fre-

quency of each group and the deviations from this formula are plotted it is immediately seen, as shown in Fig. 2, that in each of the six branches there is the "*staggering*" characteristic of $\Pi-\Pi$ transitions of molecules with equal nuclei of spin 0. Conversely this staggering forms an unambiguous proof that the emitter of the bands is a homonuclear molecule with nuclear spin $=0$, such as C_2 and O_2. Of these two, O_2 is excluded by the conditions of excitation as well as by the fine structure analysis (cf. below).

Since the magnitude of the staggering is different for the different branches the above mentioned alternation in the spacing of successive groups results.

The presence of *six branches*, each showing staggering, is only compatible with the assumption that the electron transition responsible for these bands is $^3\Pi-{}^3\Pi$, that is, the same type as for the well-known Swan bands of the C_2 molecule.[1] Indeed, as we shall show, the two systems have the lower electronic state, $^3\Pi$, in common.

In Tables I, II, III and IV the wave numbers of the lines of the four new bands are given. For the reasons given above the bands at 3129 and 3283A are only very incompletely measured whereas the bands at 2855 and 2987A have been measured down to fairly low J values. For still lower J values we have not been able to assign the lines unambiguously.

The *relative numbering* of the lines was found by a *perturbation* (splitting into two components) occurring in the center branches R_2 and P_2 of the two bands (see Fig. 2). The *absolute numbering* was found by the requirement that

$$\Delta_2 F_i'(K) = R(K) - P(K)$$

and

$$\Delta_2 F_i''(K) = R(K-1) - P(K+1)$$

plotted as a function of K should go through $-\frac{1}{2}$, at least for the center component.

Table V gives the $\Delta_2 F_i'$ values of the two bands 0–3 and 0–4. They show as good an agreement as can be expected, thus giving a further check on

[1] The possibility of a $^1\Pi-{}^3\Pi$ transition, which might be considered since the triplet splitting in the upper state is unmeasurably small (see below), is ruled out because a perturbation in the upper state appears only in the P_2 and R_2 branches. (Cf. below.)

TABLE I. *Wave numbers of the lines in the (0–3) band.* $\nu_0 = 35022.14$.

J	$^3\Pi_0-{}^3\Pi_0$		J	$^3\Pi_1-{}^3\Pi_1$		J	$^3\Pi_2-{}^3\Pi_2$	
	$R_3(J)$	$P_3(J)$		$R_2(J)$	$P_2(J)$		$R_1(J)$	$P_1(J)$
			5		34998.51			
			6		990.84	7		34998.51
			7		983.45	8	35025.23	990.01
7		34969.88	8		974.40	9	020.85	980.78
8	35005.25	960.21	9		965.48	10	015.74	970.92
9	000.68	951.26	10		954.56	11		960.21
10	34994.19	939.92	11	34998.51	944.33	12	003.11	948.84
11	988.04	929.06	12	990.84	931.91	13	34995.62	936.74
12	979.83	916.20	13	983.45	919.75	14	987.65	923.98
13	971.90	903.66	14	974.40	905.98	15	978.58	910.23
14	962.15	889.14	15	965.48	892.50	16	969.01	896.06
15	952.63	874.87	16	954.56	876.88	17	958.53	880.79
16	941.34	858.88	17	944.33	861.90	18	947.26	865.03
17	929.93	843.07	18	931.91	844.87	19	935.26	848.28
18	917.11	825.61	19	920.31 919.75	828.35	20	922.74	831.04
19	904.13	807.89	20	905.98	809.62	21	908.98	812.67
20	889.96	788.94	21	892.50	791.66 791.06	22	894.95	793.91
21	875.30	769.55	22	876.88	771.08	23	879.63	773.88
22	859.53	749.04	23	861.90	751.55	24	864.12	753.75
23	843.07	728.17	24	844.42	729.45	25	847.14	732.05
24	825.61	706.17	25	827.79	708.42	26	830.08	710.50
25	807.89	683.75	26	808.96	684.65	27	811.43	687.27
26	788.94	660.04	27	791.06	662.17	28	792.86	664.06
27	769.24	635.74	28	770.48	637.00	29	772.73	639.27
28	749.04	610.83	29	750.84	612.74	30	752.71	614.61
29	727.69	585.10	30	728.67	586.09	31	730.80	588.15
30	705.71	558.53	31	707.63	560.48	32	709.23	562.08
31	682.91	531.09	32	683.75	531.93	33	685.80	534.00
32	659.44	503.16	33	661.22	505.01	34	662.87	506.50
33	634.92	474.09	34	635.74	474.86	35	637.72	476.85
34	609.96	444.52	35	611.59	446.22	36	613.15	447.63
35	583.72		36	586.09		37	586.63	
36	557.38		37	558.96		38	560.48	
37	529.44		38	530.22		39	531.93	
38	501.63		39	503.16		40	504.49	
			40			41	474.09	
			41	444.52		42	445.43	

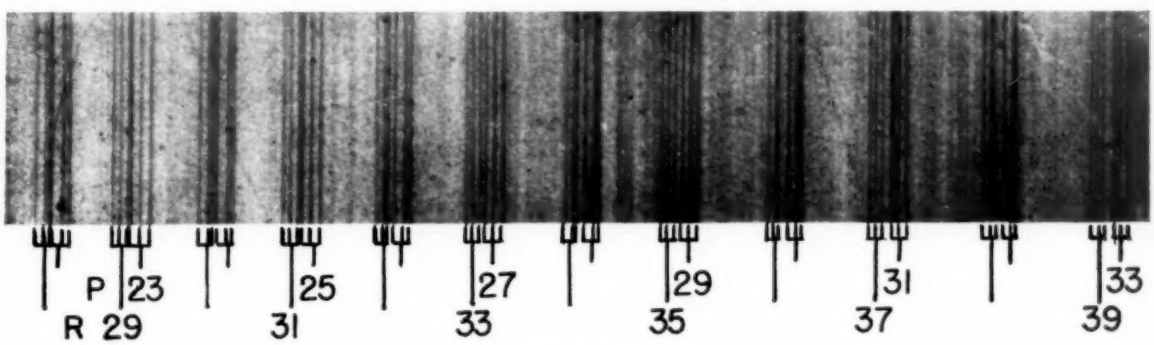

FIG. 1. Part of 0—4 band.

the analysis. As can be seen there is no systematic deviation between the Δ_2F_1', Δ_2F_2' and Δ_2F_3' values, indicating that the triplet splitting in the upper $^3\Pi$ state is very small for $K>7$.

The Δ_2F' values of the two incompletely measured bands (Tables III and IV), as far as they go, also coincide with the values in Table V. Therefore the upper state in all the bands is the same. Since no other bands have been found it must be the $v'=0$ state of the upper electronic level. Thus the four bands form a v'' *progression*, the v'' values being 3, 4, 5 and 6 as will be shown below.

The *rotational constants B and D* of the upper and lower states were determined according to the method given by Budó[2] for $^3\Pi$ states, i.e., from the average of the $\Delta_2F_i(J)$ values for $i=1$, 2, 3. The values obtained are given in Table VI. The accuracy of the B values for $v'=0$ and $v''=3$ and 4 is probably within 2 or 3 units of the last decimal place given, whereas for $v''=5$ and 6 an error of ± 0.0010 does not seem impossible due to the incompleteness of the data. Also for these latter an average D'' value from the other bands was adopted.

In Table VI are also given the B and D values of the $v''=0$ and 1 states of the lower $^3\Pi$ state of the Swan system as given by Budó.[2] It is at once apparent that the B_0'' and B_1'' values of the Swan system and the B_3'', B_4'', B_5'' and B_6'' values of the new system form a single series. They can all be represented extremely well by the formula

$$B_v''=1.6320-0.01659(v''+\tfrac{1}{2})$$

with the residuals given in Table VI in the

TABLE II. *Wave numbers of the lines in the (0–4) band.* $\nu_0=33474.07$.

J	$^3\Pi_0-{}^3\Pi_0$		J	$^3\Pi_1-{}^3\Pi_1$		J	$^3\Pi_2-{}^3\Pi_2$	
	$R_3(J)$	$P_3(J)$		$R_2(J)$	$P_2(J)$		$R_1(J)$	$P_1(J)$
						3		33476.67
			3	33479.67		4		471.30
			4	478.35	33457.28	5	33487.18	465.07
4		33442.67	5	476.67	451.07	6	484.93	458.54
5		437.62	6	473.99	443.99	7	481.87	451.07
6		429.90	7	471.30	436.15	8	478.35	442.67
7	33463.38	423.04	8	467.33	427.34	9	473.99	434.01
8	458.55	413.80	9	463.38	418.71	10	469.20	424.43
9	454.47	404.89	10	457.91	408.33	11	463.38	413.80
10	448.34	393.99	11	452.51	398.37	12	457.28	403.09
11	442.67	383.61	12	445.36	386.45	13	450.17	391.24
12	434.83	371.15	13	438.54	374.88	14	442.67	379.00
13	427.34	359.05	14	429.90	361.55	15	434.01	365.74
14	418.17	345.15	15	421.48	348.48	16	425.05	352.05
15	409.08	331.35	16	411.25	333.54	17	414.97	337.20
16	398.37	316.00	17	401.44	319.06	18	404.56	322.16
17	387.76	300.69	18	389.64	302.55	19	393.00	305.91
18	375.42	283.81	19	378.61 377.98	286.61	20	381.18	289.44
19	363.18	266.95	20	364.87	268.58	21	367.94	271.58
20	349.61	248.51	21	352.05	251.40 250.79	22	354.65	253.67
21	335.70	229.98	22	337.20	231.49	23	340.00	234.34
22	320.64	210.34	23	323.00	212.74	24	325.34	215.00
23	305.15	190.18	24	306.49	191.51	25	309.09	194.08
24	288.63	169.05	25	290.80	171.29	26	292.98	173.40
25	271.58	147.29	26	272.76	148.52	27	275.19	150.99
26	253.67	124.81	27	255.68	126.91	28	257.66	128.85
27	234.89	101.43	28	235.95	102.51	29	238.25	104.85
28	215.54	077.48	29	217.52	079.50	30	219.36	081.30
29	195.17	052.60	30	196.22	053.54	31	198.39	055.71
30	174.49	027.26	31	176.33	029.12	32	177.99	030.77
31	152.53	33000.75	32	153.49	001.62	33	155.46	003.65
32	130.31	32973.99	33	132.08	32975.80	34	133.71	32977.33
33	106.84	945.85	34	107.59	946.68	35	109.55	948.59
34	083.23	917.70	35	084.92	919.42	36	086.38	920.94
35	058.07	888.02	36	058.78	888.78	37	060.61	890.71
36	033.03	858.53	37	034.66	860.16	38	036.03	861.57
37	006.31	827.31	38	006.93	827.94	39	008.71	829.64
38	32979.78	796.25	39	32981.32	797.86	40	32982.74	799.19
39	951.44		40	952.06		41	953.78	
40	923.71		41	925.17		42	926.47	
41	893.60		42	894.23		43	895.86	
42	864.47		43	865.94		44	867.52	
43	832.84		44	833.36		45	834.86	
44	802.18		45	803.56		46	805.54	

TABLE III. *Wave numbers of the lines in the (0–5) band.* $\nu_0=31949.59$.

J	$^3\Pi_0-{}^3\Pi_0$		J	$^3\Pi_1-{}^3\Pi_1$		J	$^3\Pi_2-{}^3\Pi_2$	
	$R_3(J)$	$P_3(J)$		$R_2(J)$	$P_2(J)$		$R_1(J)$	$P_1(J)$
23		31675.70	24		31677.00	25		31679.66
24		655.58	25		657.83	26		660.03
25		634.50	26		635.65	27		638.20
26		613.07	27		615.26	28		617.28
27		590.55	28		591.59	29		593.91
28		567.73	29		569.79	30		571.65
29	31686.26	543.60	30	31687.28	544.68	31	31689.47	546.69
30	666.77	519.50	31	668.68	521.46	32	670.42	523.21
31	645.71	493.83	32	646.59	494.71	33	648.68	496.81
32	624.86	468.46	33	626.73	470.31	34	628.28	471.94
33	602.21	441.24	34	603.08	442.08	35	604.98	443.98
34	580.02	414.56	35	581.83	416.33	36	583.38	417.83
35	555.83	385.82	36	556.58	386.57	37	558.45	388.44
36	532.39	357.79	37	534.06	359.43	38	535.48	360.99
37	506.70	327.52	38	507.32	328.22	39	509.10	329.93
38	482.35	298.23	39	483.38	299.81	40	484.87	301.24
39	455.07		40	455.76		41	457.33	
40	429.83		41	430.57		42	431.84	
41	400.76		42	401.69		43	402.65	
42	374.33		43	375.10		44	376.26	

TABLE IV. *Wave numbers of the lines in the (0–6) band.* $\nu_0=30448.19$.

J	$^3\Pi_0-{}^3\Pi_0$		J	$^3\Pi_1-{}^3\Pi_1$		J	$^3\Pi_2-{}^3\Pi_2$	
	$R_3(J)$	$P_3(J)$		$R_2(J)$	$P_2(J)$		$R_1(J)$	$P_1(J)$
18		30270.44	19		30273.42	20		30276.23
19		254.94	20		256.71	21		259.76
20		237.99	21		240.93 240.25	22		243.10
21		220.99	22		222.56	23		225.41
22		202.81	23		205.20	24		207.49
23	30298.74	184.40	24	30300.65	185.73	25	30302.85	188.38
24	284.39	165.07	25	286.60	167.00	26	288.12	169.09
25	268.58	144.53	26	270.44	146.12	27	272.88	148.61
26	252.80	124.06	27	254.94	126.08	28	256.71	127.96
27	235.68	102.30	28	237.27	103.91	29	239.66	106.19
28	218.53	080.49	29	220.47	082.67	30	222.26	084.14
29	200.13	057.22	30	201.63	058.90	31	203.70	061.10
30	181.43	034.16	31	183.22	036.43	32	184.73	037.56
31			32	162.97	011.08	33	164.85	013.19
32	141.41		33	143.11		34	144.92	
33	120.88		34	121.46		35	123.52	
34	099.90		35	100.15		36	102.30	

[2] A. Budó, Zeits. f. Physik **98**, 437 (1936).

TABLE V. *Combination differences of the upper state.* $\Delta_2F_i'(K)=R_i(K)-P_i(K)$.

	0–3 BAND			0–4 BAND		
K	$\Delta_2F_1'(K)$	$\Delta_2F_2'(K)$	$\Delta_2F_3'(K)$	$\Delta_2F_1'(K)$	$\Delta_2F_2'(K)$	$\Delta_2F_3'(K)$
4				22.11	21.07	
5				26.39	25.60	
6				30.80	30.00	
7	35.22			35.68	35.15	
8	40.07			39.98	39.99	40.34
9	44.82		45.04	44.76	44.67	44.75
10			49.42	49.59	49.59	49.58
11	54.27	54.18	54.27	54.19	54.15	54.35
12	58.88	58.93	58.98	58.93	58.91	59.06
13	63.67	63.70	63.63	63.66	63.66	63.69
14	68.35	68.42	68.24	68.27	68.35	68.28
15	72.95	72.98	73.01	73.00	73.01	73.02
16	77.74	77.68	77.76	77.77	77.71	77.74
17	82.23	82.43	81.46	82.40	82.38	82.37
18	86.98	87.04	86.86	87.09	87.09	87.07
19	91.70	91.40 91.96	91.50	91.75	91.37 92.00	91.60
20	96.31	96.36	96.24	96.36	96.29	96.23
21	101.04	100.84 101.44	101.02	100.99	100.65 101.26	101.10
22	105.75	105.80	105.75	105.67	105.72	105.72
23	110.37	110.35	110.49	110.34	110.26	110.30
24	115.09	114.97	114.90	115.01	114.98	114.97
25	119.58	119.37	119.44	119.58	119.52	119.58
26	124.16	124.31	124.14	124.20	124.23	124.29
27	128.80	128.89	128.90	128.81	128.77	128.86
28	133.46	133.48	133.50	133.40	133.44	133.46
29	138.10	138.10	138.21	138.06	138.02	138.06
30	142.65	142.58	142.59	142.68	142.68	142.57
31	147.15	147.15	147.18	147.22	147.21	147.23
32	151.80	151.82	151.82	151.81	151.87	151.77
33	156.37	156.21	156.28	156.38	156.28	156.32
34	160.87	160.88	160.83	160.95	160.91	161.00
35	165.52	165.37	165.44	165.44	165.51	165.53
36				169.90	170.00	170.05
37				174.46	174.49	174.51
38				179.07	179.00	179.01
39				183.55	183.46	183.53

TABLE VI. *Rotational constants of the upper and lower state.*

STATE	v	B (cm^{-1})	OBS.-CALC.	D (cm^{-1})	
lower $^3\Pi$	0	1.6239	+0.0002	$6.4\cdot10^{-6}$	from Budó[2]
	1	1.6068	−0.0003	$6.6\cdot10^{-6}$	
	2				
	3	1.5742	+0.0003	$6.8\cdot10^{-6}$	this paper
	4	1.5572	−0.0001	$6.6\cdot10^{-6}$	
	5	1.5408	+0.0005	$(6.6\cdot10^{-6})$	
	6	1.5233	−0.0009	$(6.6\cdot10^{-6})$	
upper $^3\Pi$	0	1.1804		$6.05\cdot10^{-6}$	

column obs.-calc. Since these residuals are within the accuracy of the determinations it follows conclusively that the *lower electronic state of these two systems is the same* and also that the vibrational numbering is correct. The same conclusion is obtained from the vibrational analysis (cf. below). Thus it is definitely proven that the *emitter of the new bands is the C_2 molecule.*

In the upper part of Table VII the *rotational constants* B_e, B_0, α, D and the *moments of inertia* I_e, I_0 and the *nuclear distances* r_e, r_0 for the upper and lower electronic states of the new bands are given. The I and r values have been calculated using Bearden's[3] values for e, h and N. We consider the values of the constants of the ground state to be improved over those at present in the literature while the constants for the upper state are of course entirely new.

In the new bands, as is usual in $^3\Pi-{}^3\Pi$ transitions,[4] the *triplet splitting* between the lines of equal K increases rapidly with decreasing K (see Fig. 2). It is about 4 to 5 times larger than in corresponding triplets of the 0–0 band of the Swan system, as can be seen from the data of Johnson[5] and Shea.[6] The line splitting is the difference (or possibly sum) of the term splitting in the upper and lower state. The individual term splitting can therefore not be determined accurately. But an approximate value for the term splitting can be obtained from the difference between Δ_2F_1, Δ_2F_2, Δ_2F_3 for equal K. The differences between the Δ_2F_i'' values of the 0–3 and 0–4 bands are are about equal to those for the 0–0 and 0–1 Swan bands. This is to be expected if, as shown above, the lower electronic state for the two systems is the same, since the multiplet splitting does not depend appreciably on the vibrational quantum number. The Δ_2F_i' values for equal K do not show any consistent difference (cf. Table V), indicating that the triplet splitting in the upper $^3\Pi$ state of the new bands is much smaller than in the ground state, whereas in the upper state of the Swan bands it is nearly as large as in the ground state. This explains why the triplet splitting in the new bands is so much larger than in the Swan bands.

The *staggering* (cf. Fig. 2) is also considerably larger for the new bands than for the Swan bands (about 3 to 5 times in the center branches). Again

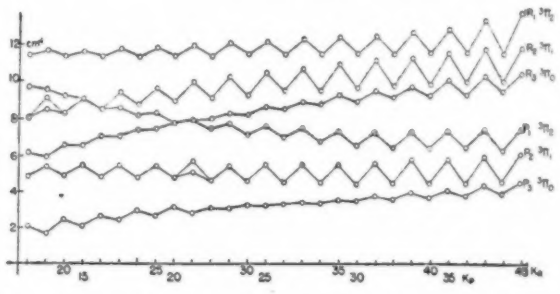

FIG. 2. Staggering and triplet splitting in the branches of the 0–4 band.

[3] J. A. Bearden, Phys. Rev. **47**, 883 (1935).

[4] W. Jevons, *Report on Band Spectra of Diatomic Molecules.*

[5] R. C. Johnson, Phil. Trans. Roy. Soc. **226**, 157, 1926/27.

[6] J. D. Shea, Phys. Rev. **30**, 825 (1927).

TABLE VII. *Constants of the C_2 molecule.*

	LOWER $^3\Pi$ (GROUND) STATE	UPPER $^3\Pi$ STATE
B_e	1.6320 cm^{-1}	—
B_0	1.6237 "	1.1804 cm^{-1}
α	0.01659 "	—
D	$6.6 \cdot 10^{-6}$ "	$6.05 \cdot 10^{-6}$ "
I_e	$17.104 \cdot 10^{-40}$ g cm^2	—
I_0	$17.192 \cdot 10^{-40}$ "	$23.648 \cdot 10^{-40}$ g cm^2
r_e	1.3101A	—
r_0	1.3135A	1.5405A
Excitation energy	0	39806.70 cm^{-1}
ω_e	1641.70 cm^{-1}	—
ω_0	1629.99 "	1047 "
$\omega_e x_e = \omega_0 x_0$	11.71 "	

the staggering in the branches is equal to the difference (or possibly sum) of the Λ doubling in the upper and lower states. Therefore the latter cannot accurately be determined. But the fact that the $\Delta_2 F''$ values stagger appreciably whereas for the $\Delta_2 F'$ values the staggering is just barely noticeable shows that the Λ doubling in the upper state of the new bands is much smaller than in the ground state. Thus most of the large staggering in the branches is due to the Λ doubling of the lower state. However, for the upper state of the Swan bands the Λ doubling is not very different from that in the ground state so that the staggering in the Swan bands is small.

As can be seen from Fig. 2, for large K values the staggering tends to be about the same for the three components. This is to be expected since both states are close to Hund's case (*b*) for large K values. However for small K values the staggering is largest for the $^3\Pi_0 - {}^3\Pi_0$ component, smaller for $^3\Pi_1 - {}^3\Pi_1$, and very small for $^3\Pi_2 - {}^3\Pi_2$. In fact this is how the correlation of the branches to $^3\Pi_0$, $^3\Pi_1$, $^3\Pi_2$ was found (cf. Mulliken[7]).

Figure 2 shows further that for about $K' = 25$ a *reversal of the staggering* in the P_3 and R_3 branches ($^3\Pi_0 - {}^3\Pi_0$) occurs: for larger K values all the three lines in a group of equal K stagger in the same way whereas for smaller K the P_3 and R_3 lines stagger in the opposite direction to the corresponding lines of the P_1, P_2, R_1, R_2 branches. Since the Λ doubling in the upper state is small compared to that in the lower it follows that there is a reversal in the Λ doubling of the $^3\Pi_0$ component of the ground state. Such a reversal has been previously found by Funke[7a] for the $^3\Pi_0$ state of the NH molecule. Since there is no such reversal in the Swan bands one must conclude that for them both in the upper and lower state the Λ doubling reverses.

Finally it may be noted that, while for the Swan bands the lines with even K are shifted to higher frequencies, for the new bands the lines with odd K are shifted in that direction (except for the P_3, R_3 branches for $K < 25$).

D. VIBRATIONAL ANALYSIS

The *zero lines* ν_0 of the bands are given in Table VIII. They were obtained in the following way: according to Budó's formulae one can easily see that $R_1(J)+R_2(J)+R_3(J)+P_1(J)+P_2(J)+P_3(J) = 6\nu_0 + 6B' + 6(B'-B'')\ J(J+1)$

TABLE VIII. *Zero lines ν_0 and vibrational quanta $\Delta G''$.*

$v'-v''$	ν_0	$\Delta G''$	OBS.–CALC. (Johnson's formula)
0−3	35022.14		
		1548.07	−0.12
0−4	33474.07		
		1524.48	−0.37
0−5	31949.59		
		1501.40	−0.11
0−6	30448.19		

apart from very small terms with higher powers of $J(J+1)$. Therefore, by plotting the sum $\Sigma R_i(J)+\Sigma P_i(J)$ against $J(J+1)$ very nearly a straight line is obtained whose intercept with the ordinate axis gives $6\nu_0+6B'$ and therewith ν_0.

The third column of Table VIII contains the *vibrational quanta* $\Delta G''$ of the lower state derived from the observed ν_0 values. In the next column are given the deviations of these observed $\Delta G''$ values from those following from Johnson's formula for the lower state of the Swan system:

$$\nu = 19373.87 + 1773.42\ v' - 19.35\ v'^2 - (1629.88\ v'' - 11.67\ v''^2).$$

The deviations are of the same order as those of Johnson's own $\Delta G''$ values derived from the Swan bands. This is another conclusive proof that the lower state of the new bands is identical with that of the Swan bands, and also of the correctness of the vibrational numbering.

The slight systematic deviations from Johnson's formula for the higher v'' values available here can be used to improve the formula for the vibrational quanta of the lower state. We obtain

[7] R. S. Mulliken, Rev. Mod. Phys. **3**, 89 (1931).
[7a] G. W. Funke, Zeits. f. Physik **96**, 787 (1935).

the following equation for the new bands.

$$\nu = 39806.77 - (1629.99\, v'' - 11.71\, v''^2).$$

This formula represents our zero lines within less than $\pm 0.10\ \text{cm}^{-1}$. The new vibrational term of the ground state $1629.99\, v'' - 11.71\, v''^2$, if introduced into the formula for the Swan system, gives just as good a representation of the Swan bands as the old formula.

The improved *vibrational constants* of the ground state of the C_2 molecule are given in the lower part of Table VII. An approximate value for the vibrational frequency ω' of the upper state is also given. It was obtained from the rotational constant D' and Kratzer's formula $D = 4B^3/\omega^2$.

The absence of the 0–0, 0–1 and 0–2 bands of the new system is easily accounted for by the Franck-Condon principle, since the nuclear distance in the upper state is so much larger than in the lower. As can be seen by plotting the potential curves, the 0–5 or 0–6 band should be the most intense of the progression in agreement with visual estimates. Bands with higher v'' would be overlapped by the much stronger Deslandres and Swan systems and have not been observed.

E. Electron Configurations

According to Mulliken the lower state of the Swan bands is $^3\Pi_u$ the upper state $^3\Pi_g$. The electron configurations are

$$(K)(K)\sigma_g^2(2s)\sigma_u^2(2s)\pi_u^3(2p)\sigma_g(2p)\ ^3\Pi_u,$$
$$(K)(K)\sigma_g^2(2s)\sigma_u(2s)\pi_u^3(2p)\sigma_g^2(2p)\ ^3\Pi_g.$$

The upper state of the new bands must also be $^3\Pi_g$. The first electron configuration, next to the above, that gives rise to a $^3\Pi_g$ state is

$$(K)(K)\sigma_g^2(2s)\sigma_u^2(2s)\pi_u^2(2p)\sigma_g(2p)\pi_g(2p).$$

Table IX. *Other C_2 bands. R means "shaded to the red;" V means "shaded to the violet;" N means "headless band."*

	λ(A)	ν(cm⁻¹)		λ(A)	ν(cm⁻¹)
R	4996.74*	20007.5	R	3599.2	27776
R	4910.99*	20356.8	R	3560.7	28076
R	4836.13*	20671.9	R	3506.6	28510
R	4770.13*	20958.0	R	3434.0	29112
R	4496.9	22231	R	3384.4	29539
R	4339.6	23037	V	2421.5	41284
R	4324.4	23118	N	2313.7	43208
R	4147.8	24102	V	2218.5	45061
R	3688.7	27102	V	2216.6	45100
R	3670.8	27234	V	2143.0	46649
R	3618.0	27632			

In fact four different $^3\Pi_g$ terms arise from this configuration. The orbital $\pi_g(2p)$ is well known to be *strongly anti-bonding*. It is therefore significant and a strong argument in favor of our assignment that the upper state of the new bands has a considerably larger nuclear distance r_0 and a much smaller vibrational frequency ω_0 than the ground state (or the upper state of the Swan bands).

F. Other C_2 Bands

In addition to the new bands, discussed in detail above, a number of further bands have been found under the conditions of excitation given in section *A* which in all likelihood are also due to the C_2 molecule. In Table IX the wavelengths and wave numbers of these bands are collected together. Except for the band marked by *N*, band heads have been measured. For the headless band marked by *N* the intensity minimum of the center was measured. The bands marked by an asterisk have been measured on grating plates whereas the others have only been measured with small dispersion. The former have also been recorded by Johnson. Possibly they form the tail bands 13–12, 12–11, 11–10 and 10–9 of the $\Delta v = +1$ sequence of the Swan bands. Similarly the bands 3618.0 and 3599.2A very probably form the tail bands 6–5 and 5–4 of the Deslandres system. Thus far we have not been able to obtain a satisfactory vibrational analysis of the other bands of Table IX.

The strong headless band at 2313.7A has been observed by a number of investigators, but its fine structure has not yet been satisfactorily analyzed. According to Mulliken[8] it is a $^1\Sigma - {}^1\Sigma$ transition of the C_2 molecule while Hori[9] claims it to be due to a C_3 molecule. An incomplete fine structure analysis by L. Herzberg confirms Mulliken's interpretation. It is possible that the weak band at 2421.5A is the 0–1 band of the same system.

It will be shown in a later paper by one of us that the so-called high pressure bands of carbon[10] belong to the Swan system and do not have a new electronic state as the upper level.

[8] R. S. Mulliken, Zeits. f. Electrochem. **36**, 603 (1930).
[9] T. Hori, Zeits. f. Physik **83**, 495 (1934).
[10] Cf. e.g. R. C. Johnson and R. K. Asundi, Proc. Roy. Soc. **124**, 668 (1929).

An Extension of the Analysis of the Spectrum of Neutral Samarium, Sm I

WALTER ALBERTSON*
George Eastman Research Laboratory of Physics, Massachusetts Institute of Technology,† Cambridge, Massachusetts
(Received July 9, 1937)

The term $4f^6(^7F)6s7s\ ^9F$ has been found, which yields 5.6 volts as the approximate ionizing potential of Sm I. The triad of terms $4f^6(^7F)6s6p\ ^9GFD^0$ have been completely identified. Several new energy states have been located, which account for all previously unidentified low temperature lines. Experimental proof of the existence of more than 910 energy states which are necessary to account for existing data is pointed out. The extreme difficulty of analyzing the remaining data is discussed.

INTRODUCTION

A PARTIAL analysis which included most of the low temperature lines of the spectrum of Sm I has been published by the writer.[1] These lines result from transitions from high odd energy states to $4f^6 6s^2\ ^7F$, the normal state of the atom. An extension of the Sm I analysis and a discussion of the problems involved in that part of the analysis which remains to be done is presented in this paper.

IDENTIFIED TERMS OF SM I

The main electron transition of Sm I is $4f^6 6s6p \rightarrow 4f^6 6s^2$. The basic terms from these configurations have now been identified and are presented in Table I. a^7F is from $4f^6 6s^2$ and the triad of terms z^9GFD^0 is from $4f^6 6s6p$. The combinations between these sets of terms are presented in Table II. In Table I, column 1 gives the energy state; column 2 the symbol used to identify the state in the earlier paper;[1] column 3 the energy in cm^{-1}. In Table II, column 1 gives the wave-length; column 2 the arc emission, furnace emission (with temperature class in Roman numerals), and furnace absorption intensities; column 3 the energy in cm^{-1}; column 4 the two states involved in the transition.

The term e^9F from $4f^6(^7F)6s7s$ has been located. This term is the second member of the series from $4f^6 6sns$, $4f^6(6s)^2\ ^7F$ being the first. From these two terms one may calculate 5.4 volts as the energy of $4f^6 6s$ of Sm II. The energies and combinations of e^9F are given in Tables I and II, respectively. The identifications of the z^9GFD^0 states were made after a study of the intervals involved, and of the intensities of their combinations with a^7F and e^9F. Only for $z^9G_1^0$ and z^9G_0 are the assignments in doubt. Strictly speaking, the assignments have no meaning because of the intermediate type of coupling and configuration interaction. The assignment given here is to be interpreted as meaning that the state seems to contain more of the quantum numbers assigned to it than it does any other set of quantum numbers. It is useful to know which single set of quantum numbers the state seems most nearly to correspond to. A few more new states are given at the end of Table I with their combinations at the end of Table II.

COMPLEXITY OF THE ANALYSIS OF SM I

The temperature classification of Sm I as published by King[2] contains 2710 lines between 8706A and 2911A. Of this number 422 are of class I and II, while the remaining are of class III, IV, and V. All of the class I lines, nearly all the class II lines, and for wave-lengths less than 4000A many lines, of all temperature classes, have been classified as transitions between upper states and a^7F. These lines are strongly absorbed,[3] even those which appear faint in emission, hence their low level origin is clearly indicated. At the shorter wave-lengths the lines show much more readily in absorption than in emission, in fact, Paul[3] has measured 540 absorption lines between 3070A and 2500A that have not been observed in emission at all. Several class II lines in the deep red are not absorbed; these lines are due to $z^9G^0 - e^9F$.

* National Research Fellow in Physics.
† This work was conducted at the Mount Wilson Observatory of the Carnegie Institution of Washington, Pasadena, and the Department of Physics, University of California, as well as at the above named institution.
[1] W. E. Albertson, Phys. Rev. **47**, 370 (1935).
[2] A. S. King, Astrophys. J. **82**, 140 (1935).
[3] F. W. Paul, Phys. Rev. **49**, 156 (1936).

As one goes to shorter wave-lengths the temperature class of the absorption lines becomes progressively higher and higher, due to the difficulty of exciting the high states in the furnace, so that it is almost certain that all the lines below 4000A, regardless of temperature class, originate from transitions to a^7F. Many of these lines have not as yet been classified. This is to be expected since, for many of the states, only one of the three possible combinations of the state with a^7F will appear. Hence, for wave-lengths less than 4000A every unclassified line represents the only recorded combination between a high state and one of the seven low states. It is, of course, impossible to determine which of the seven low states the combination is with and thus to fix the energy of the upper state. The latter will be within ± 2000 cm^{-1} of the value obtained by adding 2000 cm^{-1} to the wave number of the line. From the above, it follows that at least 910 high energy states are represented by the observed absorption data for Sm I. Here is an indication of the true complexity of the energy system of a rare earth element.

Nearly 1700 lines between 8700A and 4700A have not as yet been classified. Although many of the lines are very intense in emission, not a single one appears with any appreciable intensity in absorption. Included among these lines are eleven intense class II lines, which either do not appear in absorption or only faintly so. This is contrasted with the intense absorption of all class II lines that involve the ground state. A few of the numerous intense class III lines are also faintly absorbed. It is obvious that these lines must originate in transitions from high states to metastable states.

The recent analysis of Sm II by the writer[4] shows that terms from the configuration $4f^6(^7F)5d$ are about 10,000 cm^{-1} above the ground state. One would expect the corresponding terms from $4f^6(^7F)6s5d$ in Sm I to be present at approximately the same energy region. So far as comparisons can be made, there is a fairly close agreement between related energy structures in Sm I and Eu I and also between Sm II and Eu II. The recent extension of the analysis of Eu I by Russell and King[5] also indicates that the $4f^6(^7F)6s5d$ terms of Sm I should be found at exactly the same energy region as indicated by the analysis of Sm II. The lines from the transition $4f^75d6s - 4f^75d6p$ in Eu I fall in the wave-length region in question for Sm I. Their character is similar to the Sm I lines, consisting chiefly of intense class III lines and a few intense class II lines, the only difference being that there are many more Sm I lines than Eu I lines. This is to be expected on comparing the relative complexity of the term systems involved. Nearly all of the previously unclassified intense Eu I lines were found to belong to this transition.

There is little doubt, in the writer's opinion, that most of the 1700 unclassified lines between

[4] W. E. Albertson, Astrophys. J. **84**, 26 (1936).
[5] H. N. Russell and A. S. King, unpublished material.

TABLE I. *Certain energy states of Sm I.*

STATE	SYMBOL	ENERGY
a^2F_0	1	0.00
1	2	292.58
2	3	811.92
3	4	1,489.55
4	5	2,273.09
5	6	3,125.46
6	7	4,020.66
$z^9G_6^0$		*13,796.36*
1	10	*14,863.85*
2	14	*15,567.32*
3	18	*16,211.04*
4	21	*16,890.59*
5	26	*17,587.44*
6	34	*18,298.29*
7		*19,005.64*
8		*19,753.30*
$z^9F_1^0$	8	*13,999.43*
2	9	*14,380.44*
3	11	*14,915.83*
4	15	*15,579.11*
5		*16,344.77*
6		*17,193.75*
7		*18,118.85*
$z^9D_2^0$	12	*15,039.59*
3	13	*15,507.35*
4	17	*16,131.53*
5	20	*16,859.31*
6	27	*17,654.53*
e^9F_1		28,708.14
2		29,037.20
3		29,551.86
4		30,191.24
5		30,921.99
6		31,725.70
7		32,567.76
2	176	*26,786.82*
2	177	*16,681.74*
2,3	178	*16,748.30*
1	179	*16,112.33*
1,2	180	*16,116.42*
1	181	*17,003.28*

TABLE II. *Certain classified lines of Sm I.*

I. A.	Int. and Temp. Class Arc	Furn.	Abs.	ν (vac.)	Designation
.....	.....	.....	.....	.....	$a^7F_6-z^9G_6^0$
7262.69	3	20IIA	3	13,765.21	$a^7F_5-z^9G_5^0$
7172.67	40	30I	5	13,937.88	$a^7F_4-z^9G_4^0$
7101.46	10	50I	5	14,077.74	$a^7F_3-z^9G_3^0$
7114.50	10	80I	10	14,051.93	$a^7F_2-z^9G_2^0$
7403.30	8	60IA	15	13,503.78	$a^7F_1-z^9G_1^0$
7002.03	2	60IA	2	14,277.64	$a^7F_6-z^9G_6^0$
6912.79	3	100IIA	3	14,461.96	$a^7F_5-z^9G_5^0$
6839.23	10	100IIA	1	14,617.50	$a^7F_4-z^9G_4^0$
6790.88	30	60IA	5	14,721.57	$a^7F_3-z^9G_3^0$
6775.30	60	150IA	8	14,755.43	$a^7F_2-z^9G_2^0$
6860.93	300	300I	15	14,571.27	$a^7F_1-z^9G_1^0$
6671.51	800	400I	10	14,984.98	$a^7F_6-z^9G_7^0$
6588.91	500	300I	10	15,172.83	$a^7F_5-z^9G_6^0$
6528.02	200	250I	12	15,314.36	$a^7F_4-z^9G_5^0$
6491.28	15	100IA	8	15,401.03	$a^7F_3-z^9G_4^0$
6492.05	5	25IIA	1	15,399.11	$a^7F_2-z^9G_3^0$
6544.95	40	150IA	12	15,274.75	$a^7F_1-z^9G_2^0$
6725.88	300	200I	15	14,863.85	$a^7F_0-z^9G_1^0$
.....	.....	.....	.....	.....	$a^7F_6-z^9F_5^0$
8027.5	1−	15IIA	0	12,453.6	$a^7F_5-z^9F_4^0$
7907.48	5	40IA	2	12,642.78	$a^7F_4-z^9F_3^0$
7755.32	?	80IA	4	12,890.83	$a^7F_3-z^9F_2^0$
7580.91	5	60IA	8	13,187.40	$a^7F_2-z^9F_1^0$
.....	.....	.....	.....	.....	$a^7F_6-z^9F_6^0$
7562.7	—	2IV	.....	13,219.1	$a^7F_5-z^9F_5^0$
7513.3	2	8IIA	2	13,306.1	$a^7F_4-z^9F_4^0$
7446.2	1−	5IIA	2	13,426.0	$a^7F_3-z^9F_3^0$
7367.9	1−	4IIA	1	13,568.6	$a^7F_2-z^9F_2^0$
.....	.....	.....	.....	.....	$a^7F_1-z^9F_1^0$
7091.16	100	150I	10	14,098.19	$a^7F_6-z^9F_7^0$
7106.23	100	150I	18	14,068.29	$a^7F_5-z^9F_6^0$
7104.54	150	200I	18	14,071.63	$a^7F_4-z^9F_5^0$
7095.50	150	200I	18	14,089.56	$a^7F_3-z^9F_4^0$
7088.30	150	250I	15	14,103.87	$a^7F_2-z^9F_3^0$
7096.33	100	150I	18	14,087.91	$a^7F_1-z^9F_2^0$
7141.13	30	100I	15	13,999.53	$a^7F_0-z^9F_1^0$
7787.02	8	60IA	2	12,838.35	$a^7F_6-z^9D_5^0$
7686.70	8	60IA	4	13,005.91	$a^7F_5-z^9D_4^0$
7554.14	8	60IA	10	13,234.14	$a^7F_4-z^9D_3^0$
7378.04	5	60IA	12	13,550.01	$a^7F_3-z^9D_2^0$
7332.65	60	100I	15	13,633.88	$a^7F_6-z^9D_6^0$
7279.25	80	100I	15	13,733.90	$a^7F_5-z^9D_5^0$
7213.82	80	100I	18	13,858.47	$a^7F_4-z^9D_4^0$
7131.80	100	150I	15	14,017.84	$a^7F_3-z^9D_3^0$
7026.62	100	200IA	15	14,227.67	$a^7F_2-z^9D_2^0$
6880.86	20	200II	5	14,529.07	$a^7F_5-z^9D_6^0$
6853.92	15	150IIA	8	14,586.17	$a^7F_4-z^9D_5^0$
6827.81	40	150IA	5	14,641.95	$a^7F_3-z^9D_4^0$
6802.96	50	150IA	12	14,695.43	$a^7F_2-z^9D_3^0$
6779.16	100	200IA	10	14,747.03	$a^7F_1-z^9D_2^0$
7006.04	5	6IV		14,269.47	$z^9G_6^0-e^9F_7$
7071.10	8	5III		14,138.18	$z^9G_5^0-e^9F_6$
7124.86	?	2IV		14,031.40	$z^9G_4^0-e^9F_5$
7151.03	4	4III		13,980.15	$z^9G_3^0-e^9F_4$
7148.8	2	2III		13,984.5	$z^9G_2^0-e^9F_3$
7053.54	8	10II		14,173.38	$z^9G_1^0-e^9F_2$
6704.25	40	20III		13,796.36	$z^9G_0^0-e^9F_1$
7371.51	30	5IV		13,562.01	$z^9G_7^0-e^9F_7$
7445.41	150	2IV		13,427.60	$z^9G_6^0-e^9F_6$
7497.26	8	V		13,334.54	$z^9G_5^0-e^9F_5$
.....	.....	.....		.....	$z^9G_4^0-e^9F_4$
.....	.....	.....		.....	$z^9G_3^0-e^9F_3$
.....	.....	.....		.....	$z^9G_2^0-e^9F_2$
7221.14	6	10III		13,844.42	$z^9G_1^0-e^9F_1$
7801.54	150	100II	1	12,814.46	$z^9G_6^0-e^9F_7$
7859.53	100	30III		12,719.91	$z^9G_7^0-e^9F_6$
7919.44	80	10III		12,623.69	$z^9G_6^0-e^9F_5$
7931.92	250	50II		12,603.82	$z^9G_5^0-e^9F_4$
7895.96	250	50II		12,661.23	$z^9G_4^0-e^9F_3$
7794.50	100	25II		12,826.03	$z^9G_3^0-e^9F_2$
7607.74	80	30III		13,140.89	$z^9G_2^0-e^9F_1$

TABLE II.—*Continued.*

I. A.	Int. and Temp. Class Arc	Furn.	Abs.	ν (vac.)	Designation
6502.57	2	3IV		15,374.29	$z^9F_6^0-e^9F_7$
.....	.....	.....		.....	$z^9F_5^0-e^9F_6$
.....	.....	.....		.....	$z^9F_4^0-e^9F_5$
6544.66	40	4IV		15,275.42	$z^9F_3^0-e^9F_4$
6589.56	?	12III		15,171.34	$z^9F_2^0-e^9F_3$
6648.12	25	15III		15,037.70	$z^9F_1^0-e^9F_2$
6919.03	20	15III		14,448.91	$z^9F_7^0-e^9F_7$
6879.50	80	20III		14,531.94	$z^9F_6^0-e^9F_6$
6858.12	15	10III		14,577.24	$z^9F_5^0-e^9F_5$
6841.75	60	25III		14,612.12	$z^9F_4^0-e^9F_4$
6830.54	80	25III		14,636.10	$z^9F_3^0-e^9F_3$
6820.91	40	15III		14,656.76	$z^9F_2^0-e^9F_2$
6796.82	40	15III		14,708.71	$z^9F_1^0-e^9F_1$
7347.30	150	8IV		13,606.70	$z^9F_7^0-e^9F_6$
7282.21	20	4IV		13,728.32	$z^9F_6^0-e^9F_5$
7220.10	50	15II		13,846.41	$z^9F_5^0-e^9F_4$
7154.83	25	10II		13,972.73	$z^9F_4^0-e^9F_3$
7079.50	10	10II		14,121.40	$z^9F_3^0-e^9F_2$
6977.55	5	20III		14,327.73	$z^9F_2^0-e^9F_1$
6703.61	150	25III		14,913.23	$z^9D_6^0-e^9F_7$
6724.73	150	30III		14,866.39	$z^9D_5^0-e^9F_6$
6759.25	60	15III		14,790.46	$z^9D_4^0-e^9F_5$
6808.31	60	20III		14,683.89	$z^9D_3^0-e^9F_4$
6888.81	40	25III		14,512.30	$z^9D_2^0-e^9F_3$
7104.54	?	? ?		14,071.63	$z^9D_6^0-e^9F_6$
7109.06	4	4III		14,062.69	$z^9D_5^0-e^9F_5$
7110.56	12	6III		14,059.70	$z^9D_4^0-e^9F_4$
7118.28	15	10II		14,044.47	$z^9D_3^0-e^9F_3$
7142.09	4	4III		13,997.65	$z^9D_2^0-e^9F_2$
.....	.....	.....		.....	$z^9D_6^0-e^9F_5$
7498.71	6	V		13,331.96	$z^9D_5^0-e^9F_4$
7449.28	15	2IV		13,420.42	$z^9D_4^0-e^9F_3$
7389.03	6	2IV		13,529.85	$z^9D_3^0-e^9F_2$
7314.00	4	1IV		13,668.65	$z^9D_2^0-e^9F_1$
6580.53	50	200IA	8	15,192.16	a^7F_3-177
6551.80	200	300I	15	15,258.77	a^7F_3-178
6533.96	200	300I	15	15,300.44	a^7F_2-179
6532.25	200	300I	15	15,304.44	a^7F_2-180
6319.49	2	2IV		15,819.70	a^7F_1-179
6317.81	15	15III		15,823.90	a^7F_1-180
6273.29	50	80IA	10	15,936.20	a^7F_2-178
6174.45	150	150I		16,191.30	a^7F_2-181
6099.90	40	200IA	10	16,389.19	a^7F_1-177
5879.57	6	4III		17,003.34	a^7F_0-181

8700A and 4700A in Sa I are due to the electron transition $4f^65d6s-4f^65d6p$. Indeed, many of the high states already found to combine with a^7F are probably from $4f^65d6p$. With faith in this view, a rather extensive program of research was undertaken to unravel the spectrum and locate at least the main terms of the two electron configurations in question. Not a single energy state was found, although several hundred hours of time were devoted to the search. The tremendous line density is the cause of failure and will always remain as the chief barrier to surmount in any future attempt to bring order to this line group. Allowing a reasonable tolerance for experimental error, any wave number interval, chosen at random, will be found to occur in the data up to one hundred times. Fortuitous arrays can easily be built up from this start. A tremendous amount of labor must be expended

before a promising term array can be proven fortuitous. In fact, many fine looking arrays, involving hundreds of lines, were obtained only to be discarded later as entirely fortuitous. As there are many possible intervals between the known high states that one can start with in the search for the lower metastable states, there are many intervals to eliminate. So much can be obtained by chance alone that the real is hidden by the false.

A glance at the theoretical possible terms from the two electron configurations in question will show the cause of the great line density from this electron transition.

There will be 114 states from $4f^6(^7F)5d6s$ including

$$^{9,7,7,5}(HGFDP)$$

and 334 high states from $4f^6(^7F)5d6p$ including

$$^{9,7,7,5}(IHG, IHGF, GFD, FDP, DPS).$$

The intense lines from the transition $4f^65d6s - 4f^66s6p$ will be in the inaccessible infrared.

The writer wishes to thank the National Research Council for the Fellowship that made this research possible, the Mount Wilson Observatory of the Carnegie Institution of Washington, and the Physics Departments of the University of California and the Massachusetts Institute of Technology for placing their resources at his disposal.

SEPTEMBER 15, 1937 PHYSICAL REVIEW VOLUME 52

Electromagnetic Waves in Conducting Tubes

LEIGH PAGE AND N. I. ADAMS, JR.
Sloane Physics Laboratory, Yale University, New Haven, Connecticut

(Received June 24, 1937)

It is shown that the waves in a hollow conducting tube described by Carson and by Barrow may be represented as semi-standing waves due to the superposition of plane waves with normal phase velocity $c/(\kappa\mu)^{\frac{1}{2}}$ reflected back and forth from one side of the tube to the other. It is also shown that certain types of waves can be transmitted without attenuation in tubes of triangular, rectangular and hexagonal cross section.

THE theory of the propagation of electromagnetic waves in cylindrical conducting tubes of circular cross section has been presented by Carson, Mead and Schelkunoff[1] and independently by Barrow,[2] and has been verified experimentally by Southworth.[3] While the mathematical analysis in these papers pursues the most direct and obvious method of attack, it fails to reveal the details of the physical process involved in the transmission of waves in the interior of a hollow tube. Fundamentally the "*E*" and "*H*" types of wave described by Carson and by Barrow are the result of the superposition of an infinite number of elementary plane waves traveling at an angle with the axis of the tube and having the normal phase velocity $c/(\kappa\mu)^{\frac{1}{2}}$ characteristic of the permittivity κ and permeability μ of the homogeneous isotropic nonconducting medium filling the interior of the tubular conductor, these waves being reflected back and forth from one side of the tube to the other. The two types of wave differ only in the state of polarization of the component elementary plane waves to whose superposition they are due. The elementary plane wave with normal phase velocity is more fundamental physically than the waves discussed by Carson and by Barrow for the reason that the Poynting flux is everywhere in the direction of wave propagation.

It is the object of this communication to show that the superposition of the specified plane waves yields the waves described by Carson and by Barrow. Incidentally we shall discuss the possibility of the propagation of electromagnetic waves in cylindrical conducting tubes of polygonal cross section. In all cases we shall limit ourselves to tubes which are perfectly conducting, using

[1] J. R. Carson, S. P. Mead and S. A. Schelkunoff, Bell System Tech. J. **15**, 310 (1936).
[2] W. L. Barrow, Proc. I. R. E. **24**, 1298 (1936).
[3] G. C. Southworth, Bell System Tech. J. **15**, 284 (1936).

the symbol v for the normal phase velocity $c/(\kappa\mu)^{\frac{1}{2}}$.

(1) Parallel Planes

First consider waves propagated in the X direction in a homogeneous isotropic medium between two conducting planes $y=0$ and $y=a$. Solutions of the field equations satisfying the boundary conditions are

$$\mathbf{E}=\mathbf{j}A\cos(lx-\omega t),\quad l=\omega/v; \tag{1}$$

$$\mathbf{E}=A\{\mathbf{i}m\sin my\cos(lx-\omega t) - \mathbf{j}l\cos my\sin(lx-\omega t)\}, \tag{2-1}$$

$$\mathbf{E}=B\{\mathbf{k}m\sin my\cos(lx-\omega t)\}, \tag{2-2}$$

$$m=k\pi/a,\quad l^2+m^2=\omega^2/v^2,$$

where k is an integer; and

$$\mathbf{E}=A\{\mathbf{i}(m^2+n^2)\sin my\sin nz\cos(lx-\omega t) - \mathbf{j}lm\cos my\sin nz\sin(lx-\omega t) - \mathbf{k}nl\sin my\cos nz\sin(lx-\omega t)\}, \tag{3-1}$$

$$\mathbf{E}=B\{-\mathbf{j}n\cos my\sin nz\cos(lx-\omega t) + \mathbf{k}m\sin my\cos nz\cos(lx-\omega t)\}, \tag{3-2}$$

$$m=k\pi/a,\quad l^2+m^2+n^2=\omega^2/v^2.$$

As (1) represents a plane wave with normal phase velocity v no special comment is needed.

Waves (2–1) and (2–2) are transmitted only for frequencies greater than $c/2a(\kappa\mu)^{\frac{1}{2}}$. In Carson's notation (2–1) is an "E" wave and (2–2) an "H" wave. The first may be written in the form

$$\mathbf{E}=\tfrac{1}{2}A\{(\mathbf{i}m-\mathbf{j}l)\sin(lx+my-\omega t) - (\mathbf{i}m+\mathbf{j}l)\sin(lx-my-\omega t)\}, \tag{4-1}$$

showing that it is due to the superposition of two plane waves with normal phase velocity v traveling in the XY plane in directions making angles with the X axis whose tangents are $\pm m/l$. Each component elementary wave is polarized with the electric vector in the plane determined by the direction of propagation and the X axis. Similarly (2–2) may be resolved into the two plane waves

$$\mathbf{E}=\tfrac{1}{2}B\{\mathbf{k}m\sin(lx+my-\omega t) - \mathbf{k}m\sin(lx-my-\omega t)\} \tag{4-2}$$

with normal phase velocity v traveling in the XY plane in directions making angles with the X axis whose tangents are $\pm m/l$. In this case the component elementary waves are polarized with the electric vector perpendicular to the plane determined by the direction of propagation and the X axis. The physical process underlying the propagation of these waves, therefore, consists in the back and forth reflection from the two conducting planes of plane waves traveling at an angle with the X axis with the normal phase velocity v. The phase velocity ω/l along the X axis of the resultant wave represents the reciprocal of the component in this direction of the wave slowness of either of the component elementary waves, and for this reason it is greater than v. As the limiting frequency is approached the angles which the directions of propagation of the component waves make with the X axis approach $\pm\pi/2$, and consequently these waves are reflected back and forth between the two conducting planes without progressing in the X direction. Hence the velocity of propagation of the resultant wave becomes infinite.

Waves (3–1) and (3–2) permit the introduction of the conducting planes $z=0$, $z=b$, with $n=k'\pi/b$, in addition to the conducting planes $y=0$, $y=a$, with $m=k\pi/a$. In the first we have an "E" wave and in the second an "H" wave propagated in a conducting tube of rectangular cross section. Excepting the special cases where m or n is equal to zero, these waves are transmitted only for frequencies greater than $(a^2+b^2)^{\frac{1}{2}}c/2ab(\kappa\mu)^{\frac{1}{2}}$. If $n=0$, (3–2) becomes

$$\mathbf{E}=B\{\mathbf{k}m\sin my\cos(lx-\omega t)\},$$

which is a wave identical with (2–2) having the limiting frequency $c/2a(\kappa\mu)^{\frac{1}{2}}$ independent of b, and if $m=0$, we have the analogous wave

$$\mathbf{E}=-B\{\mathbf{j}n\sin nz\cos(lx-\omega t)\}$$

with the limiting frequency $c/2b(\kappa\mu)^{\frac{1}{2}}$ independent of a. The first of these waves satisfies the boundary conditions for any z dimension of the rectangular tube, and the second for any y dimension. In a manner similar to the method employed in the cases of (2–1) and (2–2), it is easily shown that each of the waves (3–1) and (3–2) can be resolved into four elementary plane waves traveling with the normal phase velocity v in directions making equal angles with the X axis. These waves, however, differ from those

previously discussed in that they do not travel, in general, in directions lying in planes determined by the normals to the conducting planes and the X axis.

(2) Cylindrical Tube of Circular Cross Section

We shall now show that the Carson-Barrow waves, like the simpler waves just described, are due to the superposition of plane waves traveling with normal phase velocity $v=c/(\kappa\mu)^{\frac{1}{2}}$ at an angle with the axis of the tube and reflected back and forth one side to the other. As the normal component of the wave slowness of each elementary plane wave is reversed on reflection we shall save labor by taking as primary waves those specified by (2–1) and (2–2) instead of the pairs (4–1) and (4–2) of elementary plane waves into which they may be resolved. We shall need the expansions[4]

$$\sin(mr\cos\theta)=2J_1(mr)\cos\theta-2J_3(mr)\cos 3\theta+2J_5(mr)\cos 5\theta-\cdots, \quad (5\text{–}1)$$

$$\cos(mr\cos\theta)=J_0(mr)-2J_2(mr)\cos 2\theta+2J_4(mr)\cos 4\theta-\cdots, \quad (5\text{–}2)$$

and the recurrence formulas

$$(2n/mr)J_n(mr)=J_{n-1}(mr)+J_{n+1}(mr), \quad (6\text{–}1)$$

$$2J_n'(mr)=J_{n-1}(mr)-J_{n+1}(mr). \quad (6\text{–}2)$$

Take the axis of the tube as X axis and let the circle in Fig. 1 with center at O represent a cross section of the tube. Let the Y axis have the direction of the projection on this cross section of the velocity of propagation of an elementary plane wave. A point P lying on a wave front MN is located by the cylindrical coordinates x, r, ϕ.

First consider the "E" waves. The complete solution of the electromagnetic equations of the form (2–1) is

$$E_x=m[a_1\cos my-a_2\sin my]\cos(lx-\omega t), \quad (7\text{–}1)$$

$$E_y=l[a_1\sin my+a_2\cos my]\sin(lx-\omega t), \quad (7\text{–}2)$$

where a_1 and a_2 are independent arbitrary constants. This solution is obtained immediately from (2–1) by replacing y by $y-\delta$. Now let the number of such primary plane waves propagated in the range of θ between θ and $\theta+d\theta$ be $\cos n(\theta+\phi)d\theta$ where n is an integer. Then, as $y=r\cos\theta$, the X component of the resultant amplitude at P is

$$A_x=ma_1\int_0^{2\pi}\cos(mr\cos\theta)\{\cos n\theta\cos n\phi-\sin n\theta\sin n\phi\}d\theta - ma_2\int_0^{2\pi}\sin(mr\cos\theta)\{\cos n\theta\cos n\phi-\sin n\theta\sin n\phi\}d\theta$$

$$=\begin{cases}(-1)^{n/2}2\pi ma_1J_n(mr)\cos n\phi, & n \text{ even},\\ (-1)^{(n+1)/2}2\pi ma_2J_n(mr)\cos n\phi, & n \text{ odd},\end{cases} \quad (8\text{–}1)$$

from (5–1) and (5–2). Similarly the component of the resultant amplitude in the direction of increasing ϕ is

$$A_\phi=\tfrac{1}{2}la_1\int_0^{2\pi}\sin(mr\cos\theta)\{[\sin(n+1)\theta-\sin(n-1)\theta]\cos n\phi+[\cos(n+1)\theta-\cos(n-1)\theta]\sin n\phi\}d\theta$$

$$+\tfrac{1}{2}la_2\int_0^{2\pi}\cos(mr\cos\theta)\{[\sin(n+1)\theta-\sin(n-1)\theta]\cos n\phi+[\cos(n+1)\theta-\cos(n-1)\theta]\sin n\phi\}d\theta$$

$$=\begin{cases}(-1)^{n/2}\pi la_1\{J_{n-1}(mr)+J_{n+1}(mr)\}\sin n\phi, & n \text{ even},\\ (-1)^{(n+1)/2}\pi la_2\{J_{n-1}(mr)+J_{n+1}(mr)\}\sin n\phi, & n \text{ odd},\end{cases}$$

$$=\begin{cases}(-1)^{n/2}2\pi(ln/m)(a_1/r)J_n(mr)\sin n\phi, & n \text{ even},\\ (-1)^{(n+1)/2}2\pi(ln/m)(a_2/r)J_n(mr)\sin n\phi, & n \text{ odd},\end{cases} \quad (8\text{–}2)$$

[4] Gray, Mathews and Macrobert, *Bessel Functions*, p. 16 and 32.

from (5–1), (5–2) and (6–1). In the same manner we obtain for the resultant amplitude in the direction of increasing r

$$A_r=\left\{\begin{matrix}-(-1)^{n/2}2\pi la_1J_n'(mr)\cos n\phi, & n \text{ even},\\ -(-1)^{(n+1)/2}2\pi la_2J_n'(mr)\cos n\phi, & n \text{ odd},\end{matrix}\right\} \tag{8–3}$$

from (5–1), (5–2) and (6–2).

Therefore the components of the electric intensity at P due to the superposition of the group of elementary plane waves reflected back and forth from one side of the tube to the other, for n either even or odd, are

$$E_z=Am^2J_n(mr)\left\{\begin{matrix}\cos n\phi\\ \sin n\phi\end{matrix}\right\}\cos(lx-\omega t), \tag{9–1}$$

$$E_r=-AlmJ_n'(mr)\left\{\begin{matrix}\cos n\phi\\ \sin n\phi\end{matrix}\right\}\sin(lx-\omega t), \tag{9–2}$$

$$E_\phi=A\ln\frac{1}{r}J_n(mr)\left\{\begin{matrix}\sin n\phi\\ -\cos n\phi\end{matrix}\right\}\sin(lx-\omega t), \tag{9–3}$$

the lower factors in the braces having been obtained from the upper by replacing $n\phi$ by $n\phi-\pi/2$, which is equivalent to making the number of primary waves in the range $d\theta$ proportional to $\sin n(\theta+\phi)$ instead of to $\cos n(\theta+\phi)$. These are, however, just the components of **E** obtained for the "E" type wave by Carson and by Barrow, who have discussed the circumstances under which the boundary conditions are satisfied.

The "H" waves are due to the superposition of primary plane waves of the other state of

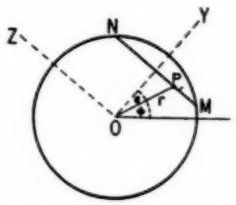

FIG. 1. Cross section of circular tube.

polarization. From (2–2) we have in the primary plane wave

$$E_z=m[b_1\sin my+b_2\cos my]\sin(lx-\omega t), \tag{10}$$

and, if we take the number of such primary waves propagated in the angle $d\theta$ to be $\cos n(\theta+\phi)d\theta$, we get

$$\begin{aligned}B_\phi=\tfrac{1}{2}mb_1\int_0^{2\pi}&\sin(mr\cos\theta)\{[\cos(n+1)\theta+\cos(n-1)\theta]\cos n\phi\\ &-[\sin(n+1)\theta+\sin(n-1)\theta]\sin n\phi\}d\theta\\ +\tfrac{1}{2}mb_2\int_0^{2\pi}&\cos(mr\cos\theta)\{[\cos(n+1)\theta+\cos(n-1)\theta]\cos n\phi\\ &-[\sin(n+1)\theta+\sin(n-1)\theta]\sin n\phi\}d\theta\\ =\left\{\begin{matrix}-(-1)^{n/2}\pi mb_1\{J_{n-1}(mr)-J_{n+1}(mr)\}\cos n\phi, & n \text{ even},\\ -(-1)^{(n+1)/2}\pi mb_2\{J_{n-1}(mr)-J_{n+1}(mr)\}\cos n\phi, & n \text{ odd},\end{matrix}\right.&\\ =\left\{\begin{matrix}-(-1)^{n/2}2\pi mb_1J_n'(mr)\cos n\phi, & n \text{ even},\\ -(-1)^{(n+1)/2}2\pi mb_2J_n'(mr)\cos n\phi, & n \text{ odd},\end{matrix}\right\}&\end{aligned} \tag{11–1}$$

from (5–1), (5–2) and (6–2). Similarly

$$B_r=\left\{\begin{matrix}-(-1)^{n/2}2\pi n(b_1/r)J_n(mr)\sin n\phi, & n \text{ even},\\ -(-1)^{(n+1)/2}2\pi n(b_2/r)J_n(mr)\sin n\phi, & n \text{ odd},\end{matrix}\right\} \tag{11–2}$$

from (5–1), (5–2) and (6–1).

Therefore the components of electric intensity in the "H" wave, for n either even or odd, are

$$E_r=Bn\frac{1}{r}J_n(mr)\begin{Bmatrix}\sin n\phi\\ -\cos n\phi\end{Bmatrix}\sin(lx-\omega t), \quad (12\text{–}1)$$

$$E_\phi=BmJ_n'(mr)\begin{Bmatrix}\cos n\phi\\ \sin n\phi\end{Bmatrix}\sin(lx-\omega t), \quad (12\text{–}2)$$

in agreement with Carson and with Barrow.

Obviously the same methods can be applied to the dielectric rod of circular cross section, the analysis being complicated, however, by the fact that the elementary plane waves are partially reflected and partially transmitted at the surface of the dielectric.

(3) Cylindrical Tube of Polygonal Cross Section

Last we shall investigate the propagation of a wave inside a cylindrical tube whose cross section is a regular polygon. The square tube is a special case of the rectangular tube already considered, and we have seen that both an "E" wave and an "H" wave may be transmitted by it. For other cross sections it seems that no "E" wave can be transmitted, and an "H" wave is propagated only in the cases of a triangular or hexagonal section, the transmission in these types of tube being due to the circumstance that cos 60° is the reciprocal of an integer.

Let Fig. 2 represent a cross section of the tube, O being on the axis and the heavy lines being the traces of the faces of the tube. Primary plane waves of the "H" type (2–2) with directions of propagation in planes containing the X axis and the normals to the faces of the tube give rise to a resultant amplitude of the electric intensity at a point $P(y, z)$ equal to

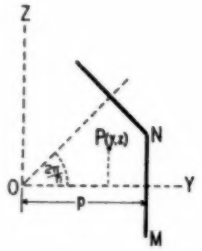

Fig. 2. Cross section of hexagonal tube. O is on the axis.

$$\begin{aligned}A_z&=a\sum_{k=0}^{n-1}\cos k(2\pi/n)\sin m[y\cos k(2\pi/n)\\&\qquad+z\sin k(2\pi/n)]\\&=a\sum_{k=0}^{n-1}\cos k(2\pi/n)\sin[my\cos k(2\pi/n)]\\&\qquad\times\cos[mz\sin k(2\pi/n)]\end{aligned} \quad (13)$$

no matter whether the number n of faces is odd or even.

The boundary condition at the face MN is that A_z should vanish for all values of z. But this condition can be satisfied only if every cos $(2\pi k/n)$ is an integral multiple of the same number. Such a situation exists only for $n=3$, 4, 6. Consequently we conclude that this type of wave can be transmitted only by triangular, square, and hexagonal tubes.

For the triangular tube $2\pi/n=120°$ and cos $2\pi k/n$ assumes the values 1, $-1/2$, $-1/2$. Therefore

$$\begin{aligned}A_z&=a\left\{\sin my+\sin(my/2)\cos\frac{(3)^{\frac{1}{2}}}{2}mz\right\}\\&=a\sin\tfrac{1}{2}my\left\{2\cos(my/2)+\cos\frac{(3)^{\frac{1}{2}}}{2}mz\right\},\end{aligned} \quad (14)$$

which vanishes for all values of z if y is an integral multiple of $2\pi/m$.

Hence the minimum frequency for transmission of this wave is $\nu=c/p(\kappa\mu)^{\frac{1}{2}}$, where p is the perpendicular distance from the axis to one of the faces.

For the hexagonal tube $2\pi/n=60°$. Here cos $2\pi k/n$ has the values 1, $1/2$, $-1/2$, -1, $-1/2$, $1/2$ and sin $2\pi k/n$ the values 0, $\sqrt{3}/2$, $\sqrt{3}/2$, 0, $-\sqrt{3}/2$, $-\sqrt{3}/2$. Hence

$$\begin{aligned}A_z&=a\left\{2\sin my+4\sin(my/2)\cos\frac{(3)^{\frac{1}{2}}}{2}mz\right\}\\&=2a\sin(my/2)\left\{2\cos(my/2)+\cos\frac{(3)^{\frac{1}{2}}}{2}mz\right\},\end{aligned} \quad (15)$$

which is just double A_z for the triangular tube.

When we pass to the tube of circular cross section by making $n\to\infty$ we see that (13) gives us A_ϕ for the "H_0" wave. No further cases of transmission are obtained by directing the elementary waves toward the corners N of the polygonal tube instead of directing them at right angles to the faces.

Short Time Lag of Spark Breakdown

MORRIS NEWMAN
University of Minnesota, Minneapolis, Minnesota
(Received July 15, 1937)

A method involving the use of a series of special electronic voltmeters along an electrical transmission line has been developed to determine the voltages of an incoming surge wave at definite time intervals in relation to another timing wave. By this method, direct readings have been obtained of the time lag of spark breakdown in steps as short as 10^{-8} second down to 10^{-9} second in some cases. A critical comparison was made of time lag measurements by the dual traveling wave method with measurements by other observers using electro-optical Kerr cell methods. Some corrections of existing results are indicated. The results obtained by the proposed method are in agreement with theoretical considerations.

INTRODUCTION

THE time lags of spark breakdown are of interest both because of their bearing on the fundamental phenomena of the spark breakdown mechanism,[1] and also for their importance in electrical engineering, particularly in lightning-protection problems.[2]

The most recent work of a quantitative character on time lags has been done by A. Tilles[3] in the interval between 10^{-5} and 1 second for low overvoltages: while for higher overvoltages the short time lags between 10^{-9} and 10^{-8} second have been further investigated by H. J. White[4] and by R. R. Wilson.[5]

It has been pointed out by L. B. Loeb[1] that in different measuring methods the definition of time lag varies. Also, in their respective papers, White[4] points out a possibility in his method of a time lag shift due to the initial time variation of the intensity of the initiating gap light and Wilson[5] points out a possibility of oscillations making the overvoltage values in his own method somewhat indeterminate.

In this paper another method of measuring short time lags is given by which the results with various definitions of time lag may be compared. Special care was taken in the design of the apparatus to eliminate oscillations as a factor. Direct readings were obtained for each individual time lag, with time resolution to less than 10^{-9} second.

[1] L. B. Loeb, Rev. Mod. Phys. **8**, 284 (1936).
[2] J. J. Torok, Trans. A. I. E. E. **47**, 177 (1928).
[3] A. Tilles, Phys. Rev. **46**, 1015 (1934).
[4] H. J. White, Phys. Rev. **49**, 507 (1936).
[5] R. R. Wilson, Phys. Rev. **50**, 1082 (1936).

THE METHOD OF MEASURING TIME LAGS

The element of time is introduced by means of an electrical transmission line on which the velocity of surge travel is easily calculable. The general principle of the time lag measurements is illustrated in Figs. 1 and 2, in which the relations of the traveling waves are given in four successive instants.

At intervals along the transmission line corresponding to the desired time of travel there are placed a series of potential-recording instruments, 1, 2, 3, $\cdots$ to 10 which respond to positive impulses of very short time duration, but which do not respond to negative potentials. At one end of the line, the surge S of positive polarity arrives, and applied at the other end is the negative timing impulse T, which is synchronized in relation to the potential causing the surge S. Fig. 1 indicates conditions for which there is no time lag between the arrival of T and S at their respective ends of the line; obviously the two waves will just meet at the center as at (*b*) and meters 10, 9, $\cdots$ to 6 inclusive will be tripped by the passage of the positive surge S. The rest of the meters will remain untripped, for the superposition of the large negative timing surge T on the positive surge S leaves no resultant positive potential to which the polarized surge trip-voltmeter can respond.

In the study of time lag characteristics of a gap, the positive surge S could be produced by the breakdown of the gap, and the time lag "t" caused by the formative spark process would delay the arrival of the surge S in relation to the timing wave T as indicated in Fig. 2a.

Then, as may be seen in Fig. 2b, when the timing wave T arrives at the center, the surge S will however be delayed by the distance $d=vt$, where v is the velocity of the wave travel along the line. The two waves will now meet only at $d/2$ to the right of the center, and the meters 6 and 7 in that interval will also be untripped. It is clear, therefore, that the number of meters remaining untripped on the positive side of the electrical center (the meeting point in the case of zero time lag) indicates the magnitude of the time lag, which determines the distance that the blocking negative timing surge T had a chance to travel in the additional interval of half the time lag of arrival of the surge S, before meeting the latter. The electrical center can be shifted by lengthening one side of the line so that the time lags are directly readable in terms of the highest untripped meter number.

Time Lag Measurements

The time lag measurements of this paper were made for the case of a pair of polished brass spheres $\frac{3}{4}$ inch in diameter separated for 10,000 volt breakdown under steady state potential, and with strong ultraviolet illumination of the surfaces from a quartz-mercury lamp at a distance of 2.5 inches from the gap.

The circuit diagram and the results of the measurements by the "dual wave" are given in Fig. 3. The results of similar measurements by electro-optical Kerr cell shutter methods by White and by Wilson are also reproduced in Fig. 3. It is difficult to make quantitative comparisons since the conditions of the surfaces and the illumination intensities are not given quantitatively. However, the agreement is rather close if the circuit factors making for discrepancies are taken into account. Thus considering White's results and his suggested shift of time lag of about 2×10^{-8} second due to delay in building up intensity in his initiating gap G_1 (diagram a), the agreement after making such a correction would be rather good. The results of Wilson, as he remarked in his paper, are apparently considerably affected by oscillations and traveling waves. His results being lower at the very short time lags than with the "dual wave" method,

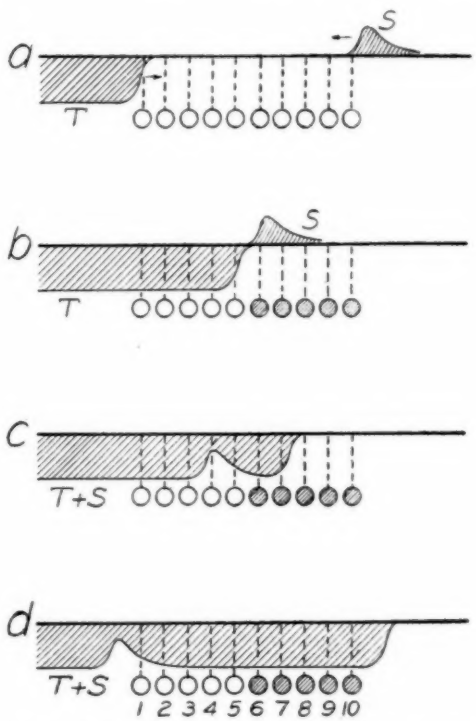

Fig. 1. Traveling wave potentials along the transmission line at the different instants of time a, b, c, and d.

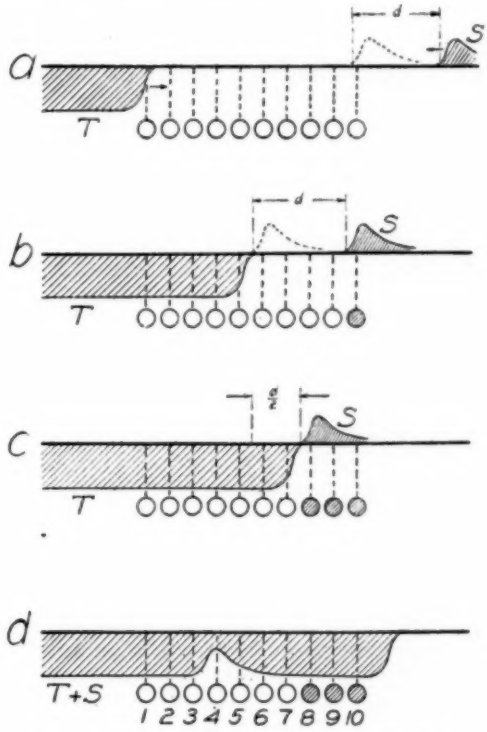

Fig. 2. The traveling wave potential relations with the surge S delayed a distance $d=vt$ corresponding to a time lag t.

would indicate overvoltage oscillations. However, considering his circuit (diagram *b*) and assuming that the transmission line did not have special compensation of its wave impedance to ground, then except for initial superposed overvoltage oscillations, actually a reduction in voltage might be expected. If such a hypothesis were correct it would bring the results by the several Kerr cell methods in rather good agreement with each other and also with the "dual wave" results.

There was little difference between the corresponding points for 98 percent and 50 percent (points *o* and *x*, respectively) approach voltages. This indicated that the presence of the approach voltage did not materially affect the breakdown mechanism over the measured range. It also showed that there were no serious disturbing oscillations in the experiments since the increase of the surge voltage increment corresponded closely to the decrease of the d.c. approach voltage. This was separately checked over the entire range of voltages with various combinations of surge and approach voltages, with the total sum agreeing to within about 2 percent, so there could scarcely have been any unforeseen oscillations of a higher order.

Some test runs were made for different ultraviolet light intensities and the results were quite similar to those obtained by White and Wilson allowing for the factors previously considered.

It appears that the time lag of breakdown is a rather definite and a similar function of the overvoltage with strong illumination for the three sets of results, which is of particular interest considering the difference of time lag definition inherent in each case. In White's work the over-potential is present at the gap for some time and initiation is accomplished by release of photoelectrons at the gap by means of another spark gap ultraviolet light source: and the time lag there is the lag between the initiation of the light source and the production of sufficient ionization in the gap being studied for visibility of the resulting light through the Kerr cell. In Wilson's work the time lag is the interval between application of surge overvoltage and the appearance of light in the gap. While in the "dual wave" method of this paper, the time lag is the interval between the application of surge overvoltage and the time of a sufficient rate of transfer of electrons to send a pulse on the transmission line of sufficient voltage to give a trip indication reading on the surge recording meters.

In conclusion, the writer gratefully acknowledges the constant interest and cooperation of Professors J. M. Bryant and H. A. Erikson in this work and also the cooperation of Professors J. T. Tate and J. H. Williams in initiating researches on a multiple oscillator acceleration scheme which occasioned the development of the time lag measuring method of this paper. Particular thanks are also due the Research Division of the General Mills Company for the loan of the kenotron power supply used in these experiments.

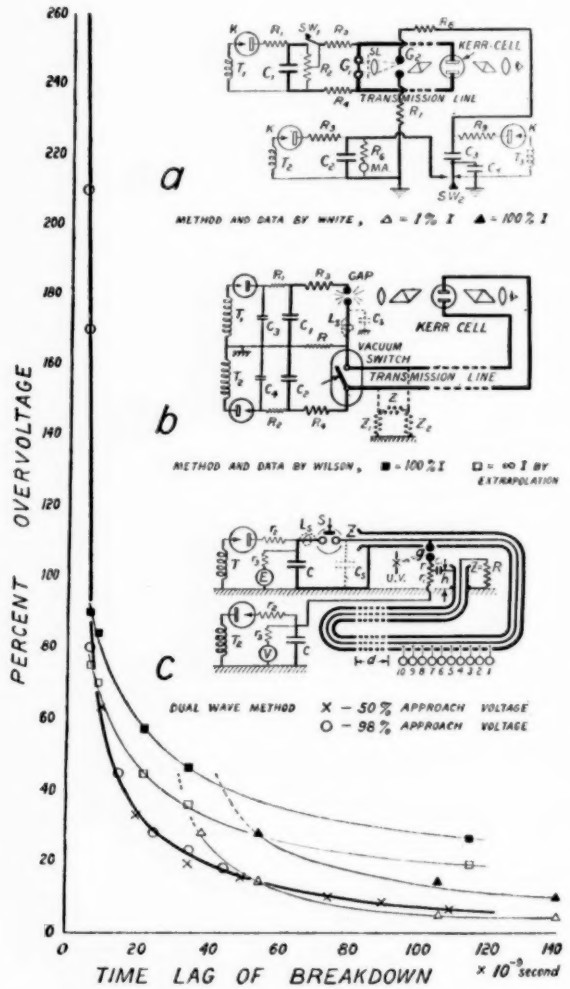

FIG. 3. Time lag of spark breakdown as a function of overvoltage for a short sphere gap with intense ultraviolet illumination of the sphere surfaces.

Low Voltage Positive Ion Source

WALTER H. ZINN
Columbia University and The College of the City of New York, New York, N. Y.
(Received July 19, 1937)

A positive ion source of the low voltage constricted arc type, which yields intense positive ion beams with small gas pumping, is described. Ion currents up to 4.3 milliamperes have been obtained using a probe canal 6 mm long and 1 mm in diameter. Magnetic analysis, when the arc was operated in hydrogen, showed a maximum of 15 to 20 percent protons.

INTRODUCTION

DURING the past few years a number of positive ion sources of the low voltage arc type for use with high voltage equipment in nuclear research have been described.[1–4] Of these, the capillary arc source gives the most promise of yielding large positive ion currents without prohibitive power consumption, enormous pumping speeds or too large and bulky apparatus. The source described herein is essentially a modification of the capillary arc design published by Tuve, Dahl and Hafstad.[1] It has been used as a source of deuterons for a relatively low voltage neutron generator. Ion currents at the target of 1.0 milliampere have readily been obtained using an outlet canal which limits the deuterium flow to an amount which is not excessive.

CONSTRUCTION

The source, drawn to scale, and the method of attaching it to the accelerating tube are shown in Fig. 1. This source differs from the capillary type of low voltage arc in that the arc instead of being confined in a cylindrical capillary passes through a narrow gap, which, in Fig. 1, is the space between the diaphragm B and the cylinder C. This gap can be made less than 1 mm wide without making the arc difficult to start or unstable in operation. The anode A is separated from the hot cathode F by the steel diaphragm B which is pushed into a thin-walled steel tube which forms the arc body. The flat nose of B is 12 mm in diameter and carries at its center a hole 3 mm in diameter and of no length. The filament is circular and surrounds the arc gap. The filament is insulated by a piece of glass tubing and it has been found that a short section of sylphon bellows (not shown) above the glass

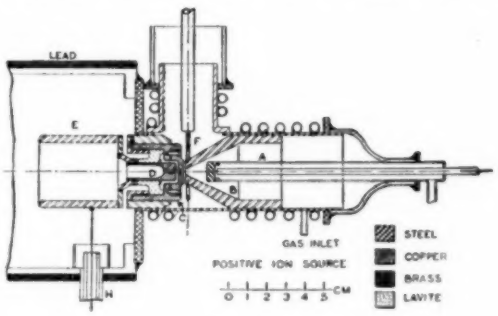

FIG. 1.

is of great assistance in centering the filament. The copper cylinder C slides in a steel sleeve soldered into the end of the steel pipe. A set-screw holds C in position; the width of the arc gap is varied by moving C. Because the gas flow around C should be a minimum a careful fit is necessary. The positive ions drift out of the arc gap through the exit hole in the face of C. An unfired lavite insulator inside C carries the probe D. Potentials up to 10,000 volts applied between D and C accelerate positive ions through the canal in the probe. The canal also limits the flow of gas into the accelerating tube. An insulated lead H in the side of the accelerating tube carries the probe potential to E. No special care has been taken to make the connection between the probe and the lavite insulator gas tight, except to seal the space between D and E with a small amount of insulute cement.

In order to facilitate the study of the dependence of the ion current on the dimensions of the exit hole, the face of C was made in the form of a

[1] Tuve, Dahl and Hafstad, Phys. Rev. **48**, 241 (1935).
[2] Lamar, Samson and Compton, Phys. Rev. **48**, 886 (1935).
[3] Lamar, Buechner and Compton, Phys. Rev. **51**, 936 (1937).
[4] Crane, Lauritsen and Soltan, Phys. Rev. **45**, 507 (1934).

TABLE I. *Output ion currents. Arc gap 1.2 mm. Probe canal 1 mm×6 mm. Exit hole (a) of Fig. 2.*

Arc Current amp.	Probe Voltage Volts					
	2000 ma	4000 ma	6000 ma	7000 ma	8000 ma	9000 ma
0.5	.27	.9	1.4	1.4		
1.0	.22	.7	1.5	1.9	2.2	2.2
1.5	.17	.7	1.9	2.6	3.1	3.2
2.0	.1	.6	1.7	2.4	3.3	4.3

plate held in place by two small screws. The glass insulators supporting the anode and filament are secured with red wax. A few turns of copper tubing provide water cooling. The source could probably be radiation cooled by making the arc-body and filament support out of stainless steel, lengthening them, and substituting a higher melting point cement.

Operating Characteristics

The arc is operated on 220 volts, the arc drop in general being 100 volts. It is started by connecting the arc-body to the anode through a resistance of 400 ohms. As the pressure, at which the arc is operated, is somewhat lower than the starting pressure, the starting procedure consists of letting in a small burst of gas and then momentarily connecting the arc-body to the anode. This invariably starts the arc even though the arc gap is less than 1.0 mm. After the arc is started the filament is connected directly to the arc-body, this seems to permit higher probe potentials without blowing out the arc. The source has been operated on both tank hydrogen and pure deuterium, and, in neither case, has it been found necessary to add any other gas to obtain a constant and persistent arc. The filament temperature is not critical but should be sufficiently high so that connecting the filament to the arc-body produces only a very small increase in the arc current.

Both oxide-coated and pure tungsten filaments have been used. Filaments of the type described by Lamar, Samson and Compton[2] are quite satisfactory although the lifetime is rather short, an average filament lasting from 30 to 40 hours. A 0.020″ tungsten filament lasts about 25 hours and a 0.040″ tungsten upwards of 50 hours. Tungsten filaments are preferred because of the ease of replacement and, in addition, there is less likelihood of contaminating the ion beam with foreign ions.

The output currents are largest when the pressure in the arc chamber is only slightly higher than the smallest pressure at which the arc can be maintained. This pressure is approximately 0.03 mm. The flow of gas is such that a 1500 cc flask of deuterium at atmospheric pressure permits operation for one hundred hours.

Ion Currents

The output ion currents depend, in a critical fashion, on the width of the arc gap and the dimensions of the exit hole. In Table I are listed the output currents for various arc currents and probe potentials for a probe canal 1 mm in diameter and 6 mm long. The dimensions of the exit hole with which the currents of Table I were obtained are shown in Fig. 2 (a).

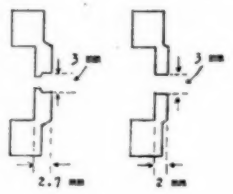

FIG. 2. Exit hole dimensions.

An inspection of Table I shows that the ion currents for the higher probe potentials are two to four times greater than those of the Tuve, Dahl and Hafstad source although, in this case, the probe canal is 50 percent longer. The currents for small probe potentials can be increased by changing the dimensions of the exit hole as will be indicated later. The current to the face of the probe (including secondaries) varied from 2.0 and 7.0 ma for the probe potentials and arc currents of Table I. The increased output currents are probably due to the higher current density in that part of the arc gap close to the exit hole and to bringing the probe close to the condensed arc. Larger arc currents produce greater output currents, but correspondingly greater probe potentials are required. For comparison, it should be noted that the source of Lamar, Samson and Compton[2] gives about the same ion current for a 2-ampere arc but, in

their case, the gas flow is much greater since the outlet hole is very short.

Measurements of positive ion currents are always complicated by the presence of secondary electrons. The method of measurement which was chosen as the one least likely to lead to spurious results is illustrated in Fig. 3. The ions are focused into a beam of smaller diameter than M by 10 to 50 kv placed across the focusing gap between L and E. All the electrodes of the accelerating tube, over a meter long, were connected and held from 90 to 300 volts positive with respect to L. The values listed in Table I are the currents to M and it is believed that very few secondaries have been counted, in fact, the true currents are probably greater since some secondary electrons from L enter M with the positive ions.

For a given arc gap and probe canal the output varies considerably with the length and diameter of the exit hole. The hole, whose dimensions are given in Fig. 2 (b), gives a current of 2.0 ma for a probe potential of 6200 volts and an arc current of only 0.4 ampere. However, the current to the probe itself was 11 ma. As the rectifier set which provided the probe potential was limited to this power, the output for larger arc currents was not measured. Larger currents than those of Table I for the smaller probe potentials are obtained by shortening the exit hole and increasing its diameter. This results in larger currents to the probe and reduces the maximum potential which can be used without extinguishing the arc. Also, decreasing the probe canal length would give greater currents for small probe potentials.[1] Holes having the shape of (a) Fig. 2 give the most satisfactory results in that the smaller diameter near the probe limits the current to the probe.

Arc gaps from 3.0 mm to 0.7 mm were investigated. The output current increases as the gap is decreased but not much was gained in using gaps less than 1.0 mm. The optimum gap is about 1.2 mm if ease of starting and steadiness are taken into consideration. The dimensions of the probe canal are determined by the available pumping speed. Systematic tests were not made to discover the way in which the ion current depends on the probe canal length or diameter. However, the conclusions of Tuve, Dahl and Hafstad[1] on this matter were roughly verified.

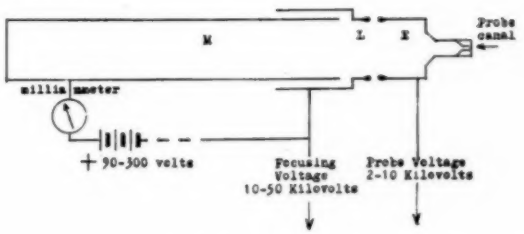

FIG. 3. Arrangement of electrodes and potentials for the measurement of output ion currents.

MAGNETIC ANALYSIS

A magnetic analysis of the ion varieties was made, using dried tank hydrogen in the source. These measurements were made with a 4 mm long probe canal and showed 15 to 20 percent atomic ions. Others[1, 2] have found similar results for the metal capillary arc and this yield apparently is all that can be hoped for from this type of source.

The source is very constant and reliable in operation. Once the pressure has been adjusted to a value slightly higher than the minimum at which the arc will run, the output current remains constant for long periods. The target currents in the accelerating tube remain constant to 1 to 2 percent although both probe and accelerating potential are turned off and on a number of times.

The author wishes to acknowledge his indebtedness to Professor Bergen Davis for making the necessary facilities available and for his helpful advice and suggestions.

Application of the Virial Theorem to Approximate Molecular and Metallic Eigenfunctions

J. O. HIRSCHFELDER AND J. F. KINCAID
Frick Chemistry Laboratory, Princeton, New Jersey

(Received July 6, 1937)

Fock showed that the virial theorem is automatically satisfied for any quantum-mechanical system whose potential is a homogenous function of the coordinates if a scale factor is introduced into the approximate charge distribution and varied so as to give the lowest energy. In this paper, we extend Fock's treatment to problems involving molecules or metals where it is customary to treat the internuclear separations as parameters. The introduction and variation of the scale factor requires very little additional work and results in considerable improvement in the physical properties. The Heitler-London-Sugiura charge distribution for molecular hydrogen has a mean potential energy, $V=-52.98$ ev; a mean kinetic energy, $T=22.79$ ev; and a total energy, $E=V+T=-30.20$ ev. When the scale factor is inserted into the eigenfunction and varied to form the Wang function: $E=-T=\frac{1}{2}V=-30.83$ ev and the virial theorem is satisfied. The total energy is improved by only 0.63 ev but the potential energy is improved by 8.67 ev and the kinetic energy by 8.04 ev. The eigenfunction for the diatomic hydrogen ion, $\Psi=N[\exp(-r_a)+\exp(-r_b)]$ where N is the normalization factor and r_a and r_b are the distances of the electrons to nuclei a and b, respectively, is another example where the scale factor results in striking improvement in the mean potential and kinetic energies. The James and Coolidge function for molecular hydrogen almost satisfies the virial theorem since $\frac{1}{2}V=-31.680$ ev and $-T=-31.588$ ev. When the scale factor, $s=1.0029$, is introduced, we obtain $E=\frac{1}{2}V=-T=-31.772$ ev. If the mean potential and kinetic energies, V_1 and T_1 respectively, are known for one nuclear separation, R_0, then on the introduction and variation of the scale factor, a lower energy is obtained for the internuclear separation, $R=-2R_0T_1/V_1$, for which $E=-T=\frac{1}{2}V=-\frac{1}{4}V_1^2/T_1$.

A FEW years ago, Professor Slater[1] pointed out that the virial theorem applies to molecular systems and that it offers a new principle to use in obtaining satisfactory charge distributions. In this paper, we develop a simple method for modifying the approximate charge distributions to satisfy the virial theorem and we find that considerable improvement in the molecular properties results. Fock[2] showed that the virial theorem is automatically satisfied for any quantum mechanical system whose potential is a homogenous function of the coordinates if a scale factor is introduced into the approximate charge distribution and varied so as to give the lowest energy. The form which Fock developed is useful for atomic problems, but his theorem requires extension for problems involving molecules or metals where it is customary to treat the internuclear separations as parameters.

In this paper, we consider only those approximate molecular or metallic eigenfunctions for the ground state which do not involve the internuclear distances explicitly but only implicitly through the electronic coordinates. These eigenfunctions are functions only of the separations of the electrons from the nuclei and from each other. There is no serious loss in generality as a result of this condition since any approximate eigenfunction can be put into this form by replacing the internuclear distances, R, in the eigenfunction by R_0, the values of the internuclear separations for a particular configuration. Let $\Psi_1(r, R)$ be an approximate eigenfunction satisfying this condition where r is symbolic for the electronic coordinates. The scale factor, s, is introduced into the charge distribution in such a way that each electronic distance is multiplied by s whilst the internuclear separations remain unchanged. Thus:

$$\Psi_s(r, R)=s^{\frac{1}{2}3n}\Psi_1(sr, R). \tag{1}$$

Here n is the number of electrons in the system. The subscripts s and 1 indicate that the eigenfunctions are for the scale factors s and 1, respectively. The effect of s is to shrink the electronic charge distribution closer to the nuclei just as though these nuclei increased their effective charge by this factor. The approximate eigenfunctions with the scale factors are related to the approximate eigenfunctions without the scale factors but for which the internuclear separations are expanded by s. For each elec-

[1] J. C. Slater, J. Chem. Phys. **1**, 687 (1933).
[2] V. Fock, Zeits. f. Physik **63**, 855 (1930).

tronic configuration, r, with the internuclear separations, R, there is a corresponding geometrically similar configuration for the nuclear separations, sR, such that the electronic separations are $r'=sr$. Because of the assumption which we have made as to the functional form of Ψ:

$$\Psi_s(r, R)=s^{\frac{1}{2}3n}\Psi_1(r', sR). \tag{2}$$

The mean value of the (electronic) kinetic energy, $T_s(R)$, is given by the relation:

$$T_s(R)=-\frac{h^2}{8\pi^2 m}\int\overline{\Psi}_s(r, R)\sum_{\text{electrons}}\Delta_i\Psi_s(r, R)d\tau. \tag{3}$$

Now using (2) and making the substitution of variables $r'=sr$, it follows that:

$$T_s(R)=s^2T_1(sR). \tag{4}$$

The mean potential energy of the system, $V_s(R)$, is given by the relation:

$$V_s(R)=\int\overline{\Psi}_s(r, R)[U_{ee}+U_{en}+U_{nn}]\Psi_s(r, R)d\tau, \tag{5}$$

where

$$U_{ee}=\sum_{\substack{\text{electron}\\ \text{pairs}}}e^2/r_{ij},\quad U_{en}=-\sum_{\substack{\text{electrons, } i,\\ \text{and nuclei, } \alpha}}e^2/r_{i\alpha},$$

$$U_{nn}=\sum_{\substack{\text{nuclear}\\ \text{pairs}}}e^2/r_{\alpha\beta}.$$

Again using (2) and making the substitution $r'=sr$, it follows that:

$$V_s(R)=sV_1(sR). \tag{6}$$

The total energy of the molecule, $E_s(R)$, is of course the sum of the mean potential and kinetic energies:

$$E_s(R)=T_s(R)+V_s(R)=s^2T_1(sR)+sV_1(sR). \tag{7}$$

Usually there will be values of s different from unity for which the energy of the system is improved. The best value of s for a particular nuclear configuration can be found from the condition that the energy is stationary for this value of the scale factor:

$$0=\left(\frac{\partial E_s(R)}{\partial s}\right)_R=2sT_1(sR)+V_1(sR)+R\left[s^2\frac{dT_1(sR)}{d(sR)}+s\frac{dV_1(sR)}{d(sR)}\right]. \tag{8}$$

For the best value of R we have the additional condition that the energy be stationary with respect to variations in the internuclear separations, R:

$$0=\left(\frac{\partial E_s(R)}{dR}\right)_s=s\left[s^2\frac{dT_1(sR)}{d(sR)}+s\frac{dV_1(sR)}{d(sR)}\right]. \tag{9}$$

Combining (8) and (9) we see that for the best value of the internuclear distances, the best value of s is

$$s=-\tfrac{1}{2}V_1(sR)/T_1(sR), \tag{10}$$

for which the lowest value for the total energy is

$$E_s(R)=-\tfrac{1}{2}V_1(sR)^2/T_1(sR). \tag{11}$$

The virial theorem is satisfied by this charge distribution since:

$$E_s(R)=-T_s(R)=\tfrac{1}{2}V_s(R), \tag{12}$$

when (10) is substituted into (4) and (6). Therefore we have the general theorem: *If the approximate charge distribution is expanded or contracted, the size which corresponds to the lowest energy gives the proper ratio between potential and kinetic energy.*

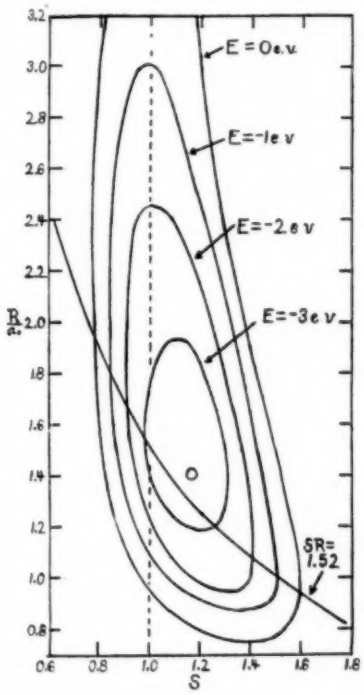

FIG. 1. The energy of H_2 as a function of R and s.

A simple example will illustrate the dependence of the molecular energy on the scale factor. Consider the Heitler-London-Sugiura[3,4] eigenfunction for molecular hydrogen:

$$\Psi_1(r, R)=N[\exp(-r_{a1}-r_{b2}) +\exp(-r_{a2}-r_{b1})]. \quad (13)$$

Here N is the normalizing factor; r_{a1}, r_{b1}, r_{a2}, r_{b2} are the separations of electron 1 from nuclei a and b and similarly for electron 2. For the lowest energy, the hydrogen nuclei are separated a distance of $R=1.52a_0$ where a_0 is the radius of the first Bohr orbit. Here:

$$E_1(R)=-30.20 \text{ ev},$$
$$-T_1(R)=-22.79,$$
$$\tfrac{1}{2}V_1(R)=-26.49.$$

These three quantities should be equal. Since they are not equal, the virial theorem is not satisfied in this case. This situation can be remedied by introducing the scale factor s into the eigenfunction to make this Heitler-London-Sugiura function into a Wang[5] eigenfunction.

$$\Psi_s(r, R)=N'[\exp(-sr_{a1}-sr_{b2}) +\exp(-sr_{a2}-sr_{b1})]. \quad (14)$$

Here N' is the new normalizing factor. Fig. 1 shows the energy as a function of both s and R. The lowest energy is for the point $s=1.166$ and $R=1.41a_0$ and this point is indicated in the figure by the small circle. For this configuration:

$$E_s(R)=-T_s(R)=\tfrac{1}{2}V_s(R)=-30.83 \text{ ev}.$$

Thus the variation of the scale factor has improved the total energy by only 0.63 ev but the mean kinetic energy is improved by 8.04 ev and the mean potential energy by 8.67 ev. This large change in potential and kinetic energies is an indication of the improvement to be expected in the other molecular properties.

The improvement in the potential and kinetic energies for the diatomic hydrogen ion, H_2^+, will show that the above is not an exceptional case. Consider as eigenfunction for H_2^+ the simple sum of atomic functions which Pauli[6] used in classical quantum mechanics:

$$\Psi_1(r, R)=N[\exp(-r_{a1})+\exp(-r_{b1})]. \quad (15)$$

For the best internuclear separation

$$E_1(R)=-15.30 \text{ ev},$$
$$-T_1(R)=-10.37 \text{ ev},$$
$$\tfrac{1}{2}V_1(R)=-12.84 \text{ ev},$$

Now introducing the scale factor to form the Finkelstein and Horowitz[7] function:

$$E_s(R)=-T_s(R)=\tfrac{1}{2}V_s(R)=-15.90 \text{ ev}$$

where $s=1.238$.

Here the improvement in the total energy is only 0.60 ev but there is a decrease of 6.12 ev in the potential energy and an increase of 5.53 ev in the kinetic energy.

In many molecular problems the computation of the energy is very laborious for each nuclear configuration. For these cases it would be difficult to construct the whole surface for energy as a function of s and R. However, knowing the mean potential and kinetic energy for just one nuclear configuration, R_0, we can use Eq. (7) to determine the energy along the rectangular hyperbola, $sR=R_0$, in the s, R diagram. Along this hyperbola the lowest energy is given for $s=-\frac{1}{2}V_1(R_0)/T_1(R_0)$ at the internuclear separation $R=R_0/s$. For this value of s the virial theorem holds and

$$E_s(R)=-T_s(R)=\tfrac{1}{2}V_s(R) =-\tfrac{1}{4}V_1(R_0)^2/T_1(R_0). \quad (16)$$

This $E_s(R)$ is always lower than $E_1(R_0)$ but it is not necessarily lower than $E_1(R)$ or $E_{s'}(R)$ where s' is some other value of the scale factor and R is the same internuclear separations. If R_0 is chosen as the best separation of the nuclei when the scale factor is unity, the point of lowest energy along the hyperbola will come close to but in general will not coincide with the configuration having both the best R and the best s. This is because the term in brackets in Eq. (8) does not vanish. Thus for the Wang eigenfunction for H_2 the best value of R is $1.52a_0$ when $s=1.00$. Following along the hyperbola $sR=1.52$ (see Fig. 1) we find the lowest energy

[3] Heitler and London, Zeits. f. Physik **44**, 455 (1927).
[4] Y. Sugiura, Zeits. f. Physik **45**, 484 (1927).
[5] S. C. Wang, Phys. Rev. **31**, 579 (1928).
[6] Pauli, Ann. d. Physik **68**, 177 (1922); also the Dissertation of K. F. Niessen, Utrecht University (1922).
[7] Finkelstein and Horowitz, Zeits. f. Physik **48**, 118 (1928).

for $s=1.162$ at which $E_s(R)=-30.79$ ev and $R=1.30a_0$. This is close to the best point on the entire energy surface for which it will be remembered that $s=1.166$, $E_s(R)=-30.83$ ev, and $R=1.41a_0$.

To show how the proper ratio of the potential to the kinetic energy can be obtained easily in a complicated case, we consider the thirteen term eigenfunction of James and Coolidge[8] for H_2. Here:

$$E_1(R)=-31.772 \text{ ev},$$
$$-T_1(R)=-31.588 \text{ ev},$$
$$\tfrac{1}{2}V_1(R)=-31.680 \text{ ev}.$$

This charge distribution is truly excellent but the physical properties of even this eigenfunction can be improved by the introduction of the scale factor, $s=1.0029$, for which

$$E_s(R)=-T_s(R)=\tfrac{1}{2}V_s(R)=-31.772 \text{ ev}.$$

The improvement in the total energy is only 0.0003 ev and hence negligible, but the mean potential and the mean kinetic energies are each improved by 0.184 ev.

N. Rosen[9] has discussed the variation of the best value of the scale factor with internuclear distance. For large separations s is less than unity so that the charge distributions are expanded. This is due of course to the charges being pulled towards the nucleus of the approaching atom. For smaller separations s is greater than unity and the charges are contracted. If the nuclei coalesce s assumes a finite value larger than for the separated atoms. This variation of s with internuclear separation makes it difficult to determine the energy as a function of the internuclear separations using the best value of s for each separation. Because of this difficulty, Wang computed the fundamental vibration frequency of H_2 on the assumption that s remains equal to 1.166 over the whole range of internuclear separations. A study of Fig. 1 will show that the energy as a function of R varies much more rapidly along the line $s=1.166$ than along the curve of best values of s. Therefore a more accurate calculation of the fundamental vibration frequency would decrease Wang's value of 4900 cm^{-1} to a value more in agreement with the experimental observation of 4260 cm^{-1}.

From Eq. (2), it follows that any molecular property which is proportional to the qth power of the electronic coordinates is multiplied by s^{-q} when the scale factor is introduced. Thus we have shown that very little additional work is required to introduce a scale factor into a molecular or metallic charge distribution and the physical properties of the system are considerably improved thereby.

The authors wish to thank Professor A. S. Coolidge and Dr. H. M. James both for helpful communications and for the use of their calculated data which enabled them to compute the mean potential and kinetic energies for their molecular hydrogen charge distribution. One of us (J.O.H.) wishes to express his appreciation to the American Philosophical Society for financial assistance.

[8] James and Coolidge, J. Chem. Phys. **1**, 825 (1933).
[9] N. Rosen, Phys. Rev. **38**, 2099 (1931).

LETTERS TO THE EDITOR

Prompt publication of brief reports of important discoveries in physics may be secured by addressing them to this department. Closing dates for this department are, for the first issue of the month, the eighteenth of the preceding month, for the second issue, the third of the month. Because of the late closing dates for the section no proof can be shown to authors. The Board of Editors does not hold itself responsible for the opinions expressed by the correspondents.

Communications should not in general exceed 600 words in length.

The Variation of the Diamagnetism of Water with Temperature

Honda and Shimizu[1] have recently derived an equation expressing the variation of the diamagnetic susceptibility of water as a function of its temperature. They cite in support of their conclusions, the experimental results of Mathur[2] and Cabrera and Fahlenbrach,[3] the general agreement between theoretical and experimental results being considered entirely satisfactory. However, in view of the estimated precision of measurement of magnetic susceptibilities, these experimental results and also the experimental results of other investigators do not show on the whole, a very satisfactory agreement.

While the values obtained by a considerable number of observers for the temperature coefficient of the susceptibility ratio χ/χ_{20} at room temperature is reasonably satisfactory, the investigations made on the variation of the susceptibility at higher temperatures show divergent results. Several observers have found the change in susceptibility to be a linear function of the temperature. The results of the investigations of Wills and Boeker,[4] however seem to indicate an anomalous variation in the region from 35°–55°C, definite breaks occurring in the slope of the mass susceptibility—temperature curve.

Using the manometric balance already described,[5] having greater sensitivity than that employed by Wills and Boeker,[4] the author, several years ago, made careful relative susceptibility measurements of water over the range of temperatures from 2°–74°C in order to investigate the reported anomalies. The results of these measurements are reproduced in Fig. 1, the indicated values of χ/χ_{20} being calculated from the values of κ/κ_{20}, the relative volume susceptibilities, obtained by interpolation with the aid of a large scale graph of the experimental results. These data are summarized in Table I.

TABLE I. *Variation of susceptibility of water with temperature.*

Temperature °C	χ/χ_{20}
0	0.9971
10	0.9985
20	1.0000
30	1.0014
40	1.0024
50	1.0030
60	1.0042
70	1.0061
75	1.0072

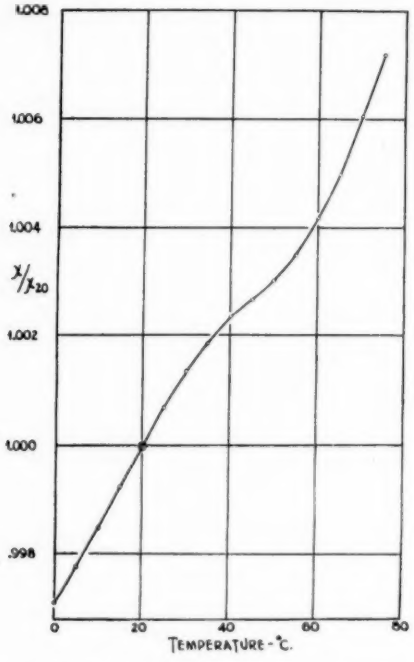

FIG. 1. Variation of susceptibility of water with temperature.

The results indicate a continuous, though irregular, increase of susceptibility with temperature, a marked change in slope occurring at 45°C. Over the range of temperature from 20°–60°C, the results are in very good agreement with the results of Wills and Boeker, as represented by the parabolic formula given by them. However, the general trend of the curve is such as to indicate divergent results for higher temperatures. Over the investigated temperature range, these results are in fair agreement with the results of Cabrera and Fahlenbrach[3] and Johner.[6] Here too, the general trend of the curve is such as to indicate divergent results for higher temperatures.

SAMUEL SEELY

Columbia University and
The College of the City of New York,
New York, N. Y.,
August 24, 1937.

[1] Honda and Shimizu, Tohoku U. Sci. Rpts. **25**, 939 (1937).
[2] Mathur, Ind. J. Phys. **6**, 207 (1931).
[3] Cabrera and Fahlenbrach, Zeits. f. Physik **82**, 759 (1933).
[4] Wills and Boeker, Phys. Rev. **46**, 907 (1934).
[5] Seely, Phys. Rev. **49**, 812 (1936).
[6] Johner, Helv. Phys. Acta **4**, 238 (1931).

A New Radioactive Isotope of Potassium

In a previous communication[1] were reported results obtained in a study of the induced radioactivity of calcium. Decay curves of calcium metal which had been activated for many hours with neutrons from a beryllium target bombarded with deuterons were published, which showed the presence of a short-lived activity. This was not identified but it was pointed out that it might be due to a fast neutron disintegration. More recently[2] it was shown that there was some evidence for the reaction:

$$Ca^{42}+n^1\rightarrow K^{42};\quad K^{42}\rightarrow Ca^{42}+\bar{e},$$

though the resulting activity was weak.

The present note is a report of experiments on the radioactivity induced in calcium by irradiation with the highly energetic neutrons from a lithium target bombarded with 14 microamperes of deuterons. Samples of the metal and of a very pure specimen of $Ca(OH)_2$ were thus activated. The samples were contained in a cadmium box filled with boric oxide placed immediately behind the brass target plate. All showed the presence of two periods, one of half-life 12.5 hours, the other a short period of half-life 18 ± 1 minutes. The metal which was activated for several hours showed also the presence of a weak period of 76 ± 6 minutes which may be due to contamination as it was not observed with the very pure hydroxide.

Chemical analysis of the activities showed both the 18 minute and 12.5 hour period to be isotopes of potassium. The samples were dissolved in dilute HCl and inactive KCl was added. The calcium was precipitated as oxalate in alkaline solution. This was filtered off and found to be practically inactive. The potassium was precipitated by the addition of perchloric acid and ethyl alcohol. It was found to be radioactive and measurements on the decay showed the presence of both the short and the long periods. Magnetic analysis of the emitted radiations using a trochoid analyzer showed them to be negative electrons. Hence as the 12.5-hour period has been shown previously[2] to be due to K^{42} the 18-minute period must be associated with a heavier isotope of potassium either K^{43} or K^{44} formed thus:

$$Ca^{43,\,44}+n^1\rightarrow K^{43,\,44};\quad K^{43,\,44}\rightarrow Ca^{43,\,44}+\bar{e}.$$

The decay curves of an unseparated sample of $Ca(OH)_2$ and of a potassium precipitate from a second sample are shown in Figs. 1 and 2. For convenience only the early portions of the decay curve of the long period activity are shown. The decay of the K^{42} was actually followed for 28 hours.

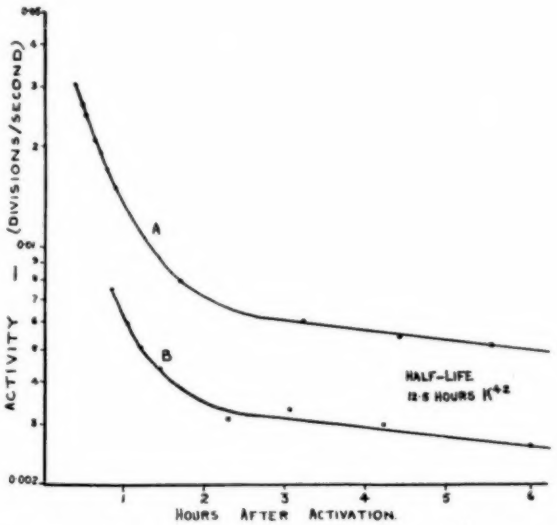

FIG. 1. Decay curves of very pure $Ca(OH)_2$ activated by $Li+H^2$ neutrons. *A*, potassium precipitate; *B*, unseparated sample.

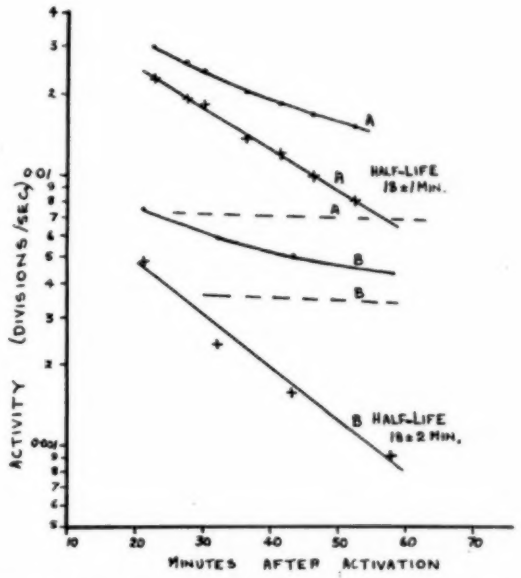

FIG. 2. Analysis of early portions of decay curves of Fig. 1. *A*, potassium precipitate; *B*, unseparated sample. Points indicated by dots; total activity; those marked with a plus sign have been corrected for the activity due to K^{42} which is shown by the dotted line.

No definite evidence was obtained of the very weak 4.5-minute positron period observed by Pool, Cork and Thornton[3] and ascribed by them to Ca^{39}. However, the samples used were activated for several hours and this period might well be masked by the increased activity due to the longer periods.

The author is grateful to Mr. E. M. Lyman for the use of the trochoid analyzer and to the staff of the Radiation Laboratory for their cooperation. His thanks are expressed to Professor E. O. Lawrence for continued encouragement.

The research has been aided by grants to the Laboratory from the Research Corporation, the Chemical Foundation, and the Josiah Macy, Jr. Foundation.

HAROLD WALKE*

Radiation Laboratory,
University of California,
Berkeley, California,
August 6, 1937.

[1] Walke, Phys. Rev. **51**, 439 (1937).
[2] Hurst and Walke, Phys. Rev. **51**, 1033 (1937).
[3] Pool, Cork and Thornton, Phys. Rev. **52**, 239 (1937).
* Commonwealth Fund Fellow.

Dielectric Strengths of CCl_2F_2 Air and SO_2 Air Mixtures

Measurement on CCl_4 air mixtures made at this laboratory several years ago indicated that CCl_4 in air may be of considerable value for high potential work. These results suggested that it might be of interest to look for similar effects due to other compounds.

With the apparatus constructed by Rodine and Herb for their work on CCl_4,[1] two other compounds, CCl_2F_2 and SO_2, have been investigated for breakdown potential as a function of concentration in air.

Results on CCl_2F_2 are shown by the curves of Fig. 1, where sparking potentials across a 3 mm sphere gap are plotted as a function of partial pressure of CCl_2F_2 for several values of total pressure. Because of the limited potential available, some of the data were taken with smaller sphere separations, but all were reduced to the common separation of 3 mm.

Each of the points plotted is an average of many determinations. However, for pressures of CCl_2F_2 in the vicinity of its vapor pressure, sparking potentials were very incon-

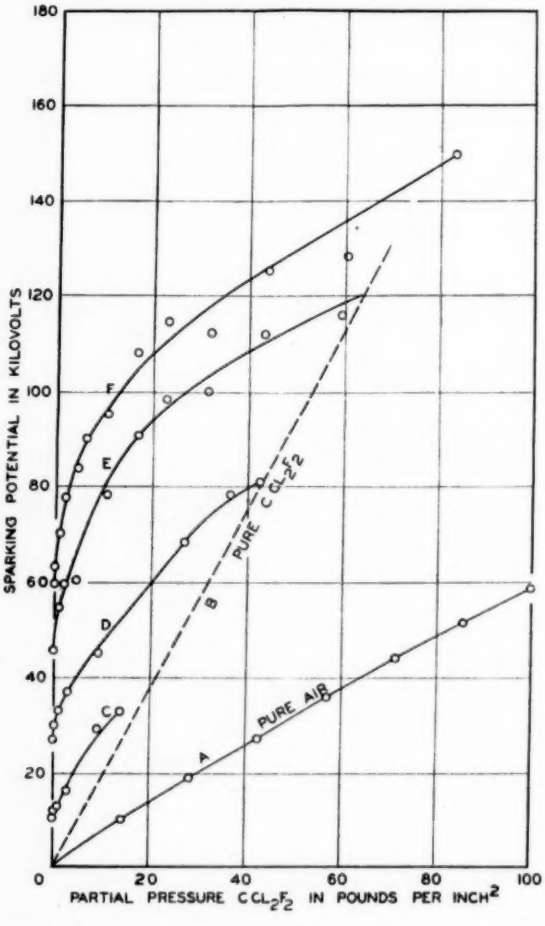

FIG. 1. Curve *A* gives sparking potential in pure air as a function of pressure. Abscissae for this curve are air pressure in pounds per sq. in. with scale as indicated. For curves *C*, *D*, *E*, and *F*, sparking potentials in CCl_2F_2 air mixtures are given as a function of partial pressure of CCl_2F_2 with total pressures as follows: curve *C*, 14.3 lb.; curve *D*, 42.9 lb.; curve *E*, 71.5 lb.; curve *F*, 100.1 lb.

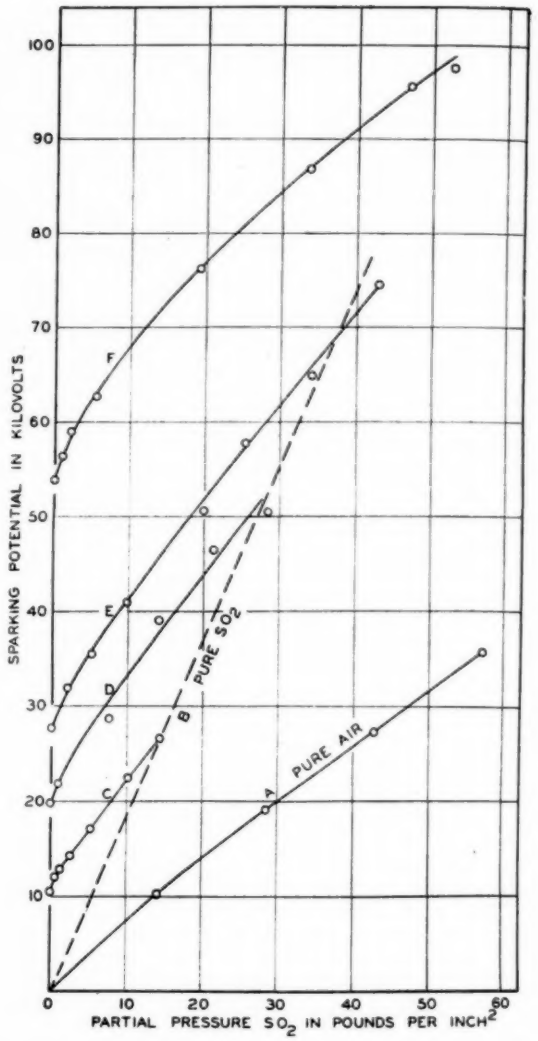

FIG. 2. Curve *A* gives sparking potential in pure air as a function of pressure. Abscissae for this curve are air pressure in pounds per sq. in. with scale as indicated. For curves *C*, *D*, *E*, and *F*, sparking potentials in SO_2 air mixtures are given as a function of partial pressure of SO_2 with total pressures as follows: curve *C*, 14.3 lb.; curve *D*, 28.6 lb.; curve *E*, 42.9 lb.; curve *F*, 100.1 lb.

sistent, occasionally as much as 30 percent below the value indicated, and therefore no claim of great accuracy can be made for the data in these regions.

That particular ordinate on each of curves *C*, *D*, and *E* which corresponds to the point at which the partial pressure of CCl_2F_2 is equal to the total pressure for that curve, is the breakdown potential for pure CCl_2F_2 at that pressure. Curve *B* is the line drawn through these points and is taken as linear to an approximation. Since curves *F* in both the case of CCl_2F_2 and the case of SO_2 were taken with total pressures in excess of the vapor pressure of the compounds at the temperature of the experiment, there exists no pure vapor point on curves *F*. From curve *B*, which shows sparking potential of pure CCl_2F_2 as a function of its pressure, and curve *A*, which is for pure air, the dielectric strength of pure CCl_2F_2 is seen to be approxi-

mately 3.0 times as great as the dielectric strength of pure air.

Curves *C*, *D*, *E*, and *F* are seen to be convex upward; and for high total pressure, the curves rise very steeply in the region of low CCl_2F_2 concentrations. If the dielectric strengths of the two components were simply additive, these curves would be straight lines connecting the end-points. The shape observed shows that the dielectric strength of the mixture is greater than the sum of the dielectric strengths of the components.

Sparking potential of the CCl_2F_2 air mixtures did not appear to depend greatly on the number of sparks that had passed. High concentrations of CCl_2F_2 appeared to have no effect on brass, Bakelite, Textolite, rubber, Picein wax, or red sealing wax.

Figure 2 shows results obtained from work on SO_2 air mixtures. The curves shown are plotted in the same manner as in the case of CCl_2F_2. To judge by the fairly permanent fog observed after sparking, the vapor seemed to be decomposed in the vicinity of the discharge.

It was also observed that the vapor corroded the spheres and pressure vessel. From a comparison of curves *A* and *B* of Fig. 2, the dielectric strength of pure SO_2 is seen to be approximately 2.7 times as great as the dielectric strength of pure air. This value, however, is very approximate since the data showed great spread.

We wish to express our appreciation to Dr. R. G. Herb for his guidance in this work, and to J. C. Bellamy, for valuable help.

C. M. Hudson
L. E. Hoisington
L. E. Royt

University of Wisconsin,
Madison, Wisconsin,
August 18, 1937.

[1] M. T. Rodine and R. G. Herb, Phys. Rev. **51**, 508 (1937).

The Elastic Constants of Crystalline Sodium at 80°K

In a recent issue of this journal[1] one of us reported values of the principal elastic constants of crystalline sodium at 80°K. These results are entirely erroneous, because an inappropriate formula was used in reducing the observations.

The experimental method is a dynamical one,[2] and the calculation of the principal elastic constants demands, in part, a relation between these quantities and the rigidity modulus corresponding to a given direction in the crystal lattice. Two such relations are available, one of which describes the behavior of a right circular cylinder over the end faces of which torsional stresses are applied. Under such a stress system the cylinder will, in general, bend as well as twist. The second relation describes the behavior of the cylinder when this bending is prevented. It appears that the propagation of supersonic torsional vibrations along thin cylinders of crystalline material is governed by the second of these relations, and not by the first.

The three crystals which yielded the data now under review were grown from sodium prepared by heating C.P. NaCl with metallic Ca. The correct values of the elastic constants of these crystals are as follows: $s_{11}=4.69$, $s_{12}=-1.94$ and $s_{44}=1.76$, all times 10^{-11} cm²/dynes. The high value of the compressibility of this material, namely 2.43×10^{-11}, suggests the presence of impurity. Accordingly we have redetermined the elastic constants from measurements made upon six crystals grown from triply distilled Mallinckrodt sodium.

The newly determined values of the principal elastic constants at 80°K are: $s_{11}=4.86$, $s_{12}=-2.17$, $s_{44}=1.76$, all times 10^{-11} cm²/dynes. The data immediately obtained from the experimental observations are the values of the velocities of propagation of longitudinal and torsional vibration along thin cylinders of the specimen material. The concordance of the observations here reported is exhibited in Table I, in which the observed velocities

TABLE I. *Observed and computed values of the longitudinal and torsional velocities in cylinders of crystal sodium.*

Direction Factor	Longitudinal Velocity $\times10^{-5}$ cm/sec.		Torsional Velocity $\times10^{-5}$ cm/sec.	
	Observed	Computed	Observed	Computed
0.0130	1.457	1.454	2.260	2.299
0.1175			1.793	1.816
0.1476	1.803	1.806	1.648	1.647
0.2128	2.104	2.104	1.387	1.378
0.2907	2.792	2.779	1.188	1.174
0.3044	2.964	2.981	1.072	1.081

may be compared with those computed from the values of the elastic constants given above. The first column contains the factor $\Sigma\alpha_i^2\alpha_j^2$, where the α's are the direction cosines of the specimen cylinder axis with respect to the principal axes of the crystal. This factor, whose value must lie between 0 and 1/3, governs the variation of the longitudinal velocity with direction, and principally that of the torsional velocity as well. It will be seen that range of possible values is well covered by the present six crystal cylinders.

Bridgman[3] has measured the variation of the compressibility of polycrystalline sodium with pressure between 2000 and 20,000 kg/cm². As the pressure is lowered the compressibility increases toward the (extrapolated) value 1.7×10^{-11} cm²/dynes at zero pressure and room temperature. The present value at 80°K is 1.56×10^{-11}.

Fuchs[4] has given a wave mechanical calculation of the quantities $(c_{11}-c_{12})$ and c_{44} for sodium at 0°K, which yields the values 1.41×10^{10} and 5.8×10^{10}, respectively. The corresponding experimental values at 80°K are 1.42×10^{10} and 5.7×10^{10}.

A complete description of the experiments will shortly be submitted for publication in this journal. The authors gratefully acknowledge their indebtedness to the Ernest Kempton Adams Fellowship of Columbia University for the financial assistance which made this work possible.

S. L. Quimby
Sidney Siegel

Pupin Physics Laboratories,
Columbia University,
New York, N. Y.
August 25, 1937.

[1] Siegel, Phys. Rev. **51**, 1015 (1937).
[2] Balamuth, Phys. Rev. **45**, 715 (1934); Rose, Phys. Rev. **49**, 50 (1936).
[3] Bridgman, Proc. Am. Acad. Arts and Sc. **70**, 94 (1935).
[4] Fuchs, Proc. Roy. Soc. **157**, 444 (1937).

On the Distribution of the Lifetimes of Radioelements

In a previous note[1] we pointed out the pseudo-Gaussian distribution of the electronic and positronic lifetimes of artificial and natural radioelements. We disposed then of about 100 lifetimes. Later on[2] with the discovery of 50 other radioelements, we found that the distribution curve was becoming more symmetrical. We pointed out then

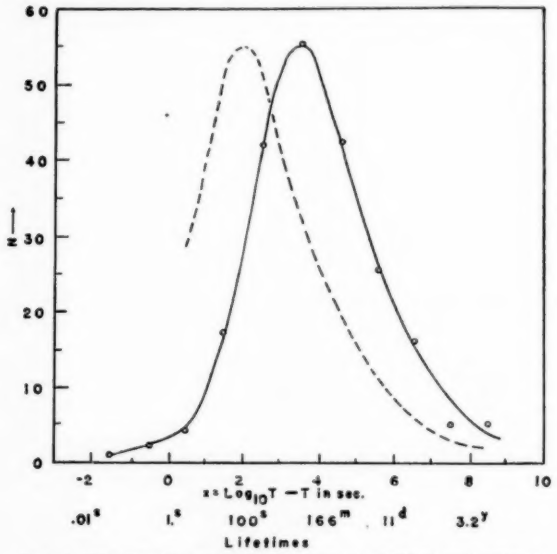

FIG. 1. Distribution curve of lifetimes of artificial and natural radioelements.

that the maximum of the curve was situated in a region of lifetimes *very easily detectable* (1 to 200 minutes) and also that there were still *too many* possibilities of discovery of new radioelements to make it worth while to discuss such a distribution. Since then some 70 more lifetimes have been measured, bringing the whole number to about 220. Fig. 1 shows the distribution curve (full line) representing the number N of radioelements as a function of $\log_{10} T$ (T being the lifetime expressed in seconds). In order to define N, let $x=\log_{10} T$ and Ndx will be the number of radioelements with values of x between x and $x+dx$. Considering the *small number* of lifetimes observed in the "easily observable" regions of 10 to 100 seconds and 3 to 30 hours, and also the *few* possible radioelements left in the proton-neutron stability diagram (neglecting the possible existence of *many* isomeric nuclei) the N distribution in Fig. 1 begins to have some interest. Furthermore some preliminary investigations for short period radioelements, with the help of the Berkeley cyclotron, by Dr. Luis Alvarez (unpublished) have proved unsuccessful. Finally, a rough calculation shows that such a distribution could be expected.

Let us take an "average" Sargent line satisfying the relation:

$$\log_{10} E=a+b\log_{10} T, \quad \text{with} \quad a=7.16, \quad b=-0.23, \quad \log T=\text{const.}-\log\lambda \qquad (1)$$

and E being the maximum energy of the spectra, expressed in volts. From this expression we get:

$$E=10^{7.16}e^{-0.53x} \quad \text{and} \quad T\propto E^{-4.3} \qquad (2)$$

in reasonable agreement with the value $T\propto E^{-4.6}$ deduced from Fermi's theory.[3]

Let us assume now that the statistical distribution of E is almost uniform for values of E from 0.5 to 6 Mev and that it drops down for higher values of E in such a way that for $E>10$ Mev it becomes very improbable. We will tentatively take $(1-10^{-12}\,(E/10)^2)$ to be proportional to the number n of radioelements of energy between E and $E+dE$, up to $E=10$ Mev, and $n=0$ for $E>10$ Mev. From this it follows that the number Ndx, as defined before, is given by

$$Ndx=ndE\propto|(1-10^{-12}(E/10)^2)|\,dE \qquad (3)$$

that is:

$$Ndx\propto|(1-10^{-14}10^{14.3}e^{-1.06x})0.53e^{-0.53x}|\,dx, \qquad (4)$$

and finally

$$N\propto e^{-0.53x}-2e^{-1.59x}. \qquad (5)$$

We have plotted N given by (5) in Fig. 1 (broken line). Thus the maximum number of radioelements seems to occur for $x=\log T\sim 2$. The observed $N_{\max}$ is for $\log T=3.5$. Considering the crude assumptions in our calculation, the agreement is satisfactory.

Taking an average value of x for $N_{\max}$, say $x=2.5$ which corresponds to a "most frequent" lifetime of about 5 minutes we get from (1) a "most frequent" maximum energy $\mathcal{E}$ of the order of 4 Mev.

Before an explanation is sought for the existence of such a "most frequent" $\mathcal{E}$ and such an N distribution, it would be very desirable to dispose of the energy spectra of most of the radioelements and thus be able to plot them according to their "degree" of transition ($L=0, 1, 2, 3\cdots$) and their mass-number "category": light or heavy nuclei (a distinction which is rather important in the case of small kinetic energies[4]) in a three dimensional Sargent diagram ($\log\lambda$, $\log E$ and N). This is hardly feasible at present, because only about 40 energy distribution curves are known.

It remains also to be seen, if there is a Gaussian-like distribution for N in each particular set of radioelements belonging to the same kind of transition, what are the respective values of $N^i_{\max}$ ($i=0, 1, 2, \cdots$ indices referring to the kind of transition: 0 stands for "allowed" transition, 1 for "first forbidden" 2 for "second forbidden" etc.).

The fact that the total N distribution for all transitions, shown in Fig. 1, is Gaussian proves either that $N^0_{\max}$, $N^1_{\max}$, $N^2_{\max}$, $\cdots$ occur for the same value of $\mathcal{E}$ (about 4 Mev), or that the N^i distributions strongly overlap; or, finally, that most of the radioelements belong to the line $L=0$ and that their N distribution is but little affected by the few radioactive nuclei of the forbidden transition lines.

I am very grateful to Professor Fermi and Professor Webster for helpful discussions.

M. E. NAHMIAS*

Department of Physics,
Stanford University,
California,
August 25, 1937.

[1] M. E. Nahmias and R. J-Walen, Comptes rendus **203**, 71 (1936).
[2] M. E. Nahmias and R. J-Walen, J. de phys. April 1937, p. 159.
[3] Fermi, Zeits. f. Physik **88**, 173 (1934).
[4] H. A. Bethe and R. F. Bacher, Rev. Mod. Phys. **8**, 194 (1936).
* Rockefeller fellow.

The Space Lattice and "Superlattice" of Pyrrhotite

Both paramagnetic and ferromagnetic solid solutions of pyrrhotite ($FeS_{1.05}-FeS_{1.12}$) may be found which are outwardly at least structurally isomorphous. The latter has anomalous ferromagnetic and gyromagnetic properties. In solutions from 50.0 to 51.2 mole percent sulfur (corresponding to $Fe_{19}S_{20}$) however, a "superlattice," in addition to the basic hexagonal lattice, has been reported.[1] As reported, the symmetry of the "superlattice" is also hexagonal, but the (110) axis of the old elementary cell (of the nickel arsenide type) becomes the a axis of the super cell, while the c axis of the old cell is doubled in length. At about 51.6 mole percent sulfur the "superlattice" is said to disappear and ferromagnetism to appear. The relation of the "superlattice" to ferromagnetism has been further investigated by us through x-ray studies of single crystals, as well as of powder specimens of both ferromagnetic and paramagnetic pyrrhotite.

The evidence for the presence of a "superlattice" in paramagnetic pyrrhotite has been confirmed by means of powder diffraction spectra made with filtered chromium radiation of samples of natural and synthetic pyrrhotite.[2] Further, identically the same evidence has been obtained from both natural and synthetic ferromagnetic pyrrhotites.[2] The diffraction lines reported[1] for the "superlattice" are found present in varying number in the diffraction patterns of all the specimens studied.

X-ray diffraction studies have been made on a ferromagnetic single crystal from Minas Geraes, Brazil,[3] and on a paramagnetic single crystal from Maggiadone, Italy.[4] In addition to Laue photograms, rotation photograms about the a, c, and (110) axes have been prepared with filtered molybdenum radiation. These photograms lead to a hexagonal lattice with the following dimensions:

$$a_0,\ 3.453\pm0.009\text{A};\quad c_0,\ 5.670\pm0.020\text{A};$$
$$d_{110},\ 5.976\pm0.029\text{A};\quad c/a,\ 1.644.$$

The same values of the parameters, within the experimental error, were found for both the ferromagnetic and the paramagnetic crystals.

All the diffractions observed from the single crystals, without exception, were identified as due to reflections from the planes of the basic lattice. In contrast to the powder diffraction data, diffraction spots corresponding to the reflections from the planes of the "superlattice" alone were not observed on the rotation photograms of either the ferromagnetic or the paramagnetic crystals, although from the point of view of intensity it was found possible for them to appear. Hence, this evidence does not support the existence of a "superlattice" in the single crystals of pyrrhotite studied in this investigation.

The Laue photograms of both crystals appear to have the symmetry D_{6h}. Diffractions from the general planes (hkl) appear in all orders. Characteristic halvings are ($00l$) and (hhl). Accordingly, the most probable space groups are D_{6h}^4, C_{6v}^4, and D_{3h}^4.

The density of certain powder specimens has been determined by us as 4.55 g/cc. Using this value, the number of molecules of pyrrhotite per elementary cell is approximately 2. The space groups D_{3d}^2 and C_{3v}^4, which give the same characteristic halvings as those found, have not been considered, since, when the number of equivalent points is only 2, these groups reduce to two of those given above as far as the atomic positions are concerned; further, these two groups are likely eliminated by virtue of the Laue symmetry observed.

The writers are very grateful to Dr. David R. Inglis for suggesting the problem and for assisting in its execution.

SURAIN S. SIDHU
VICTOR HICKS

University of Pittsburgh,
Pittsburgh, Pennsylvania.
August 23, 1937.

[1] G. Hägg and I. Sucksdorff, Zeits. f. physik. Chemie **B22**, 444 (1933).
[2] The samples of natural pyrrhotite were obtained from Kisbanya, Roumania, and Rossland, British Columbia. The synthetic pyrrhotites were kindly supplied by Dr. H. S. Roberts, Geophysical Laboratory, Washington, D. C.
[3] Kindly supplied by Professor H. Leighton, department of geology, University of Pittsburgh.
[4] Kindly supplied by Dr. F. H. Pough, The American Museum of Natural History, New York.

Further Remarks on the Saturation Property of Nuclear Forces

Certain restrictions are imposed on the relative amounts of the different kinds of exchange forces in the general symmetrical interaction operator by the requirement that the binding energy per particle in heavy nuclear systems falls below a constant upper bound which is independent of the number of particles.[1] In particular this condition must be satisfied when the statistical method is used to calculate the binding energies of heavy nuclear systems containing (1) equal numbers of neutrons and protons with zero total spin, (2) neutrons only with zero total spin, (3) equal numbers of neutrons and protons with all spins parallel, (4) neutrons only with all spins parallel. Applied to the interaction operator[1]

$$V=\sum_{i<j}\{W+MP_{ij}+BQ_{ij}+HP_{ij}Q_{ij}\}J(r_{ij}),\qquad(1)$$

with $W+M+B+H=1$, the requirement yields the set of simultaneous inequalities

$$\begin{aligned} c_1&\equiv 4W-M+2B-2H\leqq 0,\\ c_2&\equiv 2W-M+\ B-2H\leqq 0,\\ c_3&\equiv 2W-M+2B-\ H\leqq 0,\\ c_4&\equiv\ W-M+\ B-\ H\leqq 0, \end{aligned}\qquad(2)$$

each obtained from the correspondingly numbered type of nuclear system. The condition on c_4 is not independent, but follows from $c_3\leqq 0$. The conditions on c_1 and c_2 were first derived in reference 1. Kemmer[2] has recently given the third inequality. If, for reasons which have been discussed elsewhere,[3-5] we take $c_1=0$, the remaining inequalities reduce to

$$M+2H\geqq 0,\quad M-2B\geqq 0.\qquad(3)$$

An independent restriction,[6] $M-2B\geqq H$, is required by the instability of odd-odd nuclei heavier than N^{14}.

From $c_1=0$, Kemmer's inequality, and the relation $W+M-B-H\sim 0.5$ fixed by the scattering cross section

of slow neutrons in hydrogen there follows

$$W-M+B-H=-(W+M+B+H)/3+2c_3/3\leqq -1/3,$$
$$W-M-B+H=-3(W+M-B-H)+3(M-2B)\geqq -3/2. \quad (4)$$

These inequalities put one-sided limits on the triplet and singlet p interactions involved in the elastic scattering of fast neutrons and protons in hydrogen. Furthermore

$$9(W-M+B-H)+(W-M-B+H)=-6(W+M)\sim -9/2, \quad (5)$$

a useful relation establishing a connection between the p scattering of protons in hydrogen (associated with the triplet interaction) and the p scattering of neutrons in hydrogen (involving both singlet and triplet interactions). It is worth noting explicitly that the upper bound on the triplet p interaction given in (4) is a consequence of $c_3\leqq 0$ alone while Eq. (5) follows from $c_1=0$ alone.

E. FEENBERG

Institute for Advanced Study,
Princeton, N. J.,
September 2, 1937.

[1] G. Breit and E. Feenberg, Phys. Rev. **50**, 850 (1936).
[2] N. Kemmer, Nature **140**, 192 (1937).
[3] D. R. Inglis, Phys. Rev. **51**, 531 (1937).
[4] E. Feenberg, Phys. Rev. **51**, 777 (1937).
[5] H. Volz, Zeits. f. Physik **105**, 537 (1937).
[6] E. Wigner, Phys. Rev. **51**, 947 (1937). Using the experimental value for the ratio of the triplet and singlet s interactions one finds

$$W-M+B-H=-2(M-2B-H)+(W+M-3B-3H)\sim -2(M-2B-H).$$

The β-Ray Spectrum of Mn^{56}

We have measured the β-ray spectrum of Mn^{56} excited by bombarding $NaMnO_4$ solution with neutrons from a Ra-Be source. Using a field of 850 gauss, we obtain a single group with a K-U end-point at 6.5 mc^2, in agreement with Gaerttner, Turin and Crane.[1] Using a field of 425 gauss, we obtain curves similar to those of Brown and Mitchell,[2] with end-points at 3.4 and 6.5 mc^2, respectively. With a field of 637 gauss, the spectrum again shows the two groups with the same end-points as found with 425 gauss, but with the relative population of the lower energy group greatly diminished. More than 1300 tracks were measured for each field.

This work then confirms the existence of the low energy group reported by Brown and Mitchell. We attribute the discrepancy between their results and those of Gaerttner, Turin and Crane to the suppression of some of the tracks of the low energy group by the stronger magnetic fields, but our work does not permit us to draw conclusions as to the ultimate origin of the low energy group.

RALPH H. BACON
EDGAR N. GRISEWOOD
CAREL W. VAN DER MERWE

New York University,
Washington Square College,
August 31, 1937.

[1] Gaerttner, Turin and Crane, Phys. Rev. **49**, 793 (1936).
[2] Brown and Mitchell, Phys. Rev. **50**, 593 (1936).

Important Notice

THE American Institute of Physics will pay $2.00 per copy for each of the following issues of the *Physical Review:*

Volume 1, No. 6—June, 1913
Volume 2, No. 2—August, 1913
Volume 2, No. 4—October, 1913
Volume 2, No. 5—November, 1913
Volume 7, No. 1—January, 1916
Volume 7, No. 2—February, 1916
Volume 7, No. 3—March, 1916
Volume 7, No. 4—April, 1916
Volume 7, No. 5—May, 1916
Volume 9, No. 2—February, 1917

Copies should be in good condition. They should be addressed to the Publications Manager, American Institute of Physics, 175 Fifth Avenue, New York, New York, with the name and address of sender and with a covering letter.